Development of High Seismic Performance RC Piers with Object-Oriented Structural Analysis

Yoshikazu TAKAHASHI

January 2002

Development of High Seismic Performance RC Piers with Object-Oriented Structural Analysis

A Dissertation

Submitted to

the Faculty of Engineering of Kyoto University

In Partial Fulfillment

of the Requirements for the Degree of

Doctor of Engineering

by

Yoshikazu TAKAHASHI

January 2002

Summary

This dissertation is a fundamental study on the development of the high seismic performance concrete structures with the object-oriented structural analysis system and their applications.

Firstly, the object-oriented structural analysis system is developed. The system is divided into three subsystems (Structure, Load and ResponseAnalysis). Each subsystem can be used alone for the specific analytical use. And the seismic analysis can be carried out by collaborating with the subsystems. The subsystems are implemented into the class libraries in C++, but the main analysis system itself is a program code. As we placed objects in the code and define the relationship between the objects, various kind of analytical program can be made. Since the subsystems have also the rich extendibility, the object-oriented structural analysis system can support the development of new structures efficiently.

Secondly, the seismic behavior of RC tall piers with hollow section is investigated by the cyclic loading and hybrid earthquake loading tests. Results show that the shear component in the whole deformation cannot be neglected, but the seismic response is stable under the severe earthquakes if the bottom is filled and the shear reinforcement is arranged well.

Thirdly, the Unbonded Bar Reinforced Concrete (UBRC) structures is developed and proposed as the high seismic performance structure. As the results of the tests, the installed unbonded bars can add the stable positive post-yield stiffness to the load–displacement hysteresis loop and it provides the high seismic performance to the RC piers with easy construction and low cost. There are four methods to change the characteristics of UBRC structures. By the combination of the methods, many kinds of skeleton curves can be obtained. Applying the UBRC structure to railway and highway structures, the rational two-level seismic design method and the seismic response behavior are investigated. The effect of the rational design can contribute the reduction of the longitudinal reinforcement of the railway structures. The residual deformation of the UBRC structures after earthquakes becomes small by the combination of the small deformation and the effect of elastic members.

Finally, through the verification and the development of the concrete structure, the effect of the object-oriented analysis system is studied. As the results, the inheritance and the polymorphism mechanism of the object-oriented system are very effective for the addition of new ideas into the existing program code, and it helps us to develop the high performance structures rapidly.

Acknowledgements

This dissertation is synthesis of the author's research work at Structural Dynamics Laboratory of Department of Civil Engineering Systems, Kyoto University. First of all, I would like to express my sincere gratitude to Professor Hirokazu Iemura of Kyoto University for his invaluable supervision of my research, guidance, and encouragement. Professor Iemura introduced me to this field of research and has provided a splendid environment in which to conduct earthquake engineering research.

I wish to particularly express my gratitude to Professor Eiichi Watanabe and Professor Toyoaki Miyagawa of Kyoto University for their constructive suggestions and critical reading of the manuscript.

I am also indebted to Associate Professor Akira Igarashi of Kyoto University and Associate Professor Sumio Sawada of the Disaster Prevention Research Institute, Kyoto University for discussions about the object-oriented approach.

I thank Mr. Riki Honda of the Disaster Prevention Research Institute, Kyoto University, Dr. Gaku Shoji of Tsukuba University, Dr. Hitoshi Morikawa of Tokyo Institute of Technology for their kind help and continuous encouragement.

I would like to express my appreciation to Mr. Shinji Nakanishi of Kyoto University for his excellent support at experiments and laboratory life.

And Especially thanks are due to Mr. Ryoichi Fujita, Mr. Katunao Tanaka, Mr. Shinpei Maehori, Dr. Toshiaki Kato, Mr. Yasushi Ootsuka, Mr. Satoshi Ishida, Mr. Naoki Sogabe, Mr. Masahiro Ukai and Mr. Naoya Nagao and all students and alumni of Structural Dynamics Laboratory who worked with me.

Lately, I thank my father, Koji and my mother, Eiko for their heartful support and understanding. I dedicate this dissertation to my wife, Miyuki, in token of my gratitude for her belief in my abilities and constant support during my years of study.

Table of Contents

List of Figures

List of Tables

List of Photos

Chapter 1

Introduction

1.1 General Remarks

Hyogo-ken Nanbu Earthquake attacked Japan on January 15, 1995. It caused severe damage to civil infrastructures, including the lifeline such as highway and railway transportation systems. Our structural engineers were especially shocked at the severe collapse of the Route 3 of the Hanshin Expressway. To avoid such a terrible collapse again, many researches on the high seismic performance structure have been made.

In general, the behavior of the newly developed high performance structure is complicated compared with conventional structures. Therefore it is indispensable for the development to be supported by not only the experiments but also the numerical analysis. Recently the structural analysis software packages can examine the complicated behavior of structures because of the advance of the knowledge and the technique of the structural analysis field. On the other hand, the addition of functions to a system inevitably results in increased complexity. Namely it is very difficult to understand the internal code of the program. In the development of a new structure, it is necessary to try a new function or a new idea in the program code repeatedly. Therefore for the rapid development, it is important to develop the structural analysis system, which is easy to use, easy to understand the inside and easy to upgrade the function. And for the purpose, the object-oriented technique seems to be suitable.

Combined methodology based on expriments and analysis, the high seismic performance structures are developed to ensure the safty of transportational facilities.

1.2 State of the Arts on Object-Oriented Approach

1.2.1 Programming Languages

FORTRAN[1] is one of the first developed high-level programming languages. Since FORTRAN can describe programs in the form which is similar to mathematical expression, it is widely used in the engineering field. And even in the 21st century, it is still the mainstream programming language in the structural analysis field. Though FORTRAN had no object-oriented concept, such as the encapsulation, the concept of the modularization is adopted in FORTRAN90, and it is possible to express objects in programs. Some researchers try to apply the object-oriented concept using FORTRAN90/95[2,3].

Simula[4], which was developed in 1968, has the concept of class which consists of data and algorithms. Inherited Simula, Smalltalk[5] was developed in 1972. This has the basic concept of an object-oriented programming such as object, class, method and inheritance. In the early object-oriented applications to structural analysis, Smalltalk has been used[6,7].

C++ language[8,9] was developed in 1983. It is the language which expanded C language with classes. Nowadays, there are many object-oriented language (Objective-C[10], Eiffel[11], CLOS[12], Java etc.), but C++ is excellent in portability and calculation efficiency, C++ language becomes the mainstream object-oriented programming language at present.

1.2.2 The Object-Oriented Methodology / Notation

The object-oriented concept has been developed as one of the techniques of the programming. Since the concept is known to be useful not only the programming but also the analysis, the object-oriented methodology, including analysis, design and implementation, has been developed.

The Shlaer/Mellor method[13] is one of the first proposed object-oriented methodology. This methodology uses various documents in the design phase, e.g. communication, access, domain, subsystem models, etc. in addition to the object model. In the beginning of 1990's, many methodologies were proposed (Coad/Yourdon method [14,15], Booch method[16], OMT[17], OOSE method[18], Fusion methods[19], Martin/Odell methods[20], etc.). In 1994, OMT and Booch method were integrated, the work of UML (Unified Modeling Language) started. UML is a new notation method in modeling in the object-oriented methodology. By OMG (Object Management Group), which is the standardization group of the object-oriented technology, UML was approved as an object-oriented modeling language standard. In October 1999, UML 1.3[21–23] is formally approved.

1.2.3 Application to the Structure Analysis Field

Analytical systems being complicated, the management of the systems, i.e. the maintenance and the reuse, becomes very difficult. In order to avoid this software crisis, the importance of abstracting data and algorithm is indicated. In early 1990's, Fenves[6], Miller[24], Baugh and Rehak[25] are among those who emphasized the importance of the abstraction and advocated that the object orientation was useful in software development of the engineering field. The remaining part of this section will be devoted to survey some topics applied the object-oriented technology.

■ Finite Element Method

The object-oriented application began from the linear and static finite element method. In 1990, Forde et al.[26] extracted class Node, Material, Element, etc. from the linear analysis of a plane element, and the system was modeled by the graphical expression[27]. In Japan, Miki et al. also studied the introduction of the object-oriented technology of truss and beam structures in 1991[28,29]. Zimmermann and Pèlerin[7] extracted objects in the finite element method, and coded analytical programs by Smalltalk and C++. They expanded it to dynamic problems, and showed that the theory of the finite element method can be expressed in almost same way in the program code[30].

By the object-oriented technique, it is easy to express structural shapes in the program code. From the beginning of the object-oriented applications, the main interest is to model the static structure of objects in the program as well as our images. As the object-oriented methodology is being established, the dynamic behaviors are also focused. In terms of solving finite element matrices, several methods are proposed. One is to prepare the individual solver object (Forde et al.[26], Zimmermann et al.[7], Pidaparti et al.[31], Pèlerin et al.[32], etc.). It controls all other *Finite Element* objects and *Load* objects, and search the solution. Since a knowledge about solution methods is separated from *Finite Element* objects, this method can construct the simple *Structure* model. Another is a method for burying the solution method in the *Structure* object itself (Mackie[33], Ishida et al.[34,35], etc.). This method makes the main program code simple, because there are only *Finite Element* objects in the code. Recentrly, it is emphasized that each task is separated to the individual object for constructing flexible systems[36–38].

■ Constitutive Law

The material constitutive law makes the main role in the nonlinear problem. Menétrey[39] modeled the J2 plastic material by the object-oriented concept. Foerch et al.[40] carried out the

detailed modeling. They separated a *Material* object into the interface part and the behavior part. According this modeling, it is possible that it completely does not affect the *Finite Element* objects when new material behaviors would be added.

■ Matrix, Tensor

The matrix operation is indispensable for the calculation in the structural analysis and it has been indicated that it is advantageous that the matrix is modeled as an object. Though many routines were being made in the FORTRAN, they needs many arguments in the usage, and they cannot be used in the different situation. Lu et al.[41] made the matrix library in the structural analysis, and the development of the library is used by the Booch method. And the tensor object was also modeled by Jeremić et al.[42]. Using the *Tensor* objects, the mathematical expression can be realized in program code effectively.

■ Computational Algorithm

Recently algorithms of the nonlinear calculation are applied by the object-oriented concept. As the applications, there are the del operator of Tanahashi[43], the linear iteration method of Bruaset et al.[44], the nonlinear calculation by the path-following method of Olsson[45], the Regula Falsi method of Phillips et al.[46], etc.. By these research for algorithms, the range of object-oriented applications is greatly expanded.

■ Applied Object-Oriented Methodology

It is important to use the established object-oriented methodology because software engineers and structural engineers can share the same and correct image about the system. Achieving good communication is the key to developing good systems. The object-oriented methodology has been developing in 1990's, therefore the early applications of the structural engineering used their original notation. Lu[41] and Mackie[47] analyzed problems by the Booch method[16]. In the structural analysis field, the OMT was the most popular methodology. This is because it has the functional model, like the flowchart diagram besides static and dynamic models, and structural engineers were accustomed to the flowchart diagram. Hartmann et al.[48], Turk[49], Friedrich[50], Archer[38], etc. used the OMT, and especially Ishida, Taga et al.[35, 51–55] has taken some important steps in terms of their detailed dynamic and functional models. For the static and linear finite element analysis, they carried out the object-oriented analysis and design first of all, and verified the effectiveness for nonlinear problems and dynamic problems.

1.3 State of the Arts on RC Column with Hollow Section

In order to reduce weight, hollow RC members has been employed for long span girders, but hollow RC columns were not often used by 1970s[56]. One of the first researcher to give much attention to the behavior of RC columns with hollow section was Procter, who carried out tests of the hollow cylindrical and rectangle columns under axial and bending moments[56, 57].

Since the 1980s, in order to investigate the nonlinear behavior, cyclic loading tests were carried out by many researchers. Mokrin et al.[58–60] carried out tests of eight specimens to determine the ultimate moment. The parameters were the axial load and the longitudinal steel ratio. Compared the experimental results with the theoretical results, they indicated that it was reasonable to use Clough's model for the moment-curvature relationship with small axial loads, but for specimens with large axial loads, the pinching effect should be taken into account.

Since the hollow RC piers can reduce the weight, consequently can reduce the seismic inertia force, in order to investigate the seismic performance of hollow RC columns, many cyclic loading tests were carried out[61–73]. Mander, Priestley and Park carried out tests of large scale pier models[61–63]. The specimens had a height of 3.2 m, a 750 mm square cross section with 120 mm thick walls. From the results, the hysteretic performance of the hollow columns demonstrated very good energy dissipation characteristics if they were arranged well transversely. Ikeda et al. carried out cyclic loading tests of circular hollow RC columns with variable wall thickness[64, 65]. They showed that the hollow pier deteriorated rapidly after the maximum state but the pier with thick walls at the bottom had the good performance against the cyclic loading. And it should be noted that they also carried out the pseudo dynamic tests of the hollow RC column[65]. The RC tall pier with natural period of 1.6 second responded small due to the Kobe JMA record. Zahn et al.[66] and Kawashima et al.[67, 68] carried out cyclic loading tests of circular hollow RC columns without confinement on inside face. They indicated that a column with thin walls behaved in a brittle manner because of the low confinement of the walls and the spalling concrete to the void.

After the Hyogo-ken Nanbu Earthquake, it is necessary to arrange the intermediate tie in the large section for increasing the seismic performance. Suda et al. carried out tests of large scale hollow columns and investigated the arrangement of the intermediate tie for the hollow section[69–71]. They showed that designed ductility could be guaranteed by arranging transverse reinforcement according to the design codes[74, 75] revised after the Hyogo-ken Nanbu Earthquake, and structural details of the reinforcement arrangement were proposed based on relationships between the ductility and the arrangement of the transverse reinforcement.

1.4 State of the Arts on High Seismic Performance Concrete Structure

Reinforced concrete was invented in 1850 and the application of prestressing to the concrete was invented in the late of 1800s, and in this one hundred years many researchers tried to improve the performance of concrete structures. Especially after the Hyogo-ken Nanbu Earthquake, the high seismic performance concrete structures, including composite structures, have very actively been studied and developed.

In the restoration operation of the Hyogo-ken Nanbu Earthquake, many RC piers were removed because their residual deformation was large. Then the Seismic Design Specification for Highway Bridges[75] was revised so that not only a strength but also a residual deformation have to be checked for important bridges. To reduce a residual deformation, the prestressed concrete (PC) pier is proposed[76–80]. By controlling the amount of prestressing and the ratio of reinforcement appropriately, the residual deformation can be reduced and as the result, the seismic performance of RC structure can be improved.

To delay a buckling and a breakage of longitudinal reinforcement in a flexural deformation of RC piers, the RC pier with unbonding of reinforcement at the bottom is proposed[81,82]. By the unbonding treatment, the strain of reinforcements in the bottom of piers can be smoothed, and the ultimate deformation becomes large. And the RC pier with a partial unbonding of reinforcements in the footing is also proposed[83]. It can increase the base rotation significantly, and consequently increase the ultimate deformation.

For a tall pier crossing a deep valley, concrete piers with hollow section are usually used, but the shear reinforcement is difficult because of the thin walls. The steel pipe – concrete composite pier is developed for the high seismic resistance in effect of the ductile steel pipes and the spiral high strength strand[84,85]. And also using the steel pipes as the reaction frame, the rapid construction and the reduction of the skilled labor can be provided (Hybrid Slipform Method)[86]. With the similar concept, the hollow RC pier with densely arranged spiral confinement zones is proposed[87]. This structure also can improve not only the confinement but also the construction procedure. From the tests, the ductility is larger than the conventional hollow RC columns.

For the rapid construction, several members are proposed in place of longitudinal reinforcement bars. Only the steel frames are used in the steel framed concrete pier with buried precast forms[88,89]. The combination between the steel frame and the buried form can provides the rational construction work and the improvement of the ductility. The flexible strand is also proposed as longitudinal reinforcement for the construction in the narrow space area[90].

In terms of repairability, the new type of RC pier is proposed[91]. In the structure, the longitudinal bar diameter is reduced in the plastic hinge region so as to control the potential inelastic response range of the steel and the laminated rubber is put into the concrete core section of the plastic hinge in order to assist the vertical load support during returning inclined columns to the original position after an earthquake. The same idea to support the vertical load after an earthquake is also proposed by Sakai et al[92]. They use the steel frame or the steel core as the vertical load supporter.

1.5 Organization of the Thesis

This research aims a fundamental study on the development of an object-oriented structural analysis system and the high seismic performance concrete structures, and their applications.

In Chapter 2, the structural analysis system is analyzed and designed by the object-oriented technique. The system is divided into three subsystem (Structure, Load and ResponseAnalysis), and each subsystem is modeled using the UML notations and implemented in C++ programming language and applied for the specific sample problems. And finally the seismic response analysis is demonstrated as the collaboration of the subsystems.

In Chapter 3, the seismic response characteristics of RC tall piers with hollow section are investigated by the cyclic loading tests and hybrid earthquake loading tests. In addition to the conventional evaluation from the cyclic loading tests, the contribution of the shear deformation on the deformation process is focused. And finally the program for the cyclic loading analysis is developed as the application of the object-oriented analysis system developed in the preceding chapter.

In Chapter 4, the Unbonded Bar Reinforce Concrete (UBRC) structure is developed and proposed as the high seismic performance structure. At first the background and the concept of the structure are described, and then the fundamental characteristics is examined by the cyclic loading tests. And the analytical method for the UBRC structure is developed and modeled as the object in the object-oriented analysis system. Using this object, the parametric studies in terms of bars of the UBRC structure are carried out.

In Chapter 5, the UBRC structure is applied to the railway and the highway bridge structures. In the railway structure, the applicability of UBRC structures for the rational two-level seismic design method is investigated. In the highway structure, the real seismic performance is investigated by the hybrid earthquake loading tests.

Finally in Chapter 6, concluding remarks of the whole chapters of this thesis are summarized in addition to some comments for future investigations.

References

(1) Rosen, S.(ed.): *Programming Systems and Languages*, McGraw Hill, 1967.

(2) Machiels, L. and Deville, M. : Fortran 90: an entry to object-oriented programming for the solution of partial defferential equations, *ACM Transactions on Mathematical Software*, Vol. 23, No. 1, pp. 32 – 49, 1997.

(3) Takeuchi, N. and Sato, K. : Fortran90/95 and Object-Oriented Programming in Finite Element Analysis (in Japanese), *Proc. of Japan Society for Computational Engineering and Science*, Vol. 5, pp. 199 – 202, 2000.

(4) Dahl, O. and Hoare, C.: *Hierarchical program structures. In Structured Programming*, Academic Press, pp. 175 – 220, 1972.

(5) Goldberg, A. and Robson, D.: *Smalltalk-80: The language and its implementation*, Addison-Wesley, 1983.

(6) Fenves, G. L. : Object-oriented programming for engineering software development, *Engineering with Computers*, Vol. 6, pp. 1–15, 1990.

(7) Zimmermann, T., Dubois-Pèlerin, Y. and Bomme, P. : Object-oriented finite element programming : I. Governing principles, *Computer Methods in Applied Mechanics and Engineering*, Vol. 98, pp. 291 – 303, 1992.

(8) Stroustrup, B.: *The C++ Programming language*, Addison-Wesley, 1984.

(9) Stroustrup, B.: *The C++ Programming language, Second Edition*, Addison-Wesley, 1991.

(10) Cox, B.: *Object-oriented programming: An evolutionary approach*, Addison-Wesley, 1986.

(11) Meyer, B.: *Object-oriented software construction*, Prentice Hall International, 1988.

(12) Keene, S.: *Object-oriented programming in Common Lisp: A programmer's guide to CLOS*, Addison-Wesley, 1989.

(13) Shlaer, S. and Mellor, S. J.: *Object-Oriented Systems Analysis : Modeling the World in Data*, Yourdon, 1988.

(14) Coad, P. and Yourdon, E.: *Object-Oriented Analysis*, Yourdon, 1991.

(15) Coad, P. and Yourdon, E.: *Object-Oriented Design*, Yourdon, 1991.

(16) Booch, G.: *Object-Oriented Analysis and Design with Applications, Second Edition*, Addison-Wesley, 1994.

(17) Rumbaugh, J., Blaha, M., Premerlani, W., Eddy, F. and Lorensen, W.: *Object-Oriented Modeling and Design*, Prentice Hall, 1991.

(18) Jacobson, I., Christerson, M., Jonsson, P. and Overgaard, G.: *Object-Oriented Software Engineering : A Use Case Driven Approach*, Addison Wesley, 1992.

(19) Coleman, D., Arnold, P., Bodoff, S., Dollin, C., Gilchrist, H., Hayes, F. and Jeremaes, P.: *Object-oriented development: The Fusion Method*, Prentice Hall, 1994.

(20) Martin, J. and Odell, J.: *Object-oriented analysis and design*, Prentice Hall, 1992.

(21) Booch, G., Rumbaugh, J. and Jacobson, I.: *The Unified Modeling Language User Guide Version 1.3*, Addison-Wesley, 1999.

(22) Rumbaugh, J., Jacobson, I. and Booch, G.: *The Unified Modeling Language Reference Manual*, Addison-Wesley, 1999.

(23) Jacobson, I., Booch, G. and Rumbaugh, J.: *The Unified Software Development Process*, Addison-Wesley, 1999.

(24) Miller, G. : An object-oriented approach to structural analysis and design, *Computer and Structures*, Vol. 40, No. 1, pp. 75–82, 1991.

(25) Baugh Jr., J. W. and Rehak, D. R. : Data abstraction in engieering software development, *Journal of Computing in Civil Engineering, ASCE*, Vol. 6, No. 3, pp. 282 – 301, 1992.

(26) Forde, B. W., Foschi, R. O. and Stiemer, S. F. : Object-oriented finite element analysis, *Computer and Structures*, Vol. 34, No. 1, pp. 355–374, 1990.

(27) Forde, B. W.: Inside Object NAP : technical documentation for Object NAP numerical analysis program., Technical report, Univ. of British Columbia, 1988.

(28) Miki, M., Sugiyama, Y. and Uchida, Y.: Deformation Analysis of Beams by Using Object-Oriented Approach (in Japanese), *Journal of Japan Society of Mechanical Engineering*, Vol. A, Vol.57, No.541, pp. 212 – 217, 1991.

(29) Miki, M., Sugiyama, Y. and Uchida, Y.: An Object-Oriented Approach to Structural Analysis of Truss Structures (in Japanese), *Journal of Japan Society of Mechanical Engineering*, Vol. A, Vol.57, No.541, pp. 218 – 223, 1991.

(30) Dubois-Pèlerin, Y., Zimmermann, T. and Bomme, P. : Object-oriented finite element programming : II. A prototype program in Smalltalk, *Computer Methods in Applied Mechanics and Engineering*, Vol. 98, pp. 361 – 397, 1992.

(31) Pidaparti, R. and Hudli, A. : Dynamic analysis of structures using object-oriented techniques, *Computer and Structures*, Vol. 49, No. 1, pp. 149–156, 1993.

(32) Dubois - Pèlerin, Y. and Pegon, P. : Object-oriented programming in nonlinear finite element analysis, *Computer and Structures*, Vol. 67, pp. 225–241, 1998.

(33) Mackie, R. : Object oriented programming of the finite element method, *International Journal for numerical methods in engineering*, Vol. 35, pp. 425–436, 1992.

(34) Niimi, K., Ishida, E., Fukuwa, N., Nakai, S. and Katukura, H.: Analysis and Design of Finite Element Analyses using Object Modeling Technique (in Japanese), *Proc. of Symposium on Numerical Analytical Methods for Structural Engineering*, Vol. 17, pp. 477 – 482, 1993.

(35) Ishida, E., Niimi, K., Fukuwa, N. and Nakai, S. : An Object Oriented Analysis and Design of Static Linear Finite Element Analysis (in Japanese), *Journal of Structural Engineering, Japan Society of Civil Engineers*, Vol. Vol.40B, pp. 243 – 251, 1994.

(36) Rucki, M. D. and Miller, G. R. : An algorithmic framework for flexible finite element-based structural modeling, *Computer Methods in Applied Mechanics and Engineering*, Vol. 136, pp. 363 – 384, 1996.

(37) Rucki, M. D. and Miller, G. R. : An adaptable finite element modelling kernel, *Computer and Structures*, Vol. 69, pp. 399–409, 1998.

(38) Archer, G., Fenves, G. and Thewalt, C. : A new object-oriented finite element analysis program architecture, *Computer and Structures*, Vol. 70, pp. 63–75, 1999.

(39) Menétrey, P. and Zimmermann, T. : Object-oriented non-linear finite element analysis: Application to J2 plasticity, *Computer and Structures*, Vol. 49, No. 5, pp. 767–777, 1993.

(40) Foerch, R., Besson, J., Cailletaud, G. and Pilvin, P. : Polymorphic constitutive equations in finite element codes, *Computer Methods in Applied Mechanics and Engineering*, Vol. 141, pp. 355 – 372, 1997.

(41) Lu, J., White, D., Chen, W.-F. and Dunsmore, H. : A matrix class library in C++ for structural engineering computing, *Computer and Structures*, Vol. 55, No. 1, pp. 95–111, 1995.

(42) Jeremić, B. and Sture, S. : Tensor objects in finite element programming, *International Journal for numerical methods in engineering*, Vol. 41, pp. 113–126, 1998.

(43) Tanahashi, T. and Nakai, T. : Discrete Del Operator for Object-Oriented FEM (in Japanese), *Journal of Japan Society of Mechanical Engineering*, Vol. B, 62, No. 595, pp. 204 – 212, 1996.

(44) Bruaset, A. M. and Langtangen, H. P. : Object-oriented design of preconditioned iterative methods in Diffpack, *ACM Transactions on Mathematical Software*, Vol. 23, No. 1, pp. 50 – 80, 1997.

(45) Olsson, A. : An object-oriented implementation of structural path-following, *Computer Methods in Applied Mechanics and Engineering*, Vol. 161, pp. 19 – 47, 1998.

(46) Phillips, J., Price, G., Fry, S., Arcziscewski, T., DeMonsabert, S. and Menawat, A. : An object-oriented approach to numerical methods: the Regula Falsi method for solving equations with tight tolerances for environmental applications, *Journal of Hazardous Materials*, Vol. B:63, pp. 145 – 162, 1998.

(47) Mackie, R. : Using objects to handle complexity in finite element software, *Engineering with Computers*, Vol. 13, pp. 99 – 111, 1997.

(48) Hartmann, D., Fischer, A. and Holéwik, P.: Object oriented modeling of structural systems, *International Conference on Computing in Civil and Building Engineering*, Vol. 5th, pp. 78 – 85, 1993.

(49) Turk, Z., Isaković, T. and Fishinger, M. : Object-oriented modeling of design system for RC buildings, *Journal of Computing in Civil Engineering, ASCE*, Vol. 8, No. 4, pp. 436 – 453, 1994.

(50) Friedrich, J. : Object-oriented model and code for the visual examination of subsurface structures under historical buildings, *Computer and Structures*, Vol. 69, pp. 85–94, 1998.

(51) Ishida, E., Fukuwa, N., Niimi, K., Taga, N. and Nakai, S.: Research on Object-Oriented Analysis of Finite Element Analysis (1) (in Japanese), *Proc. of Annual Conference of Architectural Institute of Japan, Tokai Branch*, pp. 165 – 168, 1993.

(52) Ishida, E., Niimi, K., Fukuwa, N., Nakai, S. and Taga, N.: Object-Oriented Programming of Dynamic Finite-Element Analysis using Substructure Method (in Japanese), *Proc. of Symposium on Numerical Analytical Methods for Structural Engineering*, Vol. 17, pp. 471 – 476, 1993.

(53) Ishida, E., Niimi, K., Fukuwa, N., Nakai, S. and Taga, N.: Research on Object-Oriented Analysis of Finite Element Analysis (2) (in Japanese), *Proc. of Annual Conference of Architectural Institute of Japan, Tokai Branch*, pp. 169 – 172, 1993.

(54) Fukuwa, N., Koiso, T., Tanaka, K. and Ishida, E.: Object Oriented Analysis on the Earthquake Response Problem of Soil-Structure System (in Japanese), *Proc. of the 43rd National Congress of Theoretical & Applied Mechanics*, pp. 257 – 260, 1994.

(55) Taga, N.: A Study on the Application of Object-Oriented Approach to Earthquake Engineering, Report of Grant-in-Aid for Scientific Research, Monbusho 05452249, Kyushu University, 1996.

(56) Procter, A. : Hollow concrete columns, *Civil Engineering*, pp. 53–55, 1976.

(57) Procter, A. : Hollow rectangular reinforced concrete columns, *Civil Engineering*, pp. 45–49, 1977.

(58) Mokrin, Z. A. and Rumman, W. S.: Non-linear behavior of reinforced concrete members of hollow circular section subjected to monotonic and cyclic bending, *Proc. of the 7th World Conference on Earthquake Engineering*, Vol. 6, pp. 287–290, 1980.

(59) Mokrin, Z. A. and Rumman, W. S. : Ultimate capacity of reinforced concrete members of hollow circular sections subjected to monotonic and cyclic bending, *ACI Journal*, pp. 653–656, 1985.

(60) Mokrin, Z. A. : Energy evaluation in reinforced concrete hollow circular sections under bneding, *Engineering and Structure*, Vol. 10, pp. 281–286, 1988.

(61) Mander, J., Priestley, M. and Park, R. : Behaviour of ductile hollow reinforced concrete columns, *Bulletin of the New Zealand National Society for Earthquake Engineering*, Vol. 16, No. 4, pp. 273 – 290, 12 1983.

(62) Mander, J.: Experimental behaviour of ductile hollow reinforced concrete columns, *Proc. of the 8th World Conference on Earthquake Engineering*, Vol. 7, pp. 529–536, 1984.

(63) Priestley, M. and Park, R. : Strength and ductility of concrete bridge columns under seismic loading, *ACI Structural Journal*, pp. 61–76, 1987.

(64) Ikeda, S., Yamaguchi, T. and Etani, S. : Restoring Behavior of Concrete Hollow Circular Columns (in Japanese), *Proc. of the Japan Concrete Institute*, pp. 501–504, 1986.

(65) Osada, K., Yamaguchi, T. and Ikeda, S. : Seismic Performance and the Strengthening of Hollow Circular RC Piers Having Reinforcement Cut-off Planes and Variable Wall Thickness (in Japanese), *Journal of Concrete Research and Technology*, Vol. 10, No. 1, pp. 13–24, 1999.

(66) Zahn, F., Park, R. and Priestley, M. : Flexural strength and ductility of circular hollow reinforced concrete columns without confinement on inside face, *ACI Structural Journal*, pp. 156–166, 1990.

(67) Kawashima, K., Unjo, S., Iida, H. and Yamaguchi, M. : Seismic Retrofit of RC Hollow Piers with Cut-Off by Steel Plate Lining Method (in Japanese), *Proc. of 21st Earthquake Engineering Symposium, JSCE*, pp. 621–624, 1991.

(68) Kawashima, K. : Dynamic Strength and Ductility of Hollow Circular Reinforced Concrete Bridge Pier (in Japanese), *Report of Civil Engineering, PWRI*, Vol. 34-10, pp. 34–39, 1992.

(69) Hanada, K., Matsuda, T., Yukawa, Y., Tsukiyama, Y. and Suda, K. : Cyclic Loading Tests of RC Hollow Tall Piers (in Japanese), *Proc. of 51st Annual Conference, JSCE*, pp. 532–533, 1996.

(70) Suda, K., Niiho, H., Masukawa, J. and Murayama, Y. : Buckling Behavior of Re-bars and Role of Special Ties in PC Hollow Piers (in Japanese), *Proc. of the Japan Concrete Institute*, Vol. 18, No. 2, pp. 725–730, 1996.

(71) Yukawa, Y., Ogata, T., Suda, K. and Saita, H. : Seismic Performance of Reinforced Concrete High Pier with Hollow Section (in Japanese), *Journal of JSCE*, Vol. V-42, No. 613, pp. 103–120, 1999.

(72) Inoue, S. and Egawa, N.: Flexural and shear behavior of reinforced concrete hollow beams under reversed cyclic loads, *Proc. of the 11th World Conference on Earthquake Engineering*, Vol. 7, p. No.1359, 1996.

(73) Inoue, S., Iemura, H. and Tanaka, K. : Shear Behavior of RC Hollow Members (in Japanese), *Proc. of the Japan Concrete Institute*, Vol. 18, No. 2, pp. 677–682, 1996.

(74) Japan Society of Civel Engineers: *Standard Specification for Design and Construction of Concrete Structures (in Japanese)*, Maruzen Ltd., 1996.

(75) Japan Road Association: *Seismic Design Specification for Highway Bridges (in Japanese)*, Maruzen Ltd., 1996.

(76) Ikeda, S. : Seismic Behavior of Reinforced Concrete Columns and Improvement by Vertical Prestressing, *Proc. of the 13th FIP Congress on Challenges for Concrete in the Next Millennium*, Vol. 2, pp. 879–884, 1998.

(77) Ikeda, S., Mori, T. and Yoshioka, T. : Research on the Seismic Performance of Prestressed Concrete Piers (in Japanese), *Prestressed Concrete*, Vol. 40, No. 5, pp. 40–47, 1998.

(78) Inada, H., Mutsuyoshi, H. and Zatar, W. : Seismic Caharacteristics of Prestressed RC Piers (in Japanese), *Proc. of the Japan Concrete Institute*, Vol. 20, No. 3, pp. 739–744, 1998.

(79) Zatar, W., Mutsuyoshi, H. and Inada, H. : Dynamic Response Behaviro of Prestressed Concrete Piers under Severe Earthquake, *Proc. of the Japan Concrete Institute*, Vol. 20, No. 3, pp. 1003–1008, 1998.

(80) Mutsuyoshi, H., Zatar, W. and Maki, T. : Seismic Performance of Reinforced Concrete Piers by Prestressing (in Japanese), *Journal of JSCE*, Vol. V-50, No. 669, pp. 27–38, 2001.

(81) Hosoiri, K., Kawashima, K. and Shoji, G. : Experimental Study on Cylic Deformation Characteristics of RC piers with Unbonded Zone (in Japanese), *Proc. of the 25th JSCE Earthquake Engineering Symposium*, pp. 717–720, 1999.

(82) Hosoiri, K., Kawashima, K., Shoji, G. and Sakai, J.: Seismic Performance of Reinforced Concrete Piers with Unbonded Zone (in Japanese), *Proc. of the 4th Symposium on Ductility Design Method for Bridges*, pp. 447–454, 2000.

(83) Hoshikuma, J., Unjo, S. and Nagaya, K.: Experimental Study on Improvement of Seismic Performance of RC Piers (in Japanese), *Proc. of the 1st Symposium on the Enhancement of Earthquake Performance of Infrastructures Based on Investigation into Fracturing Process*, pp. 135–140, 3 2000. Tokyo.

(84) Watanabe, N., Imaizumi, Y., Wakama, H. and Oouchi, H. : Ductile Tests for Steel Pipe – Concrete Composite Structural Piers (in Japanese), *Proc. of the Japan Concrete Institute*, Vol. 19, No. 2, pp. 939–944, 1997.

(85) Iemura, H., Kato, T., Takahashi, Y. and Maehori, S.: Experimental Study on Seismic Performance of Steel Pipe – Concrete Composite Piers (in Japanese), *Proc. of 10th Japan Earthquake Engineering Symposium*, pp. 2099–2104, 1998.

(86) Kato, T. and Takahashi, Y.: Earthquake Design and Construction of Tall Composite Bridge Piers, *Proc. of 12th World Conference on Earthquake Engineering*, p. No.899, 2000.

(87) Kenmotsu, Y. and Kawashima, K. : Seismic Performance of Hollow Reinforced Concrete Columns with Densely Confined Zones (in Japanese), *Journal of JSCE*, Vol. I-56, No. 682, pp. 57–69, 2001.

(88) Hara, N., Ito, H., Obara, T. and Kono, I. : Experimental Study on Seismic Design for the Steel Frame Concrete Composite Structural Piers (in Japanese), *Proc. of the Japan Concrete Institute*, Vol. 21, No. 3, pp. 1015–1020, 1999.

(89) Ito, H., Hara, N., Obara, T. and Kono, I. : Experimental Study on Failure Characteristics under Earthquakes of the Steel Frame Concrete Composite Structural Piers (in Japanese), *Proc. of the Japan Concrete Institute*, Vol. 21, No. 3, pp. 1033–1038, 1999.

(90) Tsukishima, D., Nozawa, S., Imai, M. and Ishibashi, T. : Experimental Study on Failure Behavior of Concrete Member Reinforced by Strands (in Japanese), *Journal of Concrete Research and Technology*, Vol. 11, No. 1, pp. 95–103, 2000.

(91) Unjo, S., Hoshikuma, J., Nagaya, K. and Shioiri, R.: Experimental Study on the Improvement of Repairability of RC Piers with Flexural Failure (in Japanese), *Proc. of the 2nd Symposium on the Enhancement of Earthquake Performance of Infrastructures Based on Investigation into Fracturing Process*, pp. 183–188, 3 2001. Tokyo.

(92) Sakai, J., Matsui, C., Minami, K. and Hikaraka, Y. : Experimental Study on the Inelastic Behavior of RC Column Members with Steel Frame Core (in Japanese), *Proc. of the Japan Concrete Institute*, Vol. 21, No. 3, pp. 1009–1014, 1999.

Chapter 2

Development of Object-Oriented Structural Analysis System

2.1 General Remarks

A knowledge of the structural analysis field on the civil engineering has deepened more and more, and nowadays, the numerical analysis becomes an indispensable tool in all fields such as research, education, design, and construction. Especially, the computational mechanics is recognized as the third techniques to solve problems, following the analytical and experimental technique. Supported for remarkable advance and popularization of computers, the large-scale softwares are developed in the structural engineering field and would be able to analyze the complicated behavior of structures.

In the informatics field, it has widely been recognized that the object-oriented technique is effective to handle large-scale and complicated softwares. In the process of the software development, it is necessary to convert the real world phenomenon into the abstract algorithm in the program. The conventional programming methodology can only handle the procedural behavior, and the developer will be forced the leap of the idea in the early stage of the development process. On the other hand, in the development by the object-oriented methodology, the software consists of objects, which we can recognize in the real world. And the system is made to operate by the message passing between objects. Since the development process from the analysis of problem to the implementation can be promoted under the consistent concept, the object-oriented system will be comprehensible than the conventional one. And in order to enable the seamless development process, the new concepts of encapsulation and abstraction, inheritance, polymorphism, etc. are adopted in the object-oriented methodology. As the result, it would be possible not only to develop the system seamlessly but also to manage the system easily, e.g. the maintenance and the reuse of objects. Therefore, many

present new projects would have been designed under the object-oriented concept.

In the structural analysis field, the object-oriented methodology is introduced in the beginning in 1990's, and has been applied to the finite element method etc. Though, in this about 10 years, many researchers have advocated the effectiveness of the object-oriented approach, it is not used generally yet in this field. One of the reason is that programs and libraries of past structural analysis were coded in FORTRAN, and people are satisfied with system development by utilizing the enormous results. And even in the development process by FORTRAN, it has been useful and high reusability by the subroutine concept in the structuralization methodology. Since the object-oriented methodology is the advance of the structuralization one, it is considered that it will be also widely accepted in the structural analysis field. By advancing the analysis and development on the structural analysis system by the object-oriented methodology, the new structural analysis system in next generation would be proposed, and can support the flexible development of new structures.

This chapter is described on the basis on the works by Takahashi et al.[1-4].

2.2 Analysis of Structural Analysis System

In this section, the structural analysis system is analyzed in the object-oriented technique. To begin with, the conceptual domain model is made. The analysis of the system is carried out from the domain description, and finally the analysis system with three subsystems is proposed.

In this study, UML 1.3[5,6] is used in the development process. Notations of UML 1.3 were described in the **Appendix A**.

2.2.1 Domain Description

To begin with, we should describe the problem domain. In the description, it is important to clear what it does, and to indicate the direction of the detailed analysis in the next stage. Problems in this study are as follows[2].

> A structural analysis system for two dimensional static / dynamic and linear / nonlinear problems is developed. The system should allow the explicit representation of structures, loads and other entries, and the structural modeling approaches with various principles, including the finite element method, the fiber modeling, the spring model, as well as the mixed formulation. The seismic force as well as the static loads can be used in the analysis system.

2.2.2 Use Cases

Identification of Actors

An actor is a role that a user plays with respect to the system. Although a user, an other software, a hardware, etc. can be a actor, in this analysis system, only a *User* is identified as an actor because executing the system and setting and getting data are the role of the *User*.

Identification of Use Cases

A use case is a set of sequences of actions that actors require to the system. Several use cases in this system are as follows:

- The response analysis is carried out, formulating the equation of motion and solving it.
- The *User* sets the structural data, including the shape and the modeling method.
- The *User* sets the load data.
- The analytical result is informed to the *User*.
- The *User* sets the solution method of the equation.
- Inertia load is calculated by the earthquake and structural data.

2.2.3 Modeling of Conceptual Domain Model

In general, the structural analysis system is a large-scale and complicated. If it can be divided into small subsystems, the development and the maintenance become easy.

Some candidates of the subsystem appeared in the use cases. They are "Structure", "Load" and "Response Analysis". And as a relationship between these subsystems, we can recognize "A response analysis is carried out based on the data of structures and loads", "The Earthquake data converts to the load (inertia load) using the information of the structure". **Figure 2.1** shows the subsystems of the conceptual structural analysis system. The definition of these subsystems is as follows:

- Structure subsystem

  This subsystem contains the structural data and informs them to other objects. It calculates and updates the characteristic matrices according to the deformation history.

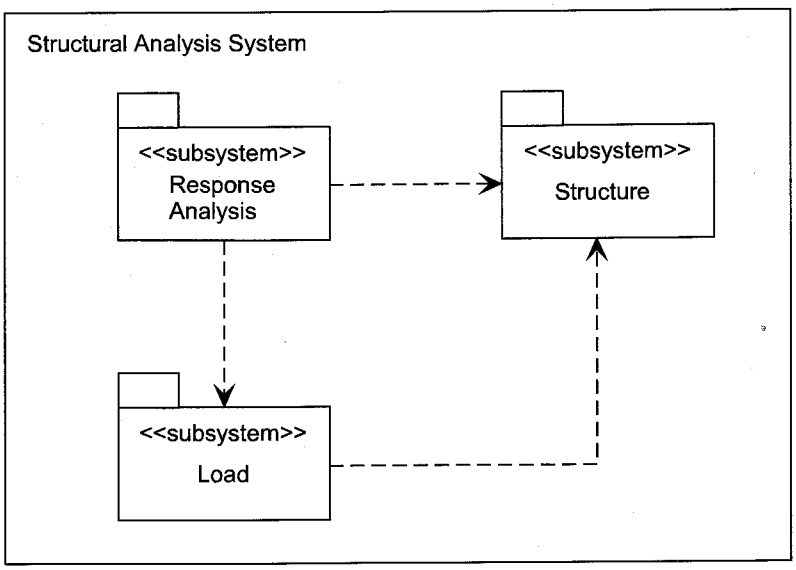

Figure 2.1: Subsystems of Structural Analysis System

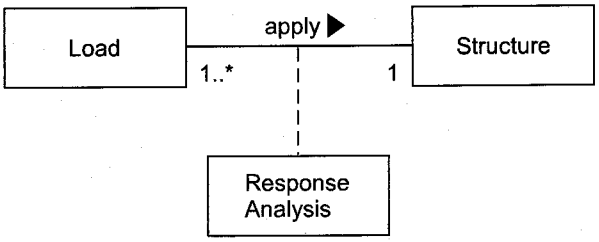

Figure 2.2: Class Diagram of Structural Analysis System

- Load subsystem

  This subsystem shows a load, which is applied to structures. Not only a static load (force) but also an earthquake (acceleration) are considered to be a kind of load.

- Response Analysis subsystem

  This subsystem formulates the equation using the data of structures and loads, and solves it.

The relationship between these subsystems is shown in **Figure 2.2**. The *Structure* itself is only a static object. When the *Loads* (external force) are applied to the *Structure*, the *Structure* is deformed. It is the *Response Analysis* to trace this deformation. **Figure 2.2** shows that the structural analysis system has been modeled in the form that there is the *Response Analysis* as a relation to the association that the *Loads* are applied to the *Structure*.

2.3 Response Analysis Subsystem

The role of the *Response Analysis* in this system is to formulate the equation and to solve it. Namely, the equation is a kernel of the *Response Analysis*. In this study, the equation is modeled as a package, so that it can be used in other systems because the equation is not a unique concept of this subsystem.

2.3.1 Background of Equation of Motion

State of the Arts on Solution Method of Equation of Motion

Many articles have been devoted to the study of solution method of an equation of motion. It is important to know the features of each solution method and to use the adequate method for the objectives.

Newmark et al.[7] proposed the Newmark β method that is the most widely used at present. By the change of β, it is possible to describe various kind of acceleration methods such as the linear and the average acceleration method. Bathe and Wilson[8] strengthened the linear acceleration method and proposed the Wilson θ method that is the implicit integration. The Wilson θ method is unconditionally stable when $\theta \geq 1.37$. Bathe et al.[9, 10] applied various solution method to the finite element analysis, and examined the characteristics. Hilber et al.[11, 12] indicated that the Newmark β method is unconditionally stable when $\beta \geq (\gamma+1/2)^2/4$ and $\gamma > 1/2$, but it has numerical attenuation which depends on the low order mode. They proposed the Hilber α method that is generalized the Newmark β method with new parameter α. Nakashima[13] investigated the stability of the Operator Splitting method, and showed that the method is adequate as an integral scheme for a substructure pseudo dynamic test method. Sun et al.[14] proposed the explicit solution method that is based on the implicit Wilson θ method, considering the correction of the solution. Sakai et al.[15] proposed the explicit solution method that is based on the implicit Newmark β method using the central difference calculus for the increment of nonlinear force vector $\mathbf{Q}$.

Uniform Expression of Equation of Motion

According to **Appendix B**, it is found that linear/nonlinear and static/dynamic equation can be described uniformly as follows.

$$\hat{\mathbf{K}}_{n+1}^{(k-1)} \Delta \mathbf{d}^{(k)} = \hat{\mathbf{R}}_{n+1}^{(k-1)} \tag{2.1}$$

where,

$$\hat{\mathbf{K}}_{n+1}^{(k-1)} = \hat{\mathbf{K}}_{dyn} + \mathbf{K}_{n+1}^{(k-1)} \tag{2.2}$$

$$\hat{\mathbf{R}}_{n+1}^{(k-1)} = \hat{\mathbf{R}}_{dyn} - \mathbf{F}_{n+1}^{(k-1)} \tag{2.3}$$

where $\mathbf{K}_{n+1}^{(k-1)}$ is a stiffness matrix at time t_{n+1} and $(k-1)$th iteration, $\mathbf{F}_{n+1}^{(k-1)}$ is a vector of nodal point forces, $\Delta\mathbf{d}^{(k)}$ is the displacement increment at k-th iteration. And in case of static problems, $\hat{\mathbf{K}}_{dyn}$ is zero and $\hat{\mathbf{R}}_{dyn}$ is just a load vector, and in case of dynamic problems, $\hat{\mathbf{K}}_{dyn}$ and $\hat{\mathbf{R}}_{dyn}$ are formulated by the adopted method. The above equations are expressed in the nonlinear form, but when $k = 1$, these equations correspond to a linear problem. The basic equation is Equation (2.1), and $\mathbf{d}_{n+1}$, as the final solution at t_{n+1}, can be obtained by adding $\Delta\mathbf{d}^{(k)}$.

2.3.2 Analysis of Equation Package

Use Cases

The demand for the *Equation* is "to solve itself". Other demands are to inform the solution to other objects, to set characteristic matrices and so on. Since in nonlinear problems characteristics of an objective model would be changing every moment, the characteristic matrices are also changing. Therefore it is necessary for the *Equation* to know the change of the characteristics of the objective model. In the structural analysis system, this objective model is corresponding to the *Structure* subsystem, but any object can be qualified as long as it has a knowledge of nonlinear handling. Therefore the object is modeled as the *Model* object, which is an interface to the *Structure*. By this modeling, the *Equation* can be used in other analytical field.

And whereas the *Load* subsystem has the time history of load, the *Equation* concerns to get the solution at only one time step. Therefore the *Load* has only the relationship to the use case "set a load vector ($\mathbf{R}_{n+1}$)" of the *Equation*.

According to the above analysis, the use case diagram of the *Equation* is shown in **Figure 2.3**. From this diagram, it is found that only the *Equation* object is visible from the *User* and the complicated nonlinear calculation kernel (*Structure*) is invisible, by which this package becomes rich in usability and maintainability.

Separation of Solution Algorithms

For the operation *solve*, which is the main objective of the *Equation* package, there are many algorithms. In order to model this operation, the *Strategy* pattern[16] is used to encapsulate algorithm itself and to be exchangeable. Therefore the algorithms of *solve* are extracted and separated as a *SolutionMethod* object. Since the *SolutionMethod* uses nonlinear characteristic matrices, it is modeled to have a relationship to the *Model*.

Figure 2.4 shows the conceptual class diagram of the *Equation* package.

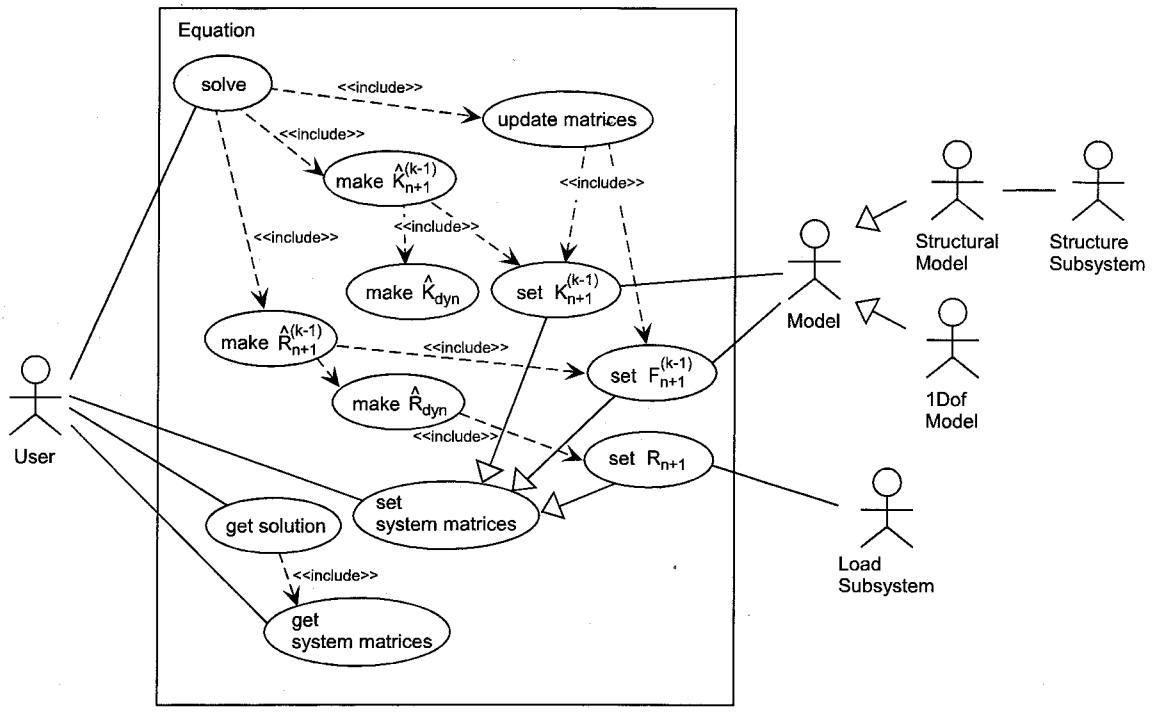

Figure 2.3: Use Case Diagram of Equation Package

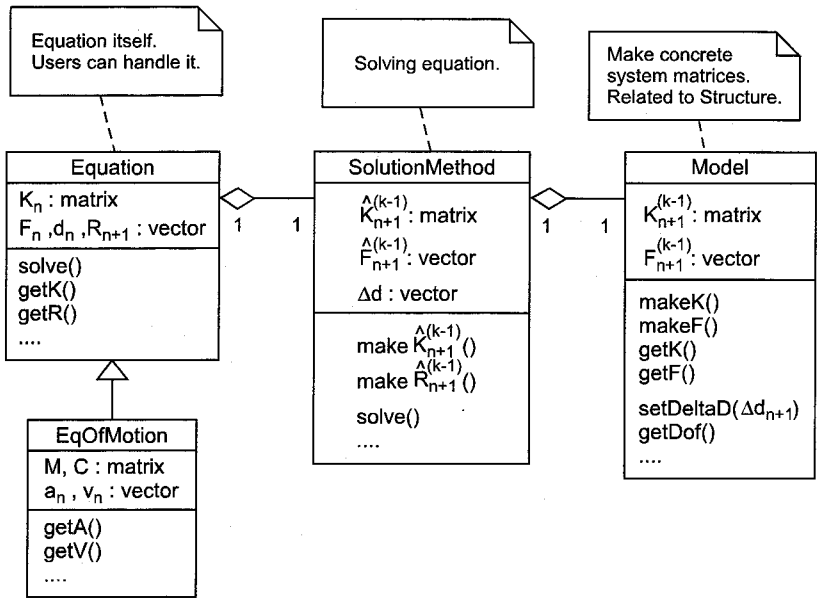

Figure 2.4: Class Diagram of Equation Package

The *Equation* object is an equilibrium equation. The user can handle it directly. It has the operation which solves itself, but actual operation is transferred to the *SolutionMethod* object. And the *EqOfMotion* object is an equation of motion and is modeled to inherit the *Equation*. The *SolutionMethod* calculates $\hat{\mathbf{K}}_{n+1}^{(k-1)}, \hat{\mathbf{R}}_{n+1}^{(k-1)}$ communicating the *Model* object, and searches the solution of the *Equation*.

Modeling Behavior and Refining Class Diagram

In order to get the solution at time t_{n+1}, it is necessary to refer to data in the iterative process. Therefore in order to decide where these data should be stored and to examine the interaction of objects, the sequence diagrams on the operation *solve* of the equilibrium equation and the equation of motion are shown in **Figure 2.5** and **Figure 2.6** respectively.

From **Figure 2.5**, it is found that the *Equation* stores data at time t_n, except for $\mathbf{R}_{n+1}$, until it has been solved, and the *SolutionMethod* has data changing in the iterative process. Especially the stiffness matrix and the nodal point force vector are stored in the *Model*.

Since characteristic matrices required in static and dynamic problems are different (corresponding to $\hat{\mathbf{K}}_{dyn}$, $\hat{\mathbf{R}}_{dyn}$), the *DynamicType* which inherits the *SolutionMethod* is modeled to store and calculate them. (To be precise, the *Static/DynamicSolutionMethod* inherits the *DynamicType* further, and they handle the difference). The algorithm which calculates these matrices has also separated using the *Strategy* pattern. On the other hand, the operation on the linearity and the nonlinearity is stored in the *IterationType*, and it carries out the actual solution operation in charge. The *IterationType* calculates $\Delta\mathbf{d}^{(k)}$, accumulates it in $\Delta\mathbf{d}_{n+1}$ and informs it to the other objects.

Based on the above analysis, the detailed class diagram is refined and shown in **Figure 2.7**. Since the *IterationType* and the *DynamicType* control the operation *solve* actually, a stereotype <<control>> is placed in the generalized class *SolutionMethod* which is a parent of the *IterationType* and the *DynamicType*. And in the *IterationType*, the *SolutionMethod* and the *Model*, the stereotype <<interface>> is placed because these classes specify a collection of operations that are used to specify a service of a class. The stereotype <<boundary>> is also placed in the *Equation* object, because the *Equation* is located in the boundary between the *User* actor and the *Equation* subsystem, and has the operations of input/output.

Here, meanings of the classes of **Figure 2.7** are described.

- *Equation*

  An equilibrium equation which consists of a stiffness matrix, a displacement vector, a load vector and a nodal point force vector. The user can handle it directly. It has the operation which solves itself at time t_{n+1}, and the actual operation is delegated to the

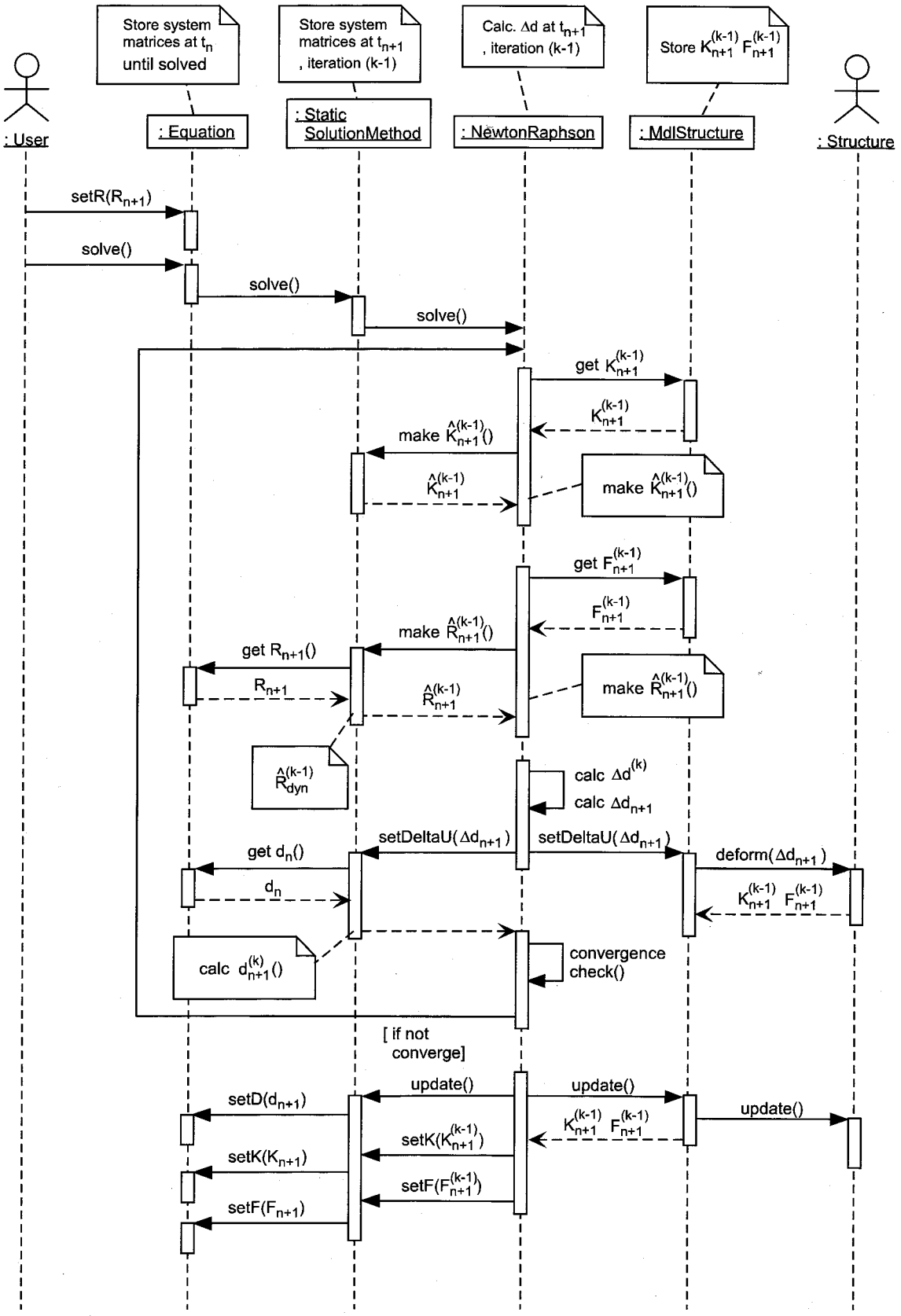

Figure 2.5: Sequence Diagram of Equation

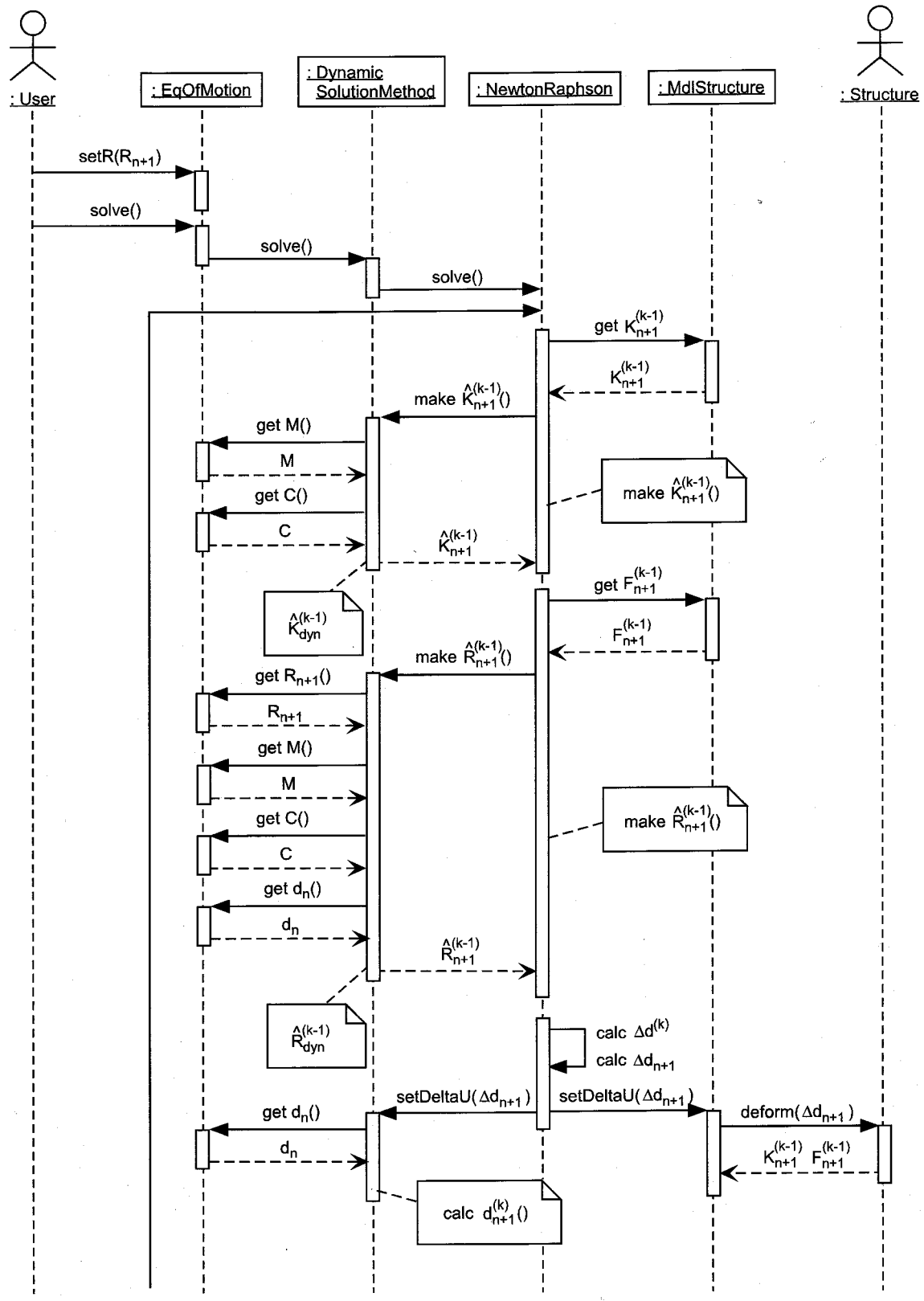

Figure 2.6: Sequence Diagram of EqOfMotion

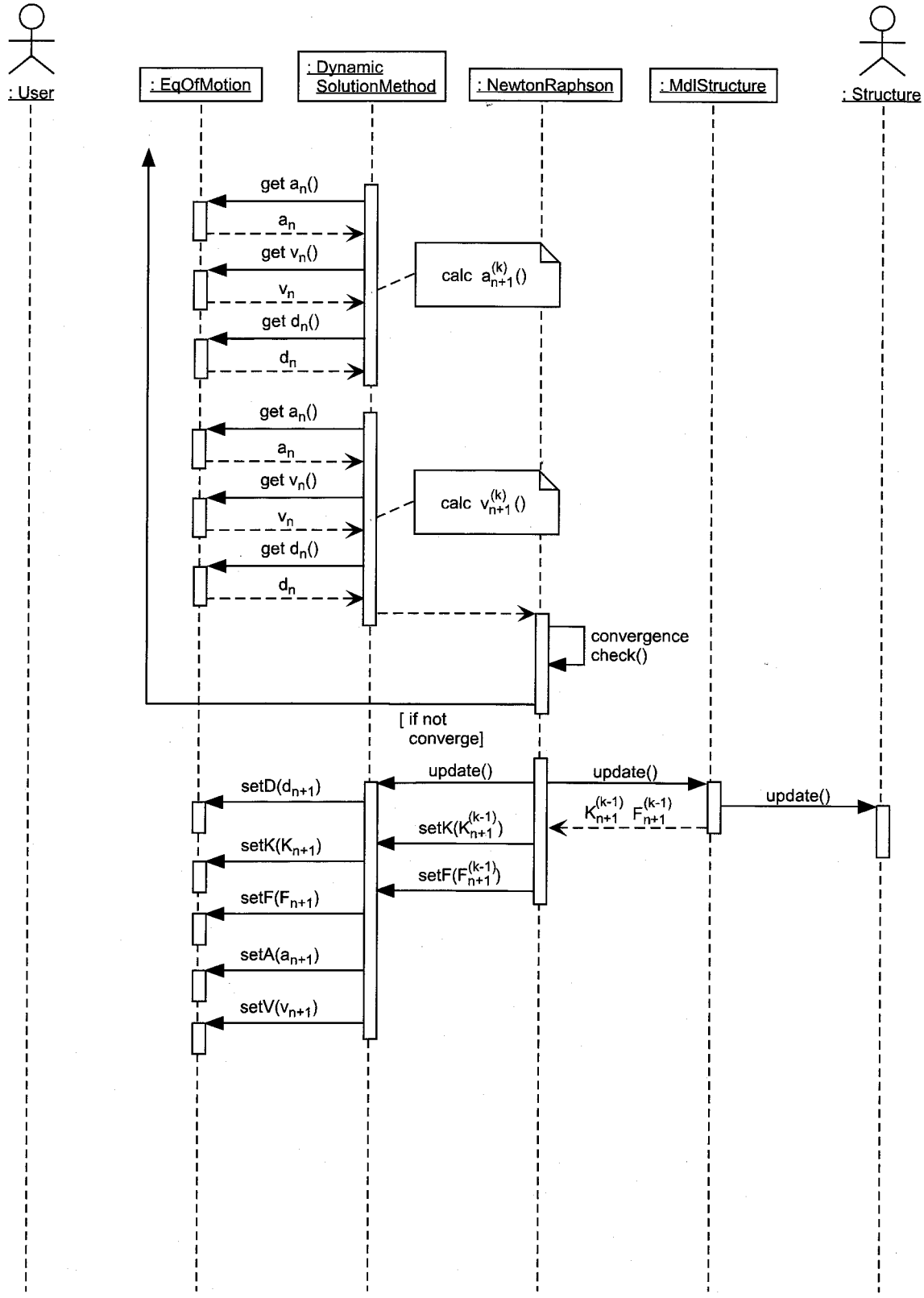

Figure 2.6: Sequence Diagram of EqOfMotion(cont'd.)

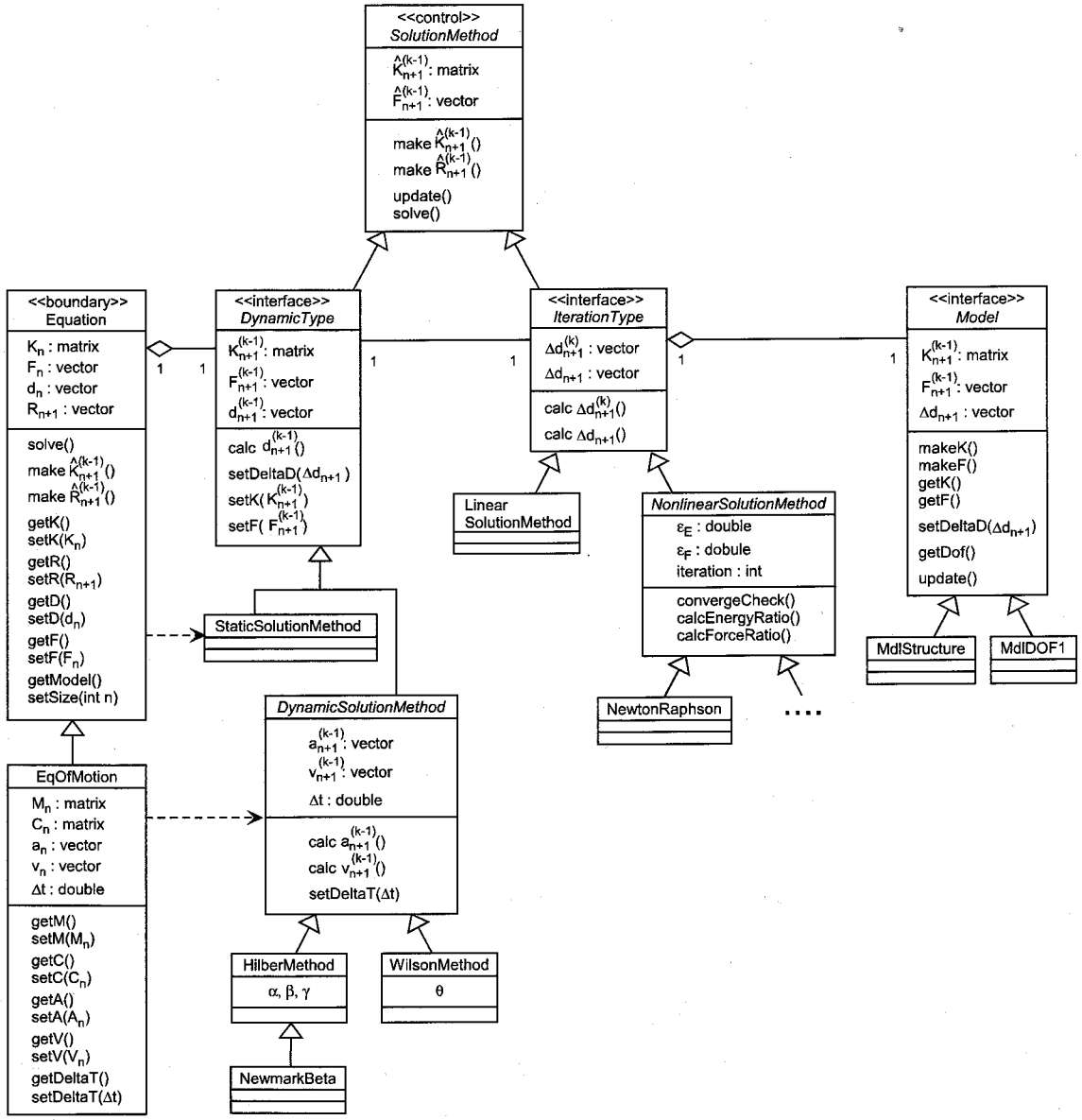

Figure 2.7: Refined Class Diagram of Equation Package

SolutionMethod, to be precise the *StaticSolutionMethod*. Until the equation is solved, the *Equation* stores these characteristic matrices at time t_n except for the load vector $\mathbf{R}_{n+1}$ at time t_{n+1}, and after it has been solved, these matrices are updated to data in time t_{n+1}.

- *EqOfMotion*

  An equation of motion which consists of a mass matrix, a damping matrix, an acceleration vector, a velocity vector in addition to the *Equation*. It has also a calculation time step Δt. The actual solution operation is delegated to the *DynamicSolutionMethod*.

- *SolutionMethod*

  An abstract class which controls the calculation. It has data and basic operations for making $\hat{\mathbf{K}}_{n+1}^{(k-1)}, \hat{\mathbf{R}}_{n+1}^{(k-1)}$. And, it has the *update* method for reporting to other objects the convergence of the calculation.

- *Model*

  An abstract class which has a relationship to a structural object with making algorithm of $\mathbf{K}_{n+1}^{(k-1)}, \mathbf{R}_{n+1}^{(k-1)}$. When the deformation since time t_n (the displacement increment $\Delta\mathbf{d}$) is received, it transfers the data to a structural object and gets the characteristic matrices.

- *IterationType*

  An abstract class which encapsulates a solution algorithm. It inherits the *SolutionMethod*. It defines a search method of getting $\Delta\mathbf{d}^{(k-1)}$ at each iterative calculation step, and reports it to the *Model*. And it also defines making operations of $\hat{\mathbf{K}}_{n+1}^{(k-1)}, \hat{\mathbf{R}}_{n+1}^{(k-1)}$.

- *DynamicType*

  An abstract class which has operations making prototypes of $\hat{\mathbf{K}}_{n+1}^{(k-1)}, \hat{\mathbf{R}}_{n+1}^{(k-1)}$. Since $\hat{\mathbf{K}}_{n+1}^{(k-1)}, \hat{\mathbf{R}}_{n+1}^{(k-1)}$ in a static and dynamic problem are different, this object handles the difference. It inherits the *SolutionMethod*. It defines the basic operation of making the part of $\hat{\mathbf{K}}_{n+1}^{(k-1)}, \hat{\mathbf{R}}_{n+1}^{(k-1)}$, which is used in *solve()* of the *IterationType*. The *Equation* requests the operation *solve* of this object, and it delegated to the *IterationType*. It stores characteristic matrices in the iterative process, such as $\mathbf{d}_{n+1}^{(k-1)}$.

- *LinearSolutionMethod*

  A class which defines a linear solution algorithm. It inherits the *IterationType*.

- *NonlinearSolutionMethod*

An abstract class which defines a nonlinear solution algorithm with an iterative calculation. It inherits the *IterationType* adding attributes and operations for checking the convergence.

- *StaticSolutionMethod*

  A class which defines operations making prototypes of $\hat{\mathbf{K}}_{n+1}^{(k-1)}, \hat{\mathbf{R}}_{n+1}^{(k-1)}$ in a static problem. It inherits the *DynamicType*. But since the static problem part of $\hat{\mathbf{K}}_{n+1}^{(k-1)}$ is made by the *IterationType*, this object does nothing to make $\hat{\mathbf{K}}_{n+1}^{(k-1)}$.

- *DynamicSolutionMethod*

  A abstract class which defines operations making prototypes of $\hat{\mathbf{K}}_{n+1}^{(k-1)}, \hat{\mathbf{R}}_{n+1}^{(k-1)}$ in a dynamic problem. It inherits the *DynamicType*. It also has operations for calculating an acceleration $\mathbf{a}_{n+1}^{(k)}$ and a velocity $\mathbf{v}_{n+1}^{(k)}$.

- *NewtonRaphson*

  A class which defines the nonlinear algorithm by the Newton–Raphson method. It inherits the *NonlinearSolutionMethod*.

- *HilberMethod*

  A class which defines the algorithm for calculating $\hat{\mathbf{K}}_{n+1}^{(k-1)}, \hat{\mathbf{R}}_{n+1}^{(k-1)}$ based on the Hilber α method. It inherits the *DynamicSolutionMethod*.

- *NewmarkMethod*

  A class which defines the algorithm for calculating $\hat{\mathbf{K}}_{n+1}^{(k-1)}, \hat{\mathbf{R}}_{n+1}^{(k-1)}$ based on the Newmark β method. Since the Newmark β method is the case that α is 0.0 in Hilber α method, it inherits the *HilberMethod*.

- *WilsonMethod*

  A class which defines the algorithm for calculating $\hat{\mathbf{K}}_{n+1}^{(k-1)}, \hat{\mathbf{R}}_{n+1}^{(k-1)}$ based on the Wilson θ method. It inherits the *DynamicSolutionMethod*.

- *MdlStructure*

  An interface class between this *Equation* package and the *Structure* subsystem. It can refer to the *Structure* in making characteristic matrices.

- *MdlDof1*

  An object which defines the algorithm for making characteristic matrices of a single degree of freedom model. The nonlinearity operation is used the other object like the

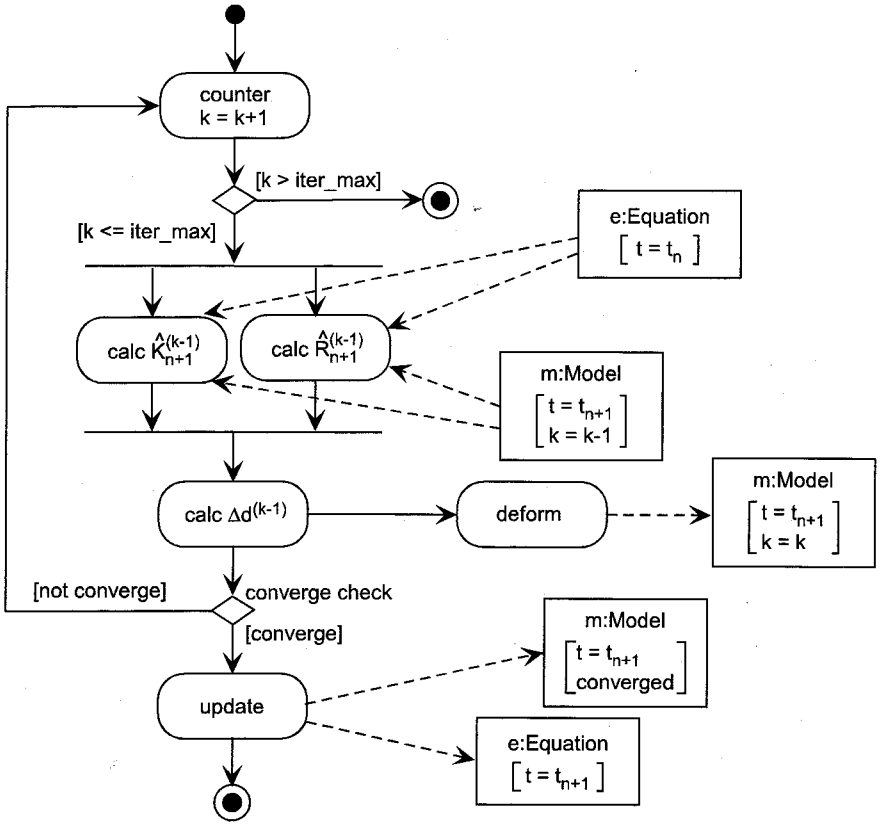

Figure 2.8: Activity Diagram of SolutionMethod

hysteresis object. It doesn't have the nonlinear operation, so it use the object like the *Hysteresis* object in the making process.

The activity diagram can show the activities in the form of the flow chart. Focusing on the dynamic behavior, the algorithm of *solve* of the *SolutionMethod* is shown in **Figure 2.8**. From this figure with object flows, it is found how each activity would affect the state of objects. Though in the solution algorithm, various data are used and generated, the *Equation* package distributes each data to corresponding objects. Therefore the complicated nonlinear solution algorithm of the *Equation* can be expressed in this simple activity diagram.

The dynamic view of the operation *solve* is shown in the statechart diagram (**Figure 2.9**). The upper part shows the operation in a nonlinear problem, and the lower part shows that in a linear problem. The trigger of a solution process is a message *solve* from the *User* actor. When the message *solve* is received, the state of the *Equation* change to *solving*. While in the state, the *Equation* also send the message *solve* to the *SolutionMethod* and the actual solution process is carried out until the solution is converged. And when the *SolutionMethod* send the message *converged* to the *Equation*, the state of the *Equation* changes to the final state *solved*. In spite of the type of a problem, the message of the solution process is the same. And compared with the upper and the lower part in **Figure 2.9**, it is found that we can cope

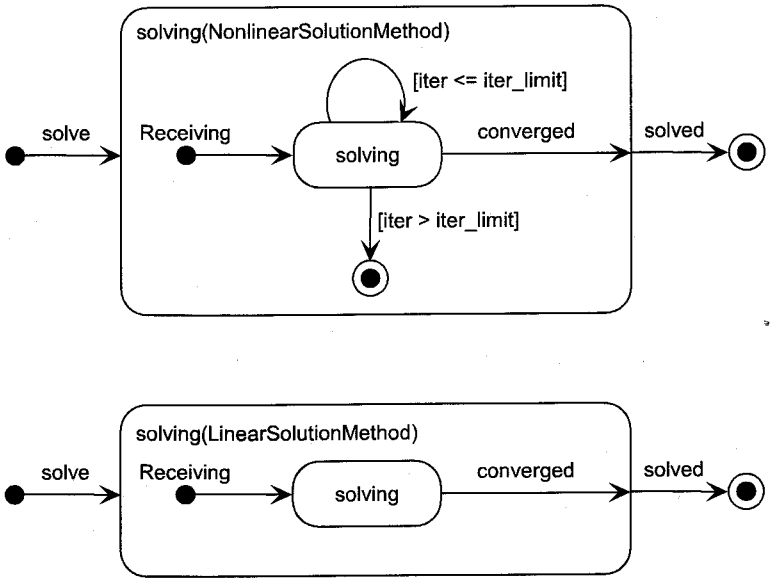

Figure 2.9: Statechart Diagram of Equation Package

with any problem only by exchanging the appropriate *IterationType*. This modeling can be realize by using the *Strategy* pattern, and can make this *Equation* robust against adding a new solution method.

2.3.3 Implementation

Equation Class Library

The *Equation* package that analyzed and designed in this section is implemented in C++ language.

C++ Header File The definitions of classes of the *Equation* package in C++ are shown in **Figure 2.10**. In the code, the line number is denoted for the explanation. In the code, the keyword "`: public Equation`" (line 22) means that this class is the inheritance of the *Equation* class and the keyword "`=0`" placed behind the method (e.g. line 40) means an abstract method. Since abstract methods are realized by a concrete class which inherits the abstract class, the abstract class defines the prototype characteristics which a child class should have. As compared this code with the class diagram (**Figure 2.7**), it is found that the code can be implemented in almost the same expression of the analytical results.

Method solve Here, the implementation of method *solve* of the *Equation* is explained. The program code of the method is shown in **Figure 2.11**. The *Linear/NonlinearSolutionMethod* (line 10 and 19) are the classes which inherit the *IterationType*, and they have the concrete operation of the linear/nonlinear solution method respectively.

```
 1: class Equation {                                    // definition of class
 2: public:
 3:  Equation(Model*, IterationType*, DynamicType*); // constructor
 4:  virtual int setSize(int size);                     // set DOF size
 5:  DynamicType* setSolutionMethod(DynamicType*);
 6:  Model* getModel();
 7:  DynamicType* getSolutionMethod();
 8:  int getSize();                                     // get DOF size
 9:  Gen_matrix calcK();
10:  Gen_matrix setK(Gen_matrix); inline Gen_matrix getK();
11:  Col_vector setR(Col_vector); inline Col_vector getR();
12:  Col_vector calcF();
13:  Col_vector setF(Col_vector); inline Col_vector getF();
14:  Col_vector setD(Col_vector); inline Col_vector getD();
15:  void solve();                                      // solve equation
16: protected:
17:  Gen_matrix Kmatrix;
18:  Col_vector Rvector, Fvector, Dvector;
19:  DynamicType *sMethod;                              // have DynamicType
20: };
21:
22: class EqOfMotion : public Equation {               // definition of class
                                                       // inherit class Equation
23: public:
24:  EqOfMotion(Model* n, IterationType* s, DynamicType* d);
25:  virtual int setSize(int size);
26:  double setDeltaT(double dt);                      // set time interval
27:  double getDeltaT();                               // get time interval
28:  Gen_matrix setM(Gen_matrix); inline Gen_matrix getM();
29:  Gen_matrix setC(Gen_matrix); inline Gen_matrix getC();
30:  Col_vector setA(Col_vector); inline Col_vector getA();
31:  Col_vector setV(Col_vector); inline Col_vector getV();
32: protected:
33:  double deltaT;                                    // time interval data
34:  Gen_matrix Mmatrix, Cmatrix;
35:  Col_vector Avector, Vvector;
36: };
37:
38: class SolutionMethod {   // definition of class
39: public:
40:  virtual void storePreData(Col_vector) = 0;
41:  virtual void storeDataAtT(Col_vector) = 0;
42:  virtual int setSize(int size);
43:  virtual void setUp();
44:  virtual void solve() = 0;
45: protected:
46:  Gen_matrix EffectiveK;
47:  Col_vector EffectiveR;
48:  virtual Gen_matrix makeEffectiveK() = 0;
49:  virtual Col_vector makeEffectiveR() = 0;
50: };
51:
52: class DynamicType : public SolutionMethod {
53: public:
54:  ....
```

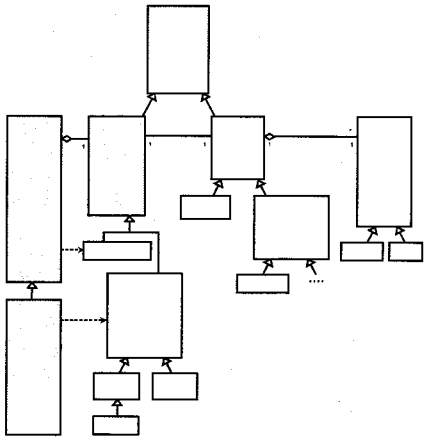

Figure 2.10: Static Structure of Implementation of Equation Package

```
52: class DynamicType : public SolutionMethod {     // definition of class
                                                    // inherit class Equation
53: public:
54:  virtual Gen_matrix makeEffectiveK() = 0;       // define the prototype
55:  virtual Col_vector makeEffectiveR() = 0;       // methods to calc K^(k-1)_(n+1), F^(k-1)_(n+1)
56:  virtual void storePreData(Col_vector);         // save data in iteration
57:  virtual void storeDataAtT(Col_vector);         // save data at t_(n+1)
58:  virtual void setUp();                          // initial setup
59:  virtual DynamicType* clone() = 0;              // define the prototype
                                                    // method to duplicate itself
60:  Equation* setEquation(Equation* eq); Equation* getEquation();
61:  IterationType* setIterationType(IterationType*); // set IterationType object
62:  IterationType* getIterationType();
63:  virtual int setSize(int size);                 // set DOF size
64:  virtual void solve();                          // solve equation
65: protected:
66:  Equation *equation;                            // relate to Equation
67:  IterationType* iterationType;                  // relale to IterationType
68:  Col_vector preFvector;
69:  Col_vector preDvector;
70: };
71:
72: class IterationType : public SolutionMethod { // definition of class
                                                   // inherit class SolutionMethod
73: public:
74:  friend IterationType* DynamicType::setIterationType(IterationType*);
                 // this method in DyanmicType can access data of IterationType
75:  Model* setModel(Model*); Model* getModel();  // set and get class Model
76:  virtual void storePreData(Col_vector);
77:  virtual void storeDataAtT(Col_vector);
78:  virtual int setSize(int size);
79:  virtual void setUp();
80:  virtual void solve() = 0;                     // solve equation
81:  virtual IterationType* clone() = 0;
82:  Col_vector& getRn();                          // get Rvector in previous time
83: protected:
84:  Model *model;                                 // have Model
85:  DynamicType* dynamicType;                     // relate to DynamicType
86:  LU_matrix *lu;                                // matrix for inverse
87:  Col_vector deltaD;                            // solution of equation
88:  Col_vector Rn;
89:  virtual void calcDeltaD();                 // calc K^(k-1)_(n+1), F^(k-1)_(n+1) and solve Δd^(k)
90:  virtual Gen_matrix makeEffectiveK();
91:  virtual Col_vector makeEffectiveR();
92: };
93:
94: class Model {                                 // definition of class Model
95: public:
96:  Equation* setEquation(Equation* eq);
97:  inline Gen_matrix getK();  // get Kmatrix
98:  inline Col_vector getF();  // get Fvector
99:  virtual int setSize(int size);
100:  virtual void setUp();
101:  virtual void setDeltaD(Col_vector) = 0;
        //  define prototype method to transfer
        //  the step deformation data
102:  virtual void update() = 0;
        //  define prototype method to update data
103:  virtual int getDof() const = 0;
104: protected:
105:  Equation *equation;
106:  Gen_matrix Kmatrix;
107:  Col_vector Fvector, Disp;
108: };
```

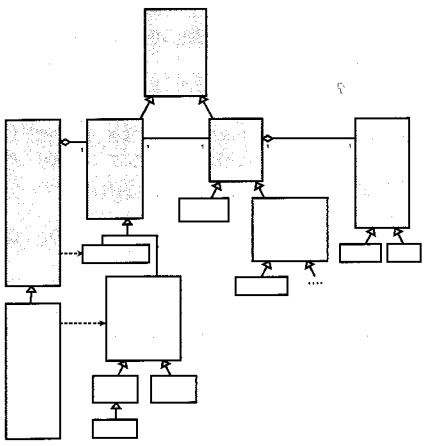

Figure 2.10: Static Structure of Implementation of Equation Package(cont'd.)

```
 1: /*-------------------------------------------------------------------*/
 2: void Equation::solve() {     // method solve() in class Equation
 3:  sMethod->solve();                      // delegate to DynamicType
 4: }
 5: /*-------------------------------------------------------------------*/
 6: void DynamicType::solve() {  // method solve() in class DynamicType
 7:  iterationType->solve();                // delegate to IterationType
 8: }
 9: /*-------------------------------------------------------------------*/
10: void LinearSolutionMethod::solve() {
                                 // method solve() in LinearSolutionMethod
11:  setUp();
12:  calcDeltaD();                          // make K_{n+1}, F_{n+1} and solve ΔD_{n+1}
13:  model->setDeltaD(deltaD);              // report ΔD_{n+1} to structural model
14:  storePreData(deltaD);
15:  model->update();                      // update model property
16:  storeDataAtT(deltaD);                 // store data at time t_{n+1}
17: }
18: /*-------------------------------------------------------------------*/
19: void NonlinearSolutionMethod::solve() {
                                 // method solve() in NoninearSolutionMethod
20:  setUp();
21:  iteration = 0;
22:  accum_dD = 0;
23:  do {
24:   iteration++;
25:   calcDeltaD();                         // make K_{n+1}^{(k-1)}, F_{n+1}^{(k-1)} and solve Δd^{(k)}
26:   checkEnergyConv();                    // calc energy convergence
27:   accum_dD += deltaD;                   // calc ΔD_{n+1}
28:   model->setDeltaD(accum_dD);           // report ΔD_{n+1} to structural model
29:   storePreData(accum_dD);               // store data at time t_{n+1} ,iter(k)
30:   checkForceConv();                     // calc force convergence
31:   if(iteration>=20) {                   // convergence check in iteration
32:    cerr << "\nDivergence..." << endl;   // error message
33:    exit(1);                            // terminate forcely
34:   }
35:  } while(convergenceCheck()!=1);        // convergence check
36:  storeDataAtT(accum_dD);                // store data at time t_{n+1}
37:  model->update();                       // update model property
38: }
39: /*-------------------------------------------------------------------*/
```

Figure 2.11: Implementation of *solve()* of Equation Package

In the object-oriented analysis, the *Equation* is the interface with the *Users*, and it has no concrete solution method itself, and the *Equation* is modeled to delegate the solution process to the *SolutionMethod* (see **Figure 2.9**). Therefore, in the program code, it is also found that when the message *solve* is sent to the *Equation* (line 2), the message *solve* is transferred to the *DynamicType* (here, `sMethod`) (line 3), and the *DynamicType* is also transferred to the *IterationMethod* which has a concrete solution method (line 7). `Equation::sMethod` and `DynamicType::iterationType` are related to the appropriate concrete object when the program is executed. For example, the `DynamicType::iterationType` is related to the *LinearSolutionMethod* (line 10) or the *NonlinearSolutionMethod* (line 19) in the executed program. Since the *Equation* doesn't have algorithms directly, not only the *Equation* but also the *User* operation is not affected by adding a new algorithms.

Next, looking inside the code *solve* in the linear/nonlinear solution method (from line

10/19), it is found that the algorithm corresponds to the sequence diagram such as **Figure 2.5**. In the program code, the nonlinear solution method algorithm can be realized in the simple code, because the nonlinear behavior is calculated outside of the *Equation* package (through the *Model*) (line 13 and 28).

Furthermore, since this package uses the *Matrix* class library which defines the linear algebra operations, the code is similar with the mathematical expression (e.g. line 27 shows the summation of vector).

Example

In order to show the advantage of the *Equation* package, the complete program code of the static linear/nonlinear analysis of a single degree of freedom is shown in **Figure 2.12**. In the program, a single degree of freedom object (MdlDof1) uses the *Hysteresis* object (line 8, 9). It cannot be discussed about the *Hysteresis* object here, but it is modeled to be an object to handle the nonlinearity.

At first of the linear or nonlinear analysis, the equilibrium equation or the equation of motion is formulated. In the program code, we can do so (line 11, 12). And in the solution process : Step 1, we set the loading condition (line 19) and solve the equation (line 21, 22). In this example, the nonlinear *Equation* object carries out the iterative calculation by the Newton–Raphson method inside (see line 12). But deserving special mention, the solution process can express in the same form exactly in spite of the nonlinearity of the problem (line 21, 22). And, in Step 2, we analyze the unloading state (line 28). For the conventional programming technique, this kind of program becomes complicated, because the calculation needs the previous condition. But in this program, the solution operation is completely the same of the loading state (compare line 34, 35 with line 21, 22).

In the program code, the equations is expressed explicitly and the same expression can be used in spite of solution methods. This is the reason that code can be implemented with the high readability.

2.4 Structure Subsystem

The structure is the object which has been modeled actively since the beginning of the research on the object-oriented application. But almost all objective applications were FEM, in which the model of the structure can be relatively simple. However, on the modeling methods (methods for making element matrices), there are the fiber model method, the spring model, etc. as well as FEM, and in the future, the more and more new methods will be proposed. In this section, the *Structure* subsystem is modeled to handle these various methods

```
 1: #include <fstream.h>                          // include definition files
 2: #include "equation.h"
 3: #include "mdlusr.h"
 4: #include "hyst.h"
 5:
 6: int main()                                    // start main program
 7: {
 8:  Hysteresis *hysL = new HysLinear(1.0, 2.0);   // generate linear hysteresis
 9:  Hysteresis *hysN = new HysBilinear(1.0, 4.0, 3.0, 6.0);
                                                  // generate bilinear hysteresis
10:
11:  Equation *eqL = new Equation(new MdlDof1(hysL)
                   , new LinearSolutionMethod
                   , new StaticSolutionMethod);    // setup static-linear equation
12:  Equation *eqN = new Equation(new MdlDof1(hysN)
                   , new NewtonRaphson
                   , new StaticSolutionMethod);    // setup static-nonlinear eq.
13:
14:  int num_dof = 1;                             // set DOF
15:  Col_vector R(num_dof), D(num_dof);           // generate load, displ. vectors
16:
17:  // ------------------------ Step 1: -----------------------------
18:  R[1] = 6.0;                                  // set load data (loading)
19:  eqL->setR(R); eqN->setR(R);                  // set load vector to equations
20:
21:  eqL->solve();                                // solve static-linear equation
22:  eqN->solve();                                // solve static-nonlinear equation
23:
24:  D = eqL->getD(); D.print("D_L");             // get result of analysis and display
25:  D = eqN->getD(); D.print("D_N");             // get result of analysis and display
26:
27:  // ------------------------ Step 2: -----------------------------
28:  R[1] = 2.0;                                  // set load data (unloading)
29:  eqL->setR(R); eqN->setR(R);
30:
31:  eqL->solve();                                // solve static-linear equation
32:  eqN->solve();                                // solve static-nonlinear equation
33:
34:  D = eqL->getD(); D.print("D_L");             // get result of analysis and display
35:  D = eqN->getD(); D.print("D_N");             // get result of analysis and display
36:
37:  return 0;                                    // terminate protram normally
38: }
```

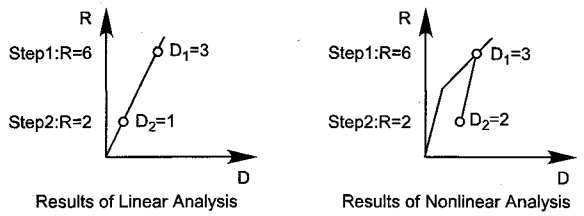

Figure 2.12: Example of Static Linear/Nonlinear Program and Results

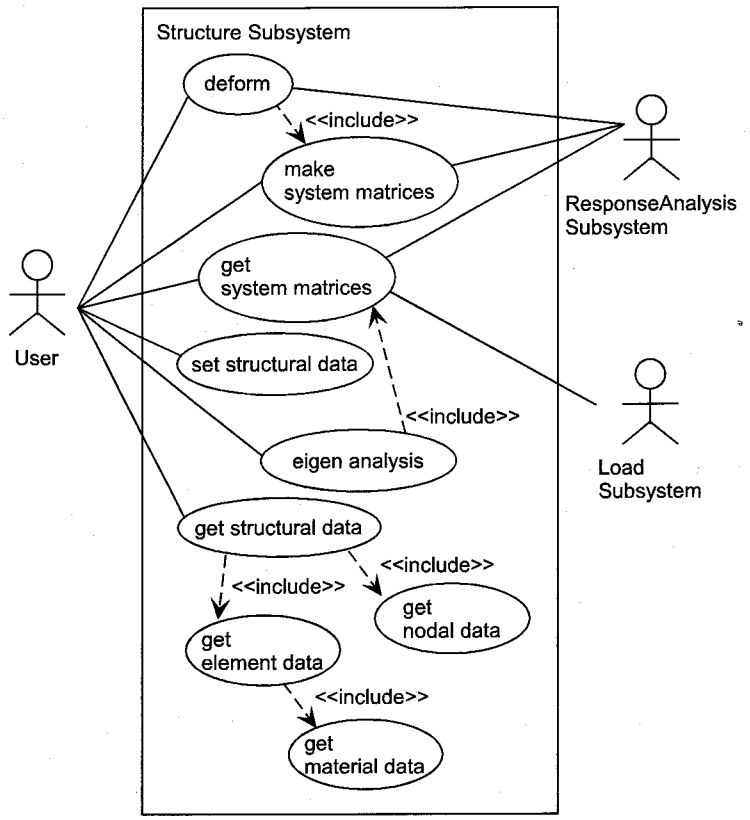

Figure 2.13: Use Case Diagram of Structure Subsystem

efficiently and simultaneously.

2.4.1 Requirement Analysis

Since the knowledge on the response analysis is delegated to the *ResponseAnalysis* subsystem, it is not necessary to include the knowledge in the *Structure* subsystem. Therefore, the demand for the *Structure* is "that the shape of real structures is represented in the program code as much as possible" and "that the characteristic matrices are made based on the modeling method". And, when the deformation state is reported to the *Structure*, the *Structure* must be *deformed*. The reference of the characteristic matrices is also required by not only users but also the *ResponseAnalysis* subsystem. Use cases of the *Structure* are shown in **Figure 2.13**.

The most important use case is to make the characteristic matrices. Although there are various methods for making characteristic matrices, there is only one "shape" when we recognize the structure. Therefore, the *Structure* subsystem is divided into two packages, the *Shape* and the modeling methods (*Method*)[3] and the methods are encapsulated by the *Strategy* pattern (**Figure 2.14**). In **Figure 2.14**, the *Material* and *Hysteresis* packages have also been divided from the *Structure* subsystem. Since the *Material* and *Hysteresis* are general ob-

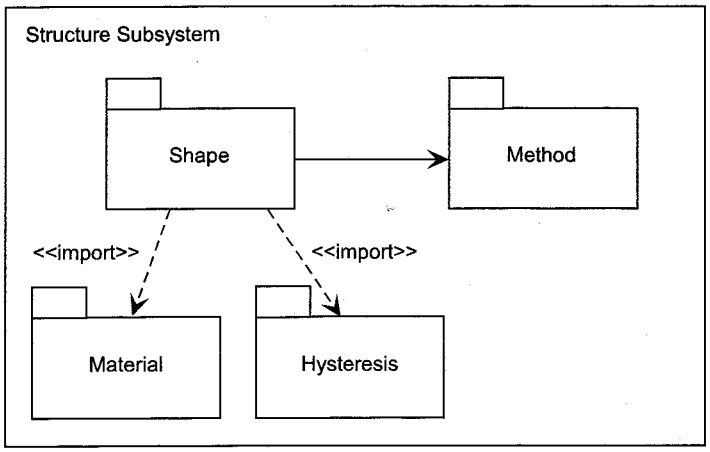

Figure 2.14: Packages in Structure Subsystem

jects which can be used in other problems, they are modeled and encapsulated as a package, and these packages are imported by the *Shape* packages as shown later. The class diagram of the *Hysteresis* package is shown in **Figure 2.15**. regardless of the type of the hysteresis, we can get the result corresponding to the given value in the same expression `getY(double x)` because the hysteresis data is stored in the object. The *Material* package handles the specific stress–strain relationship of materials. As same as the *Hysteresis* object, the stress in consideration for the strain history can be obtained by the unique method `getStress(double e)`. In this section, the *Shape* and *Method* packages are analyzed in detail.

2.4.2 Shape Package

Class Diagram

A structure, e.g. a bridge in the real world, is an assemblage of elements, like piers and girders. However, when the structure is analyzed, it is general to be simplified as the analytical model (**Figure 2.16**). The objective of the *Shape* package is the modeling of this simplified structure.

In **Figure 2.16**, objects in the *Shape* are identified. The *Structure* and the *Element* class can be identified, and the *Structure* is modeled to be an assemblage of *Elements*. And, among the *Structure* and the *Element*, there are common attributes and operations as follows.

- Characteristic matrices, such as stiffness matrix and nodal point force vector, etc. are constructed.
- They can be represented as an assemblage of *Nodes*.
- They can be deformed.

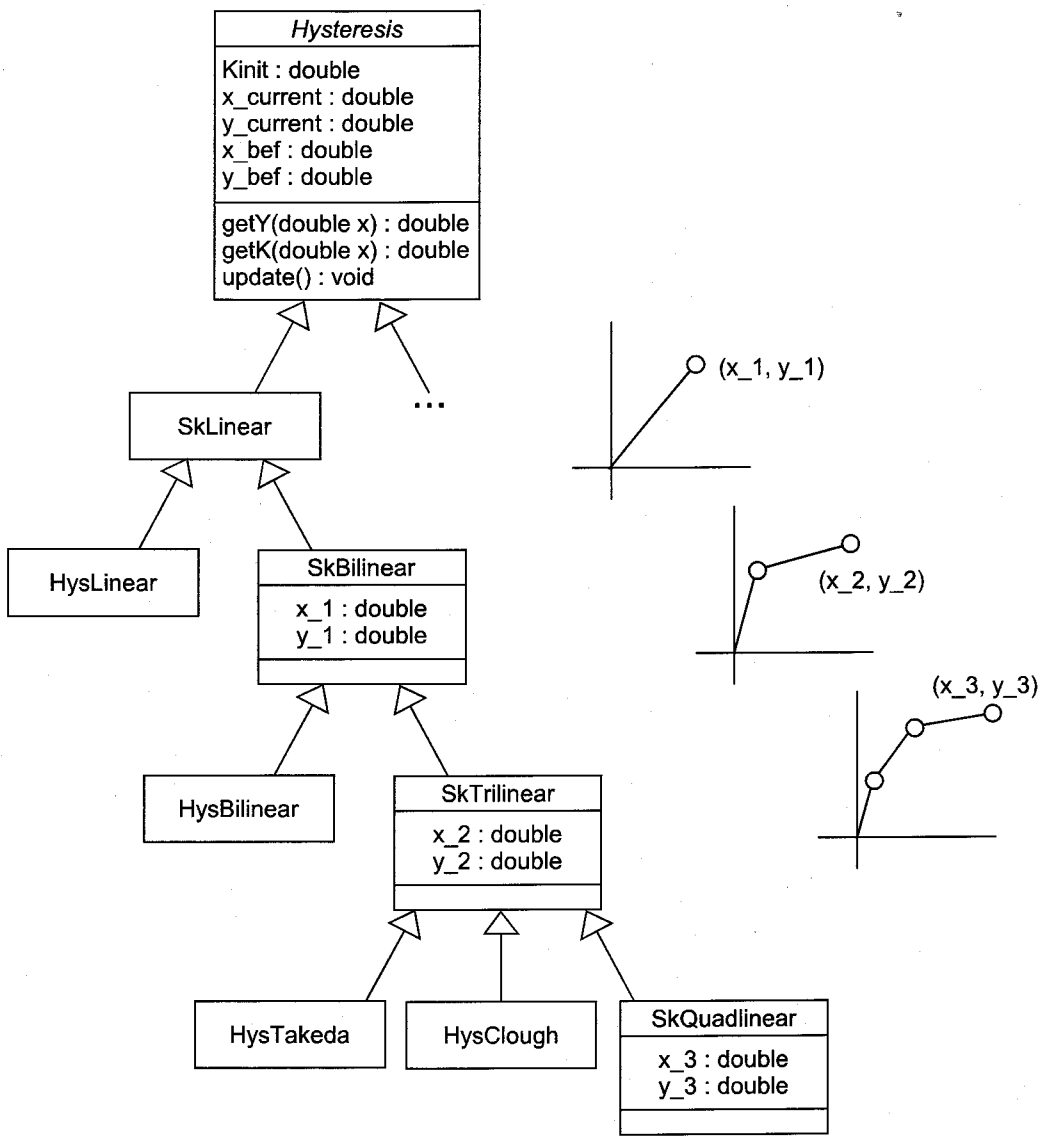

Figure 2.15: Hysteresis Package

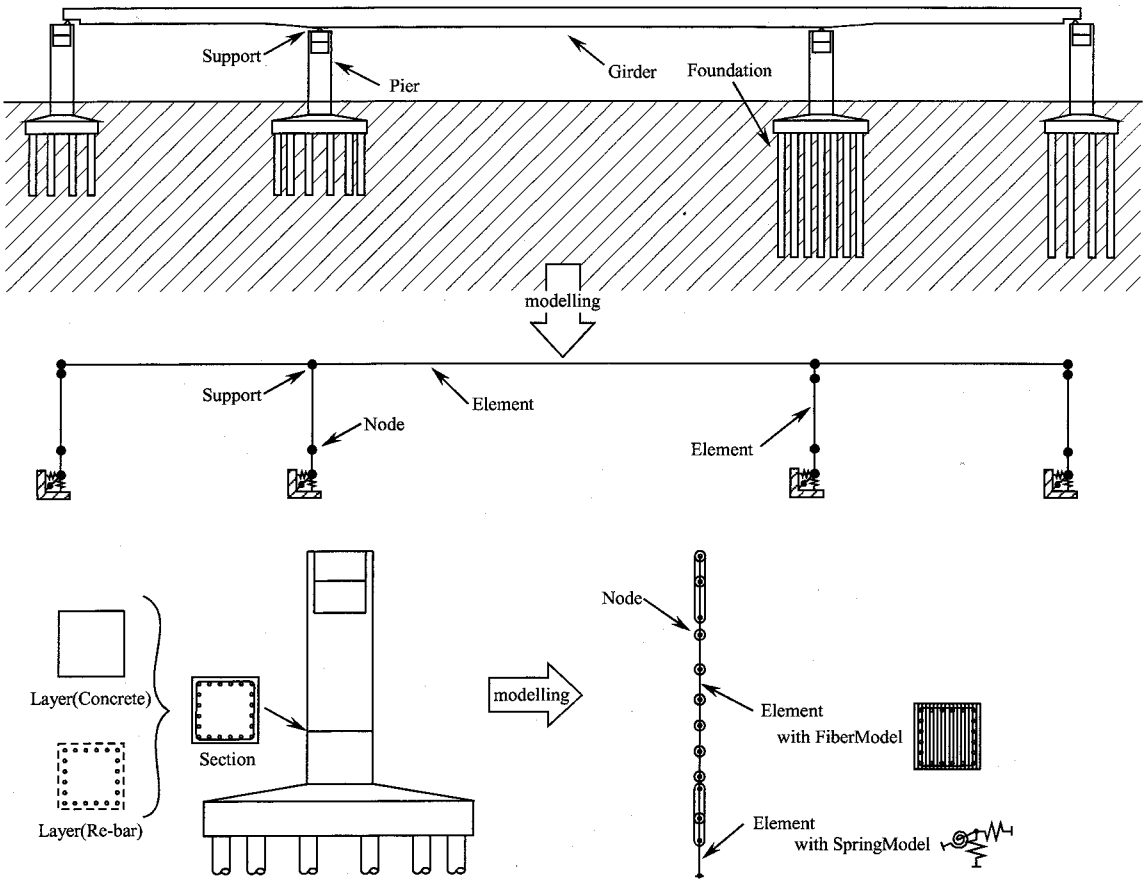

Figure 2.16: Shape of Structures

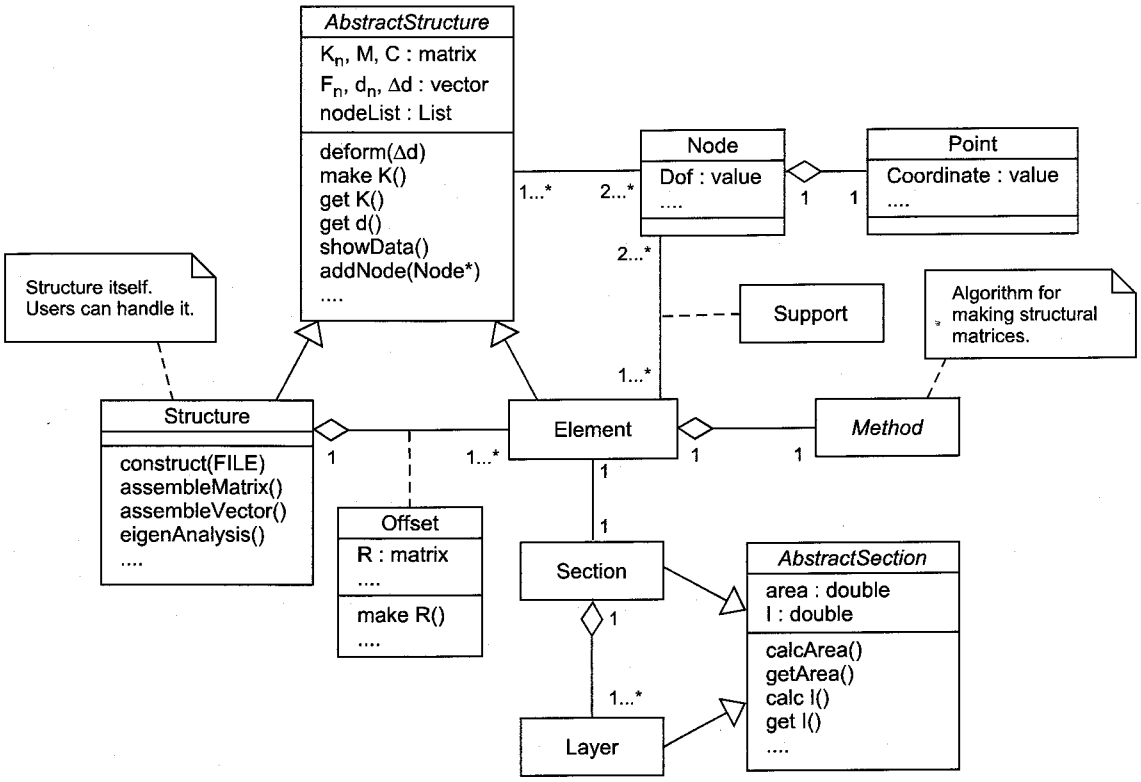

Figure 2.17: Class Diagram on Shape (part 1)

Therefore, a super class (*AbstractStructure*) which has the common attributes and operations mentioned above is extracted, and the *Structure* and the *Element* objects are modeled to inherit the *AbstractStructure*.

The *Element* is modeled to have the *Method* in order to make element matrices. And in order to define the location of each *Element* in the *Structure*, the *Offset* class is made as a relationship between the *Structure* and the *Element*. And the *Support* class is also made because there are many shoes in a bridge structure. The *Support* is modeled as a relationship between the *Node* and the *Element*. The *Element* has a *Section*, and in order to cope with composite structures, *Layer* is identified and the *Section* is modeled to have multiple *Layers*. The class diagram is shown in **Figure 2.17**.

Here, th classes are described as follows.

- *AbstractStructure*

  An abstract class which have the common properties between the *Structure* and the *Element*. The following attributes are defined : A list of *Nodes*, a stiffness matrix, a nodal point force vector, a mass matrix, etc.. And, it defines the abstract operations of making characteristic matrices and of deforming the structure.

- *Structure*

A structure which is an assemblage of *Elements*. By assembling element characteristic matrices, the structure characteristic matrices are constructed. When the deformation state is received from the *User*, this object calculates an element deformation corresponding to the element coordinate, and reports it to each element. It can also carry out the eigen analysis.

- *Element*

  A line element which composes a structure. Based on the *Method* package, a element stiffness matrix and a nodal point force vector are calculated. And, an element mass matrix and an element damping matrix are also constructed. It has the cross-sectional information (*Section*).

- *Point*

  A class which locates the position.

- *Node*

  A node which has the information on degree of freedom. *Structures* and *Elements* can be represented as an assemblage of *Nodes*. The position is informed by referring to the *Point* class.

- *Section*

  A cross section of an *Element*. It has the cross-sectional data such as the area, the moment of inertia, etc.. It consists of multiple *Layers* in order to express composite structures, and the cross-sectional data are calculated by referring the *Layers*.

- *Layer*

  An abstract layer which has a relation to one *Material*. It has operations to calculate the area, the moment of inertia, etc..

- *Offset*

  A class which define the location of each *Element* in the *Structure*. It has operations which make a rotation matrix, etc..

Next, detailed objects in a cross section (*Layer*) are analyzed. In order to be able to apply various modeling methods, it is necessary to relate different nonlinear characteristics to a *Layer*. Then, as it is shown in **Figure 2.18**, the *GaussPoint* object is set up as the relationship between the *Layer* and the nonlinearity, and in case of FEM, the *Layer* has several *GaussPoints* related to the *Material*, and in case of the Moment–Curvature method,

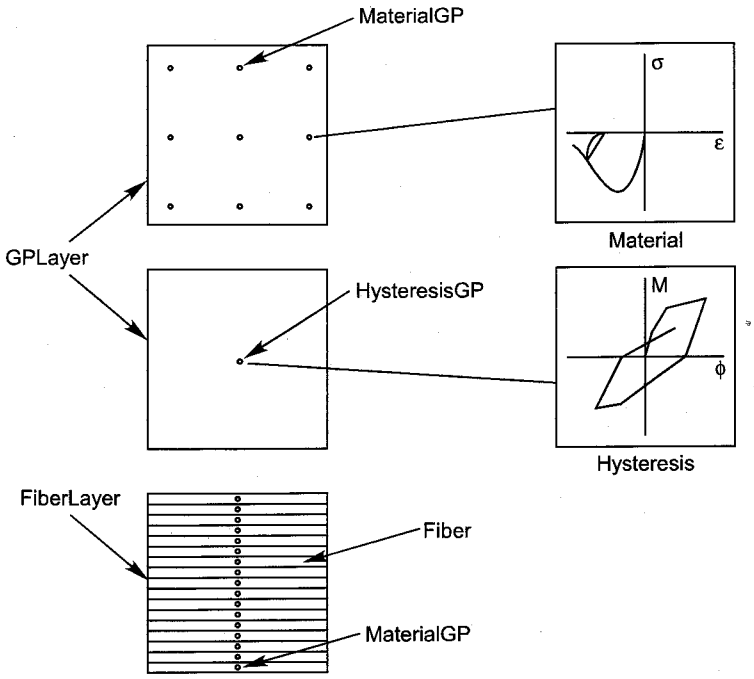

Figure 2.18: Conceptual Diagram of GaussPoint Object

the *Layer* has a *GaussPoint* related to the *Hysteresis*. And in case of the fiber model method, the *Layer* is an assemblage of *Fibers*, and the *Fiber* has the information of the area in addition to the *Material* property.

Class diagram of the shape related to the *Layer* is shown in **Figure 2.19**. The description of classes on **Figure 2.19** are as following.

- *FiberLayer*

  A layer which is an assemblage of *Fibers*. It can represent an arbitrary shape. The cross-sectional data, such as the area, are calculated using *Fibers*.

- *GPLayer*

  An abstract layer which has a relationship to *GaussPoints*. The cross-sectional data are calculating by a numerical integration.

- *RectLayer*

  A layer with a rectangle shape. It has data of a height and a width of a *Layer*.

- *CircleLayer*

  A layer with a circular shape. It has a diameter data of a *Layer*.

- *GaussPoint*

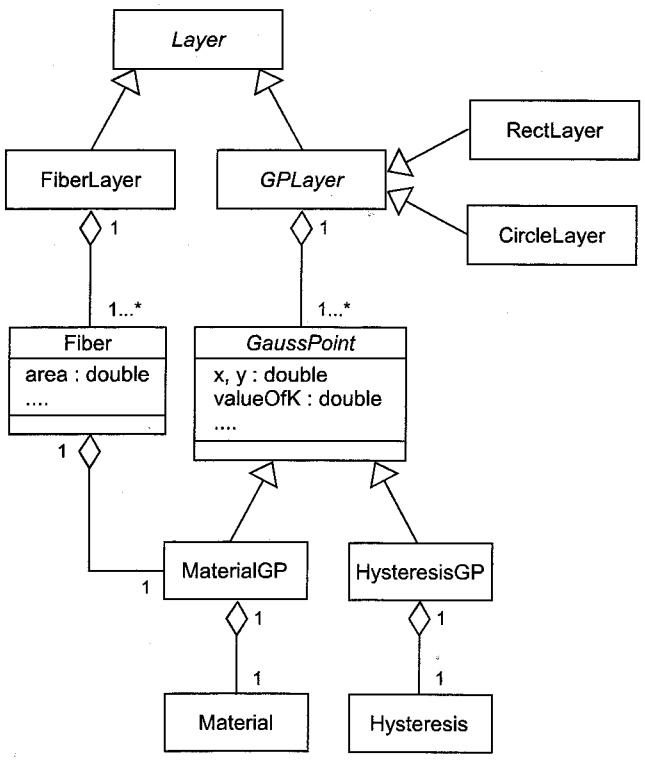

Figure 2.19: Class Diagram of Shape (part 2)

An abstract Gauss point used in a numerical integration. It remembers the hysteresis information considering the deformation history at a position in a *Layer*.

- *MaterialGP*

  A Gauss point with relates the *Material*.

- *HysteresisGP*

  A Gauss point with relates the *Hysteresis*.

- *Fiber*

  A piece for the fiber model. It has the area as the attribute, and it can get the information about the *Material* and the position in the cross section from the *MaterialGP*.

- *Material*

  An abstract material which has the stress – strain relationship.

- *Hysteresis*

  An abstract hysteresis relationship, such as linear, bilinear, trilinear, etc..

Modeling on Dynamic Behavior

The purpose of the *Structure* subsystem is to make the characteristic matrices. However, for a structure, the characteristic matrices is only the mean of expressing the deformation condition, and the essential behavior of the *Structure* is how to respond by given deformation state.

The sequence diagram is shown in **Figure 2.20** when the *Structure* subsystem receives the message of deformation from the *User* actor with a displacement increment vector. This displacement increment is converted into the increment on each *Node* and *Element*, and the *Structure* object sends the increment to corresponding *Element* as the message of the deformation. Each *Element* requests the making of element characteristic matrices to *Method* package. Since this *Method* package is a kind of black box from the *Shape* package, it is not necessary to know what kind of modeling method is related to the element. The only information the *Shape* package should have is that the procedure to get the characteristic matrices corresponding to the deformation history is to request the *Method* package to create the matrices. Therefore the modeling of the *Shape* can be very simple.

2.4.3 Method Package

In this study, objective modeling methods are the finite element method[10], the fiber model method[17], the moment–curvature model and the spring model (load–displacement model). Especially the fiber modeling of the Timoschenko beam is developed in **Appendix C**. These concrete methods inherit the *Method* class. The *Element* object can make the characteristic matrices using the *Method* object, not the concrete method object (e.g. through the operation `Element::makeK()` in **Figure 2.21**). Therefore there is no influence on the *Shape* package by adding a new modeling method.

According to **Appendix D**, it is found that in term of the algorithm about making element characteristic matrices, the finite element method, the fiber model method and the moment–curvature model calculate these matrices by integrating cross-sectional characteristic matrices in axial direction of the element. On the other hand, the spring model has no common part of other analytical method in the calculating process of element characteristic matrices. Class diagram based on the knowledge arrangement of the analytical method is shown in **Figure 2.21**.

For the finite element method, the fiber model method and the moment–curvature model, the *SectionBased* class is made as the super class of them. In the *Shape* package, the relationship between the *Element* and the *Section* is the one-to-one, because the purpose is to represent the shape. But the *Method* package should know the nonlinear hysteretic in-

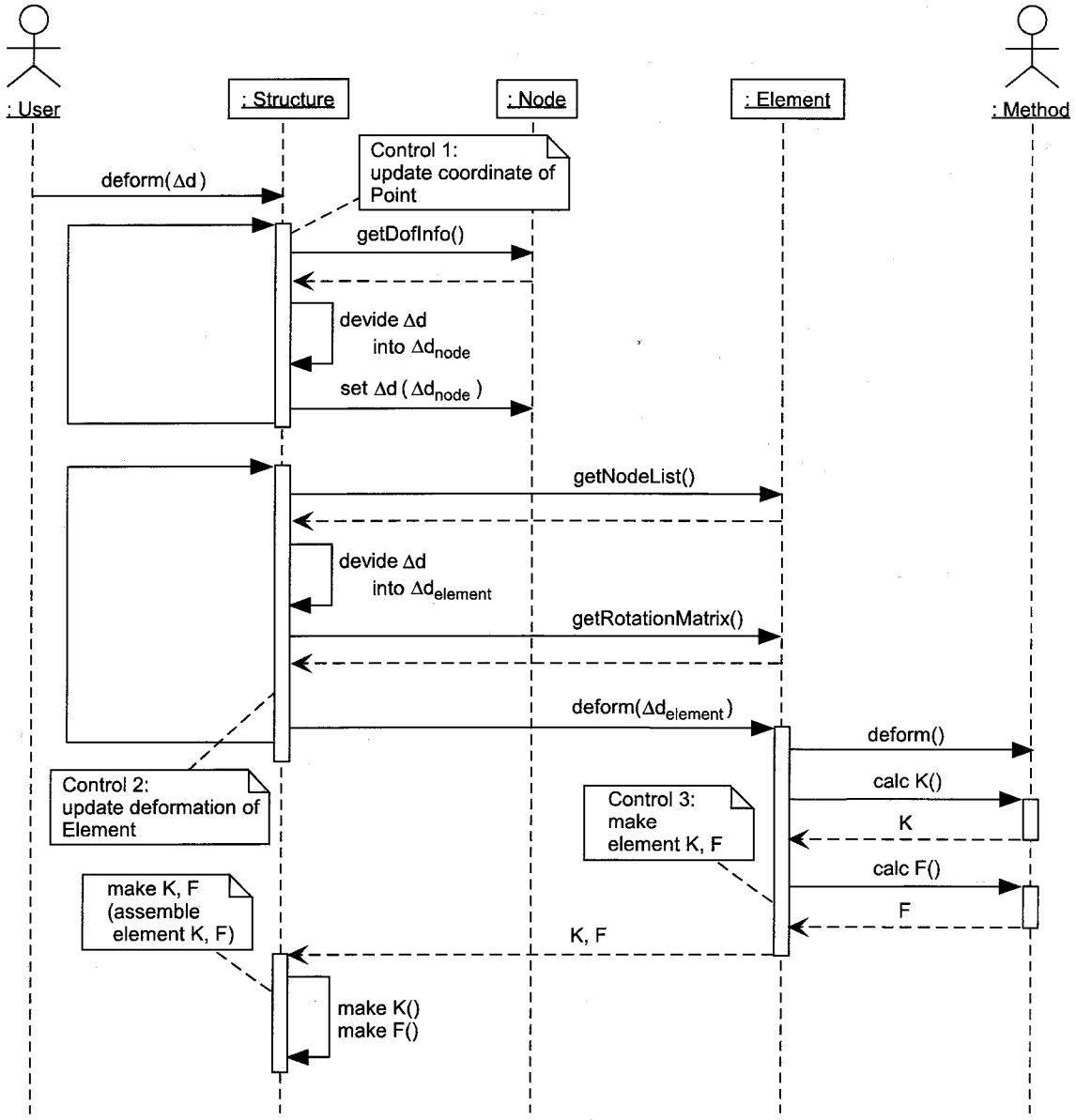

Figure 2.20: Sequence Diagram of Structure (Shape)

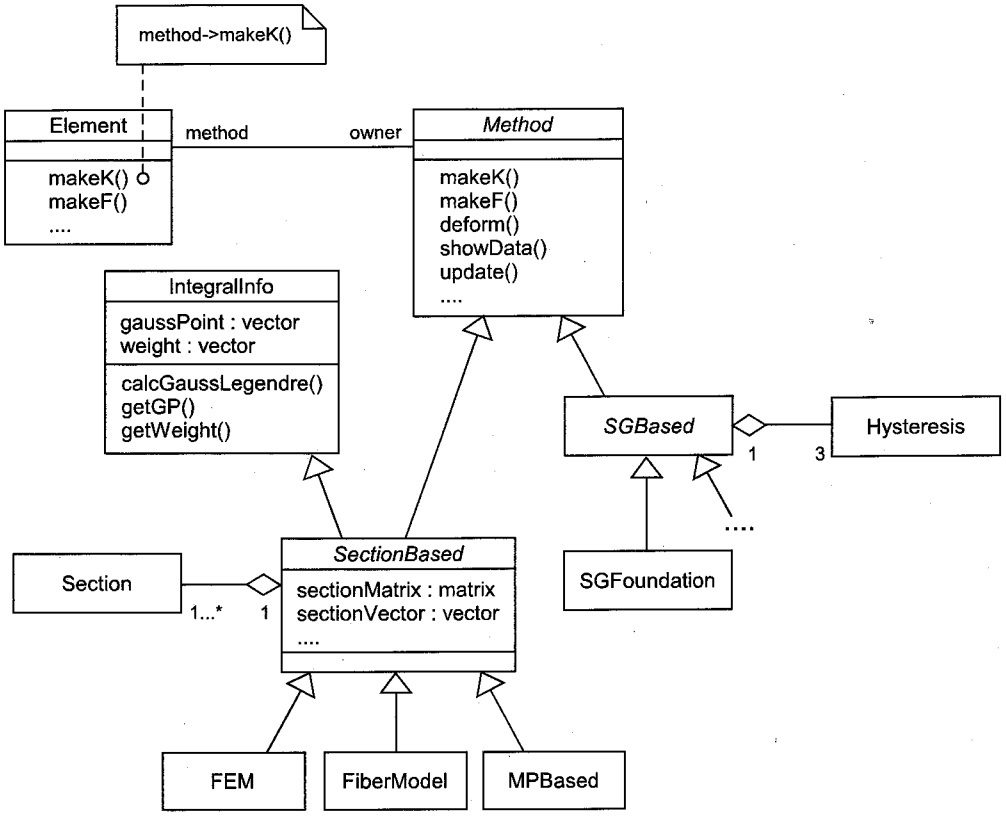

Figure 2.21: Class Diagram of Analytical Method Package

formation of each cross-sectional position. Therefore the *SectionBased* object has multiple *Sections* by copying the *Section* in the *Shape* package. And, in order to carry out a numerical integration, the *IntegralInfo* class which has operations to calculate the Gauss points and the weight is made, and the *SectionBased* class also inherits it.

The spring model is represented by the *SGBased* class, and the subclasses, which specialized in the axial, lateral, rotational direction and the foundation, are made. About the hysteretic behavior of the spring, the *Hysteresis* objects are used.

Since the *Method* package defines extracted algorithms, the dynamic behavior only follows the specific algorithm, like conventional programs in FORTRAN.

2.4.4 Implementation

Structure Class Library

The *Structure* subsystem is implemented in C++ language. The classes in the C++ header file are converted the object-oriented analytical results as well as the *Equation* package. Here, the program code of method *deform* in the *Structure* class is shown in **Figure 2.22** to explain how to implement the results of the object-oriented analysis. All variables cannot be explained here, and the outline of the code is explained.

```
 1: /*-------------------------------------------------------------------*/
 2: Col_vector Structure::deform(Col_vector du) {
 3: //-----------------------------------------------------------------
 4: // Control 1 in Figure 2.19: update coordinate of Point
 5: //   deviding the Dvector into displacement increments of each Node
 6: //-----------------------------------------------------------------
 7:  Col_vector disp(3);
 8:  for(int i=1; i<=NumNode; i++) {            //-----------------------
 9:   Node *node = (*NodeList)(i);              //
10:   for(int j=1; j<=3; j++) {                //
11:    if(node->getDof()->value(j)==0) {       //    devide Δd
12:     disp[j] = 0.0;                         //
13:    } else {                                //        into Δd_node
14:     disp[j] = du[node->getDof()->value(j)]; //
15:    }                                       //
16:   }                                        //-----------------------
17:   if(node->getDof()->getSize()==3) {
18:    node->getPosition()->addCoordinate(disp[1], disp[2]); // move Point
19:   }
20:  }
21: //-----------------------------------------------------------------
22: // Control 2 in Figure 2.19: update deformation of Element
23: //   deviding the Dvector into disp. increment of each Element
24: //-----------------------------------------------------------------
25:  int irow, idegree;
26:  Col_vector inc_disp(6);
27:  disp.setsize(6);
28:  ObjectList<Node> *nodeList;
29:  for(int i=1; i<=NumElem; i++) {
30:   nodeList = ((*ElementList)(i))->getNodeList();// get NodeList
31:   for(int j=1; j<=nodeList->getSize(); j++) {  //-------------------
32:    for(idegree=1; idegree<=3; idegree++) {     //
33:     irow = (((*nodeList)(j))->getDof())        //
34:          ->value(idegree);                     //
35:     if(irow==0) {                              //    devide Δd
36:      inc_disp[3*(j-1)+idegree] = 0.0;          //
37:      continue;                                 //        into Δd_element
38:     }                                          //
39:     inc_disp[3*(j-1)+idegree] = du[irow];      //
40:    }                                           //
41:   }                                            //-------------------
42:   disp = ((*ElementList)(i))->getR()*inc_disp; // get R and calculate
43:                                                // Δd_element in elem. coord.
44:                                                //-------------------
45:   ((*ElementList)(i))->deform(disp);           // report the deformation
46:  }                                             //        to each Element
47:  deltaD = du;
48:  return deltaD;
49: }
50:
51: /*-------------------------------------------------------------------*/
52: Col_vector Element::deform(Col_vector du) {
53: //-----------------------------------------------------------------
54: // Control 3 in Figure 2.19: make element K, F
55: //-----------------------------------------------------------------
56:  deltaD = du;
57:  method->deform();                  // report the deformation to Method
58:  makeF();                           // calculate F vector of model
59:  makeK();                           // calculate K matrix of model
60:  return deltaD;
61: }
62:
63: /*-------------------------------------------------------------------*/
```

Figure 2.22: Implementation of Method deform() in the Structure module

When the displacement increment vector is reported to the *Structure* (line 2), the *Structure* calculates the new location of each node (*Node*) and deformation of each element (*Element*) in element coordinate system (line 3 ~ 41). What the *Structure* should do is only above mentioned, and the other works are delegated to the *Elements* (line 40 calls line 46, `ElementList->deform(disp)`).

And when the deformation message is reported. In the deformation method of the *Element* (line 46), the data are transferred to the *Method* object, and the *Method* object also transfers them to the concrete *Model* object. And the *Element* also calculate the characteristic matrices based on the *Model* object (line 58, 59). The *Element* is not necessary to know how to calculate the matrices. Compared with **Figure 2.20**, these operations can be coded in the same manner.

Example

A program using the *Structure* object is shown in **Figure 2.23**. In the input file (line 7), structural data and analytical method are described. This program is to analyze the deformation of the structure corresponding to the designated top displacements. At first, we can recognize that the *Structure* itself can be represented in the program code (line 6). And though the *Structure* can make the characteristic matrices according to the deformation history (line 10 and 15), it is not necessary to mention the loading history (line 10 and line 15 are the same).

Program using the *Structure* subsystem are very easy to understand what the program carry out.

2.5 Load Subsystem

2.5.1 Outline

The *Load* subsystem shows a general external load, and is an object that is applied to a structure. The demand for the *Load* in the structural analysis problem is to make a load vector. In the earthquake engineering field, an earthquake causes a seismic force to a structure. Although an earthquake itself is not a force, it is a good idea to model it as a load object.

2.5.2 Object-oriented Analysis

Static Load

The load object is only a series of force data. When the object is applied to structures, it has the meaning as the load. The static load has to know the applied point in a structure, and

```
 1: #include <fstream.h>                          // include definition files
 2: #include "structure.h"
 3:
 4: int main()                                    // start program
 5: {
 6:  Structure *structure = new Structure(1); // generate structure object(ID:1)
 7:  structure->construct("str.dat");          // setup structure
 8:  structure->showData(cout);                // show data of structure
 9:
10:  structure0->makeF();                      // calculate nodal point force vector
11:
12:  Col_vector D(structure->getNumDof());
13:  D[1] = 1.0;                               // set deformation vector
14:
15:  structure->deform(D);                     // deform structure object
16:
17:  structure->makeK();                       // calculate stiffness matrix
18:  structure->makeF();                       // calculate nodal point force vector
19:
20:  return 0;                                 // terminate program normally
21: }
```

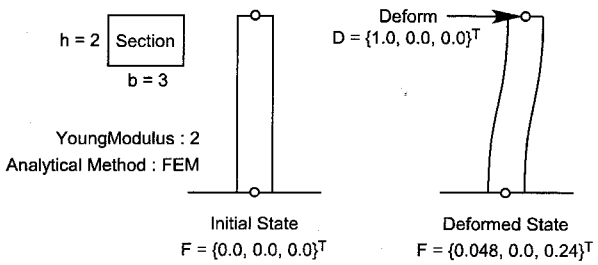

Figure 2.23: Program Example using Structure Object and Results

based on the information, the *Load* object makes a load vector.

Seismic Load (Earthquake Package)

The earthquake wave is a series of acceleration data, which is not a force. When the earthquake is applied to structures, seismic load occurs as the inertia load. Therefore, in order to make a load vector, it is necessary to know the structural data, such as the mass matrix.

Generally the earthquake wave is represented as three components of NS, EW and UD. There are time histories in one direction, and the time history is used by the calculation of the Fourier analyses, etc. in order to verify the characteristics of the wave. Therefore, first of all, the time history wave class (*Wave*) is made, and the *Waves* class is made as a set of three *Wave* objects.

The characteristics of the seismic wave is expressed by not only the time history and the Fourier spectrum but also the response spectrum, the evolutionary power spectrum, etc.. Therefore, the *Earthquake* class is modeled to inherit the *Waves*, and it has operations to calculate a response spectrum analysis, etc.. When a response spectrum or a strength demand spectrum is calculated, it is necessary to carry out the response analysis. Since the analysis is to solve a linear/nonlinear equation of motion of a single degree of freedom, the *Earthquake*

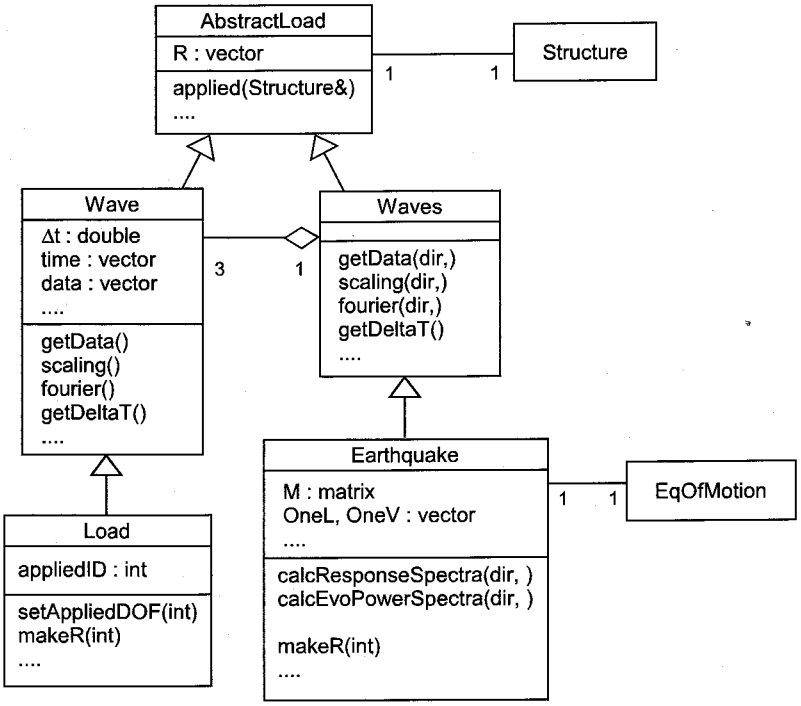

Figure 2.24: Class Diagram of Load Subsystem

object is modeled to reuse the *Equation* package.

According to the analysis of the *Load* subsystem, including the *Earthquake* package, the class diagram is shown in **Figure 2.24**.

2.5.3 Implementation

The *Load* subsystem is also implemented in C++ language. The example program using the *Load* subsystem is shown in **Figure 2.25**.

In this program, we introduce a static (line 14) and a seismic load (line 20), and apply them to the structure (line 17 and 22). Therefore they can make the appropriate load vectors (line 25 and 26). And although the *Earthquake* is a part of the *Load* subsystem, it can be used alone. In this program, it is found that only the earthquake object can be used for the calculation of the response spectrum (line 29).

2.6 Structural Analysis System

2.6.1 User Interface of System

The conventional analysis system has the user interface program, but our structural analysis system have no specific interface program. In the sense of users' usage, the main program

```
 1: #include <fstream.h>                          // include definition files
 2: #include <stdlib.h>
 3: #include "load.h"
 4: #include "earthq.h"
 5:
 6: int main()                                    // start program
 7: {
 8:   // ------- Setup Structure -------
 9:   Structure *structure = new Structure(1);
10:   structure->construct("str.dat");
11:   structure->showData(cout);
12:
13:   // ------- Setup Static Load -------
14:   Load* load = new Load;                       // generate load
15:   load->setWaveDataWithTime("static.dat"); // read data
16:   load->setAppliedDOF(5);                      // set DOF number(5) of loading
17:   load->applied(structure);                    // applied to structure
18:
19:   // ------- Setup Seismic Load -------
20:   Earthquake* earthq = new Earthquake;     // generate earthquake
21:   earthq->setOneDirWaveDataWithTime(NS, "kobe_ns.dat"); // read data
22:   earthq->applied(structure);
          // applied to structure; earthquake object knows how to make
          // load vector referring the dof list of structure
23:
24:   // make Load Vector at 427th time step for structural analysis
25:   load->makeR(427);
26:   earthq->makeR(427);
27:
28:   // Earthquake object itself can calculate the ResponseSpectra
29:   earthq->calcResponseSpectra(NS, "res_ns.dat", 0.05);
30:
31:   return 0;                                    // terminate program normally
32: }
```

Figure 2.25: Program Example using Load and Earthquake Object

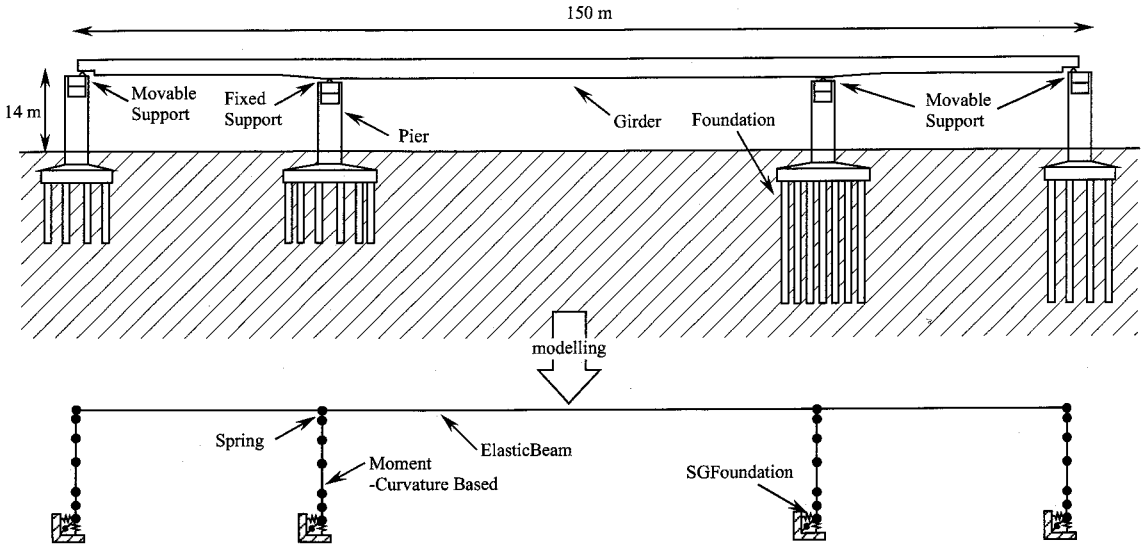

Figure 2.26: Objective Bridge

code (for example in C++, `main(){...}`) should be corresponding to it. Since three subsystems have been developed understandably and implemented as class libraries in C++, the main program wouldn't be complicated from the user. This structural analysis system has no limitation about the usability and the extendibility, because the system is just the program code and we can rewrite the system itself according to the objective problem.

2.6.2 Example (Seismic Response Analysis)

The seismic response analysis of the bridge is introduced. The objective bridge is a three-span continuous girder bridge shown in **Figure 2.26**. As shown in the lower part of the figure, it is modeled a flame structure, which consists of line elements, shoes and foundations. And as the modeling method, the moment–curvature model (Takeda hysteresis model) is used for the bridge piers, the elastic FEM beam is used for the girders and the spring model is used for the shoes and the foundations. As the input earthquake motion, the JR Takatori Station record (1995) is used.

In **Figure 2.27**, the whole program of the seismic analysis system is shown. And it is found that the seismic response analysis itself can be expressed by only few codes (in this case, 51 lines, including comments). At first of the analysis, the bridge object is constructed (line 12). And in order to know the vibration characteristics of the bridge, the eigen analysis is carried out. Then the earthquake object (line 18) is generated and is applied to the bridge (line 21). In line 24, the equation of motion is generated and the analysis is carried out by the message passing (line 37 ~ 48). As the results, the displacement and acceleration response of the girder are obtained (line 46, 47).

```
 1: #include <fstream.h>                              // include definition files
 2: #include "equation.h"
 3: #include "load.h"
 4: #include "earthq.h"
 5: #include "structure.h"
 6: #include "method.h"
 7: #include "mdlstr.h"
 8:
 9: int main()
10: {
11:   // ------ Setup Structure ------
12:   Structure *bridge = new Structure(1);          // generate bridge object
13:   bridge->construct("5span.dat");                // setup bridge
14:
15:   bridge->eigenAnalysis();                       // eigen analysis
16:
17:   // ------ Setup Earthquake ------
18:   Earthquake *earthq = new Earthquake;           // generate earthquake object
19:   earthq->setOneDirWaveDataWithTime(NS, "kobe_ns.dat"); // read data
20:
21:   earthq->applied(*bridge);                      // apply earthquake to bridge
22:
23:   // ------ Setup Equation of Motion ------
24:   EqOfMotion *equation;                          // generate equation object
25:   equation = new EqOfMotion(new MdlStructure(bridge)
26:                           , new NewtonRaphson(
27:                             new NewmarkMethod(0.25))); // setup equation
28:   equation->setM(bridge->getM());                // set mass matrix from structure
29:   equation->setDeltaT(earthq->getDeltaT());      // set analysys interval time
                                                     // from earthquake
30:
31:   in size = bridge->getNumDof();                 // get DOF from structure
32:   Col_vector R(size), acc(size), dsp(size);
33:
34:   // ------ Seismic Response Analysis ------
35:   ofstream ACC("accout.dat");                      // setup output files
36:   ofstream DSP("dspout.dat");
37:   for(int j=0; j<earthq->getNumData(); j++) {    // start analysis
38:     R = earthq->makeR(j);                       // get load vector from load object
39:     equation->setR(R);                          // set load vector to equation
40:
41:     equation->solve();                          // solve equation
42:
43:     acc = equation->getA()+earthq->getData(NS,j)*One;  // get absolute acc.
44:     dsp = equation->getD();                    // get displacement
45:
46:     ACC << ' ' << earthq->getTime(j) << ' ' << dsp << endl; // output data
47:     DSP << ' ' << earthq->getTime(j) << ' ' << acc << endl;
48:   }
49:
50:   return 0;                                    // terminate program normally
51: }
```

Figure 2.27: Seismic Response Analysis Program

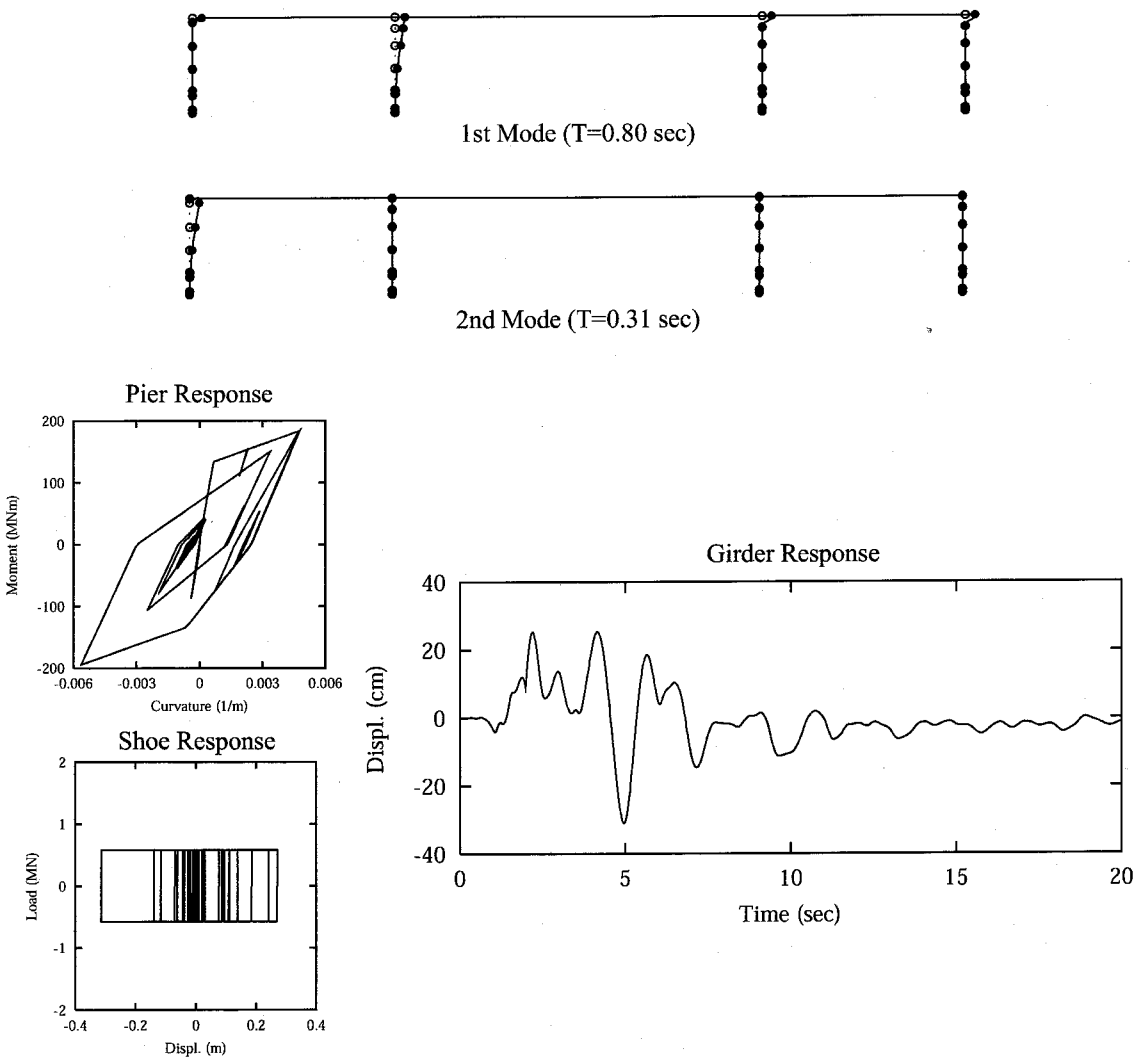

Figure 2.28: Results of Seismic Response Analysis

The results of this analysis, including the hysteresis, is shown in (**Figure 2.28**). This is the nonlinear problem, but the complicated calculations are completely concealed from the user. This program is very simple and easy to understand what happens in the program.

2.7 Summary

In this study, the structural analysis system is analyzed, designed and implemented in the object-oriented technique, and the structural analysis system in next generation is proposed. The conclusions drawn from this chapter are summarized as follows.

1. The structural analysis system is divided into three subsystems of *Structure*, *Load* and *ResponseAnalysis*. The proposed system can carry out an analysis by message passing to each other. The analysis system itself is a program code. Since, this system

allows the explicit representation of structures, loads, equations and so on, it is easy to understand, maintain and extend to other problem domains. This is an advantage in not only the research field where new solution method is often developed but also the educational field where it is important to understand the meaning of the whole system.

2. The *ResponseAnalysis* subsystem is modeled that the *Equation* package is the kernel. And in the *Equation* package, we propose the model to express solution methods by three objects, *DynamicType*, *IterationType* and *Model*. The *DynamicType* defines the operations making prototypes of the effective matrices in a static and dynamic problem. The *IterationType* encapsulates concrete solution algorithms and solves the equation. The *Model* has a relationship to a structural object which calculate the stiffness matrix and the nodal point force vector for the *Equation*. The *Equation* is the interface between users and solution algorithms and can be accessed by the users. The other objects are invisible from the users. Furthermore, since the solution methods are modeled by the *Strategy* pattern, the *Equation* has no influence on adding a new solution algorithm. As the results, this package becomes robust against the modification and the expansion.

3. The *Structure* subsystem is divided into the *Shape* and the *Method* packages. The *Shape* shape represents only the shape of the structure from the view of the users. The structural modeling methods are separated from the *Shape*, and are encapsulated as the *Method* package. As similar to the *Equation* package, the users can only access the *Shape* subsystem directly. Therefore in spite of the modeling method, the same expression can be used in the program code to denote a structure. And inheriting the *Method*, any modeling method can be used in the *Structure* subsystem. In this study, the FEM, the fiber model, the moment–curvature model and the spring model are implemented as the modeling principles.

4. The *Load* subsystem shows a series of external load, and has a role to make external load vectors for the structural analysis system. Besides the static load object (*Load*), the *Earthquake* package is introduced. These objects can make the appropriate load vectors as they are applied to the *Structure* object. These objects can be used alone, e.g. for the calculation of the Fourier spectrum, and especially the *Earthquake* object can calculate the response spectrum and so on. Therefore the *Earthquake* object is useful in the earthquake engineering field.

5. By the object-oriented analysis of the structural analysis system by the UML notation, it is possible that not only researcher in the structure analysis field but also researcher

in the informatics field, such as programmers and system engineers, can share the same knowledge about the system, and collaboration work can be realized.

References

(1) Takahashi, Y., Igarashi, A. and Iemura, H. : Object-Oriented Analysis and Design of Structural Analysis System (in Japanese), *Journal of JSCE*, Vol. I-57, No. 689, pp. 301–320, 10 2001.

(2) Takahashi, Y., Igarashi, A. and Iemura, H. : Application of Object-Oriented Approach to Earthquake Engineering (in Japanese), *Journal of Civil Engineering Information Processing System , JSCE*, Vol. 5, pp. 123–130, 1996.

(3) Fujita, R., Takahashi, Y. and Iemura, H. : Development of Structure Module on Object-Oriented Structural Analylsis System (in Japanese), *Journal of Civil Engineering Information Processing System , JSCE*, Vol. 6, pp. 119–126, 1997.

(4) Takahashi, Y., Igarashi, A. and Iemura, H. : Application of Object-Oriented Approach to Earthquake Engineering, *Journal of Civil Engineering Information Processing System , JSCE*, Vol. 6, pp. 271–278, 1997.

(5) Booch, G., Rumbaugh, J. and Jacobson, I.: *The Unified Modeling Language User Guide Version 1.3*, Addison-Wesley, 1999.

(6) Rumbaugh, J., Jacobson, I. and Booch, G.: *The Unified Modeling Language Reference Manual*, Addison-Wesley, 1999.

(7) Newmark, N. : A Method of Computation for Structural Dynamics, *J. eng. mech. div. ASCE*, Vol. 85/EM3, pp. 67 – 94, 1959.

(8) Bathe, K. and Wilson, E. : Stability and Accuracy Analysis of Direct Integration Methods, *Earthquake eng. struct. dyn.*, Vol. 1, pp. 283 – 291, 1973.

(9) Bathe, K. and Cimento, A. : Some Practical Procedures for the Solution of Nonlinear Finete Element Equations, *Comp. meths appl. mech. eng.*, Vol. 22, pp. 59 – 85, 1980.

(10) Bathe, K.: *Finite Element Procedures*, Prentice Hall, 1996.

(11) Hilber, H., Hughes, T. and Taylor, R. : Improved Numerical Dissipation for Time Integration Algorithms in Structural Dynamics, *Earthquake eng. struct. dyn.*, Vol. 5, pp. 283 – 292, 1977.

(12) Hughes, T. : Analysis of Transient Algorithms with Particular Reference to Stability Behavior, *Computational Methods for Transient Analysis*, pp. 67 – 155, 1983.

(13) Nakashima, M., Ishida, M. and Ando, K. : Integration Techniques for Substructure Pseudo Dynamic Test (in Japanese), *Journal of Structu. Constr. Engng, AIJ*, Vol. 417, pp. 107 – 117, 1990.

(14) Sun, K., Pires, J. and Tao, J. : A Post-Correction Integration Algorithm for Non-Linear Dynamic Analysis of Structures, *Earthquake eng. struct. dyn.*, Vol. 20, pp. 1083 – 1097, 1991.

(15) Sakai, H., Sawada, S. and Toki, K. : Non-iterative Computation Scheme for Nonlinear Dynamic Finite Element Method, *Journal of JSCE*, Vol. 507/I-30, pp. 137 – 147, 1995.

(16) Gamma, E., Helm, R., Johnson, R. and Vlissides, J.: *Design Patterns : Elements of Object-Oriented Architecture*, Addison Wesley, 1995.

(17) Ristić, D., Y.Yamada and H.Iemura: Nonlinear behaviour and stress - strain based modeling of reinforced concrete structures under earthquake induced bending and varying axial loads, KUCE No.88 - ST - 01, Kyoto University, 1986.

Chapter 3

Seismic Response Characteristics of RC Tall Piers with Hollow Section

3.1 General Remarks

The preparation of expressway can not only support the global activity but also construct multiple transportation network, and the new expressway, such as the 2nd Tomei expressway, is under construction in Japan. Since an expressway often crosses over a deep valley, it requires many tall bridge piers. Generally for a tall pier, a hollow section is adopted in order to reduce the seismic force.

Though the hollow section can give the high flexural stiffness rationally, it is difficult to confine the concrete of the web part effectively, and the thinner web causes the deterioration of the seismic performance, such as concrete shear resistance, flexural ductility, etc., compared to the filled section. A great deal of effort has been made on the research of structures with hollow section, but almost all results are based on the static loading tests, and what seems to be lacking is the research of the real behavior under earthquakes. Only few attempts have so far been made at the dynamic evaluation experimentally[1)], and it is hardly to say that the behavior under severe earthquakes is examined sufficiently.

In this study, to begin with, in order to investigate the fundamental characteristics of RC columns with hollow section, the static cyclic loading tests were carried out. The study of quantative evaluation on shear deformation of a hollow pier has been strangely neglected until now although many researchers indicated that a hollow member often causes a shear failure. Therefore, in these tests, in addition to the conventional evaluation, such as the load–displacement relationship, the deformation characteristics were examined by separating the whole deformation to the flexural, shear and rotational components. Next, the seismic performance is evaluated by hybrid earthquake loading tests. Considering the similarity law, the

Table 3.1: Parameters of Test Units in Static Tests

	l/d	Axial Load (MPa)	Stirrup Ratio (%)	Intermediate Tie
H4-1	4.0	0.0	0.34	w
H4-2		3.7	0.17	w/o
H4-3				w
H4-4			0.34	w/o
H4-5				w
H2-1	2.0		0.17	w/o
H2-2			0.34	w

actual seismic response of the bridge can be reproduced in the tests.

This chapter is described on the basis of the works by Iemura and Takahashi[2–5].

3.2 Deformation of RC Piers with Hollow Section

3.2.1 Fundamental Performance

Description of Test Units

All test units had the same section dimensions, which is a 320 mm square cross section with 85 mm thick walls (**Figure 3.1**). The test parameters were the shear span ratio l/d, the axial load, the stirrup ratio and the usage of intermediate tie (**Table 3.1**). In the table, the first character of the unit name "H" denotes the hollow section type and the second character denotes the shear span ratio. In order to evaluate the effect of the hollow section clearly, the hollow section starts the bottom. The basic model was the column with l/d = 4.0 (the height of 1200 mm). And, the test units with l/d = 2.0 were prepared in order to examine the effect of the hollow section on the shear behavior.

The material properties of steel and concrete are shown in **Table 3.2**, **Table 3.3** respectively. The high-early-strength Portland cement was used and the maximum aggregate size was 15 mm.

Loading System and Test Procedure

Two digitally controlled actuators were used for loading (**Figure 3.2**, **Photo 3.1 ~ Photo 3.6**). The actuators are made by Tokyo Koki – Schenck, and the loading capacity of ±400 kN. These actuators were controlled by the control unit made by Shimazu Co. Ltd. In order to apply the vertical load, the linear roller way (Nippon Tomson – IKO) was installed at

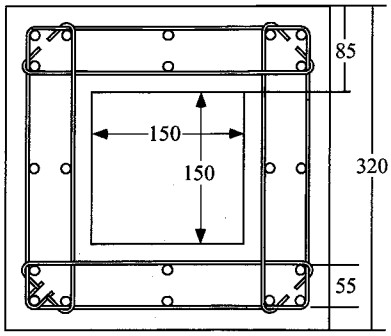

a) Hollow Section

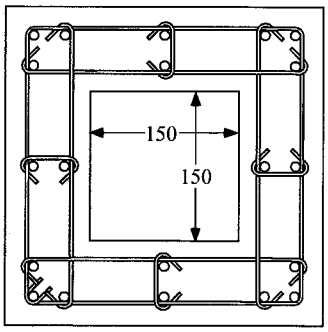

b) Hollow Section with Intermediate Ties

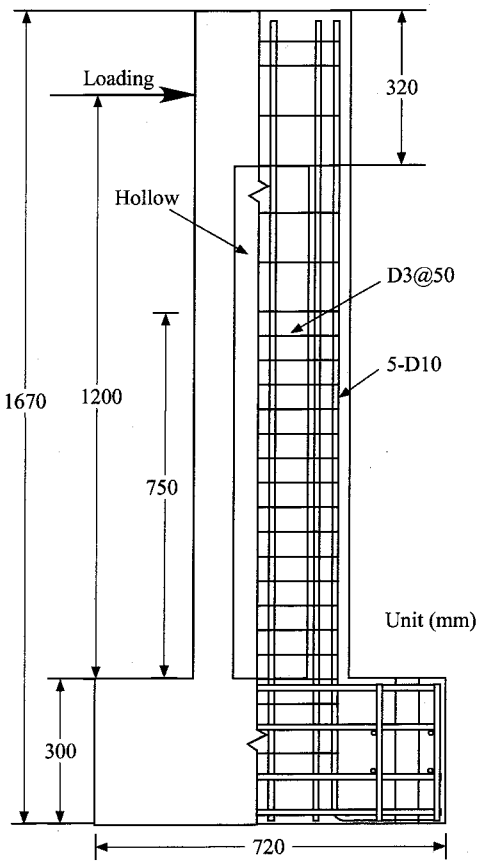

c) H4 series (H4-4)

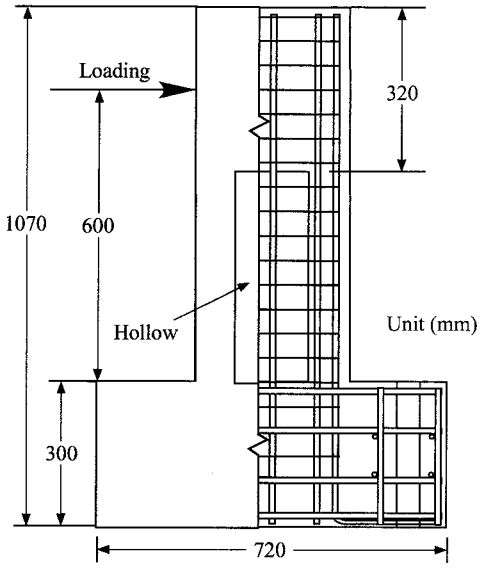

d) H2 series (H2-2)

Figure 3.1: RC Pier Test Units with Hollow Section

Table 3.2: Properties of Steel

		Yield Strength (MPa)	Ultimate Strength (MPa)
Longitudinal Bar	D10	373	545
Stirrup	D3	299	378

Table 3.3: Properties of Concrete

Compressive Strength (MPa)	Tensile Strength (MPa)	Bending Strength (MPa)
32.8	3.6	6.7

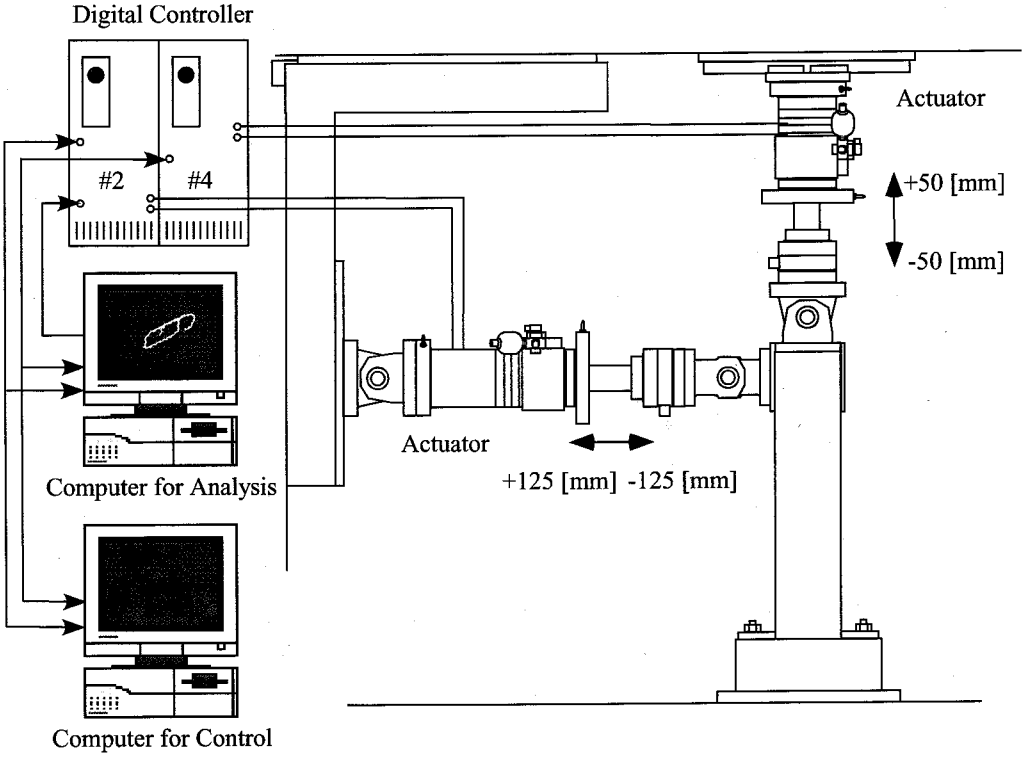

Figure 3.2: Loading System

the base of the vertical actuator (**Photo 3.2**). Two computers were used, and the one controls the actuator controllers and the other controls the test (generate loading waves, save data, etc.) (**Photo 3.5**). The displacement and the strain were measured by the static strain measurement (**Photo 3.6**).

The horizontal actuator imposed the horizontal displacements and the other one applied the axial load. The horizontal displacement was applied at a quasi-static rate in displacement-controlled cycles to rotation angles $R = \pm 0.01, \pm 0.02$, etc., until failure of the column occurred, where $R = l/\Delta$; l = shear span; and Δ = actuator's displacement. The axial load is shown in **Table 3.1**

Load–Displacement Hysteresis Loops

Figure 3.3 shows the hysteresis loops for horizontal load – horizontal displacement at the top of columns. And, **Table 3.4** shows the numerical data such as ductility factor etc.. In this study, the ultimate displacement is defined as the displacement at which the load decreases to the 80 percent of the maximum load.

From the results of H4 series, it is found that the H4-4, 5 of which the stirrup spacing was short, exhibited a large ductility. Also, as for H4-5 with intermediate ties, the restoring force after the maximum state decreased more gradually than that of H4-4. On the other hand, H4-2, 3 had almost the same performance of H4-4, while H4-3 had the intermediate ties. From the above results, it is found that the intermediate ties can prevent the buckling of longitudinal bars and improve the confinement of concrete.

H4-1, in case of no axial load, showed very large ductility compared with the others. Generally, The compressive stress of piers with hollow section is about 3 ~ 5 MPa while that of normal piers with filled section is about 1 MPa. It is well known that the deformation performance around the ultimate state is deteriorated as the axial load becomes large. Therefore piers with hollow section have a great influence of the axial load.

In the case of H2 series, in spite of the amount of stirrup, soon after the yielding of longitudinal bars, the rapid decrease of restoring force occurred.

As the overall tendency, restoring force is rapidly decreasing after the maximum state. The main reasons are the spalling of concrete occurs not only outside but also the void and the buckling of longitudinal bars.

Failure Mode

Figure 3.4 shows the damage process of each specimen in the loadings. H4 series finally failed in flexure at the bottom. After the maximum state, the buckling of longitudinal bars and the spalling the concrete were observed, and the restoring force decreased rapidly. Fo-

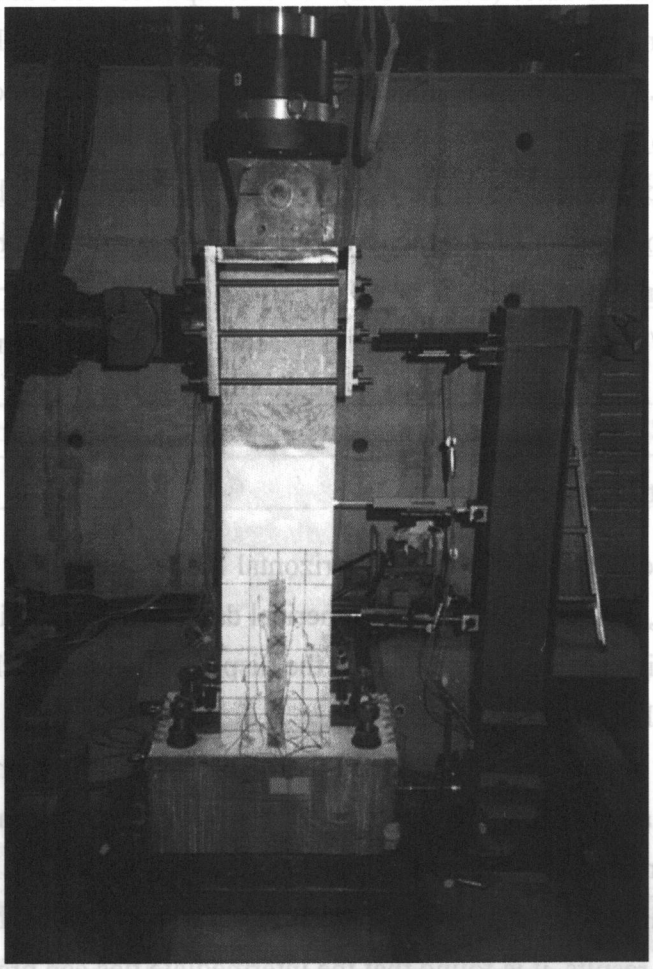

Photo 3.1: Test Setup for H4 Series

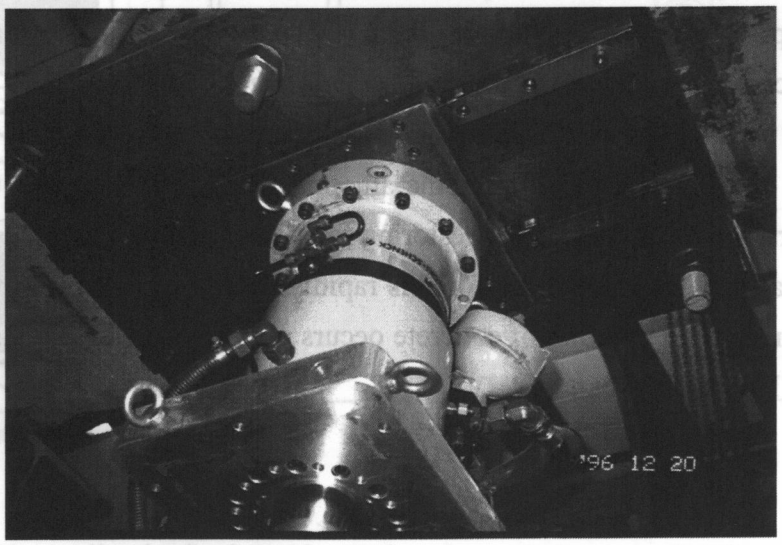

Photo 3.2: Linear Roller Way for Vertical Actuators

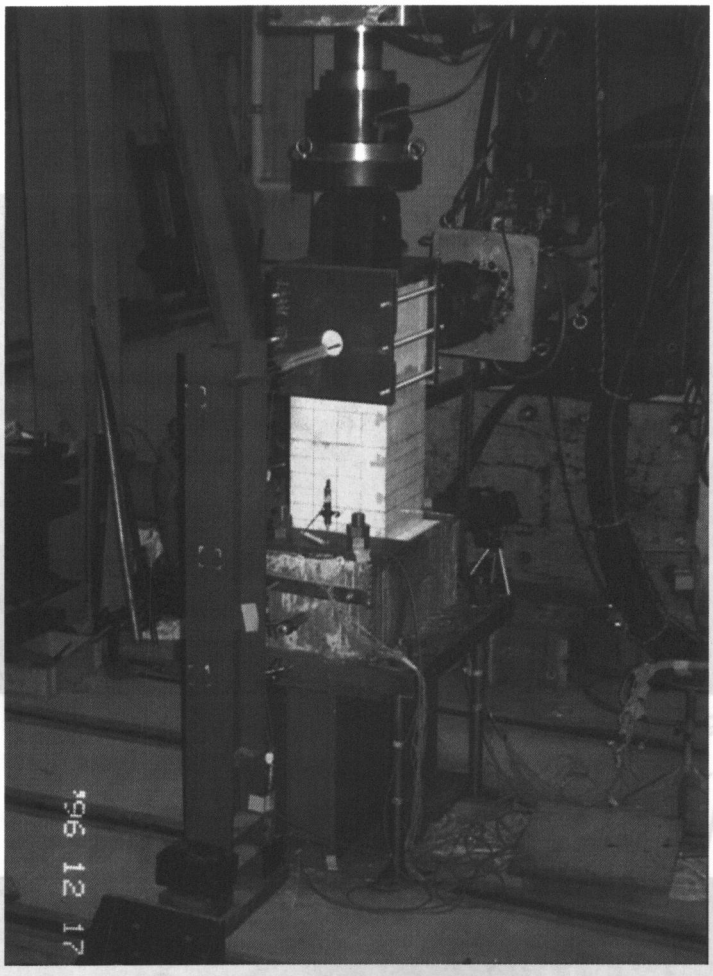

Photo 3.3: Test Setup for H2 Series

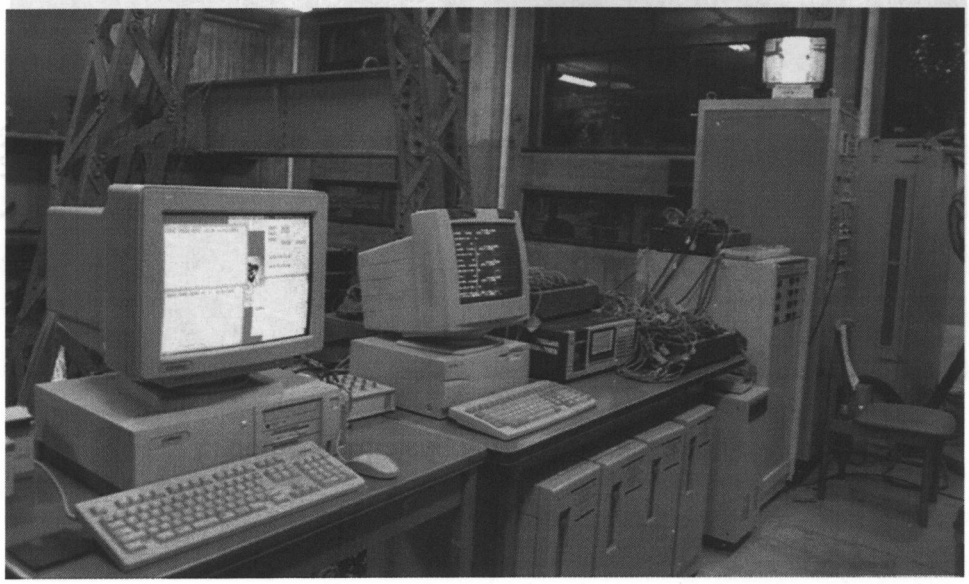

Photo 3.4: Control System

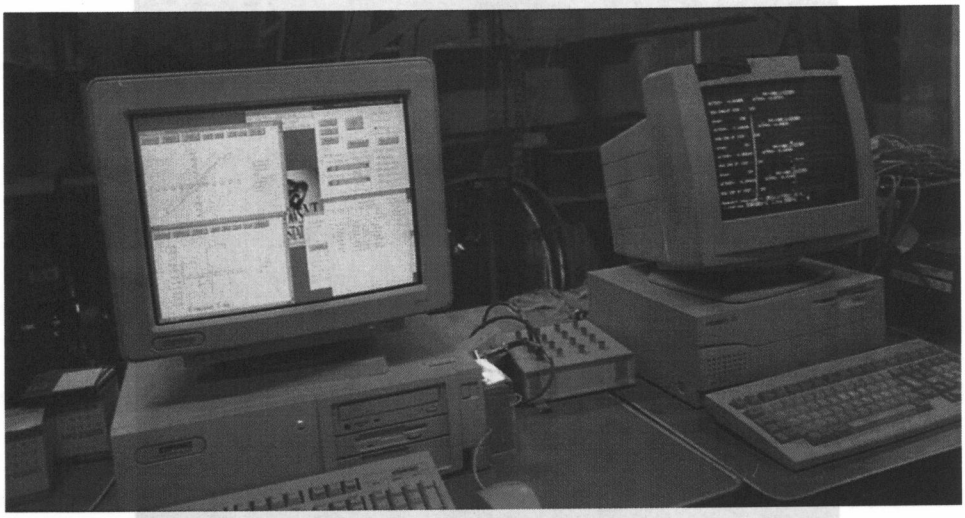

Photo 3.5: Computers for Controlling Tests

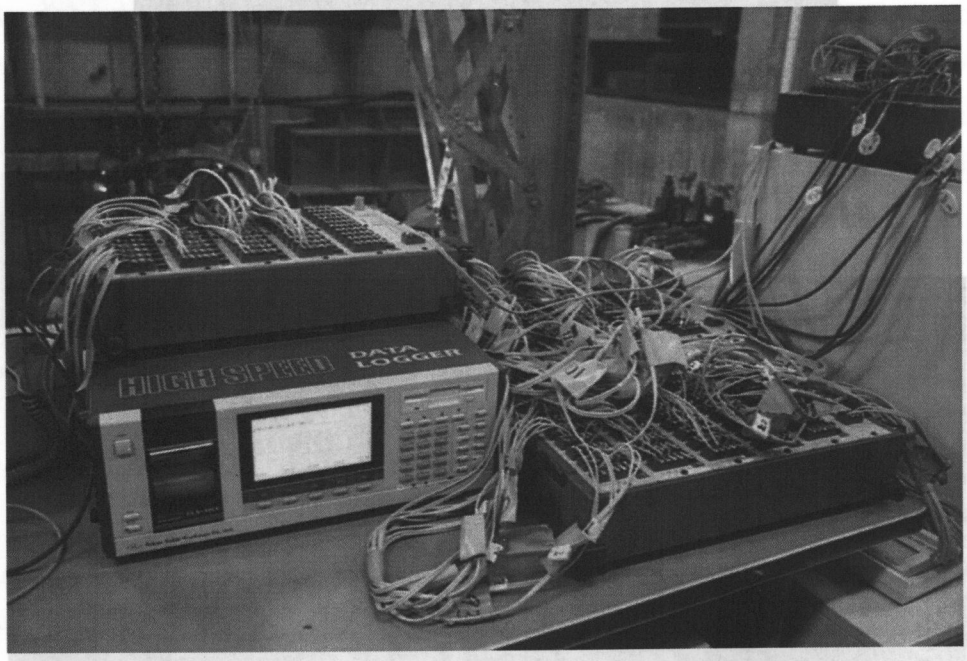

Photo 3.6: Measuring System for Strain

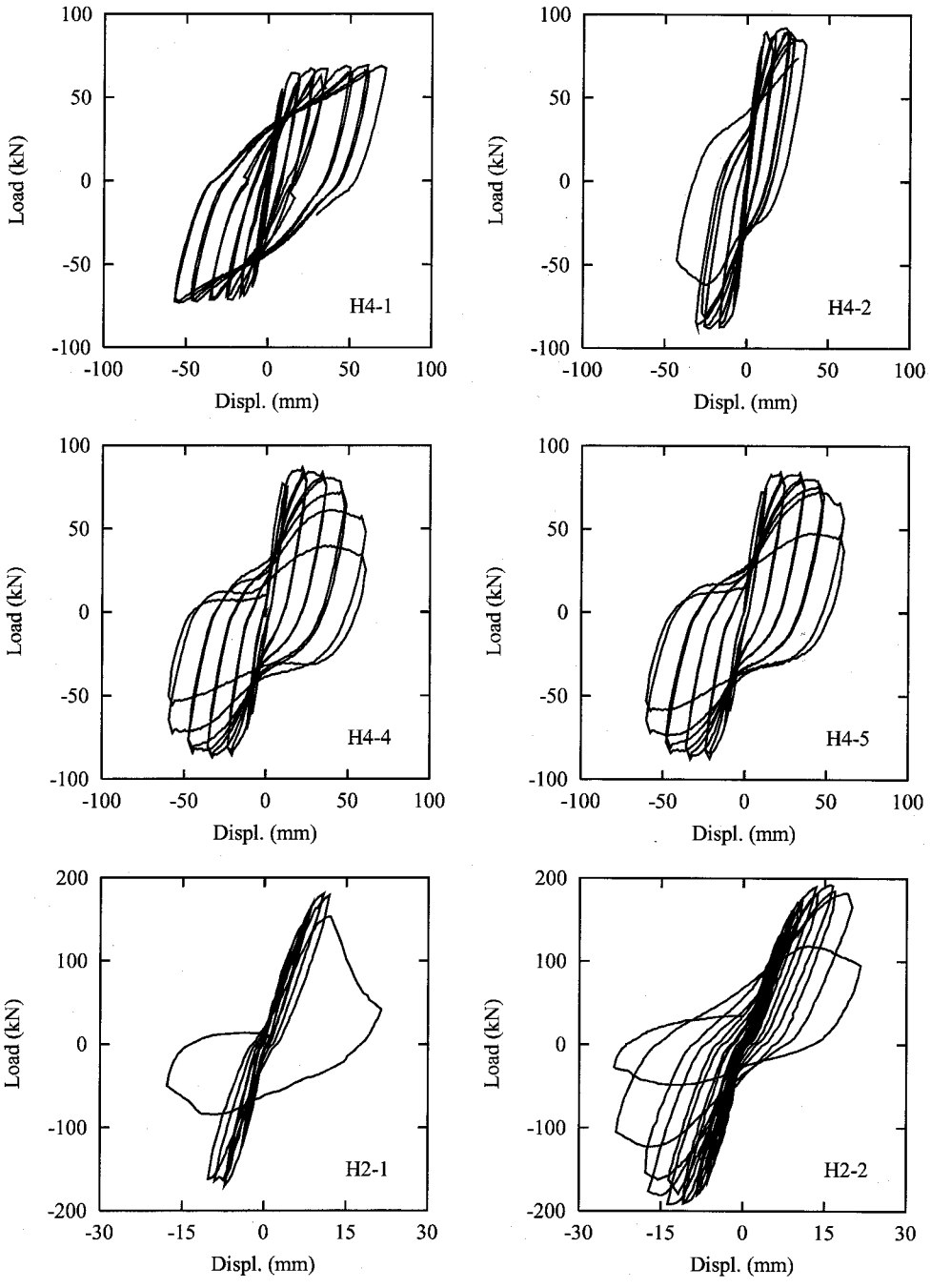

Figure 3.3: Load–Displacement Relationship

Table 3.4: Results of Static Tests of RC Piers with Hollow Section

	Yield Displ. (mm)	Maximum Load (kN)	Ultimate Displ. (mm)	Ductility Factor
H4-1	14.4	68.9	71.81	4.99
H4-2	10.2	91.9	28.90	2.83
H4-3	12.1	91.4	33.89	2.79
H4-4	9.6	86.9	41.04	4.25
H4-5	9.3	86.1	40.66	4.36
H2-1	9.1	181.7	11.88	1.31
H2-2	7.8	191.0	17.59	2.25

cusing on the crack patterns, the flexural cracks were dominant, but the diagonal cracks were observed in the web part. In H4-1 under no axial load, horizontal cracks were dominant.

In case of H2 series, the diagonal cracks were observed in the web part at an early stage of loading. Finally these columns failed in shear by about 60-degree diagonal cracks.

The characteristics of the hollow RC columns are shown in crack pattern well. That is, the flexural cracks in the flange part changed into the diagonal cracks drastically when they progressed into the web part (**Figure 3.5**). These diagonal cracks intersected under the cyclic loading, and the cracks of vertical direction generated in the center of the sections. Though this phenomenon occurs even in case of filled section, it is a particularly problematic issue when it occurs in the thin web part of hollow sections, generating large cracks of a sharp angle in case of hollow sections. These facts indicate that the influence of shear cannot be neglected in hollow piers and it is necessary to examine the shear behavior under cyclic loadings carefully.

Strain of Stirrups

The strains of stirrups at each peak of input waves are shown in **Figure 3.6**. Whereas the strains of H4 series gradually increased, the strains of H2 series became quite large from the early stage of the loading. This result also means that the shear deformation was large in the H2 series. Also, the peak of strain about height of 25 cm is observed. This height was just the same of the intersection of the diagonal cracks, and the width of cracks became large during the cyclic loading. It is possible to assume that this fact shows the performance deterioration by cyclic loading from the viewpoint of the stirrup strain, too.

Compared H4-3 with H4-4, the strains of H4-3 which had low amount of stirrup were small. In the test, it is observed that the longitudinal bars of H4-3 were buckled between

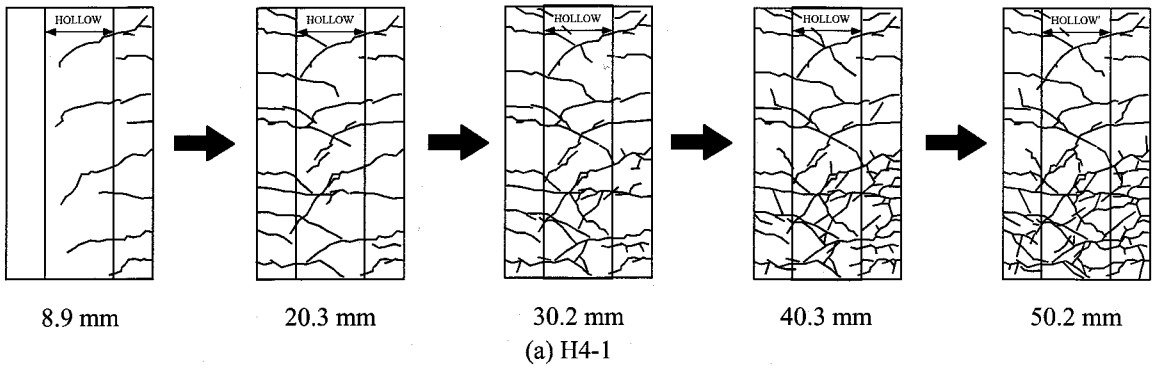

(a) H4-1

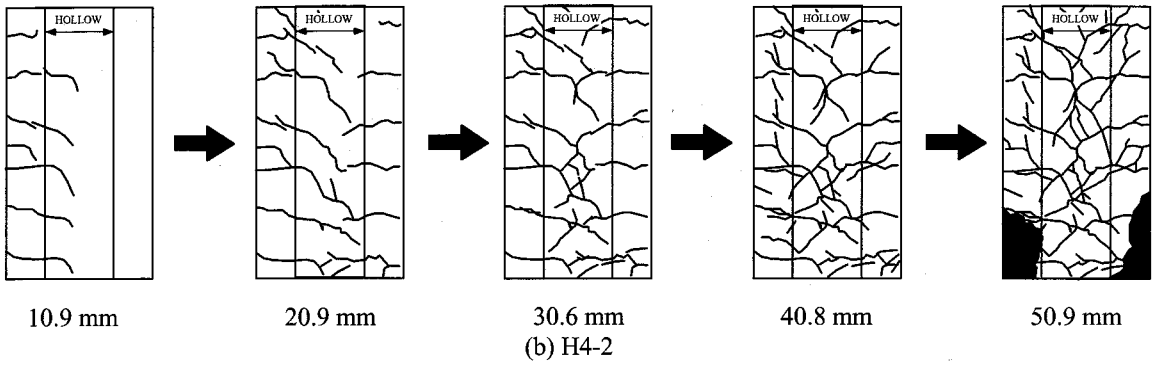

(b) H4-2

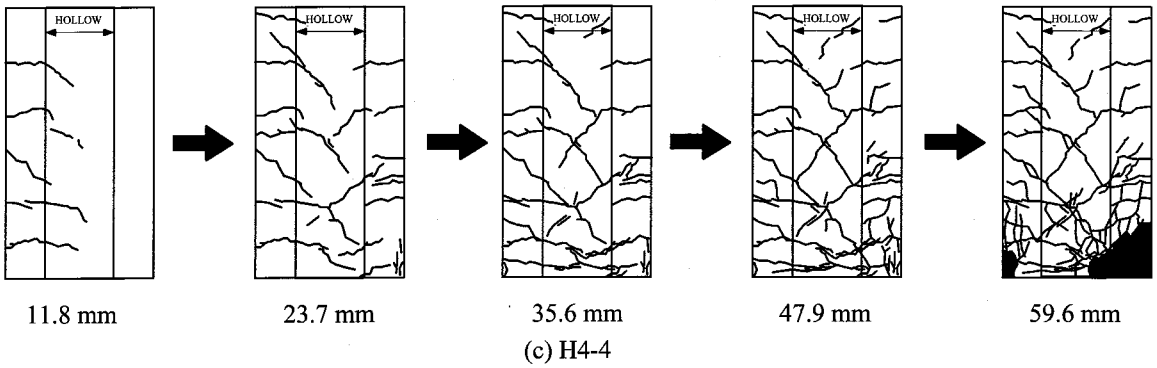

(c) H4-4

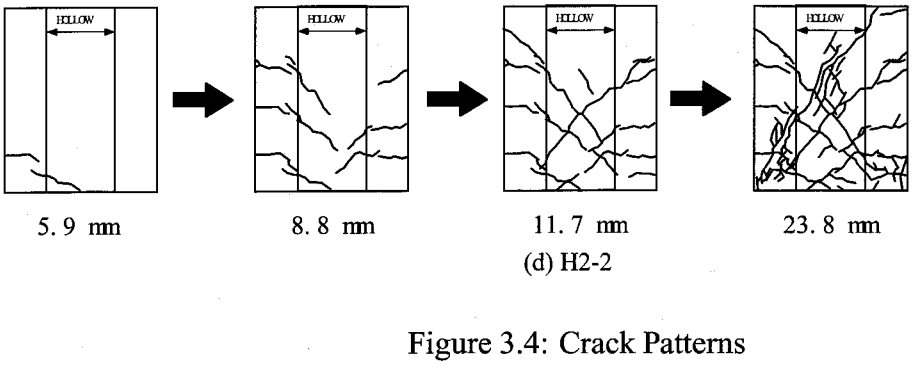

(d) H2-2

Figure 3.4: Crack Patterns

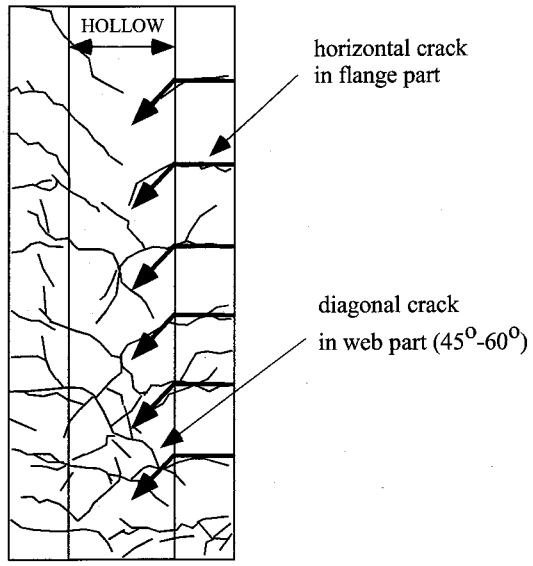

Figure 3.5: Crack Pattern (H4-2)

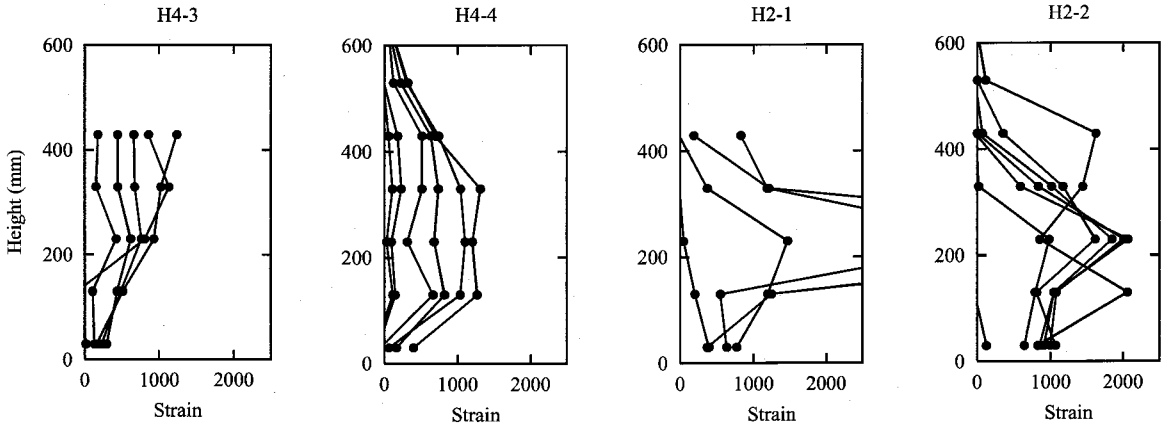

Figure 3.6: Strain of Stirrups

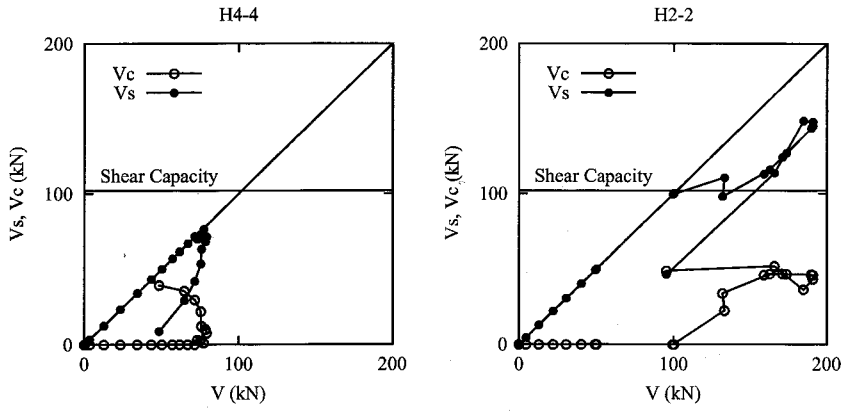

Figure 3.7: Shear Force of Concrete and Stirrup

stirrup intervals. Therefore it seemed that the ultimate state of H4-3 is caused by the buckling of longitudinal bars, and the stirrups couldn't exhibit the performance effectively.

Shear Capacity

In the JSCE Standard Specification for Design and Construction of Concrete Structures (JSCE Code)[6], the design shear capacity of RC members (Vyd) is defined as the summation of the design shear capacity of concrete without shear reinforcement (Vcd) and the design shear capacity carried by transverse reinforcement (Vsd). Also, after the crack occurrence, Vcd is constant and the increment of shear force is resisted by the transverse reinforcements. **Figure 3.7** shows the sharing ratio of the concrete contribution (Vc) and the stirrup contribution (Vs) to the applied shear force (V), in which the Vc is simply calculated by subtracting Vs estimated based on the stirrup strain from the applied shear force. The design shear capacity of these specimens is 102 kN (Vc = 56.1 kN, Vs = 45.9 kN).

As for H4-4, the shear force of experiment was less than the shear capacity, but this is because this specimen failed in flexure. On the other hand, the shear force of H2-2 is larger than the design capacity. But around the ultimate state, the resistant load decreased rapidly and finally became smaller than the design load. This phenomenon is remarkable in case of cyclic loading state. Therefore it is necessary to establish the rational shear design method considering the deterioration of concrete shear resistance due to cyclic loading, especially earthquake loading.

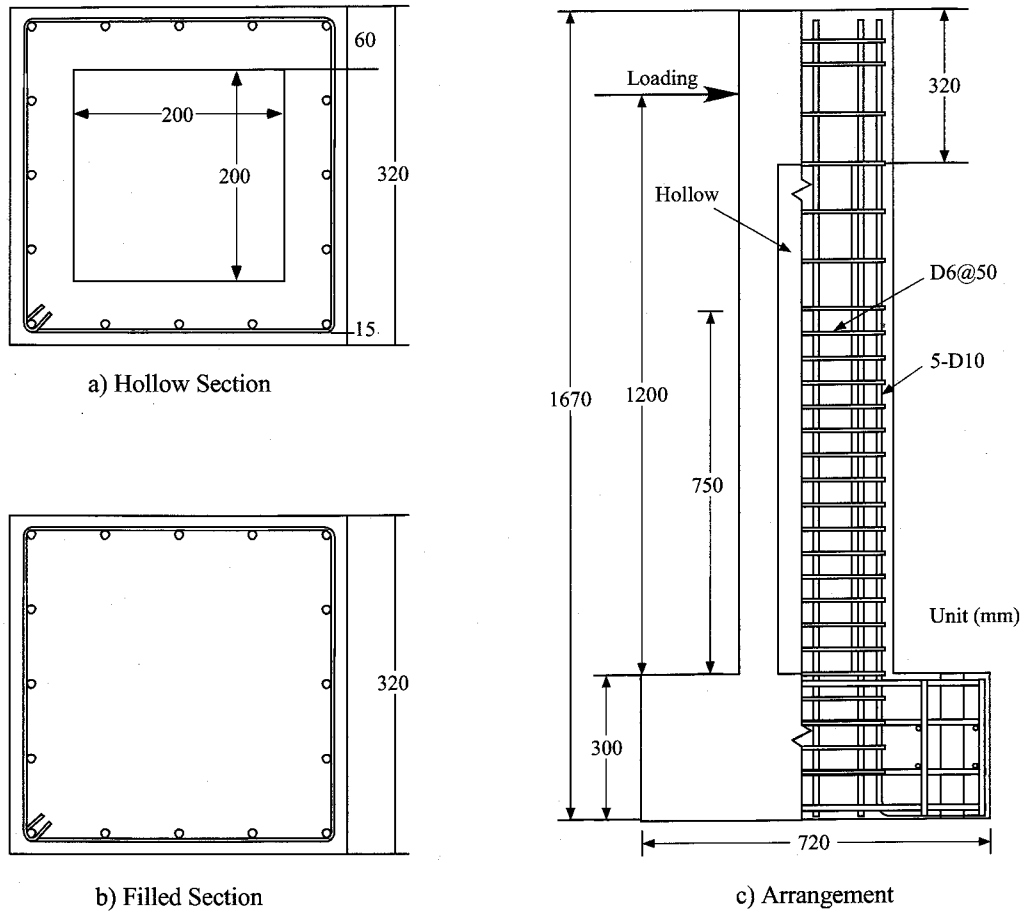

Figure 3.8: Cross Section of Specimen

3.2.2 Evaluation on Deformation Components

Outline

As mentioned in the previous section, it became clear that the RC pier with hollow section cannot neglect the effect by the shear behavior, and that especially it is necessary to pay attention to the deterioration of shear resistance due to cyclic loading. These facts are also indicated by previous researchers, but these facts were based on the load–displacement relationships and the crack pattern, and no studies have been tried to measure the shear deformation directly. Therefore, in this section, cyclic loading tests of hollow RC columns with potentiometers were carried out, and the three components, the flexural, the shear and the rotational components were measured.

The hollow RC specimens had the section dimension, which was a 320 mm square cross section with 60 mm thick walls (**Figure 3.8**(a)). In order to emphasize the effect of on the hollow section, the specimens of this study (H4-6 ~ H4-8) had the thinner web than **Figure 3.1**. Furthermore the specimens didn't have the stirrup on inside face. H4-8 was designed so that the shear capacity may be smaller than the flexural capacity. In addition,

Table 3.5: Parameter of Specimen

	Section Shape	Flexural Capacity (kN)	Shear Capacity (kN)	Repetition (cycles)
H4-6	Hollow	78.	125.	10
H4-7				3
H4-8		76.	40.	
F4-1	Filled	79.	146.	

a pier model with filled section (F4-1) was also made for the comparison (**Figure 3.8**(b)). Here, the first character of the name "F" denotes the filled section. Compared it with the others, the difference of the failure mode due to the cross-sectional shape is also examined.

The axial load of 3.7 MPa was applied to the specimens. The horizontal displacement was imposed at a quasi-static ratio in cycles to displacement ductility factor each of $\mu = \pm 1, \pm 2$, etc, until premature failure of the specimens caused. In order to examine the effect of earthquake characteristics such as Type I and Type II earthquake, in this study, the number of repetition of the constant amplitude in the loading wave was selected as a test parameter

The test parameters of specimens were the cross-sectional shape, the shear capacity and the repetition of the loading (**Table 3.5**). In the Seismic Design Specification of Highway Bridges[7], the 10 times repetition in cyclic loading tests means the Type I earthquakes (plate boundary earthquakes) and the 3 times repetition means the Type II earthquakes (inland direct strike earthquakes).

Instrumentation

The shear deformation was measured by the potentiometers between embedded marks in the front of columns and the flexural deformation was measured by the potentiometers attached to the sides. The displacement of the pull-out of the longitudinal bars from the footing was measured by the bottom potentiometers attached to the sides. And the load and the displacement at the loading point, the strain of longitudinal bars and stirrups were also measured (**Figure 3.9**, **Photo 3.7**, **Photo 3.8**).

Calculation of Deformation Components

The deformation of piers, δ, is composed of the flexural component δ_f, the shear component δ_s and the rotational component δ_r.

$$\delta = \delta_f + \delta_s + \delta_r \tag{3.1}$$

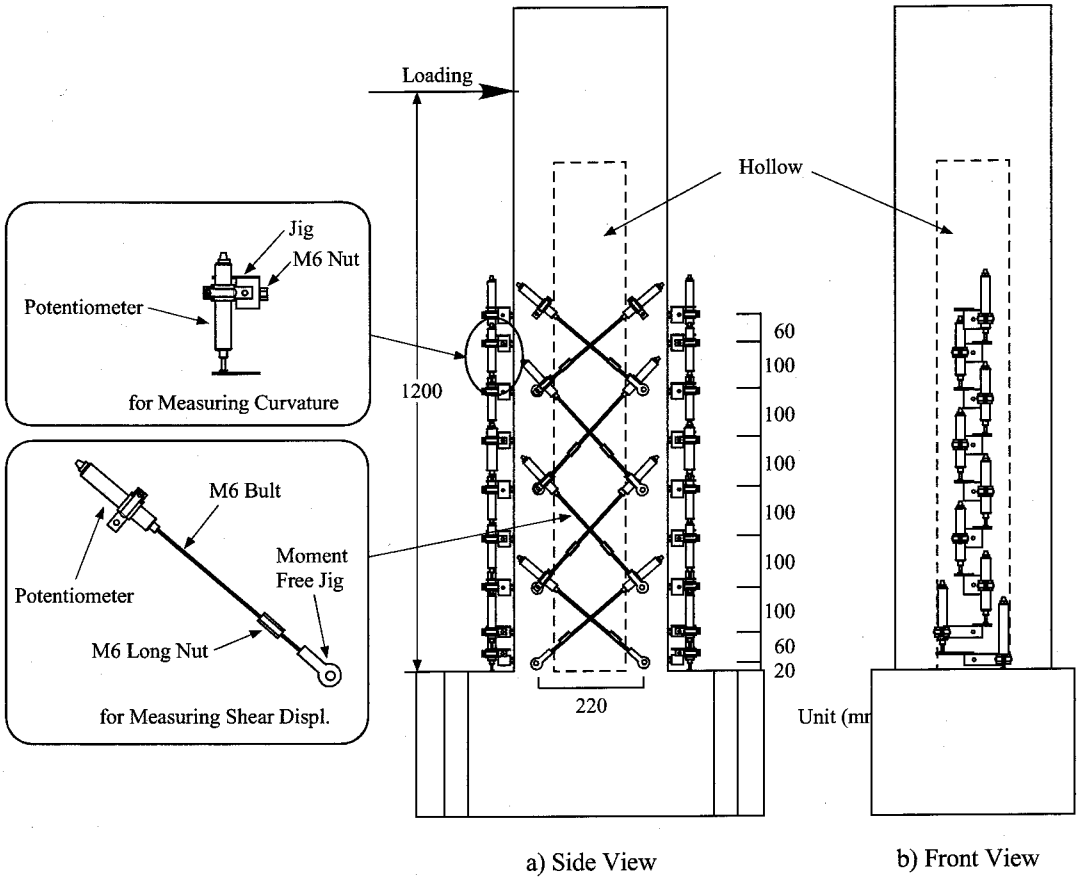

Figure 3.9: Arrangement of Potentiometers

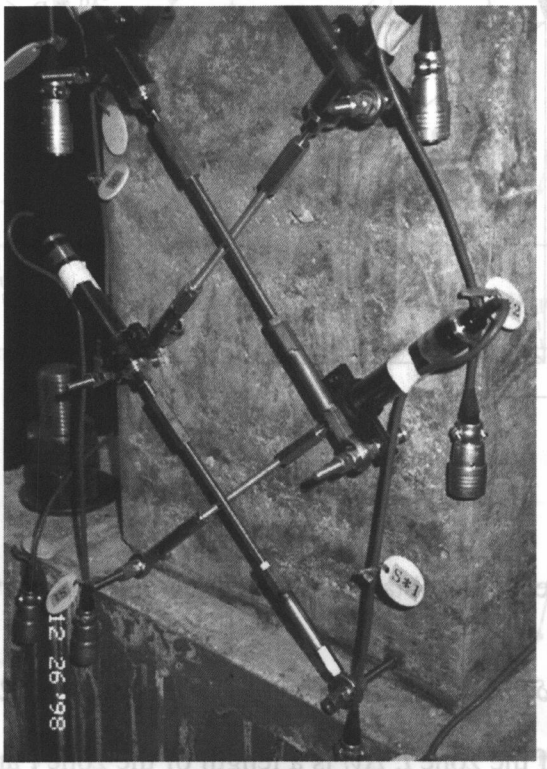

Photo 3.7: Potentiometers for measuring shear deformation

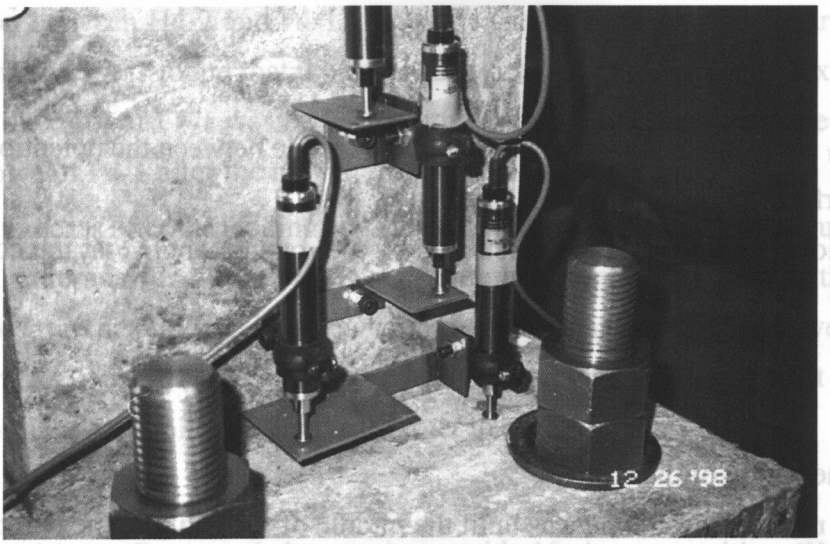

Photo 3.8: Potentiometers for measuring flexural deformation

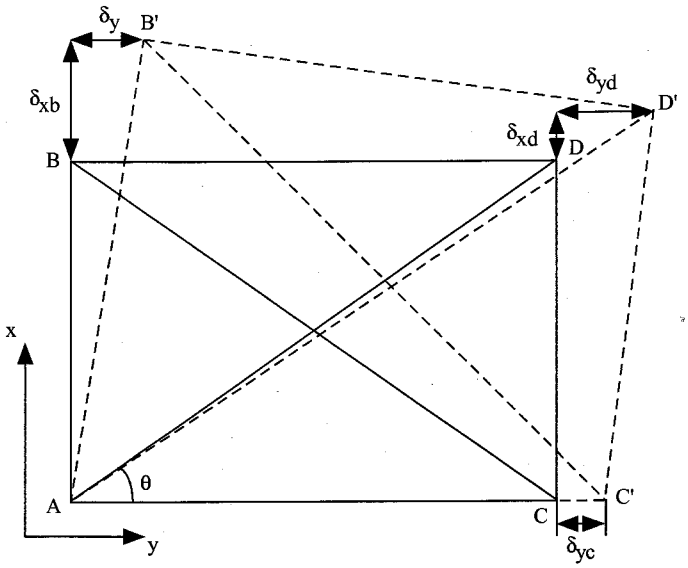

Figure 3.10: Shear Deformation

The flexural component δ_f is obtained by the integral of the curvature.

$$\delta_f = \int \phi \cdot y dy = \sum (\phi_i y_i + \phi_{i-1} y_{i-1}) \Delta y_i / 2 \tag{3.2}$$

where ϕ is a curvature of the zone i, Δy_i is a length of the zone i and y_i is a distance of i-th section from the loading point.

According to the research of Maeda et al.[8], the shear component δ_s is calculated by the following equation, which is derived from the geometric relationship in **Figure 3.10**.

$$\delta_s = (\Delta_{1i} - \Delta_{2i}) / 2 \cos\theta_i \tag{3.3}$$

where Δ_{1i}, Δ_{2i} are a diagonal displacements, θ_i is an angle between the potentiometer and the horizontal surface.

The rotational component δ_r is calculated by the rotation angle θ at the column base as following.

$$\delta_r = H \cdot \theta \tag{3.4}$$

where H is the height of the column.

Since the measurement zone was until the middle of the column, the deformation of the upper part is calculated estimating the elastic behavior.

Experimental Results

The skeleton curves of the specimens are shown in **Figure 3.11**.

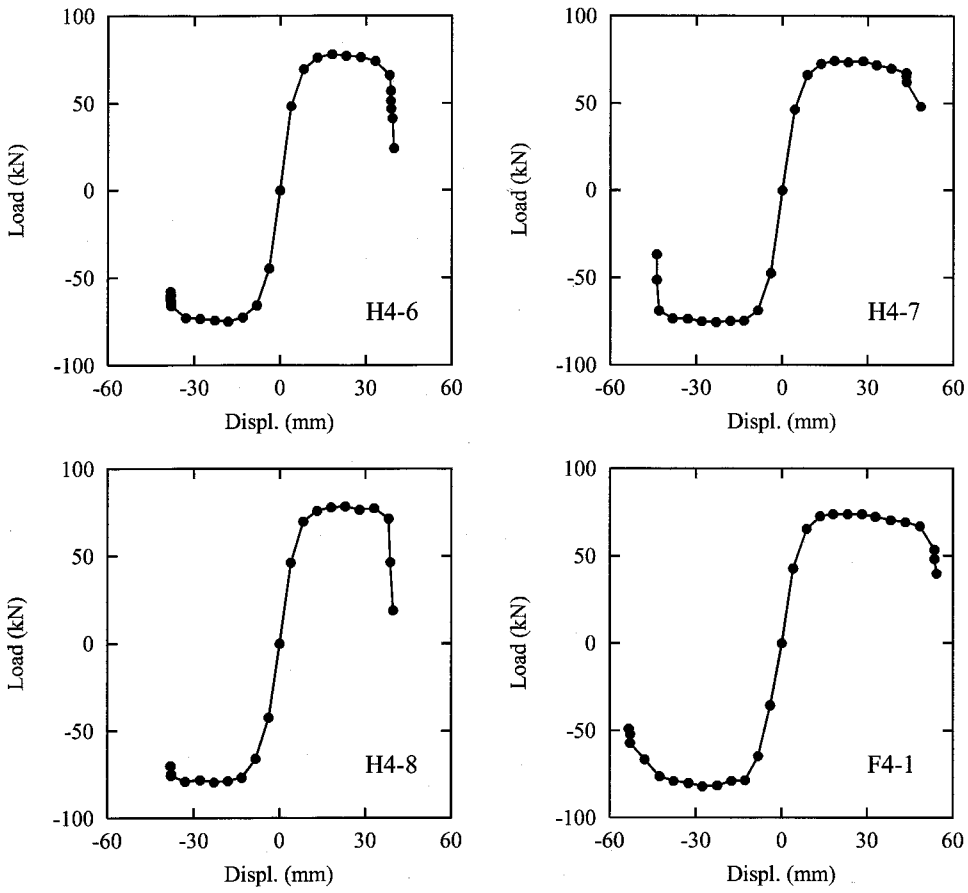

Figure 3.11: Skeleton Curve

Effect of Cross-Sectional Shape The effect of the cross-sectional shape is indicated by the comparison between H4-7 and F4-1. From the skeleton curves, the flexural capacity is almost the same, and it is found that the hollow specimen had the efficient flexural capacity. However, the ductility of F4-1 was larger than that of H4-7. Furthermore, the deterioration of restoring force of F4-1 after the maximum state was more gradual.

The crack patterns after the loading are shown in **Figure 3.12**. From the figure, it is found that the crack patterns of H4-7 and F4-1 were different in spite that both of them failed in flexure. In H4-7, the flexural cracks changed into the diagonal cracks in the web part, while the flexural cracks of F4-1 kept horizontal when they progressed. This result suggests that the shear deformation of hollow columns is larger than that of filled columns.

Effect of Repetition Compared the specimen with 10 times repetition (H4-6) with the specimen with 3 times repetition (H4-7), it is found that H4-6 deteriorated rapidly. And although the large difference could not be seen in their failure mode, the progress of the cracks in H4-6 was accelerated by the repetition, this caused the early ultimate state. These results were obtained from the results of filled section specimens. But because of the thin

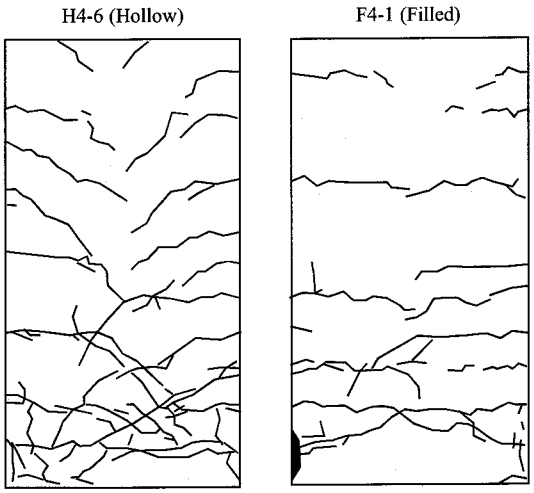

Figure 3.12: Crack Patterns

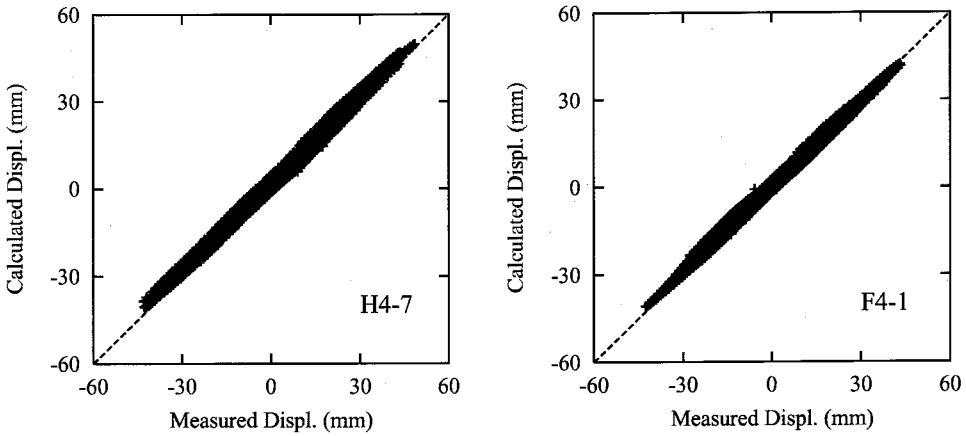

Figure 3.13: Precision of Separation of Deformation

web, this phenomenon becomes serious for the hollow columns. Therefore for tall piers with hollow section, we have to pay attention to the Type I earthquakes.

Transition of Each Deformation Components At first, the precision of separating deformations is shown in **Figure 3.13**. The x-axis denotes the direct measured displacement at the loading point and the y-axis denotes the sum of the calculated by the Equation (3.1)~(3.4). Since almost all points are plotted on the diagonal line, the separation seems to be good.

To begin with, the deformations in the each every cycle is plotted in **Figure 3.14**. Here, since the repetition cycle of H4-6 is large, the 1st, 5th and 10th cycles are extracted and plotted in order to compare with the others. As a general tendency, each component volume increases during the loading. During the repetition of the same amplitude, the shear component keeps to increase, whereas the flexural component keeps constant or decreases. It is quantitatively shown that the transition from the flexural deformation to the shear deforma-

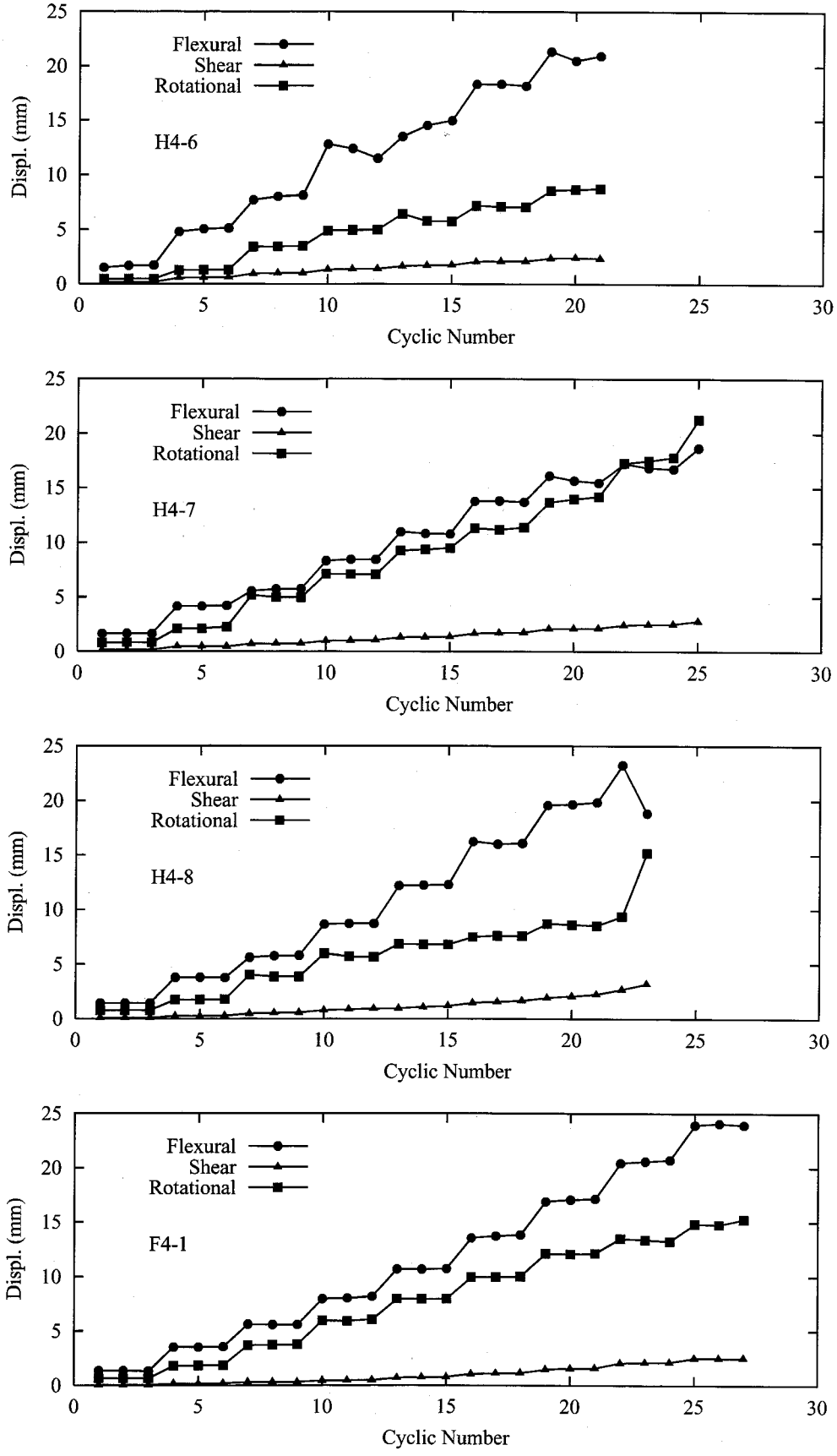

Figure 3.14: Transition of Each Component

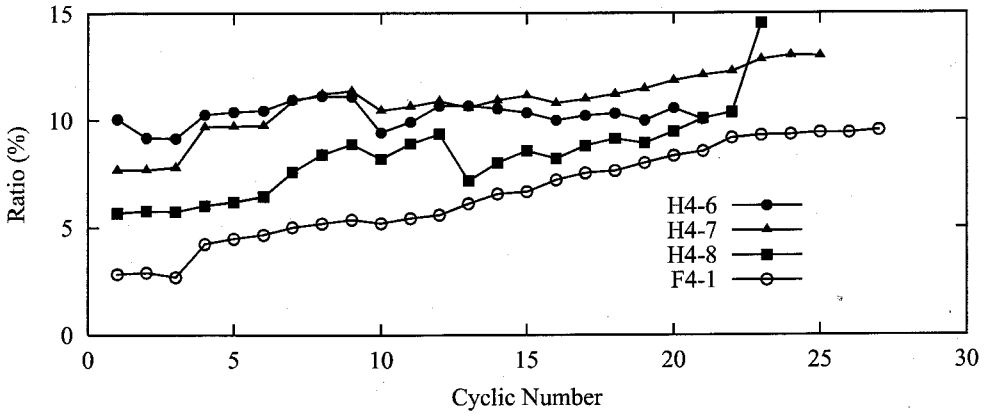

Figure 3.15: Comparison of Transition of Ratio of Shear Component

tion is induced by cyclic loadings. And, the rotational component shares large in the whole deformation, and therefore the pull-out of the longitudinal bars must take into account the evaluation of deformation of RC piers.

Next is focusing on the shear component. The ratio of the shear component to the sum of the flexural and shear components is used as the index of this study, because the shear component is quite small than the rotational one. The transition of the shear component of each specimen are compared in **Figure 3.15**. To begin with, it is found that the ratio of the shear component in the filled specimen (white circle) is smaller than the other hollow specimens (black points), and this result agrees with the engineering intuition.

And it is also found that in case of hollow section, the ratio of the shear component is large in the early loading stage, but that it only increases slightly during the loading. The reason for the moderate increase of the ratio is that the final failure is dominated by the flexural deformation because these specimens were failed in flexure. On the other hand, in case of H4-8 which failed in shear, there is a steep increase and in case of F4-1, it is small in the early loading stage, but increases with the progress of the loading and finally increases up to the 10 % of the deformation.

3.3 Seismic Response of RC Tall Pier with Hollow Section

3.3.1 General Remarks

Although several research on the seismic response of bridge piers with hollow section has been made, almost all of them were based on the static cyclic loading tests or the numerical analysis. However, as mentioned in previous section, since the failure mechanism of RC hollow piers is complicated, various assumptions have to be considered in the numerical analysis. Therefore, in this section, in order to investigate the real seismic behavior of RC

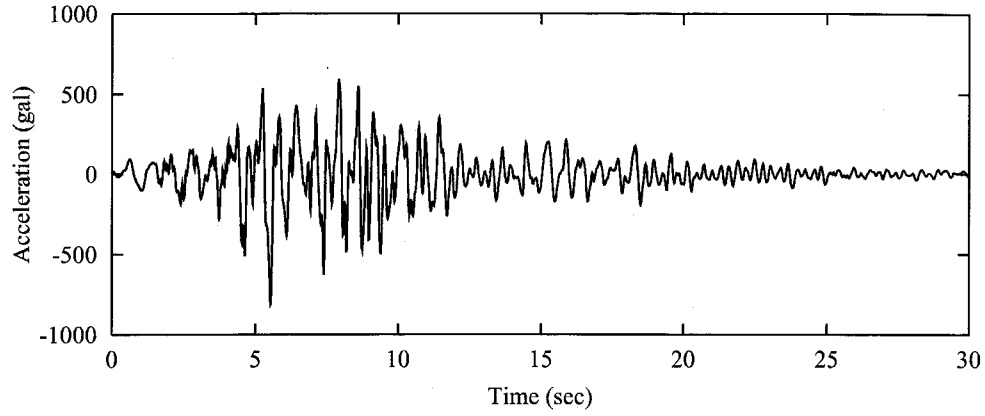

Figure 3.16: Input Earthquake Motion (Type II)

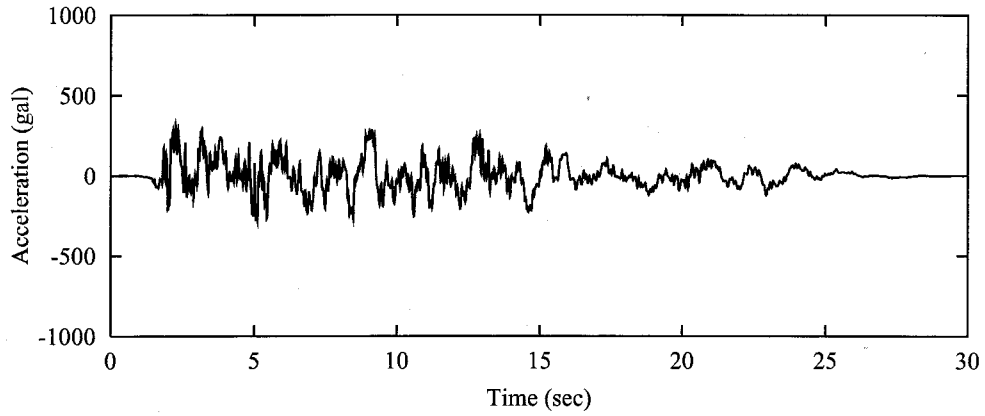

Figure 3.17: Input Earthquake Motion (Type I)

hollow piers, the hybrid earthquake loading tests were carried out.

At first, in order to examine the response characteristics considering an inland direct strike earthquake (Type II earthquake), the Kobe JMA record (NS direction) (**Figure 3.16**) in the 1995 Hyogo-ken Nanbu Earthquake was inputted into the specimen. In usual cyclic loading tests, the gradual increasing input wave is used. But an inland direct strike earthquake, like the Kobe JMA record, shows a very strong power in the beginning of the motion. Therefore the main aim of this test is to investigate the response characteristics with an initial large deformation using real response history due to the Kobe JMA record.

Second, in order to investigate the seismic performance of tall piers with hollow section designed by the seismic intensity method, the hybrid earthquake loading tests considering the similarity law were carried out. Since the tall pier has the long natural period, the Kaihokukyo record (LG direction) (**Figure 3.17**) in the 1978 Miyagiken-oki Earthquake was also used in addition to the Kobe JMA record. This earthquake is used as a plate boundary earthquake (Type I earthquake).

3.3.2 Hybrid Earthquake Loading Test Methods

The hybrid earthquake loading test (or pseudo dynamic test) is a computer-controlled experimental technique in which direct step-by-step time integration is used to solve the equations of motion. The hybrid loading test has been used to test structures that exceed the size, strength or weight limits to test on shaking tables while using only the test equipments as in static cyclic loading tests. With the test, the following characteristics are verified:

- Durability and stability against earthquake
- Residual displacement requirements
- Energy dissipation under earthquake

And considering the similarity law, this test method can evaluate the real response of structures[9]. Several techniques have been proposed, and in this study, the similarity law of the frequency characteristics is adopted. In this technique, the frequency characteristics of the model is considered to be the same as that of the real structure, and the equation of motion of the model is solved in the computer. According to this similarity law, when the length ratio of the actual bridge to the specimen is S, the amplitude of the input earthquake motion should be set to be 1/S and the time scale is the same between them. Since the response analysis in the model properties is carried out, the response of the real structure can be obtained by the results applying the similarity law.

3.3.3 Response Characteristics with Initial Large Deformation

Outline

In this test, focusing on the loading history, the failure by earthquakes is compared with the results of the cyclic loading tests. Therefore the same specimen of Section 3.2.1 was used in this test.

The specimen had a span length of 1200 mm and a spacing of stirrup of 50 mm. In the hybrid loading test, this specimen was assumed to be designed as the tall pier which natural period is 2.0 sec. The other parameters were decided from the results of the static loading tests. The damping coefficient in the numerical analysis part was set to 0.01. And, the test is carried out in about 5 minutes, and it becomes a loading rate of about 1/10 for real time.

As an input earthquake motion, the Kobe JMA record (Type II) was used. To evaluate the seismic performance after the large deformation, the input motion was adjusted to 13 % amplitude of the original wave.

Experimental Results

Load–Displacement Hysteresis and Time Histories The load–displacement hysteresis loops, the acceleration and the displacement time histories are shown in **Figure 3.18**. And, in the diagram of the hysteresis loops, the skeleton curve of H4-3 in cyclic loading test is also shown.

In the hysteresis loop of the hybrid loading test, the specimen exhibited the stable response although it had responded up to the ultimate state. But the restoring force in the negative displacement side was smaller than that in the positive side. It seems to be a reason that in the positive side the pier responded up to the ultimate state at once whereas in the negative side the deformation gradually increases. It is similar that the restoring force in the push-over loading test exhibits to be larger than that in the cyclic loading test. As Kawashima et al. pointed out[10], the loading history has the great influence on the performance of piers.

Crack Patterns Crack pattern after the test is shown in **Figure 3.19**. In this figure, it is found that the flexural crack didn't turn into the shear cracks even when they progressed into the web part in the hybrid loading test. This phenomenon is also related closely to the loading history. That is, in cyclic loading tests, the damage is accumulating gradually in the web part, and because of the deterioration of stiffness the influence of shear becomes larger. On the other hand, when large deformation would occur in the early stage of responses, the cracks are developing as the usual flexural cracks because the web part is still undamaged.

Comparing the results of the cyclic loading and hybrid loading tests, not only the hysteresis skeleton curve but also the crack pattern of the cyclic loading tests are different to that of the hybrid loading test of the Kobe JMA record. From this result, in order to assess the seismic performance of RC structures, especially with hollow section, it is necessary to take account with the effect of loading history of earthquakes.

3.3.4 Tests of Specimens Assuming Real Bridge

Outline

In the past researches on RC hollow piers, the specimen with only hollow section were used. However in actual bridges, the hollow piers have the filled section at their plastic hinge zone. This kind of structure can avoid the brittle failure at the bottom due to the hollow section, but the failure might occur at the connection between the hollow and the filled section at where the flexural capacity changes rapidly[11]. In this study, the hollow RC columns assuming the real bridge were constructed, and the seismic performance was examined by the hybrid earthquake loading tests considering the similarity law.

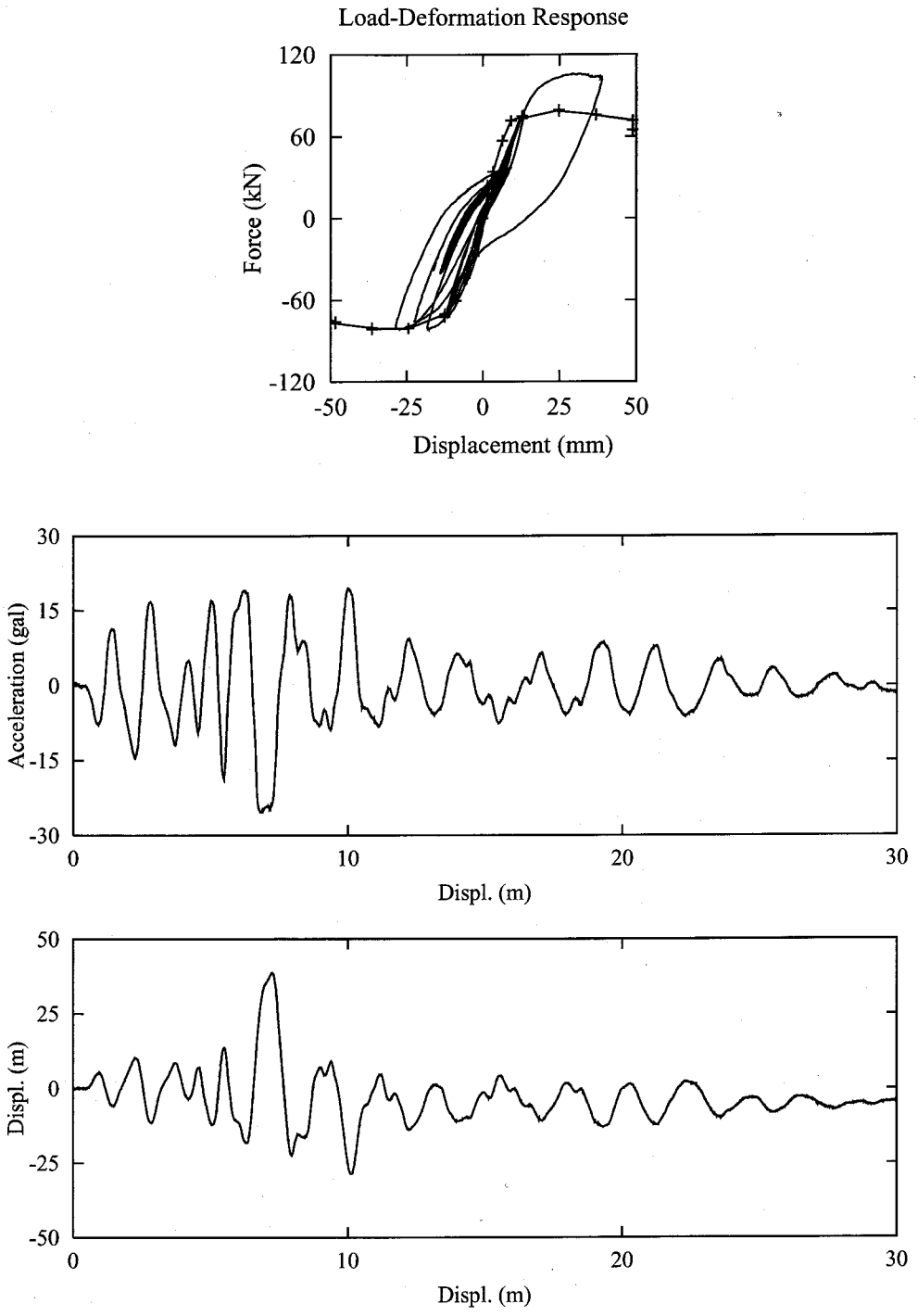

Figure 3.18: Results of Hybrid Earthquake Loading Test

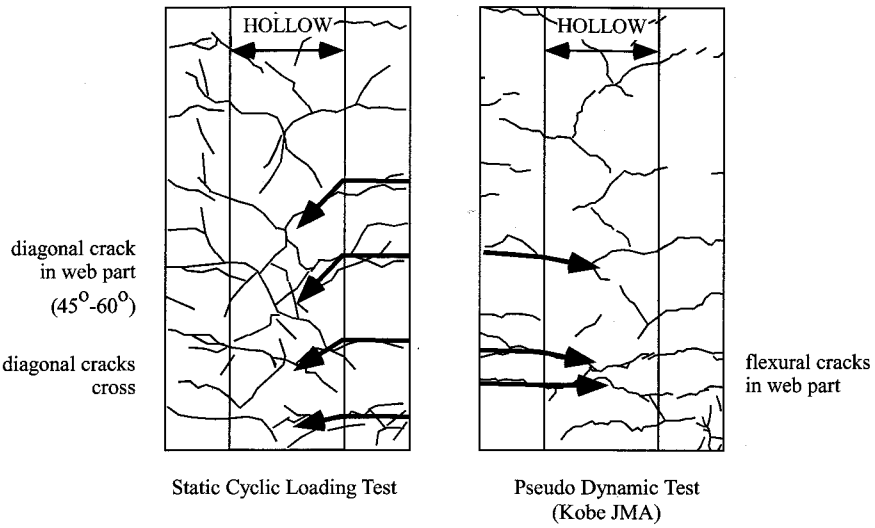

Figure 3.19: Crack Pattern

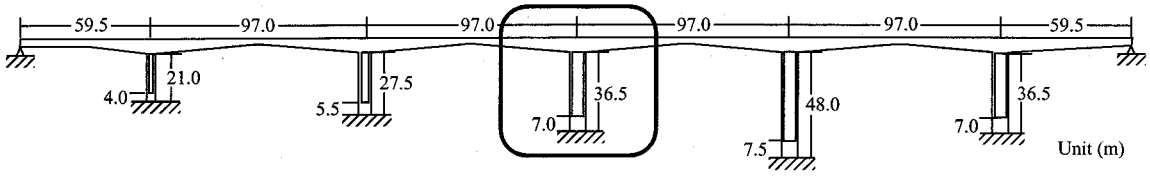

Figure 3.20: Objective Bridge

As the input earthquake motion, the Kaihoku Bridge record (Type I) and the Kobe JMA record (Type II) were used.

Assuming Real Bridge Pier and Specimens

The bridge pier of the assuming the bridge[12] is shown in **Figure 3.20**. It is the RC tall pier with hollow section, which had a 7×9 m rectangle cross section with 1.5 m thick walls and a height of 36.5 m (a/d : 5.2). This bridge was designed by the seismic intensity method in 0.25. Double of D51 and a single D32 were used as the longitudinal reinforcement. The interval of stirrup was 15 cm and the intermediate ties were arranged in the pitch of 60 cm. The weight of the superstructure was 53.8 MN and the bridge pier weight was 3.10 MN.

In this test, the specimens were constructed in the transverse direction of the bridge pier. In respect of the reinforcement ratio, the stirrup ratio and the wall-thickness ratio, specimens were designed to be almost same as the actual bridge pier. The specimen was the 1/22 scaled model, which had a 320 mm square cross section with 67 mm thick walls and a height of 1532 mm (a/d : 5.0) (**Figure 3.21**). The 6 mm diameter deformed bar (SD295) was used as the longitudinal reinforcement, and the 3 mm diameter deformed bar (SD295) was used as the stirrup. And, the plastic hinge zone of the specimen has the filled section. The

Table 3.6: Parameters of Real Bridge and Specimen

	Width of Section (m)	Shear Span (m)	Weight of Superstruct. (tf)	Weight of Pier (tf)	Ratio of Rebars (%)	Ratio of Stirrup (%)	Ratio of Wall to Section
Actual	7.0	36.5	5489.9	1167	2.99	2.25	0.214
Specimen	0.32	1.53	274	0.31	2.35	2.27	0.209

comparison between the assumed actual bridge pier and the specimen is shown in **Table 3.6**.

Based on the similarity law, time axis was scaled in 1/1, the amplitude of the input earthquake and the weight of the superstructure were scaled in 1/22.

Experimental Result

Load–Displacement Hysteresis and Time Histories The load–displacement hysteresis loops and the time histories are shown in **Figure 3.22** and **Figure 3.23**. On the hysteresis loops, the skeleton curves of results of the cyclic loading tests was shown. The test of the Type I earthquake was stopped at 15 seconds due to the accident of the equipment, but the principal response of the pier can be evaluated from this results. The results were shown in value of the actual bridge pier.

The displacement responses of both tests were almost the same in spite of the input acceleration of the Type I earthquake whose amplitude is about the half of the Type II earthquake. The value of the acceleration response spectrum of the Kaihoku Bridge record is 1037 gal around the period of 1.37 second which is the natural period of the actual bridge pier, and that of the Kobe JMA record is 1172 gal. That is to say, there is no significant difference on the acceleration response of this long-period structure like this bridge pier. It can have been confirmed experimentally that the tall piers with a long period are influenced by Type I earthquake which dominant period is a relatively long.

And, although the pier had the 6.4 m square cross section and the height of about 30 m, it has been deformed up to only 0.47 m, and in the both tests the pier exhibited the elastic response. These results tells us that the tall pier designed by the current specification is very safety against strong earthquakes such as not only the Type I earthquake but also the Type II earthquake, and it has a good seismic performance.

Failure Mode Although the displacement responses of both tests were almost the same, the difference can be observed in the failure mode, especially in the crack pattern (**Figure 3.24**). At first, in regard to the number and the region of cracks, the few cracks in the test of the

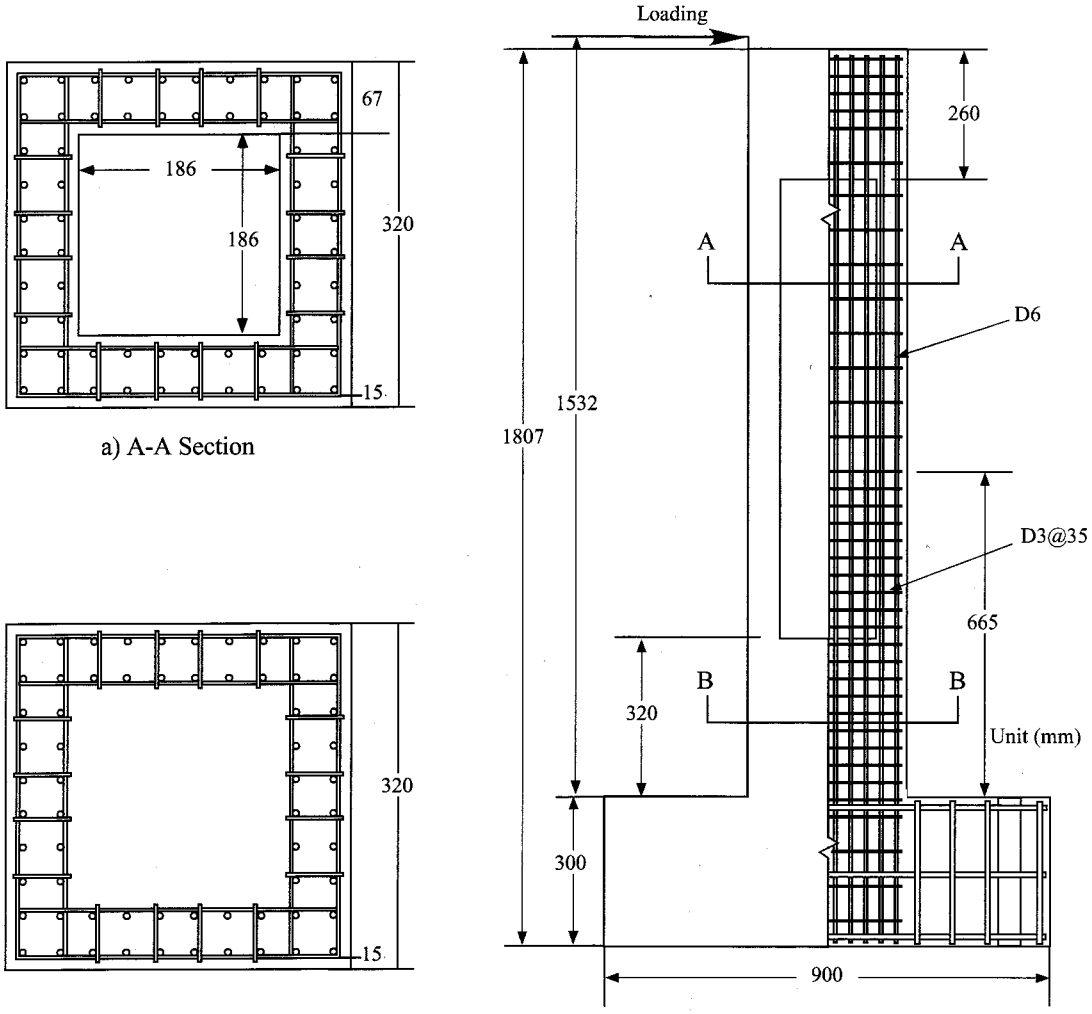

Figure 3.21: Arrangement of RC Specimen with Hollow Section

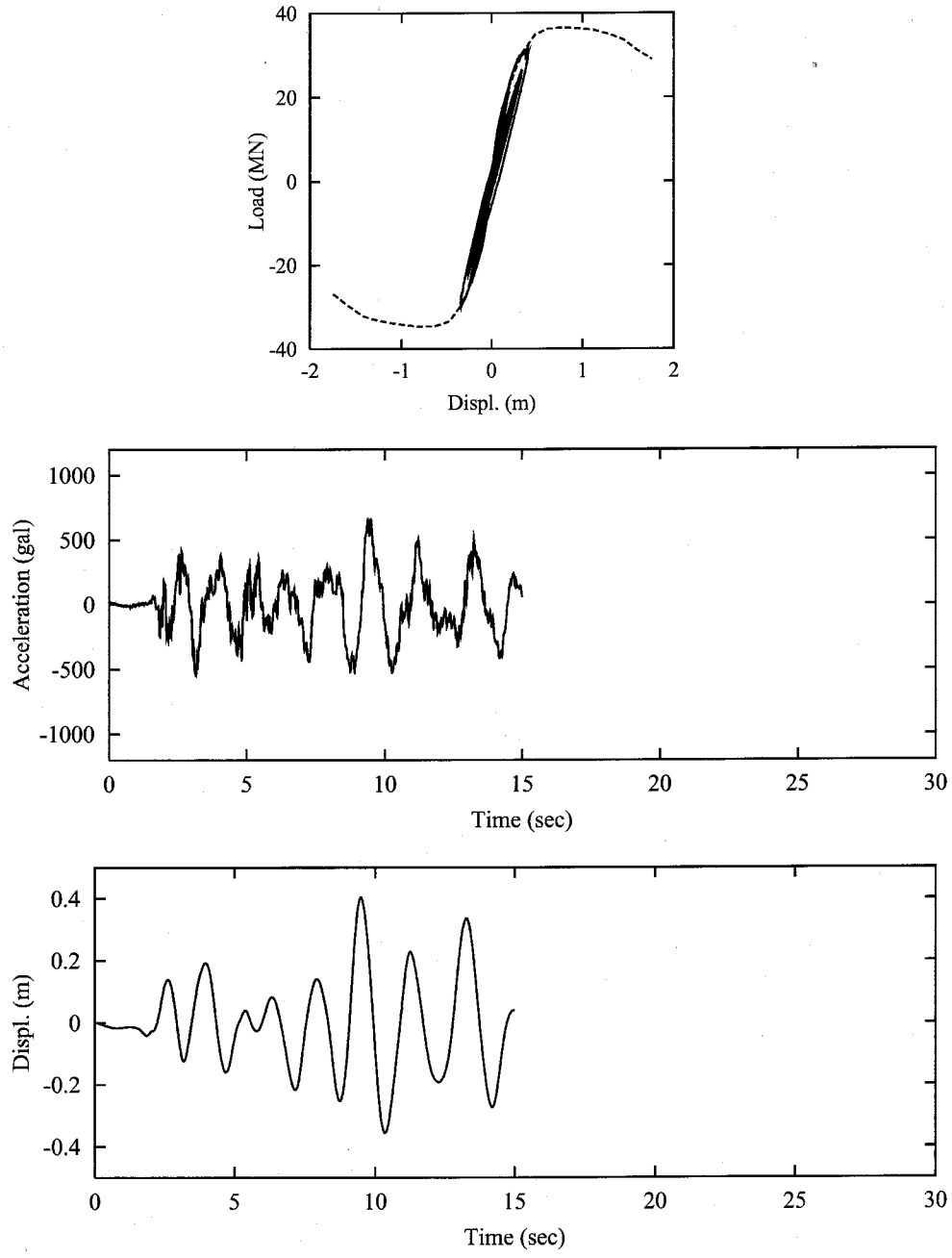

Figure 3.22: Results of Hybrid Tests (Type I Earthquake)

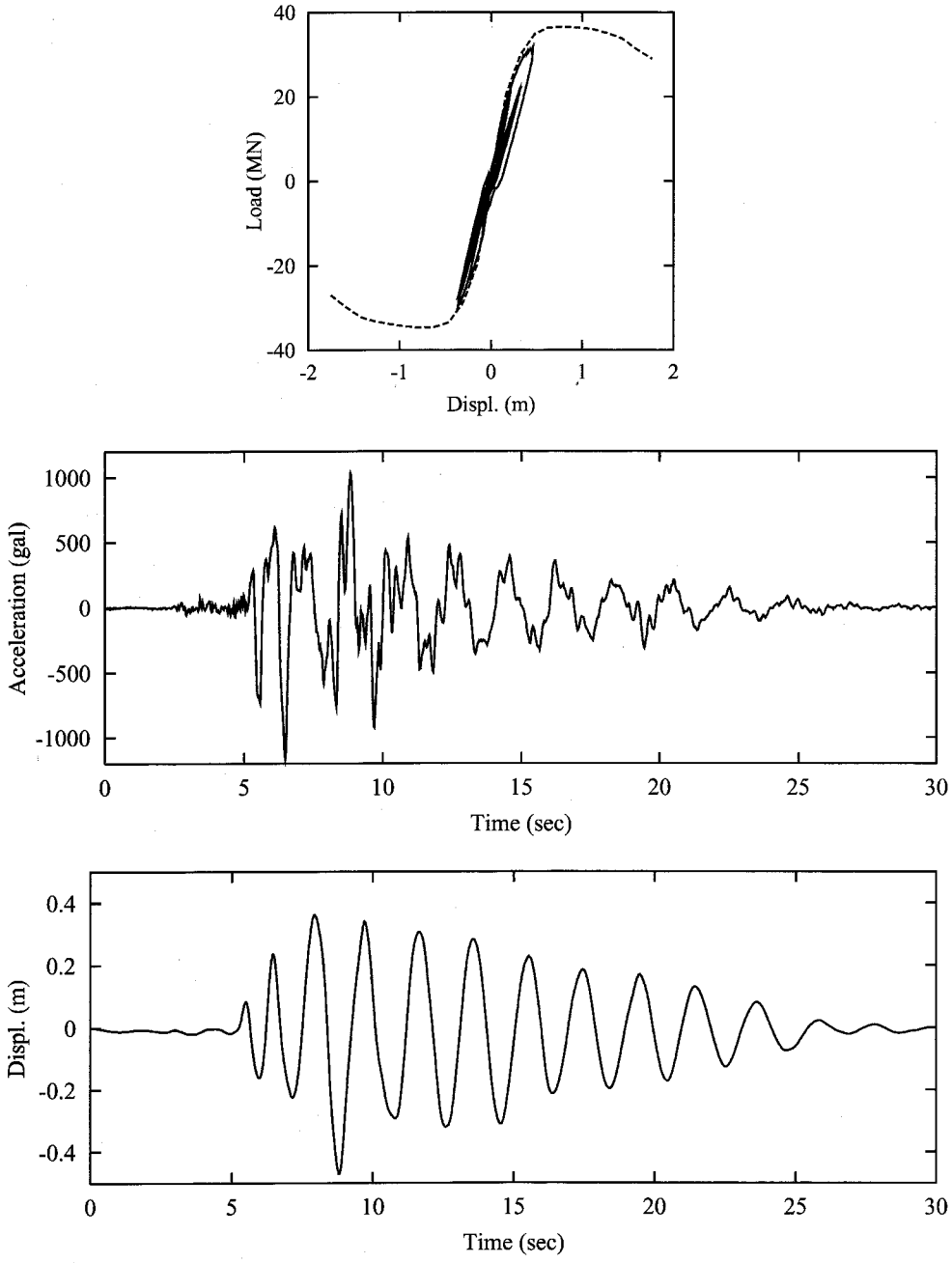

Figure 3.23: Results of Hybrid Tests (Type II Earthquake)

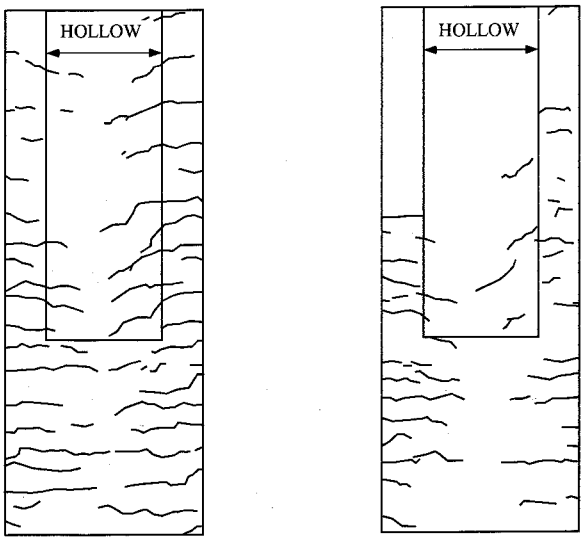

Figure 3.24: Crack Patterns in Hybrid Test

Type II earthquake only appeared in the 2D region (640 mm) above the bottom, but in the test of the Type I earthquake many cracks appeared in the 3D region (960 mm) above the bottom and the interval of cracks was almost the same. In addition, there is large difference for the cracking phenomena of right and left side in the test of the Type II earthquake. The severe crack appeared in the right side compared with the left side. On the other hand, the crack pattern of the pier under the Type I showed symmetric. It is considered that this result is affected by the characteristics of the seismic loading history of the Kobe JMA record, which might cause a large deformation in one direction.

3.4 Object-Oriented Cyclic Loading Analysis for RC Structures

3.4.1 Basic Algorithm of Cyclic Loading Analysis

The cyclic loading test is the method to force the displacement history at any point of test units. In order to simulate this test method using the multi degree of freedom system, the boundary condition is designated in terms of the combination of the displacement and the load: at the degree of freedom of the loading point, the displacement is prescribed by the loading history, and at the other degrees of freedom, the nodal point force is zero.

In this section, we make the program which takes into account various load distribution patterns, e.g. the inverse triangular pattern[13]. The objective of this problem is to find the

vector $\mathbf{d}_n^{(k)}$ which satisfies the conditions

$$\mathbf{e}^T \mathbf{d}_n^{(k)} = x_{top,n} \tag{3.5}$$

$$\mathbf{K}_{n+1}^{(k-1)}\left(\mathbf{d}_{n+1}^{(k)} - \mathbf{d}_{n+1}^{(k-1)}\right) + \mathbf{F}_{n+1}^{(k-1)} = p_{n+1}^{(k)}\mathbf{t} \tag{3.6}$$

where $\mathbf{K}_{n+1}^{(k-1)}$ is a stiffness matrix of the structure, $\mathbf{F}_{n+1}^{(k-1)}$ is a nodal force vector of the structure, $p_{n+1}^{(k)}$ is an unknown scalar value, $x_{top,n}$ is the specified top displacement, $\mathbf{t}$ is the vector which represents the loading pattern, and $\mathbf{e}$ is the vector which represents the displacement pattern. In case of the cyclic loading test which apply a loading history at the top of a structure, $\mathbf{t}, \mathbf{e} = \{0, 0, ..., 0, 1\}$. In case of the inverse triangular loading pattern, $\mathbf{t} = \{1, 2, 3, 4, ..\}$.

For the displacement increment, it is assumed that

$$\Delta\mathbf{d}^{(k)} = \mathbf{d}_{n+1}^{(k)} - \mathbf{d}_{n+1}^{(k-1)} \tag{3.7}$$

Substituting (3.7) into (3.5) and (3.5), we have

$$\mathbf{H}_{n+1}^{(k-1)}\Delta\mathbf{u}^{(k)} = \mathbf{b}_{n+1}^{(k-1)} \tag{3.8}$$

where

$$\mathbf{H}_{n+1}^{(k-1)} = \begin{bmatrix} \mathbf{K}_{n+1}^{(k-1)} & -\mathbf{t} \\ \mathbf{e}^T & \underline{0} \end{bmatrix} \tag{3.9}$$

$$\Delta\mathbf{u}^{(k)} = \begin{Bmatrix} \Delta\mathbf{d}^{(k)} \\ p_{n+1}^{(k)} \end{Bmatrix} \tag{3.10}$$

$$\mathbf{b}_{n+1}^{(k-1)} = \begin{Bmatrix} -\mathbf{F}_{n+1}^{(k-1)} \\ x_{top,n+1} - d_{n+1}^{(k-1)} \end{Bmatrix} \tag{3.11}$$

Based on (3.8), the analytical algorithm is as follows:

1. Define $\mathbf{t}$
2. Give the loading displacement of the top $x_{top,n+1}$ at time t_{n+1}
3. Make $\mathbf{H}_{n+1}^{(k-1)}$
4. Make $\mathbf{b}_{n+1}^{(k-1)}$ using the data in the previous iteration
5. Solve (3.8) and obtain the unknown increment $\Delta\mathbf{u}$ using
6. Obtain the displacement increment of the structure $\Delta\mathbf{d}$ from $\Delta\mathbf{u}$
7. Obtain the displacement vector of the structure at time t_{n+1} using the equation

$$\mathbf{d}_{n+1}^{(k)} = \mathbf{d}_{n+1}^{(k-1)} + \Delta\mathbf{d}$$

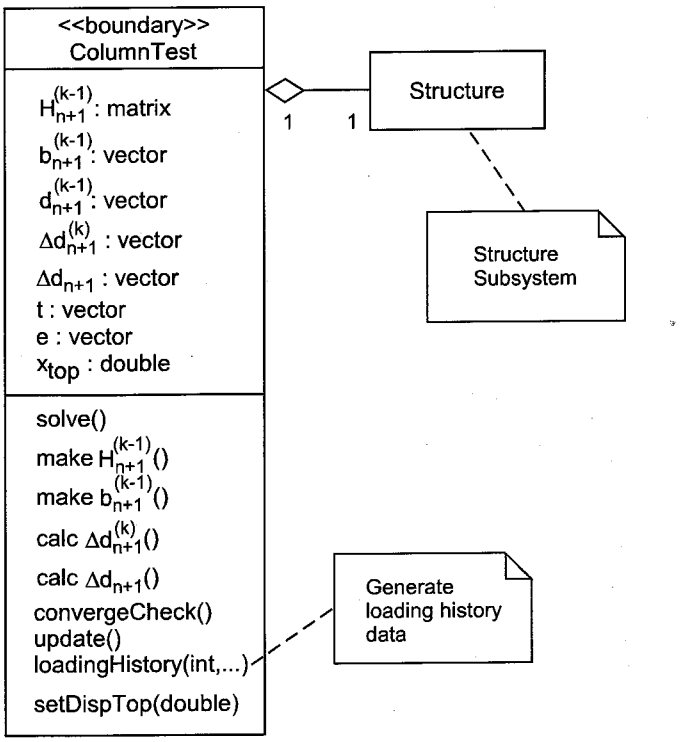

Figure 3.25: Class Diagram of Cyclic Loading Analysis

8. Convergence criteria

$$||\Delta d||_\infty < \epsilon$$

If converged, go to 2, otherwise go to 3

3.4.2 ColumnTest Object

In Chapter 2, the object-oriented structural analysis system was developed. For developing of the cyclic loading analysis for RC structures, the *Structure* subsystem can be used.

The *Structure* subsystem has already the shape of structures and the modeling methods. But the installed modeling methods are based on the displacement method. In order to simulate the cyclic loading test, the *ColumnTest* object is made. This object has a *Structure* object and calculates $\mathbf{H}_{n+1}^{(k-1)}$, $\mathbf{b}_{n+1}^{(k-1)}$, etc. using $\mathbf{K}_{n+1}^{(k-1)}$ and $\mathbf{F}_{n+1}^{(k-1)}$ of the structure, based on Eq. (3.9), (3.10), and carrys out the cyclic loading analysis according to the algorithm mentioned above.

Looking at the algorithm, it is found that the procedure is similar to the *Equation* subsystem. Since the problem is nonlinear, it is necessary to calculate the solution iteratively. Therefore as the solution method of this object, the Newton–Raphson Method is adopted. The class diagram and the sequence diagram of the *ColumnTest* are shown in **Figure 3.25** and **Figure 3.26**, respectively. Comparing **Figure 3.26** with **Figure 2.5**, it is easy to under-

stand what this object does.

The *ColumnTest* object is implemented in C++ language. The definition of class (line 7 – 37) and the main program (line 39 – 67) are shown in **Figure 3.27**. Since the *ColumnTest* object has the structural object, the *ColumnTest* object only take the sequence of the cyclic loading into account. We can get the structural data from the *Structure* object in the *ColumnTest* object.

3.4.3 Example

In order to verify the performance of the code, the cyclic loading analysis for H4-4 is carried out.

Analytical Model

As the structural model of the column, the combination of the fiber model and elastic model are used. The analytical model has seven nodes and six elements. The three element above the bottom is modeled by the fiber model, and the others are modeled by the elastic beam model. The section is divided into three layers, which are the core concrete, the cover concrete and the reinforcement layers. In the analysis, the loading histories are adjusted in order to consider the pull-out of the longitudinal bars.

Constitutive Law of Concrete

As the constitutive law for the concrete, the Ristić model is used[14] (**Figure 3.29**). This model constitutes the nine rules. This model has been implemented as the *MatConcRistic* object in the *Material* Package.

Constitutive Law of Steel

As the constitutive law for the steel, the Menegotto – Pinto model (Ristić revised version) is used[14] (**Figure 3.30**). This model can take the Bauschinger effect and the strain harding. This model has been implemented as the *MatStelRistic* object in the *Material* Package.

Results

The load–displacement hysteresis loops of this analysis and the experiment are shown in **Figure 3.31**. And the stress–strain hysteresis loops of the concrete and the reinforcement fibers are shown in **Figure 3.32**.

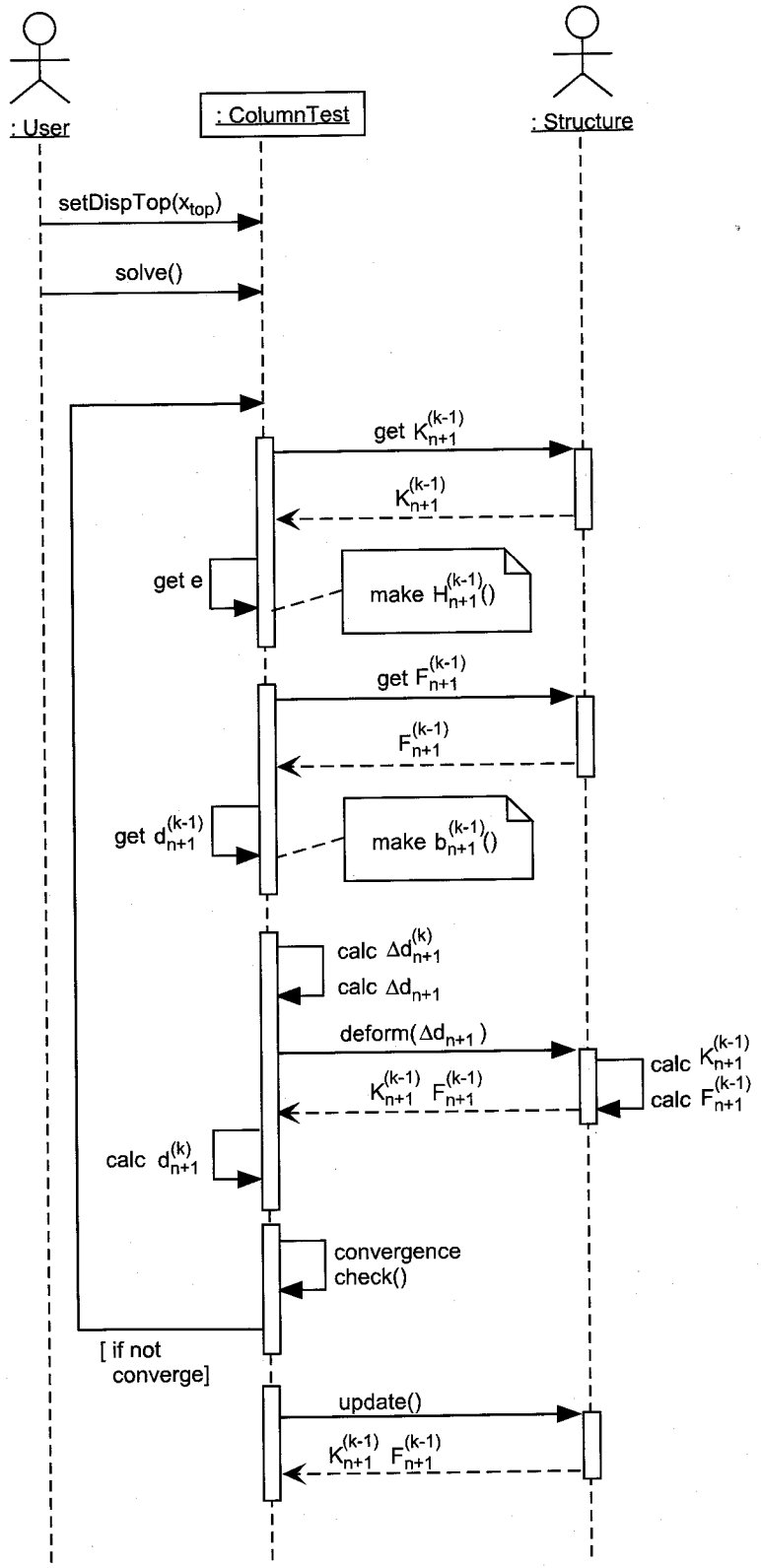

Figure 3.26: Sequence Diagram of Cyclic Loading Analysis

```
 1: #include <fstream.h>                          // read various header files
 2: #include <stdlib.h>
 3: #include <stdio.h>
 4: #include "structure.h"                        // read Structure Subsystem
 5: #include "method.h"
 6:
 7: class ColumnTest {                            // define ColumnTest object
 8: public:
 9:   ColumnTest(Structure *str);
10:   virtual ~ColumnTest() {}
11:   virtual void setUp();
12:   Gen_matrix makeH();  Gen_matrix getH();     // make H_{n+1}^{(k-1)}
13:   Col_vector makeB();  Col_vector getB();     // make b_{n+1}^{(k-1)}
14:   Col_vector calcDeltaU();                    // calc Δu^{(k)}
15:   virtual void setDeltaD(Col_vector);         // transfer Δd^{(k)} to structure
16:   void solve();                               // solve d_{n+1}^{(k)}
17:   int convergenceCheck();
18:   virtual void update();
19:   Col_vector setAxialLoad(double ax);         // set axial load
20:   double setDispTop(double x);                // set displacement at top
21:   Col_vector loadingHistory(double wamp, int ncyclic  // make loading
                          , int nredo, double udsp);    //   history data
22:   int getLoadNum() { return ntotal; }         // get total step of loading
23: protected:
24:   Structure *structure;                       // structure object
25:   double x_top;
26:   Gen_matrix H;
27:   LU_matrix *lu;
28:   Col_vector B;
29:   Col_vector t;
30:   Col_vector e;
31:   Col_vector deltaU;
32:   Col_vector R;
33:   double d;
34:   Col_vector accum_dU;
35:   Col_vector dspHistory;
36:   int ntotal;
37: };
38:
39: int main(int argc, char* argv[])
40: {
41:   if(argc<2) {
43:     cout << "Usage: static datafile" << endl;
43:     exit(1);
44:   }
45:
46:   Structure *structure = new Structure(1);  // make structure object(ID:1)
47:   structure->construct(argv[1]);            // set data from file
48:
49:   ColumnTest *test = new ColumnTest(*structure); // make test object
50:   column->setUp();
51:   column->setAxialLoad(-300.0e3);           // set axial load (300 kN)
52:   // generate loading data (amplitude : 6 mm, cyclic : 5, repeticion : 2)
53:   column->loadingHistory(0.006, 5, 2, 0.00002);
54:   ofstream result("output/pd.dat");         // set output file
55:
56:   // start cyclic loading analysis
57:   for(int i=1; i<=column.getLoadNum(); i++) {
58:     column.setDispTop(column.getDspHistory(i)); // set displacemet at top
59:     column.solve();                           // get the solution
60:
61:     F = structure.makeF();                  // get force data of structure
62:   // output p-d data
63:     result << ' ' << (structure.getUvector())[num-2]
64:            << ' ' << F[num-2] << endl;
65:   }
66:   return 0;
67: }
```

Figure 3.27: Implementation of Cyclic Loading Analysis

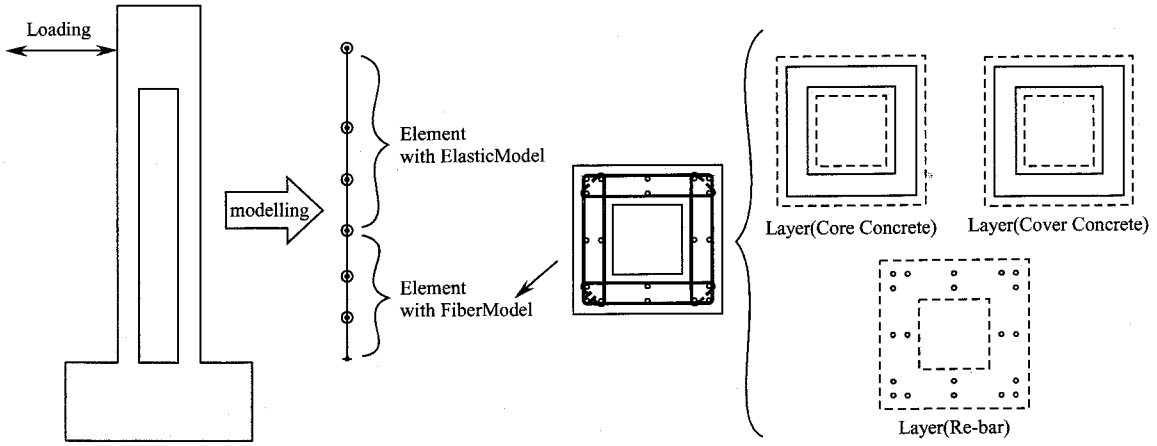

Figure 3.28: Analytical Model

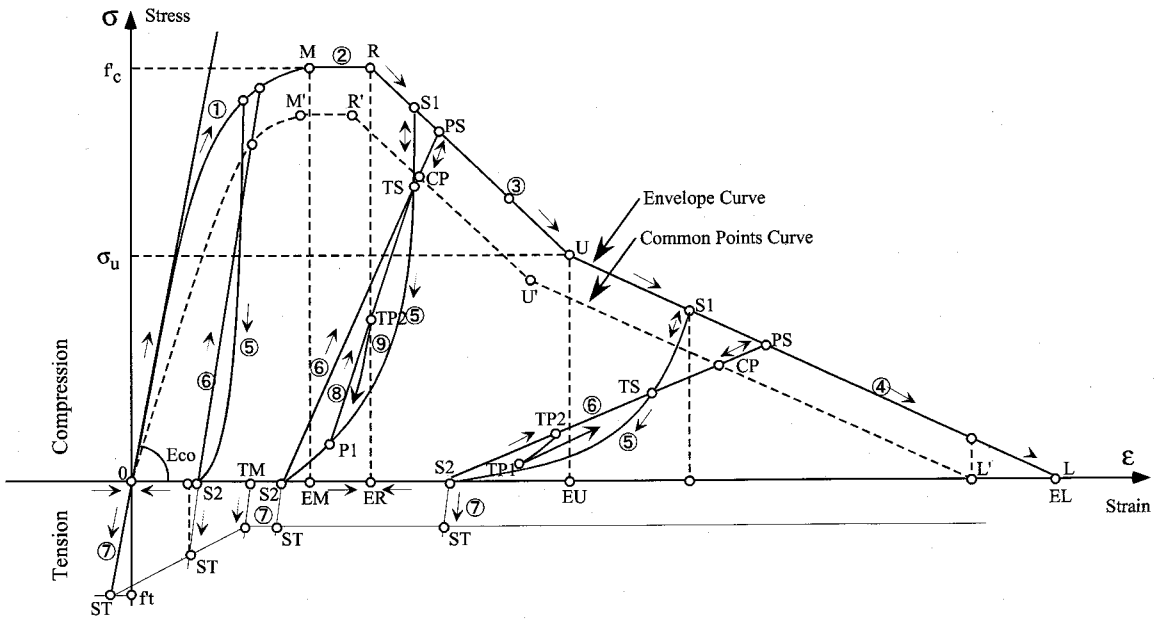

Figure 3.29: Stress – Strain Model for Concrete

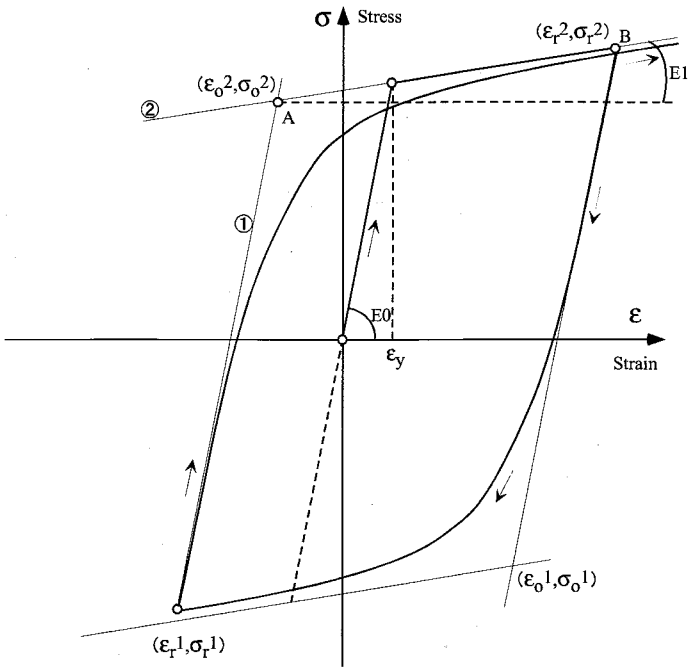

Figure 3.30: Stress – Strain Model for Steel

From this figure, it is found that this analytical program can work well, including the inside hysteretic behavior. This analytical system can simulate the real concrete structure very well.

3.5 Summary

In order to clarify the behavior of hollow RC piers under the combination of loads and earthquake loads, the static loading tests and hybrid earthquake loading tests were carried out. From this study the following results are listed:

1. From the results of the cyclic loading tests, the shear span ratio has the great influence on the failure mode and the deformation performance. The bridge pier with small shear span ratio has high possibility to fail in shear. Since in general a bridge which crosses a deep valley has various height piers, it is important to check the deformation performance of the shortest pier.

2. Under cyclic loading, the shear component cannot be neglected. Even if the amplitude of the displacement is the same, the shear deformation increases monotonously as the repetition cycle increases. That is to say, the flexural failure transits to the shear failure by the cyclic loading, and especially, the effect is significant in hollow piers of which the web is thin.

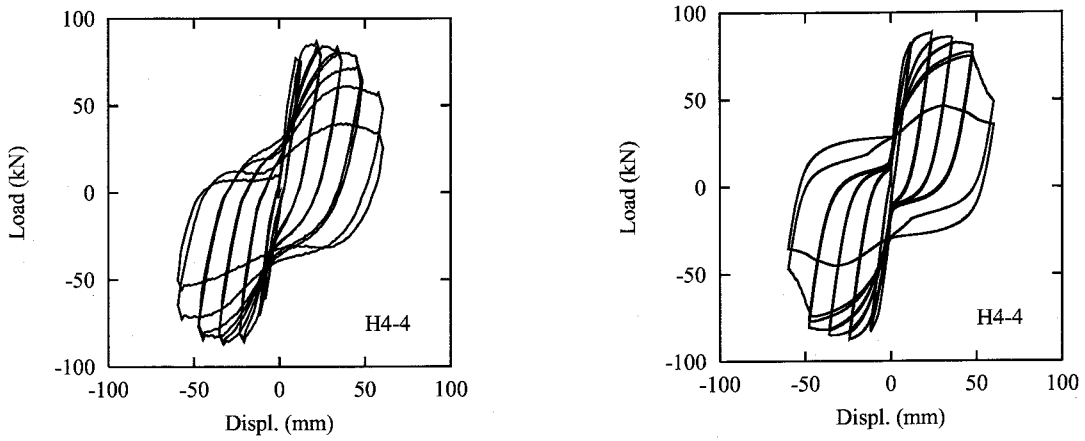

a: Test b: Analysis

Figure 3.31: Comparison of Load–Displacement Hysteresis Loops

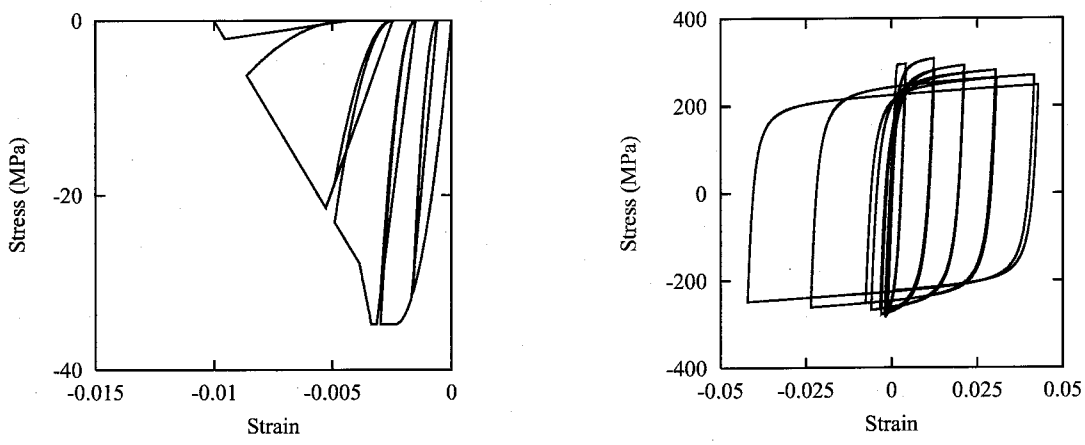

a: Concrete at Edge b: Steel at Edge

Figure 3.32: Stress–Strain Hysteresis Loops

3. Even in case of the flexural failure, shear cracks appeared in the web part under small loads. And flexural cracks in the flange part changed into diagonal cracks when they progressed into the web part.

4. From the hybrid earthquake loading tests, it was observed that the hysteresis response was stable and it can dissipate the input energy by the hysteretic action. The hollow RC piers were found to have a good performance under earthquake motions if they are arranged by the appropriate amount of stirrups.

5. When inputting the Kobe JMA record, the pier responded up to the ultimate state in the early stages of the loading. As the result, the restoring forces in the positive and negative displacement side were different. Furthermore not only the resistant forces but also the crack pattern of the hybrid loading tests were different to that of the cyclic loading tests. These results suggest that the loading history has a great influence of the failure process of RC structures, and the new experimental method have to be developed to assess the effect of the loading history due to inland direct strike earthquakes

6. The mechanism of hollow RC members cannot be explained well only by the flexural deformation. Nowadays, the performance design is spreading in the world and in the design concept it is important to check not only the force but also the displacement of the structure. If the deformation of the shear and the pull-out of the longitudinal bars can be taken into the design appropriately, the rational design can be realized. For this purpose, it is necessary to develop the quantitative evaluation of the ratio of the shear to the flexural and the pull-out deformation using the parameters of the shear span ratio, cross-sectional shape, axial load, and so on.

7. The object-oriented program for the cyclic loading analysis is developed. To cope with the boundary condition of the test method, the *ColumnTest* object is mode, and in the object the *Structure* subsystem is reused. By reusing the developed object for the structural analysis, it is easy to develop the analytical system, and the system becomes very simple in spite of the nonlinear problem. Compared the analytical results of H4-4 with the experimental results, it is found this analytical program can work well, including the inside hysteretic behavior. This analytical system can simulate the real concrete structure very well.

References

(1) Osada, K., Yamaguchi, T. and Ikeda, S. : Seismic Performance and the Strengthening of Hollow Circular RC Piers Having Reinforcement Cut-off Planes and Variable Wall Thickness (in Japanese), *Journal of Concrete Research and Technology*, Vol. 10, No. 1, pp. 13–24, 1999.

(2) Takahashi, Y. and Iemura, H.: Inelastic Seismic Performance of RC Tall Piers with Hollow Section, *Proc. of 12th World Conference on Earthquake Engineering*, p. No.1353, 2000.

(3) Iemura, H., Takahashi, Y., Tanaka, K. and Maehori, S.: Experimental Study on Seismic Performance of RC Hollow Tall Piers, *Proc. of 10th Japan Earthquake Engineering Symposium*, pp. 2105–2110, 1998.

(4) Tanaka, K., Iemura, H. and Takahashi, Y.: Experimental Study on Deformation of RC Hollow Tall Piers (in Japanese), *Proc. of 24th JSCE Earthquake Engineering Symposium*, Vol. 1, pp. 313–316, 1997.

(5) Ishida, S., Iemura, H. and Takahashi, Y.: Experimental Study on Deformation Characteristics of Hollow RC Columns (in Japanese), *Proc. of 54th Annual Conference, JSCE*, Vol. 5, pp. 490–491, 10 1999. Higashi Hiroshima.

(6) Japan Society of Civel Engineers: *Standard Specification for Design and Construction of Concrete Structures (in Japanese)*, Maruzen Ltd., 1996.

(7) Japan Road Association: *Seismic Design Specification for Highway Bridges (in Japanese)*, Maruzen Ltd., 1996.

(8) Maeda, M., Arizono, Y. and Yukimura, N. : Experimental Study on the Evaluation of Deformation of RC Beams (in Japanese), *Proc. of the Japan Concrete Institute*, Vol. 19, No. 2, pp. 861–866, 1997.

(9) Saizuka, K., Itho, Y., Kiso, E. and Usami, T. : A Consideration on Procedures of Hybrid Earthquake Response Test Taking Account of the Scale Factor (in Japanese), *Journal of JSCE*, Vol. I-30, No. 507, pp. 179–190, 1995.

(10) Takemura, H. and Kawashima, K. : Effect of Loading Hysteresis on Ductility Capacity of Reinforced Concrete Bridge Piers (in Japanese), *Proc. of Structural Engineering, JSCE*, Vol. 43A, pp. 849–858, 1996.

(11) Iemura, H., Izuno, K., Fujisawa, S. and Takahashi, Y.: Fundamental Study on Inelastic Seismic Response of RC Tall Piers with Hollow Section (in Japanese), *Proc. of 9th Japan Earthquake Engineering Symposium*, pp. 1483–1488, 1994.

(12) Highway Engineering Center: Report on Seismic Design for Bridges with Tall Piers (in Japanese), 1997.

(13) Igarashi, A., Seible, F., Hegemier, G. and Priestley, M.: The U.S.-TCCMAR Full-Scale Five-Story Masonry Research Building Test: Part III, SSRP 94/03, University of California, San Diego, 1994.

(14) Ristić, D., Y.Yamada and H.Iemura: Nonlinear behaviour and stress - strain based modeling of reinforced concrete structures under earthquake induced bending and varying axial loads, KUCE No.88 - ST - 01, Kyoto University, 1986.

Chapter 4

Development of Unbonded Bar Reinforced Concrete Structure

4.1 General Remarks

Not only civil engineers but also citizens had a great impact from collapse and severe damage of many concrete bridges in Hyogo-ken Nanbu Earthquake. In the restoration operation, a bridge pier which was greatly damaged was of course an object of the removal and the reconstruction, but a pier which was slightly damaged was also an object of the reconstruction, if the residual deformation was over 15 cm or the tilt angle was over 1 degree of its height. From the results of the detail investigation after the earthquake, in the piers of the damage level B, C and D, which means non-serious damage, there were 129 piers whose residual deformation was over 15cm (**Figure 4.1**[1]). That is, nowadays, the important infrastructures are required to have not only the high strength and the high ductility but also the usability and the repairability after earthquakes.

Then what is the high performance of RC structure? In general the high strength and the high ductility are recognized as the high performance. And we add as follows,

- Stable Seismic Response
- Low Construction Cost

The structure which has the well-balanced performance above is the high performance structure in the next generation.

In this study, the Unbonded Bar Reinforced Concrete (UBRC) structure is proposed as the high performance structure. This structure has the stable post-yield stiffness of the load–displacement skeleton curve. And it also intends to be the rational structure from the viewpoint of the two level seismic design method. In this chapter, at first, the background of the

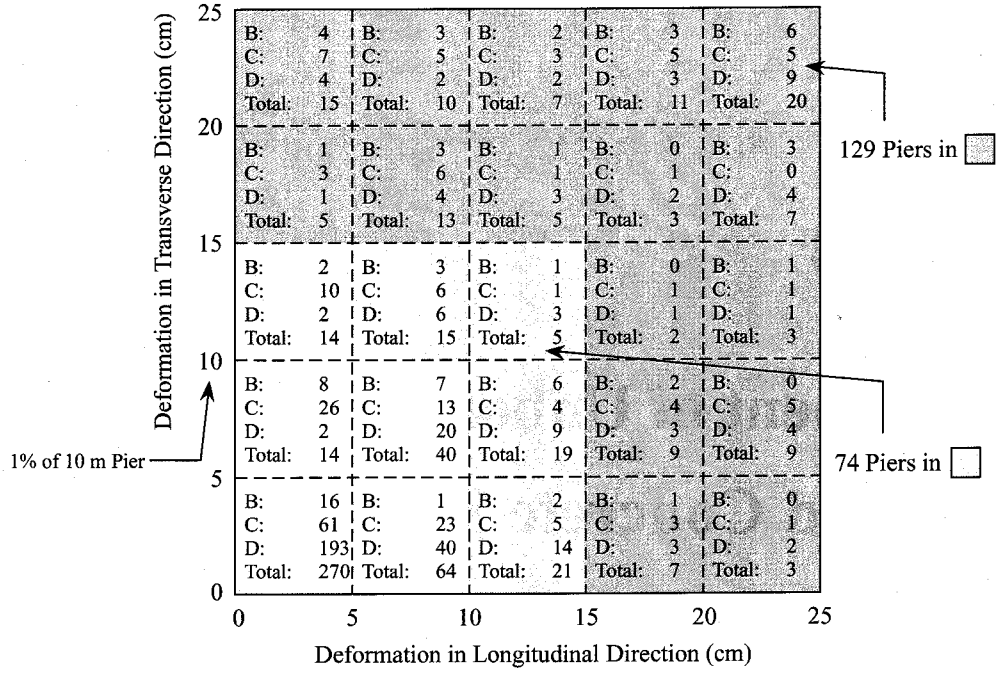

Figure 4.1: Permanent Displacement of Pier at Top and Damage Level

UBRC structure is described. Next, the structure and the concept are shown, and in order to verify the fundamental characteristics, the cyclic loading tests are carried out. And the object-oriented model for an UBRC structure is derived, and the parametric studies on bars of an UBRC are carried out.

The concept and the experimental results of this chapter are described on the basis of the works by Iemura and Takahashi[2–5].

4.2 Background

4.2.1 Steel Pipe – Concrete Composite Structure

In a series of the study of the RC tall piers in the preceding chapter, we also examined the steel pipe – concrete composite structure[6,7]. This structure consists of longitudinal reinforcements, large steel pipes and spiral hoops of the high strength PC strand. It has the high shear strength and the high ductility by the combination of steel pipes and spiral hoops, and the concrete protects the steel pipes from the buckling. Since the steel pipes are used as the reaction frame for construction works, the pier can be constructed rapidly. In order to investigate the seismic performance, the pseudo dynamic tests were carried out[7]. The results in case of the Type I earthquake input motion are shown in **Figure 4.2**. Although the pier responded up to the ductility factor of over 9.0 and the restoring force was deteriorating, the response characteristics was stable and the residual displacement after the earthquake

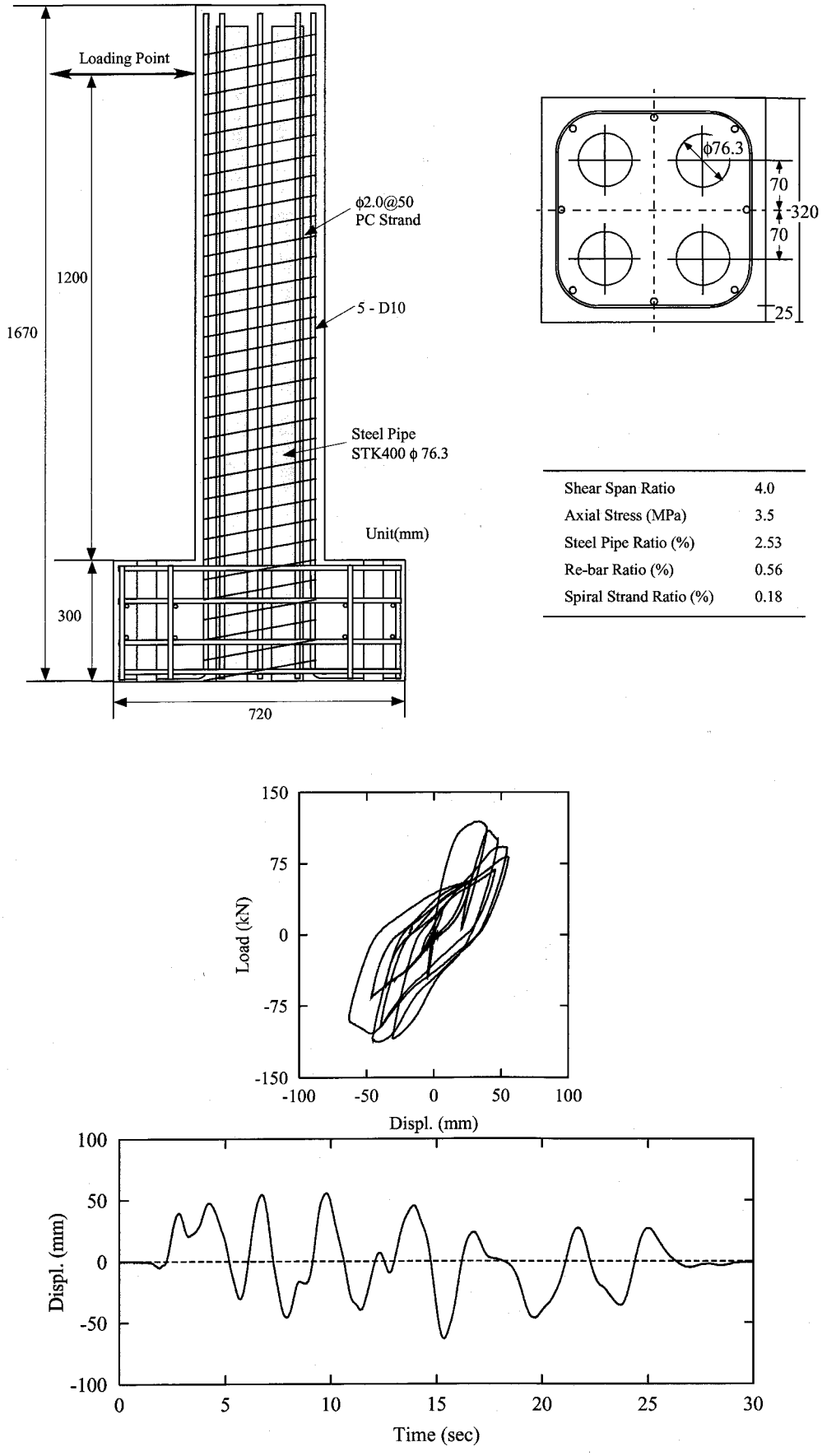

Figure 4.2: Pseudo Dynamic Test Results of Steel Pipe – Concrete Composite Pier

was almost zero. One of the reason for the small residual displacement was considered that the steel pipes had the effective restoring force because they placed inside the cross section. But since in such large deformation the strain at the bottom is very large, it is natural that the pipes would yield and cannot give the effective restoring force. Therefore in the finite element analysis of the structure, the bond slip behavior between the pipes and the concrete was focused. The original structure has the perfect bond, but when the bond slip occurs, the behavior of the pipes becomes independent of the concrete and consequently the strain of the pipes remains small. Therefore, the pipes can have the effective restoring force even in the large deformation[8].

To tell the truth, the bond slip behavior of the conventional RC structures is not taken into account in the design phase and it is accident in the large deformation. But according to the study of the steel pipe – concrete structure, it is found that the elastic member can stabilize the seismic response and reduce the residual deformation. This is one of the reason why we use unbonded members inside the structure positively.

4.2.2 Response of Structure with Post-Yield Stiffness

Since the skeleton curve of a RC structure is the elasto-plastic type, the large deformation occurs after the yield of the structure. But it is reported that the only the post-yield stiffness ratio of 0.05 has the great effect on the reduction of the maximum and the residual deformation[9]. **Figure 4.3** shows the effect of post-yield stiffness on the seismic response. The parameter of r is the post-yield stiffness ratio. From the displacement response, it is found that the residual deformation is greatly reduced by the addition of the post-yield stiffness.

And the Seismic Design Specification of Highway Bridges defines that the residual displacement after earthquakes must be evaluated from the next equation and it should not be larger then 1% of the height of the pier[10].

$$\delta_R = c_R(\mu_R - 1)(1 - r)\delta_y \tag{4.1}$$

where δ_R = the residual displacement of the pier after earthquakes, c_R = the modification factor, μ_R = the response ductility factor of the pier, r = the ratio of the post-yield stiffness to the initial stiffness, δ_y = the yield displacement. It is easily understood from this equation that the larger the ratio is, the smaller the residual displacement becomes. That is, the piers with the large post-yield stiffness are qualified as the high seismic performance piers.

From the above discussions, it becomes clear that the seismic performance of RC piers will be improved effectively by increasing the post-yield stiffness.

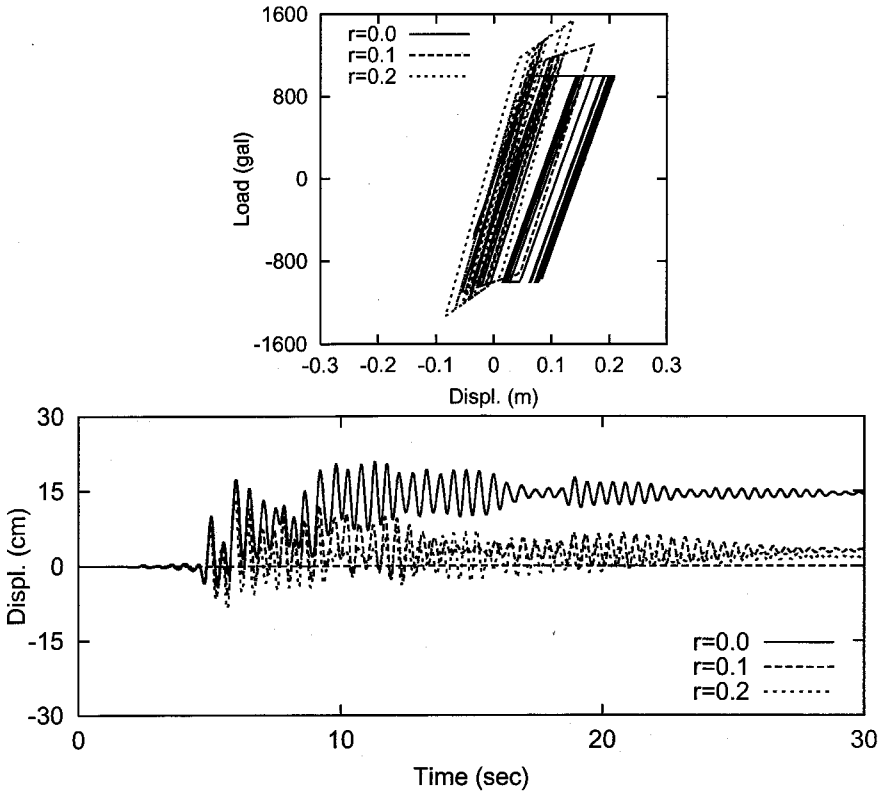

Figure 4.3: Effect of Post-Yield Stiffness

4.3 Unbonded Bar Reinforce Concrete Structure

The basic UBRC structure consists of a conventional RC pier and unbonded high-strength bars (**Figure 4.4**). The both ends of the bars are anchored in the body of the RC structure. As we shall see later in **Figure 4.5**, at the one end of the bars, the gap is installed to adjust the work range of the bars. Since this structure is also reinforced by unbonded bars, it is called Unbonded Bar Reinforced Concrete (UBRC) structure.

The characteristics of the UBRC structure are explained from the viewpoint of the load–displacement skeleton curve (**Figure 4.5**). The load–displacement relationship of a conventional RC structure is the perfectly elasto-plastic model[10]. When elastic members are installed in the RC structure, it is possible to obtain the structure with the post-yield stiffness. The UBRC structure is developed to have this skeleton relationship with the positive and the stable post-yield stiffness even in the large deformation. For actual structures, it is necessary to guarantee that the bars behave in the elastic manner in the large deformation in order to obtain the stable post-yield stiffness. Therefore, for the bars, the high-strength material is used, and the unbonding treatment is performed.

The effect of the unbonding treatment is shown in **Figure 4.6**. In general, under the low level of the loading, the strain of longitudinal bars shows the triangle distribution along the height of the pier as same as the moment distribution. When the level of the loading becomes

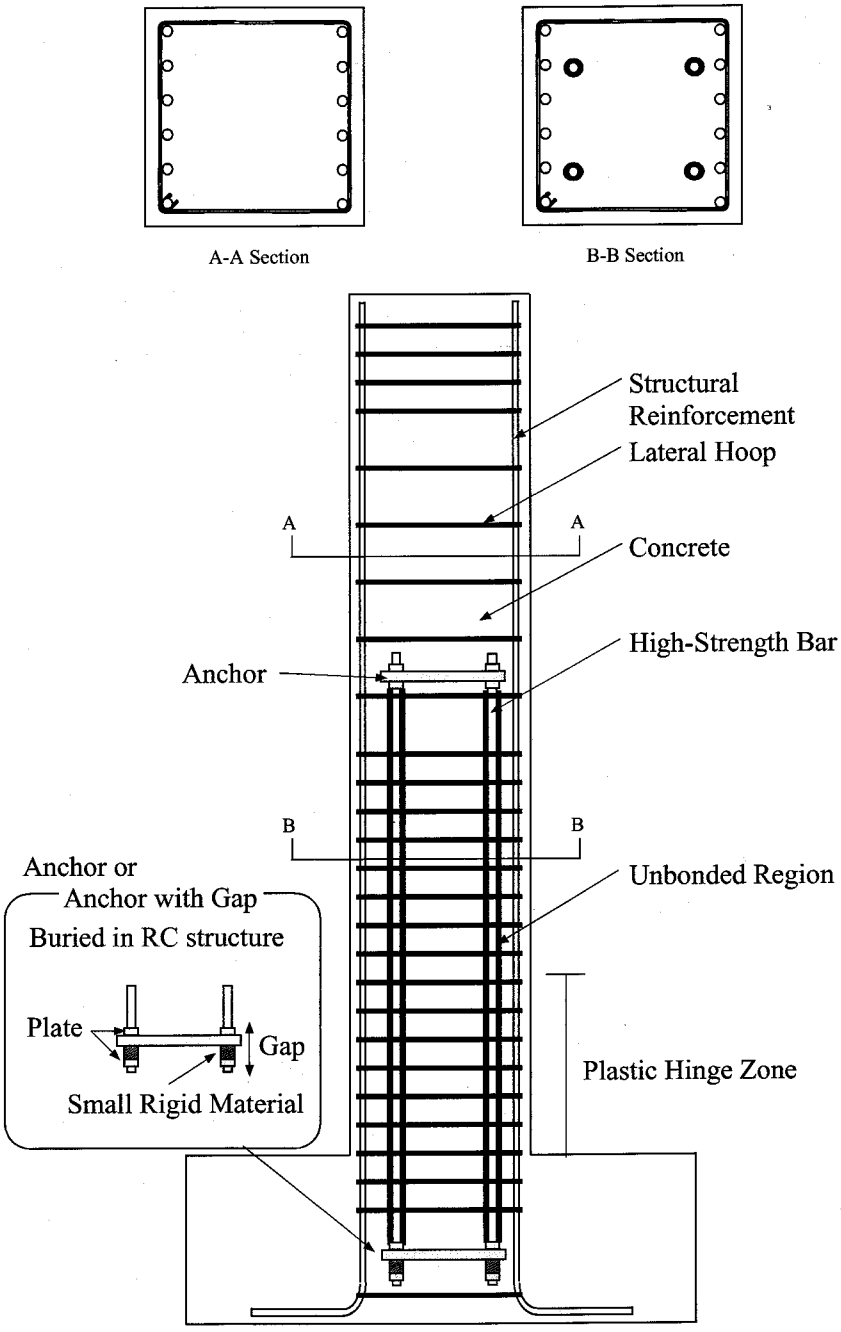

Figure 4.4: Conceptual Model of Proposed UBRC Structure

Load-Displacement Relationship of Conventional RC Structure

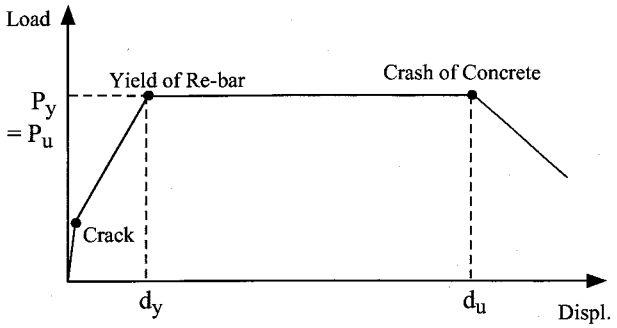

Load-Displacement Relationship of Elastic Member (Unbonded Bar)

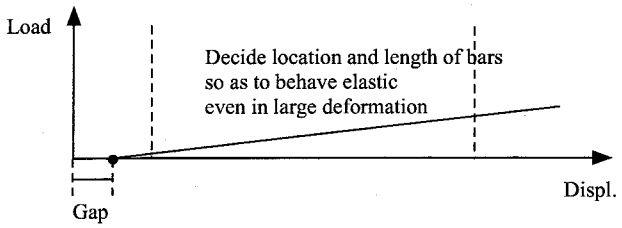

Load-Displacement Relationship of UBRC Structure = RC Structure + Bar

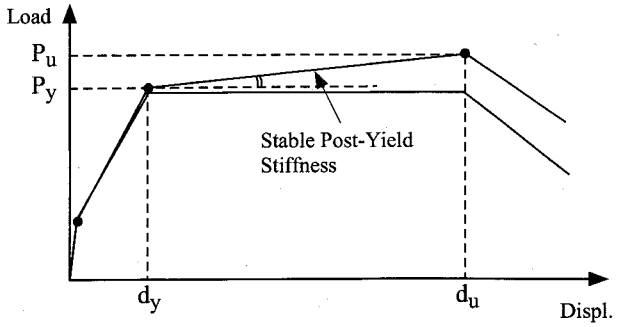

Figure 4.5: Effect of Installation of Elastic Bars

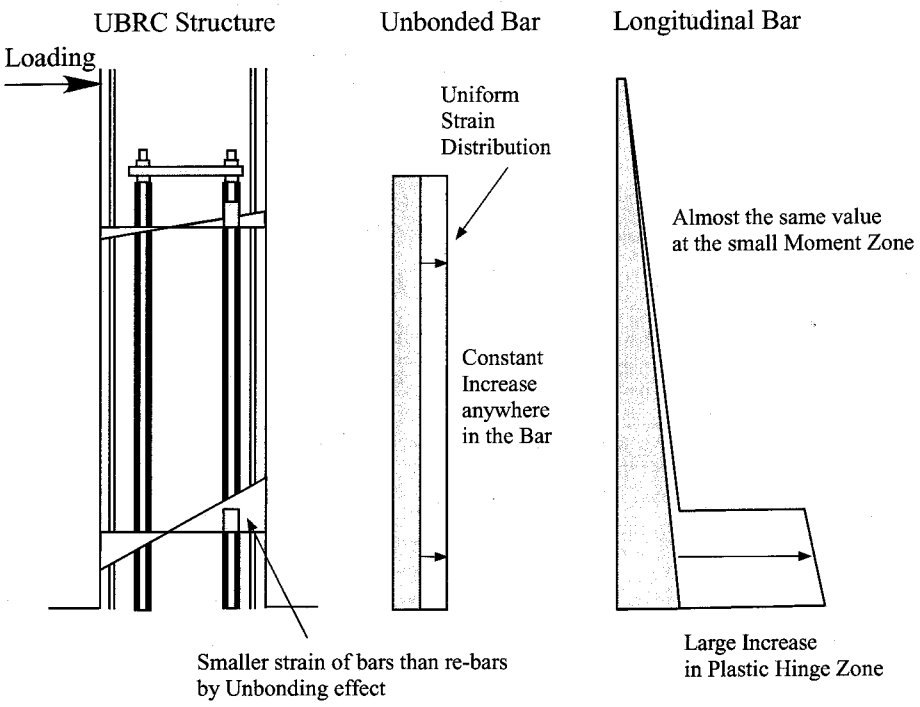

Figure 4.6: Effect of Unbonding Treatment of Bars

large, around the loading point the strain changes only a little, but at the bottom of the pier, the longitudinal bars would yield and the strain becomes large, and the plastic hinge zone is formed. On the other hand, for the unbonded bars, the strain distribution becomes constant because the bars behave independent of the RC member except for the anchors. Therefore since the whole length of the bar can resist the deformation of the RC member effectively, the strain of the bars becomes small. That is, the bars hardly yield. By this fact, the unbonded bar can be used as the elastic member even in large deformation, and the UBRC structure can show the stable post-yield stiffness.

For the UBRC's bars, a high-strength material has advantage because the yield strain is large. But in general the high-strength material is very expensive, and sometimes it is difficult to adopt it from the economical viewpoint. Since the most important characteristic of the UBRC structure is the post-yield stiffness in the large deformation, the effect of the bars in the small deformation is not so important. Therefore the gap is installed at the one end of the bars and controls the active elastic range of the bars (**Figure 4.4**, **Figure 4.5**). By this measure, the UBRC structure can be realized by using the conventional material for bars.

Since in the ultimate state the UBRC structure has a large restoring force compared with the original structure, the deterioration of the concrete may be accelerated. That is, the ultimate displacement becomes smaller than the original structure. Considering the equal energy principle for the UBRC structure (**Figure 4.7**), the ultimate displacement of the UBRC is ob-

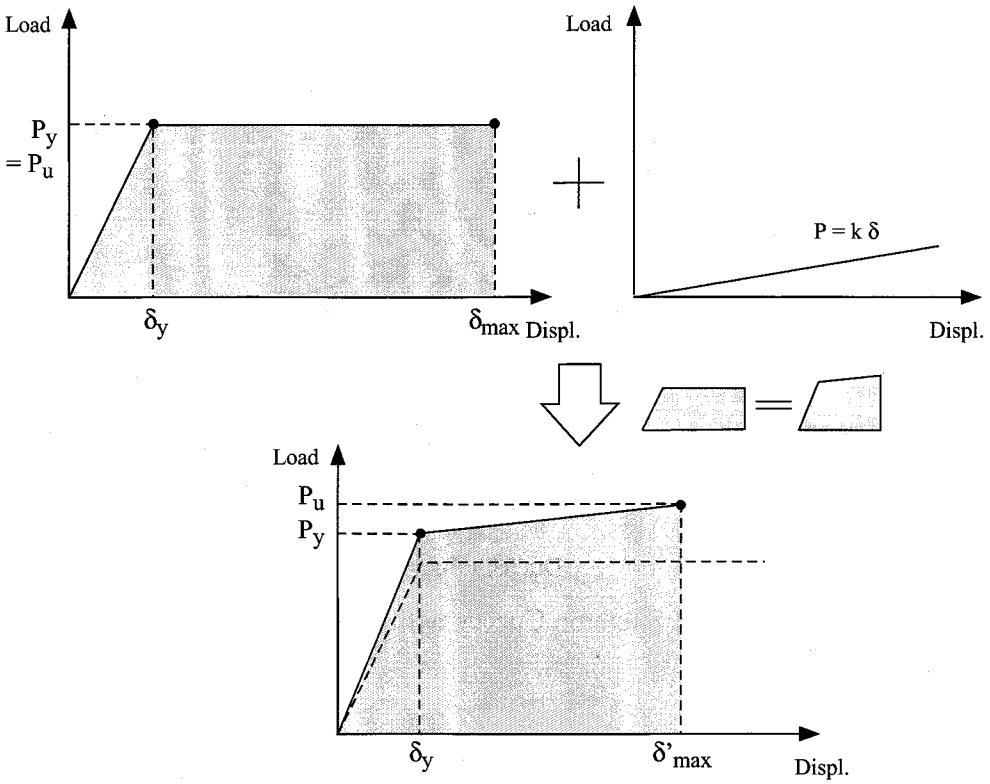

Figure 4.7: Equal Energy Principle

tained:

$$\mu_{UBRC} = \frac{1-r}{r}\left\{\sqrt{1+2\mu\frac{r}{1-r}}-1\right\} \tag{4.2}$$

where r is the post-stiffness ratio of the UBRC structure, μ is the ductility factor of the original RC structure. According to this equation, the load–displacement skeleton curves with the same energy capacity in case of $\mu = 5.0$ are shown in **Figure 4.8**. The broken line shows Equation (4.2). From this figure, it is found that the decrease of the ultimate displacement is not necessarily the deterioration of the seismic performance in this case.

Next, the characteristics of the UBRC structure are explained from the viewpoint of the hysteresis response(**Figure 4.9**). The maximum displacement response of the conventional RC structure becomes large because the post-yield stiffness is almost zero. As the result, the residual plastic deformation after the earthquake becomes also large. On the other hand, since the UBRC structure has the positive post-yield stiffness, it can be expected that the maximum displacement response can be reduced. Moreover, because the unbonded bars do not yield, they can be expected to have the effective restoring force and reduce the residual deformation. That is, the UBRC structure can reduce the residual plastic deformation by the combination of the small maximum displacement response and the elastic restoring force of the bars. Moreover, in the large deformation where the concrete and the longitudinal bars deteriorate, the existence of the elastic member can stabilize the seismic response.

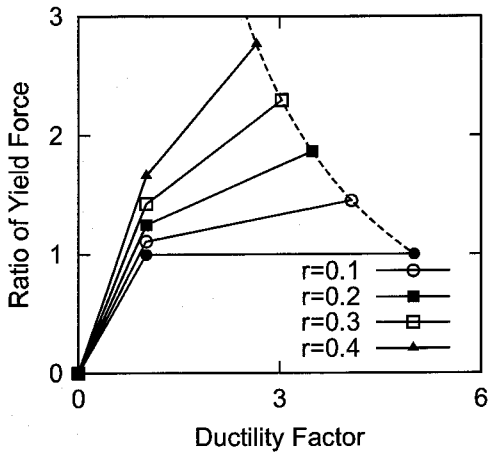

Figure 4.8: Skeleton Curves with Elastic Member

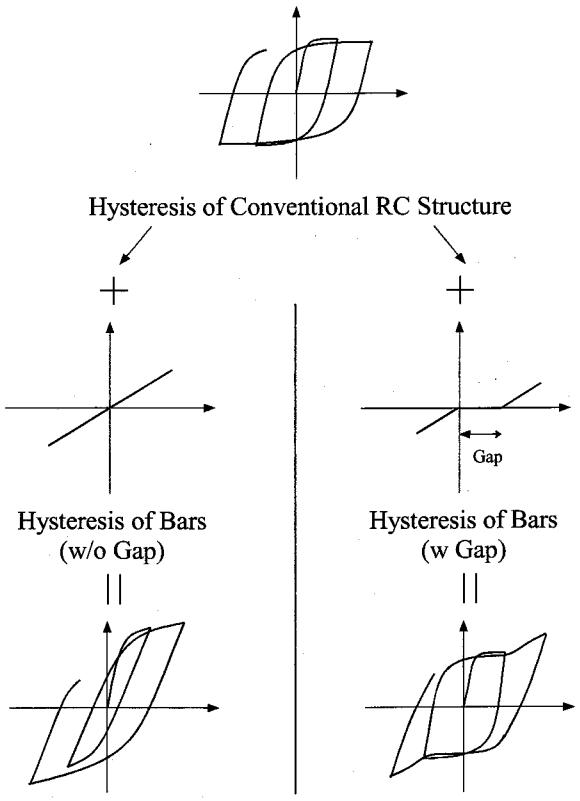

Figure 4.9: Effect on Hysteretic response

Table 4.1: Parameters of Test Units

Test Unit	Stirrup	Bar (location from center of section)	Longitudinal Bar
RC-1	D6@50 mm	—	16 – D10
UBRC-1		4×SBPR ϕ9.2 (70 mm)	
UBRC-2			8 – D10
UBRC-3		4×SBPR ϕ9.2 (100 mm)	16 – D10

The UBRC structure has the combination of different functions : for the fundamental pier structure, this is the RC structure, which can absorb energy by hysteretic action, and in order to give the post-yield stiffness, reduce the residual deformation and stabilize the dynamic response, the unbonded high-strength bars are installed.

4.4 Cyclic Loading Tests

4.4.1 Description of Test Units

In order to verify fundamental characteristics of the UBRC structure, especially focusing on the effect of the configuration of the bars, column specimens were constructed. In these specimens, the gap at the anchor was not installed. Each specimen had a 320 mm square cross section and a height of 1507 mm (**Figure 4.10**). The parameters of test units are summarized in **Table 4.1**. PC rods (SBPRϕ9.2) were used as high strength bars. The mechanical properties are shown in **Table 4.2**. In order to guarantee the unbonding behavior of the bars in the plastic hinge zone, spiral sheaths for PC rods were installed.

The basic model was the conventional RC model (RC-1). UBRC-1 was the test unit which is addition of unbonded bars to RC-1, and it was possible to investigate the effect of the addition of the elastic member. UBRC-2 was the test unit with unbonded bars and had the same flexural capacity as RC-1, and it was possible to examine the role of structural longitudinal reinforcement. UBRC-3 had the same amount of bars and longitudinal reinforcement as UBRC-1, but the location of bars in the section was different, and it was possible to verify the effect of the configuration of the bars.

4.4.2 Loading System and Test Procedure

The loading system is shown in **Photo 4.1**, **Photo 4.2**. This system is similar to **Figure 3.2**, but the connection equipment between a specimen and actuators is improved. Since the equipment in **Figure 3.2** used swivel heads, the loading point of the horizontal and the ver-

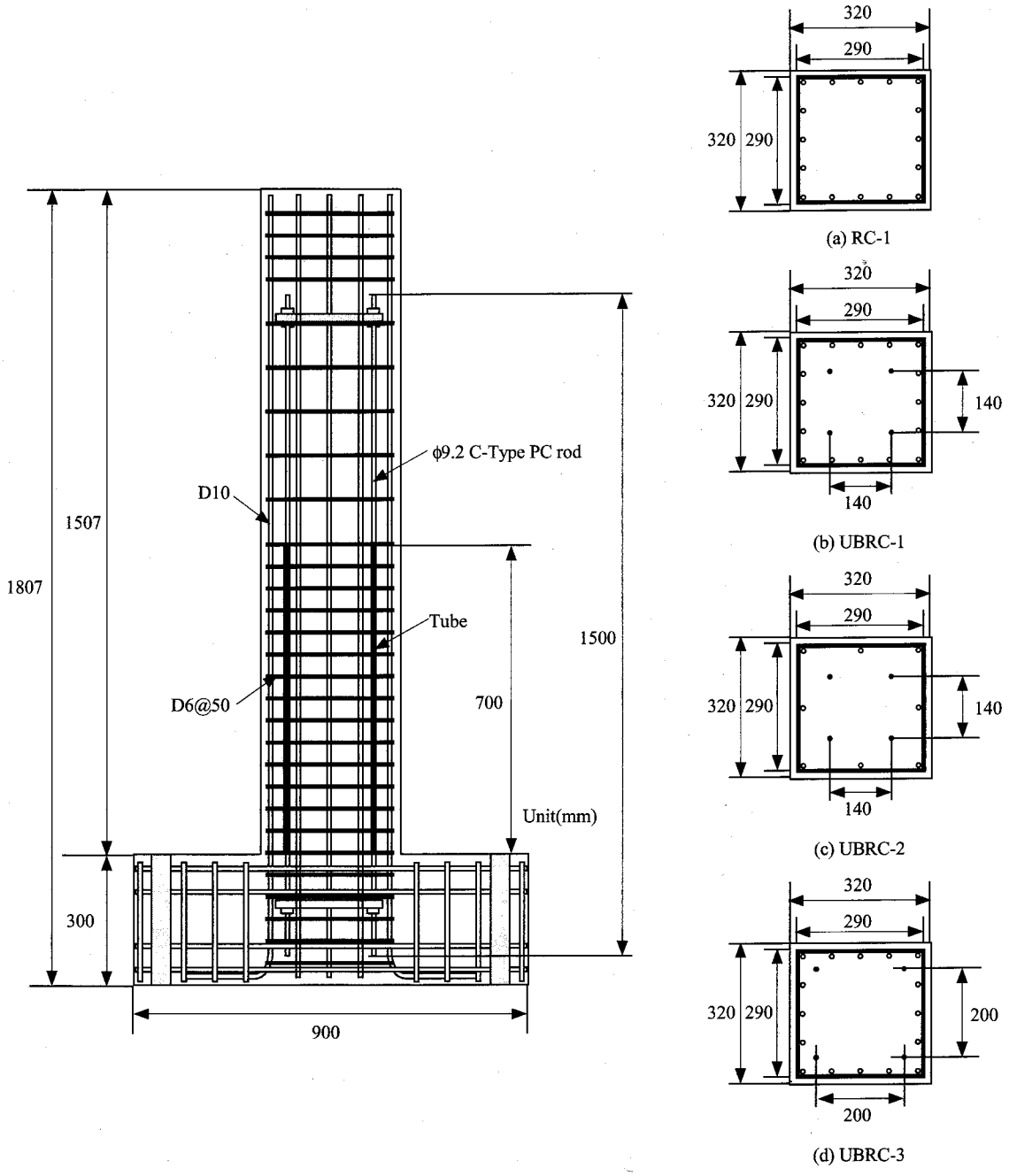

Figure 4.10: Test Units

Table 4.2: Mechanical Properties of Steel

		Yield Strength (MPa)	Tensile Strength (MPa)
Longitudinal Bar	SD295 D6	312	451
	SD295 D10	312	451
PC Rod	SBPR ϕ9.2	1185	1331

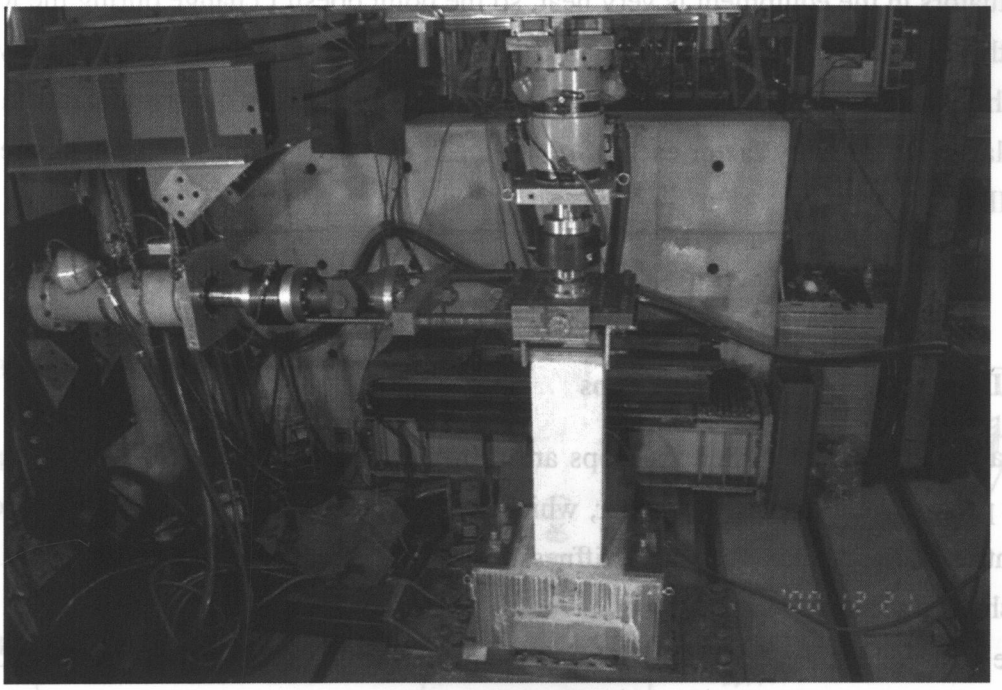

Photo 4.1: Loading System

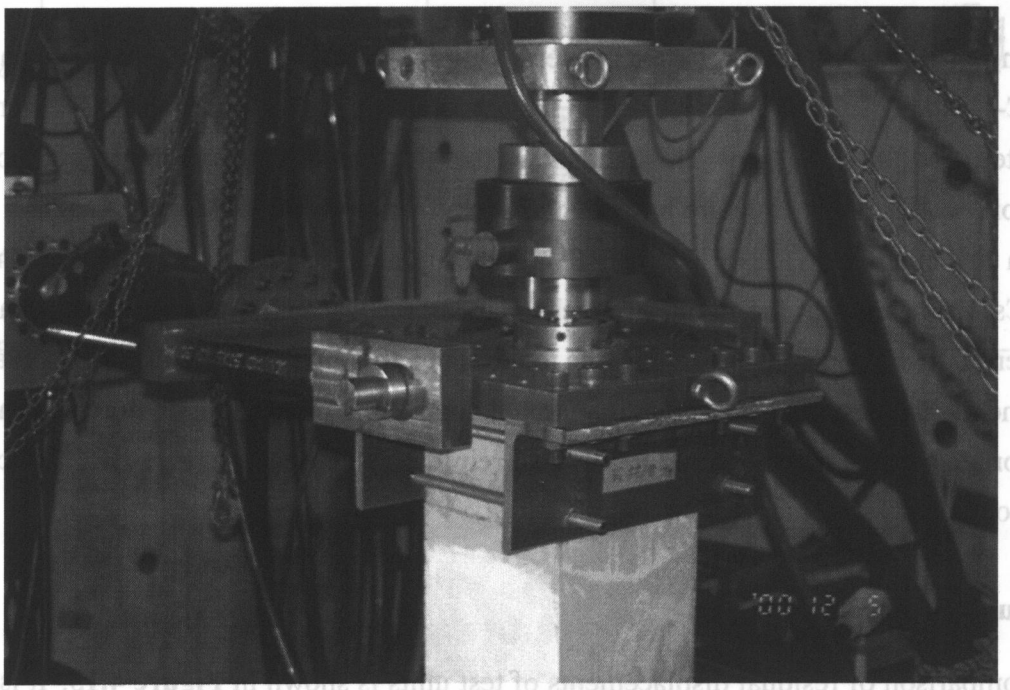

Photo 4.2: Equipment for Loading

tical actuators moves during the loading process. On the other hand, the loading point of the two actuators in the equipment is very near, so the point doesn't change during the loading. Using this equipment, we can simulate the behavior of superstructures more precisely.

In the experiments, the horizontal displacement was applied at a quasi-static rate in cycles to displacement ductility factor each of $\mu = \pm 1, \pm 2$, etc. ($\mu = 5$ mm). The axial stress was 1.46 MPa.

4.4.3 Test Results

Load–Displacement Hysteresis Loops

The load–displacement hysteresis loops are shown in **Figure 4.11**. RC-1 behaved in the almost perfectly elasto-plastic manner, which is the typical behavior of RC structures. On the contrary, the positive post-yield stiffness can be observed in the other units. But the all loops showed the spindle shape type.

The post-yield stiffness of UBRC-1 was almost the same as that of UBRC-2, and UBRC-3 showed larger than others. These results suggest that the post-yield stiffness is decided by the bar location in the section, not by the amount of longitudinal reinforcement. But in spite of the unbonding treatment, the bars of UBRC-3 yielded at the displacement of 60 mm.

Failure Mode

Looking at the crack patterns after the tests (**Figure 4.12**), it is found that the cracks of UBRC-1 and UBRC-3 were dispersed in the test units, while the cracks of RC-1 were concentrated around the bottom. This fact shows that the whole length of the UBRC columns can work well and this structure have a good performance on the flexural behavior.

On the other hand, in case of UBRC-2, the number of cracks was fewer than other UBRCs. It means that the width of cracks was large because the tension stress cannot be transferred to the concrete effectively due to the small amount of structural longitudinal reinforcement. This result suggests that in terms of controlling cracks, it is important to arrange appropriate amount of structural longitudinal reinforcement because the UBRC structure is based on the RC structure.

Residual Displacement

The comparison of residual displacements of test units is shown in **Figure 4.13**. It is found that those of UBRC test units were smaller than that of RC-1. In other word, the residual displacement can be decreased only by installing elastic members in the RC pier even if prestressing is not applied like PC structures. And, so that UBRC-2 showed the most small

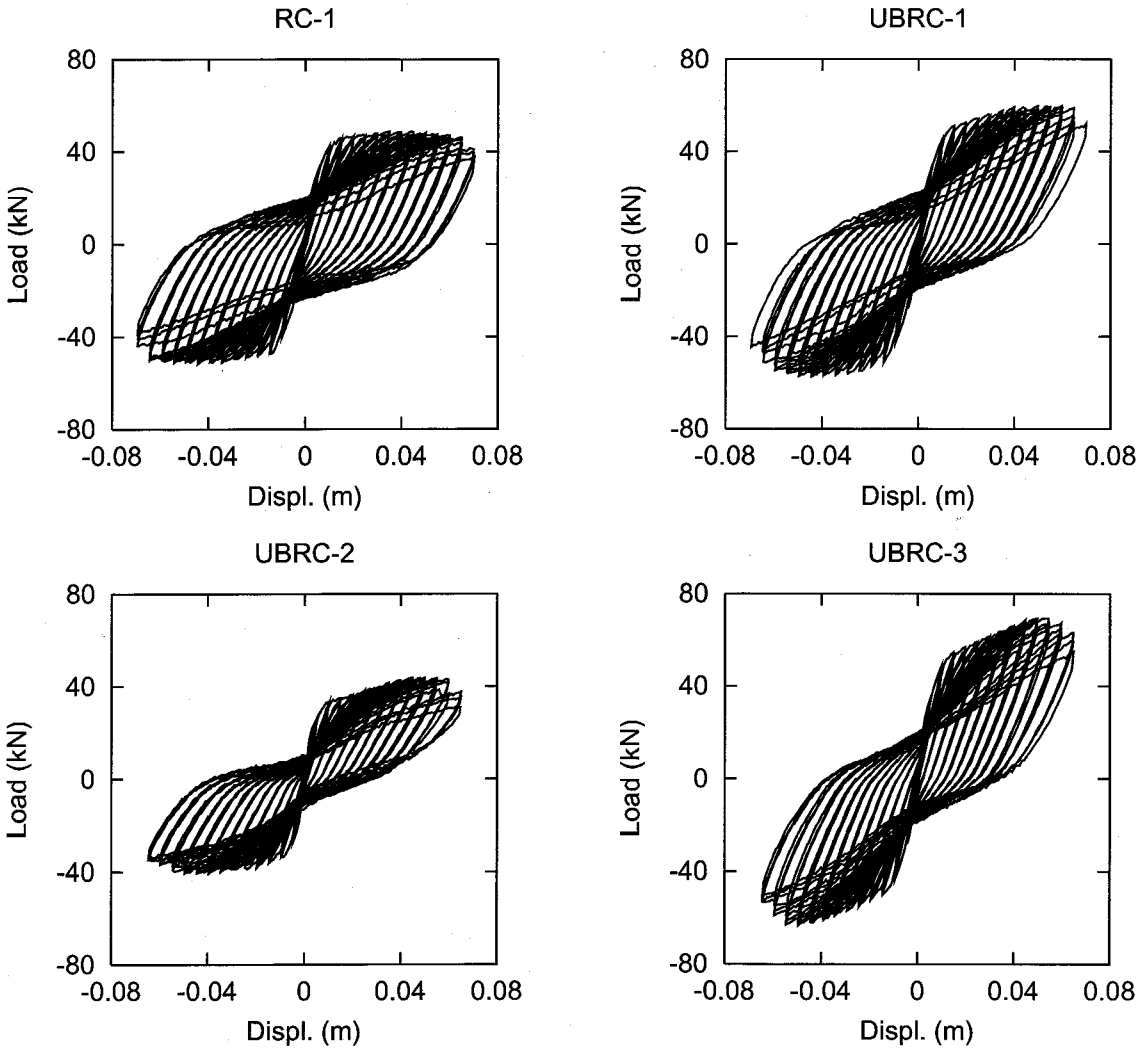

Figure 4.11: Load–Displacement Hysteresis Loops

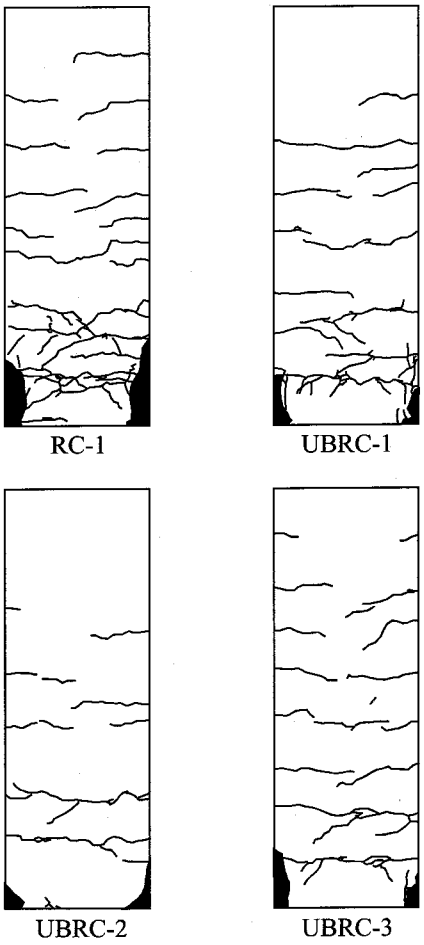

Figure 4.12: Crack Patterns

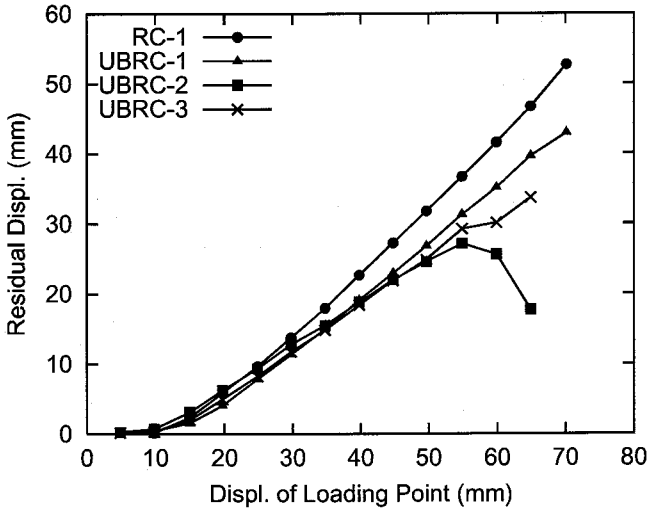

Figure 4.13: Residual Displacement

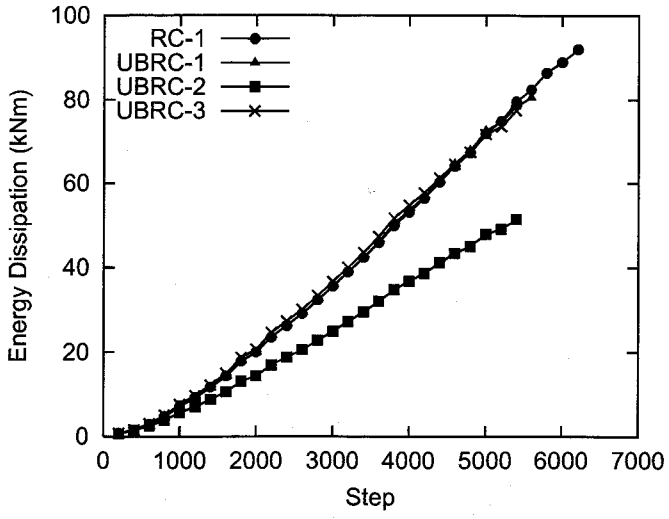

Figure 4.14: Amount of Absorbed Energy

value, the structure with the high ratio of bars to structural longitudinal reinforcement showed the small residual displacement. This results agree with the tendency in PC structures.

Performance of Absorbing Energy

The comparison of accumulated absorbed energy of test units is shown in **Figure 4.14**. From this figure, it is found that the capacity of absorbing energy, except for UBRC-2, was almost the same. This result shows that installing bars changes the stiffness without changing the area of hysteresis loops. On the other hand, UBRC-2 had poor performance of absorbing energy. That is, it is clear that the capacity of absorbing energy depends on the amount of structural longitudinal reinforcement, not of bars.

4.5 Analytical Formulation of UBRC Structure

4.5.1 Outline

As described in the preceding section, the UBRC member consists of the RC member and the unbonded bars. Therefore the analytical model is also represented as the combination of the RC member model and the unbonded bar model. The UBRC element cannot be satisfied with the Bernoulli's assumption because the behavior of the bars is independent from that of the RC member besides the anchors. The bars are only deformed following the deformation of the RC member satisfying the compatibility condition.

In this section, the force vector of the unbonded bar is formulated and the object-oriented model is derived from the *Method* object in **Figure 2.21**.

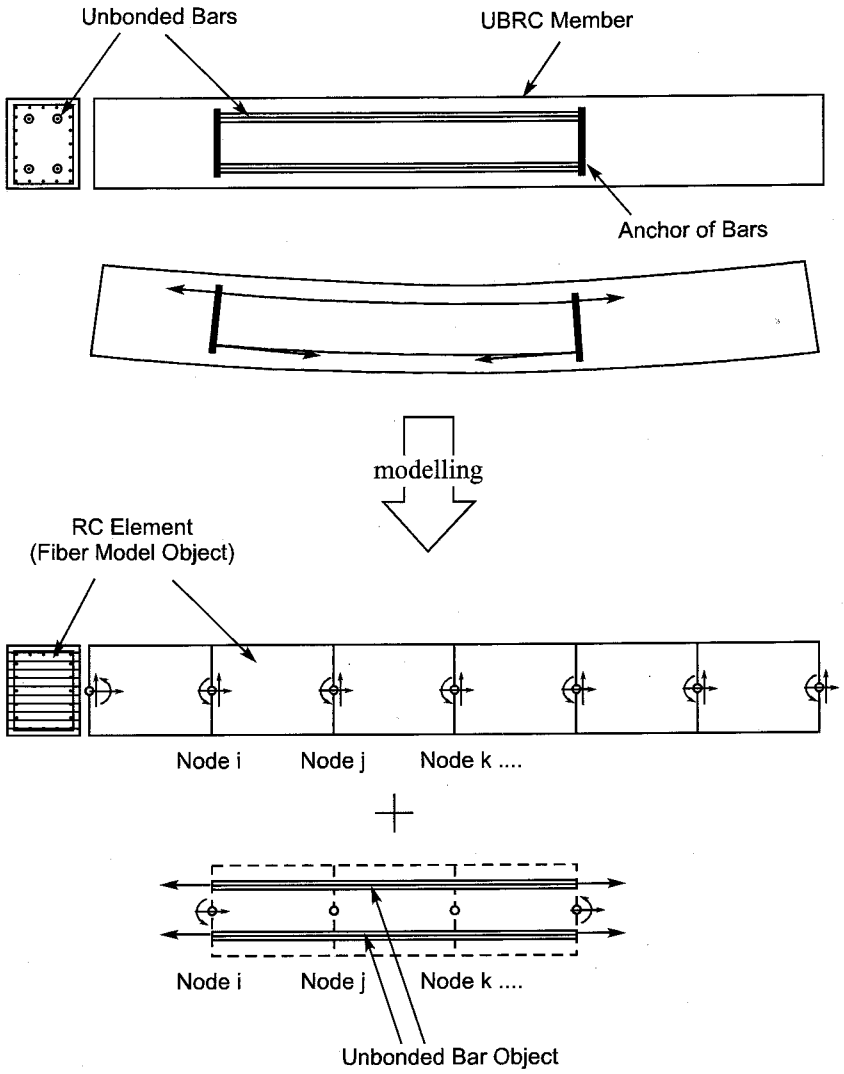

Figure 4.15: Unbonded Bar Member

4.5.2 RC Member

The RC member is modeled as the beam with the Timoschenko fiber model.

4.5.3 Unbonded Bar Member

Because of the no bonding between the bars and the RC member, the strain increment of the bar must correspond to that of the RC member at the location of the bar.

$$\Delta\epsilon_{bar} = \frac{1}{L_{ub}} \int_0^{L_{ub}} \Delta\epsilon_{ub}\, dx \tag{4.3}$$

For example, in **Figure 4.15**, the RC member is divided into 6 elements, but the strain of the bar is calculated using the information of 3 elements.

Now the calculation of the strain increment of the bar is followed using **Figure 4.16**. The

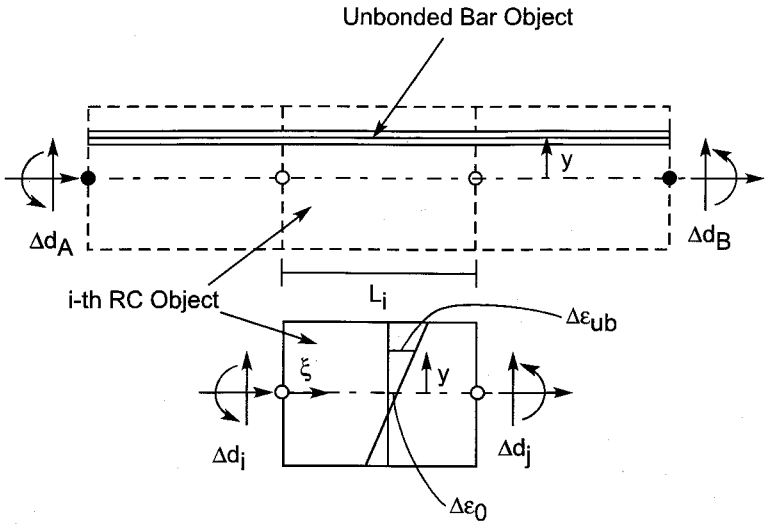

Figure 4.16: Calculation of Length of Unbonded Bar

strain of the RC member at the location of the bar is obtained:

$$\Delta\epsilon_{ub} = \Delta\epsilon_0 + y\Delta\phi = \left\{ \begin{array}{cc} 1 & y \end{array} \right\} \left\{ \begin{array}{c} \Delta\epsilon_0 \\ \Delta\phi \end{array} \right\} = \mathbf{Y}_i\, \boldsymbol{\epsilon} \tag{4.4}$$

And the strain increments at the neutral axis is calculated using the nodal displacement increments of the RC member.

$$\boldsymbol{\epsilon} = \mathbf{B}_f \left\{ \begin{array}{c} \Delta\mathbf{d}_i \\ \Delta\mathbf{d}_j \end{array} \right\} = \mathbf{B}_f\, \mathbf{d}_i^e \tag{4.5}$$

The length increment ΔL_i of the RC element i is

$$\Delta L_i = \int_0^{L_i} \Delta\epsilon_{ub}\, d\xi = \int_0^{L_i} \mathbf{Y}_i\, \mathbf{B}_f\, \mathbf{d}_i^e\, d\xi = \mathbf{Y}_i \left(\int_0^{L_i} \mathbf{B}_f\, d\xi \right) \mathbf{d}_i^e \tag{4.6}$$

where

$$\int_0^{L_i} \mathbf{B}_f\, d\xi = \left[\begin{array}{cccccc} -1 & 0 & 0 & 1 & 0 & 0 \\ 0 & 0 & -1 & 0 & 0 & 1 \end{array} \right] \tag{4.7}$$

Substituting (4.7) into (4.6), we have

$$\Delta L_i = \left\{ \begin{array}{cccccc} -1 & 0 & -y & 1 & 0 & y \end{array} \right\} \mathbf{d}_i^e = \mathbf{Y}\, \mathbf{d}_i^e \tag{4.8}$$

Therefore the strain increment of the bar is

$$\Delta\epsilon_{bar} = \frac{1}{L_{ub}} \mathbf{Y} \sum_i \mathbf{d}_i^e \tag{4.9}$$

Adding $\Delta\epsilon_{bar}$ to the strain at $t = t$, $\epsilon_{bar,n}$, we obtain the total strain at $t = t + \Delta t$, iteration step (k), $\epsilon_{bar,n+1}^{(k)}$, using the constitutive law of the material of the bar, the total stress $\sigma_{bar,n+1}^{(k)}$

is obtained. The additional axial force N and moment M due to the bar are

$$N_{n+1}^{(k)} = \sum_{i=1}^{numbar} \sigma_{i,n+1}^{(k)} A_i \tag{4.10}$$

$$M_{n+1}^{(k)} = \sum_{i=1}^{numbar} \sigma_{i,n+1}^{(k)} A_i y_i \tag{4.11}$$

As the result, the nodal force vector due to the unbonded bars is

$$\mathbf{F}_{n+1}^{(k)} = \left\{ -N_{n+1}^{(k)} \quad 0.0 \quad M_{n+1}^{(k)} \quad N_{n+1}^{(k)} \quad 0.0 \quad M_{n+1}^{(k)} \right\}^T \tag{4.12}$$

4.5.4 UnbondBars Object

According to the previous subsection, it is found how to calculate the nodal point force vector of the unbonded bars considering the compatibility condition. In this subsection, the *UnbondBars* object is modeled.

Since the *UnbondBars* is an object to make the nodal point force vector, it derives from the *Method* class. But the method of *makeK()* and *deform()* are meaningless because the behavior of the *UnbondBarss* object is decided by the compatibility condition of the deformed RC member. The class diagram is shown in **Figure 4.17**.

In order to calculate the strain increment of bars, it is necessary to know the information of all RC members which has unbonded bars. Therefore this object possesses the ID number list of the RC members and in the method *calcEffectUnbond()*, the list is used to access the corresponding RC element. The sequence model of *makeF()* is shown in **Figure 4.18**.

4.6 Comparison of Analytical Results with Experimental Results

Since the *UnbondBars* object is one of the *Method* object, the structure with *UnbondBars* is also the *Structure* object. Therefore in order to carry out the cyclic loading analysis, we can use the same program as mentioned in the RC hollow columns (Section 3.4).

The analytical results for **Figure 4.10** are shown in **Figure 4.19**. Comparing with the experimental results, it is found the the analysis can predict the effect of the unbonded bars very well.

Figure 4.20 and **Figure 4.21** show the transition of the stress distribution of RC-1 and UBRC-3, respectively. In the small deformation (until Point 4), the distributions between RC-1 and UBRC-3 are very similar. However, as the deformation becomes large, the distributions change and the compressive stress due to the bars can be recognized in UBRC-3.

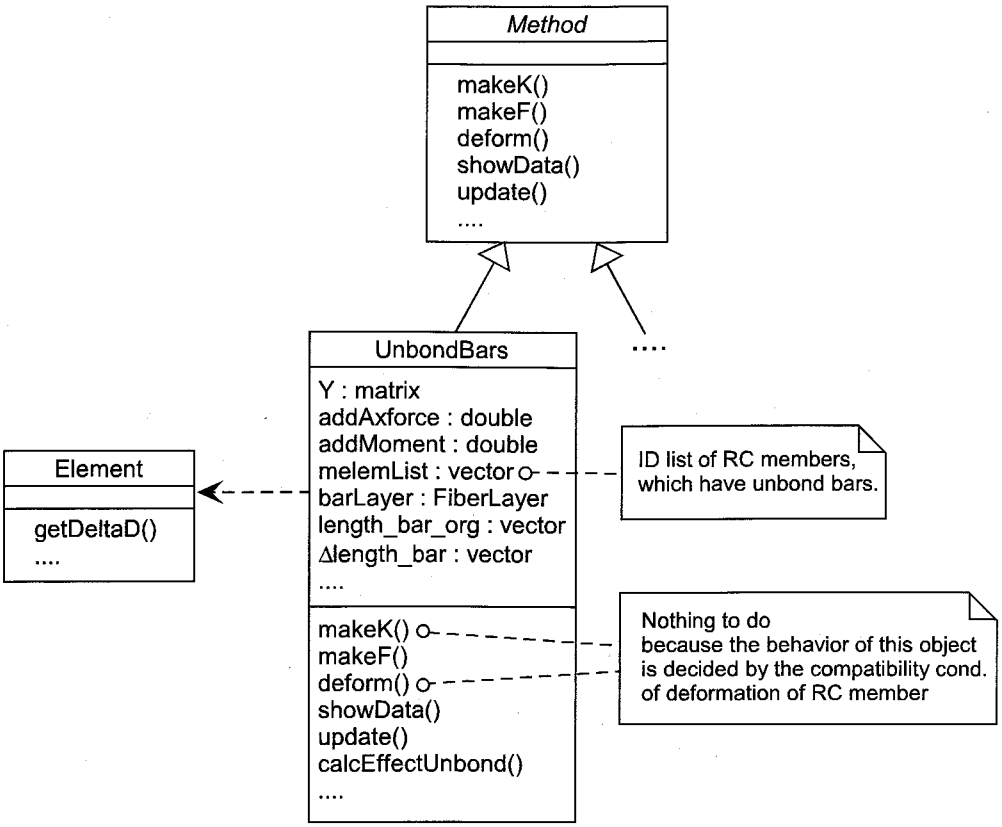

Figure 4.17: Unbonded Bar Member

For example, on Section 5, the tensile stress can be observed in the every step in RC-1, but in UBRC-3 the tensile stress is vanishing through the loading process. The phenomena can be recognized in the other sections. In the large deformation (e.g. Point 9), the compressive zone of concrete section in UBRC-3 becomes larger than that of RC-1. This is the bars' effect.

From this fact, we can explain the crack distribution of UBRC structures (**Figure 4.12**). The compressive stress due to the unbonded bars closes small cracks and makes the effective section of the RC part of UBRC structures enlarge. Therefore the behavior of UBRC structures in the large deformation becomes similar to PC or PRC structures, and the cracks are distributed along the height.

4.7 Effect of Unbonding

In **Figure 4.22**, the hysteresis loops and the strain distributions of the bar along the height are shown in case of the bonded and the unbonded bars, respectively. Each line in the strain distribution is the value at the maximum deformation of each loading cycle. The base structure used in this analysis is the UBRC-1 (**Figure 4.10**), but the pull-out of the longitudinal

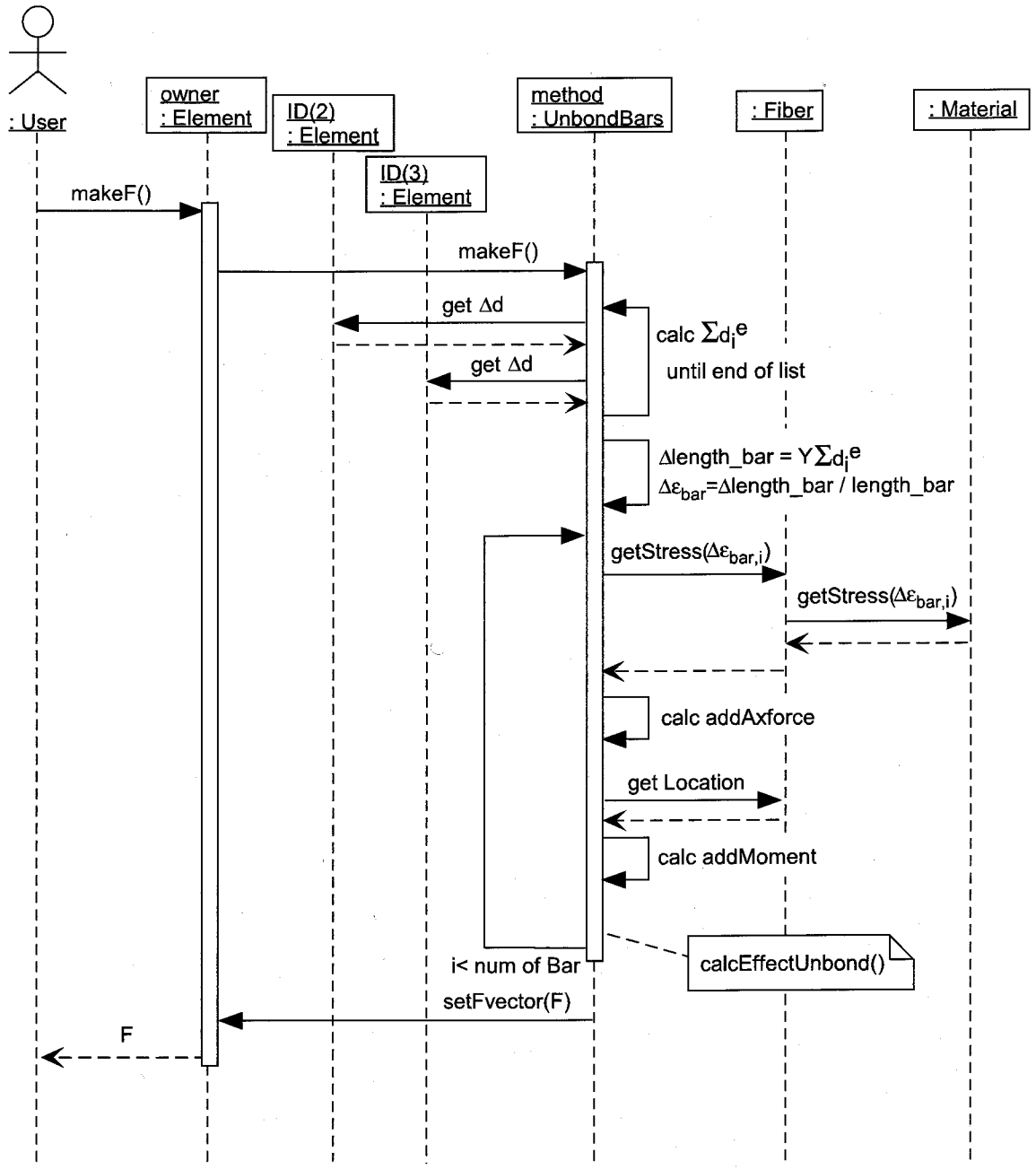

Figure 4.18: Unbonded Bar Member

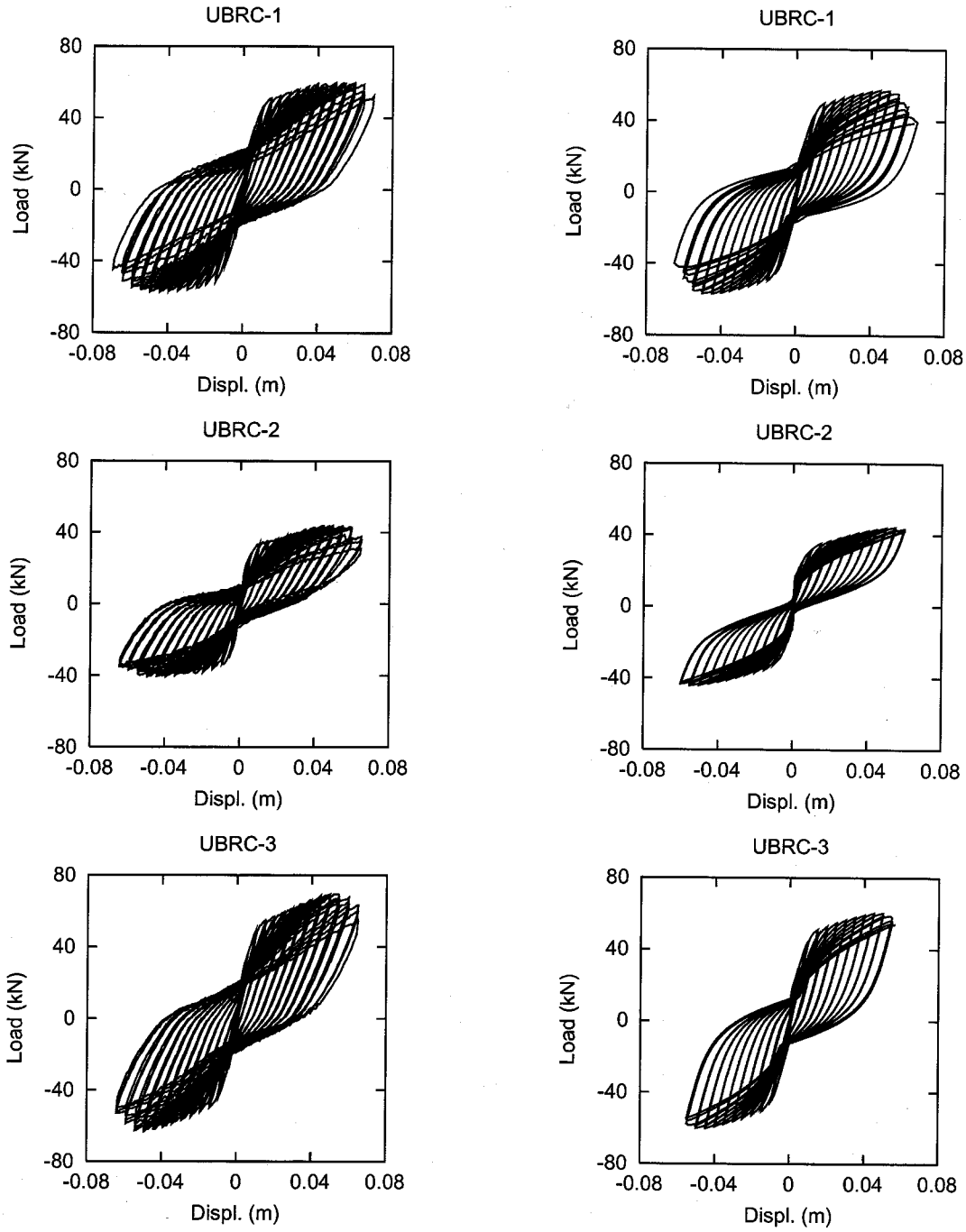

a: Experimental Results b: Analytical Results

Figure 4.19: Comparison of Load–Displacement Hysteresis Loops

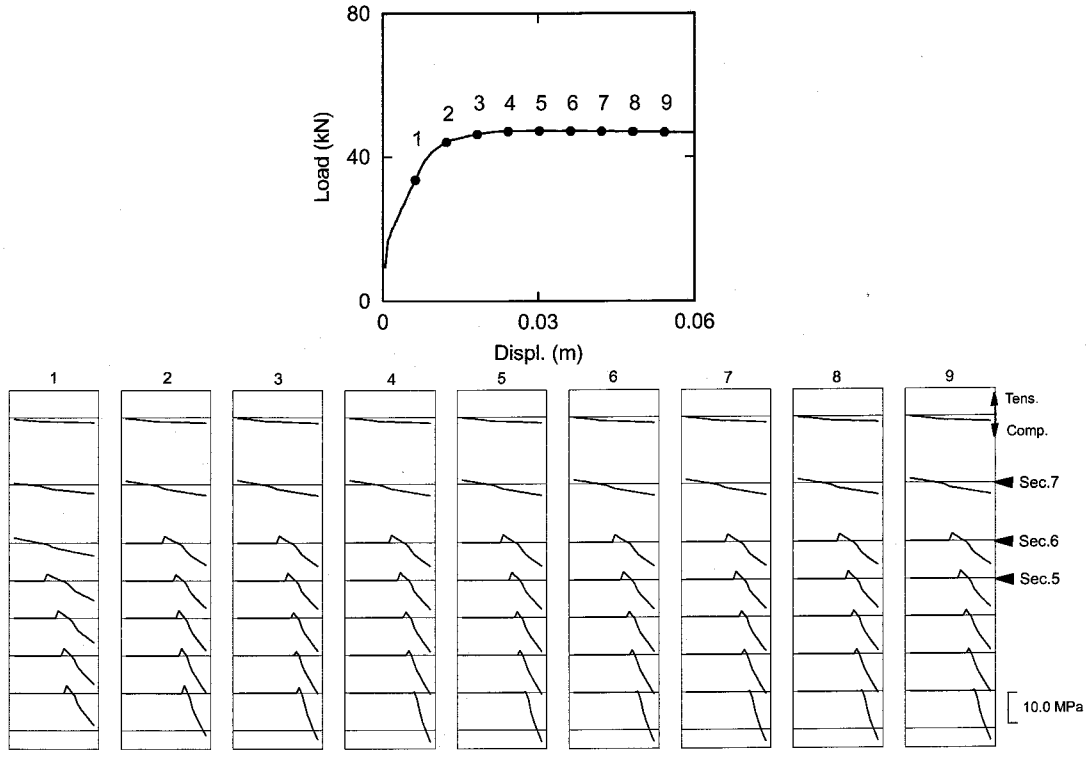

Figure 4.20: Stress Distribution of RC-1

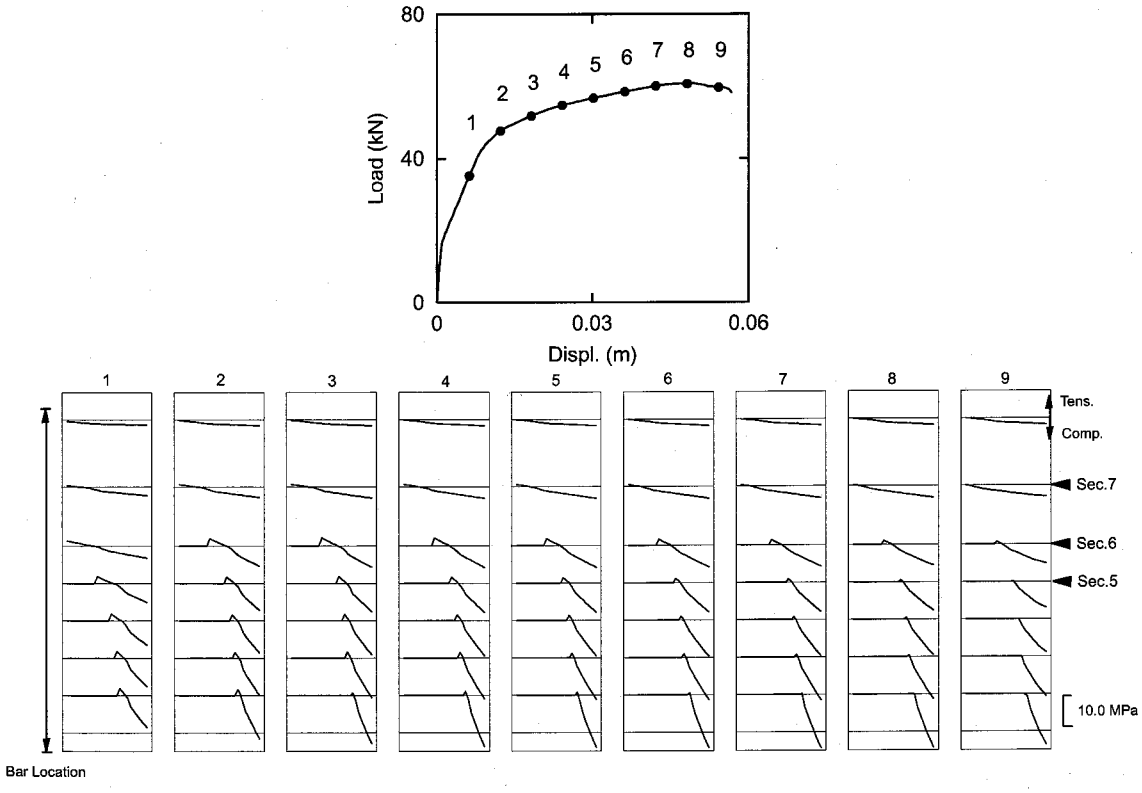

Figure 4.21: Stress Distribution of UBRC-3

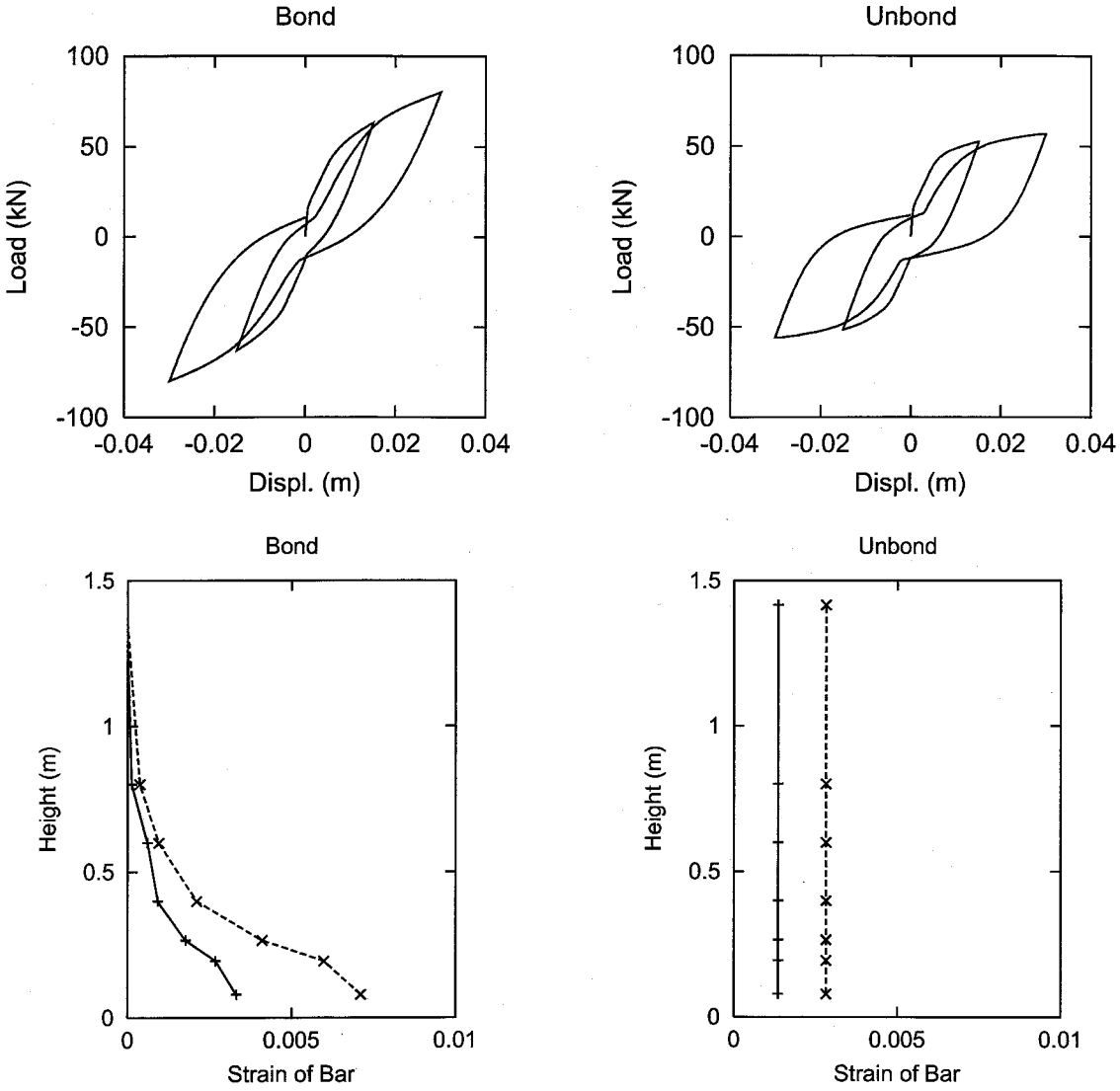

Figure 4.22: Effect of Unbonding

bars is not taken into account.

Compared with the hysteresis loops, the bond type has linearity and the restoring force is large. But from the strain distribution, the strain at the bottom exceeds 7000 μ. Considering that the yield strain of the conventional PC tendon (C-type) is about 5000 ~ 6000 μ, the bar hardly behave in the elastic manner in the large deformation. It means that the elastic restoring force is lost in the large deformation, and we cannot realize the UBRC structure using the conventional materials. On the other hand, the strain distribution of the unbond type shows constant and the level is much smaller than 5000 μ. This is because the whole length of the bars can work effectively. And due to the bars' effect, the positive post-yield stiffness can be obtained. From the results, it is found that the unbonding treatment is effective for the guarantee of the elastic behavior in the large deformation.

4.8 Parametric Studies for Bars of UBRC Structure

4.8.1 Outline

The behavior of UBRC structures is decided by the combination between the RC part and the bars. Installing the unbonded bars into the RC structure, we can obtain the structure with the positive stiffness after yielding, and can control the stiffness due to the amount and the location of the bars. In this section, we conduct the parametric studies of UBRC structures. As the parameters of bars, the area, the location in the section, the length and the gap at the anchor are selected.

In the analysis, the standard structure is UBRC-1. And the ultimate state is defined as the state that the stress of the edge of the core concrete reaches zero. As the stress-strain model for concrete the Ristić model is used and for reinforcement bar the Meneggoto-Pinto model is used. In order to verify the post-yield stiffness due to the bars well, the post-yield stiffness of the reinforcement bars is set to 0.1 % of the elastic stiffness. And the elastic model is used for unbonded bars.

In the evaluation of parameters, the load–displacement skeleton curve and the maximum and ultimate displacement and the strain of the bar are used.

4.8.2 Influence of Area of Bars

As the parameter of this study, the ratio of the area of bars to the total area of longitudinal steel bars (bar ratio) is selected. We examine the four case; 10 %, 30 %, 50 % and 70 % (**Figure 4.23**).

From the skeleton curve, it is found that the post-yield stiffness increases as the bar ratio increases. But in case of high bar ratio, the restoring force deteriorates rapidly after the maximum state. Therefore in this case, we should define the ultimate state for UBRC structures as its maximum state.

And as the bar ratio increases, the maximum and the ultimate displacement and the strain of the bar decreases. The reason for this is that the bars with high bar ratio can exert large force even if the strain is still small, and the large force deteriorates the RC part.

The advantage for increasing the bar ratio to improve the post-yield stiffness is that the bar ratio has no limitation. Large bar ratio can achieve large stiffness and large strength certainly.

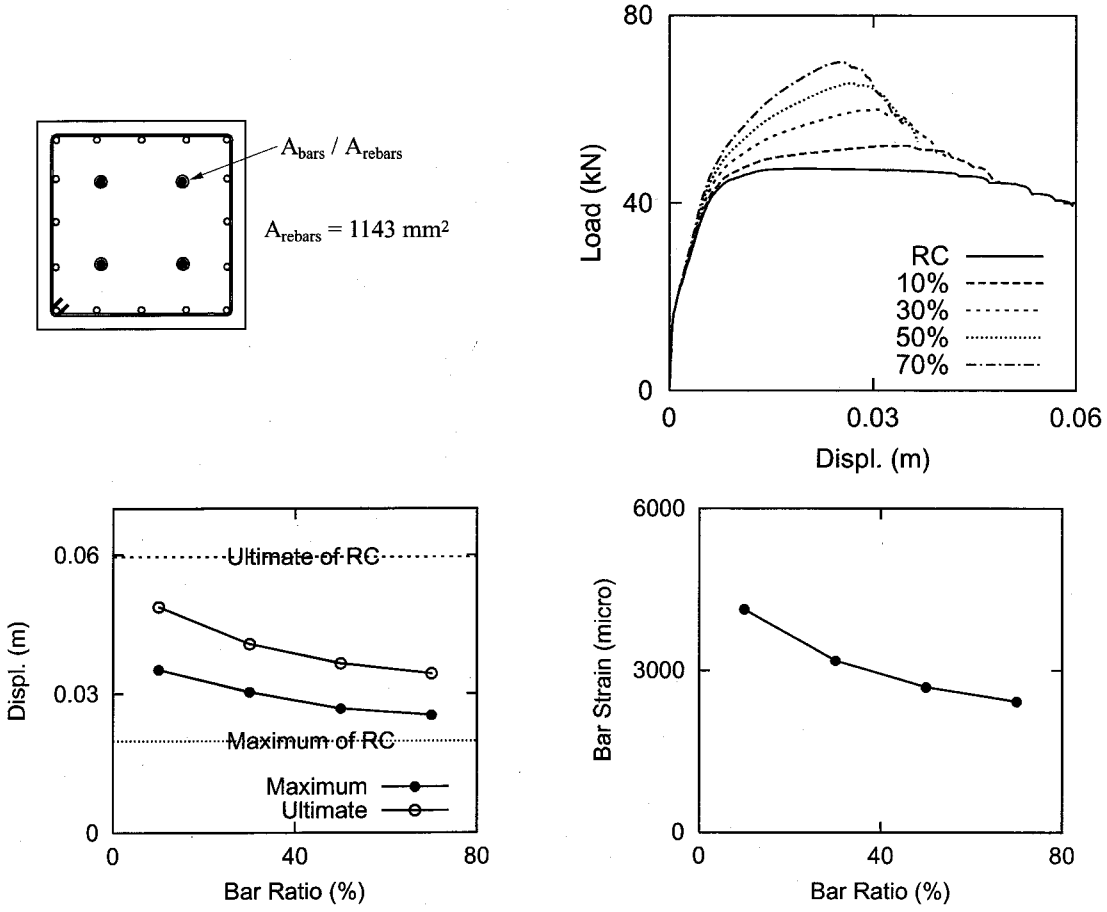

Figure 4.23: Influence of Area of Bars

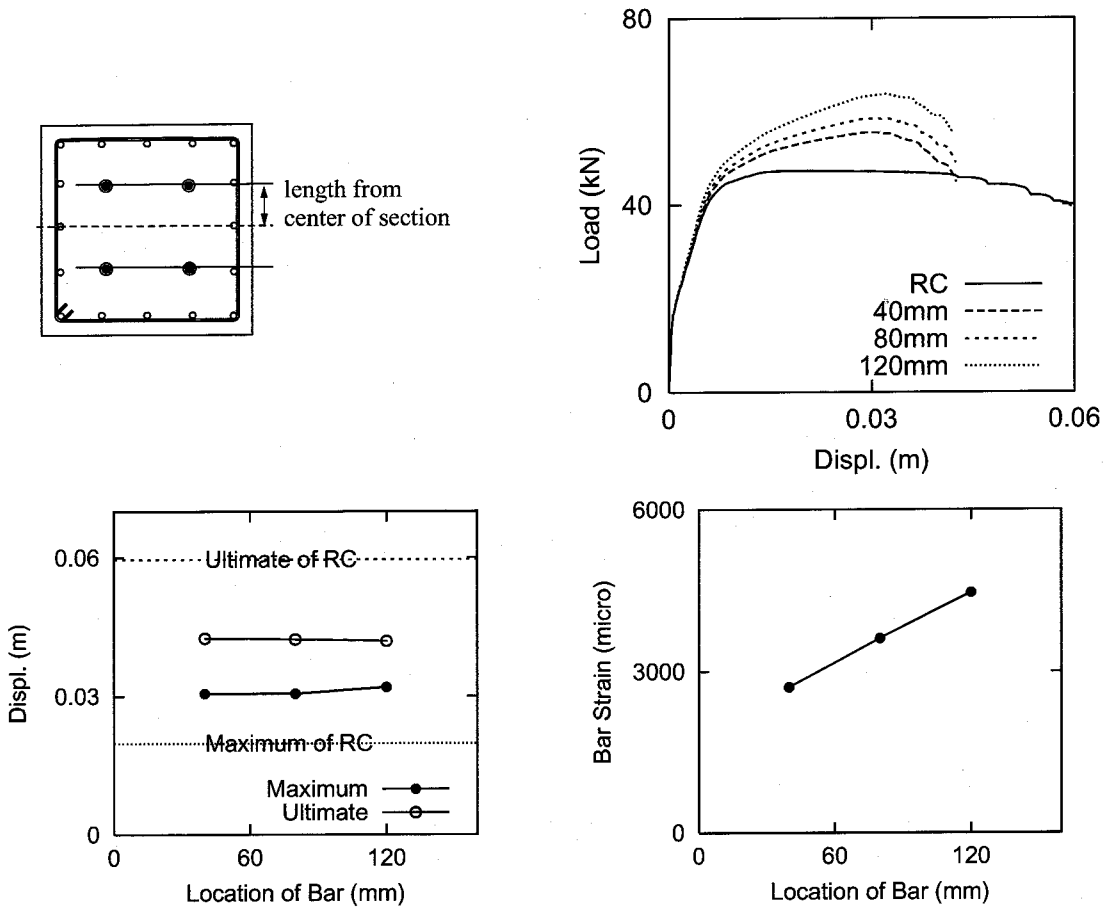

Figure 4.24: Influence of Location of Bars in the Section

4.8.3 Influence of Location of Bars in the Section

The location of bars in the section (length from the center of the section) is selected as the parameter of this study. We examine the length of 40, 80 and 120 mm (**Figure 4.24**).

From the skeleton curve, the post-yield stiffness becomes large as the bar is located apart from the center. And the rate of deterioration after the maximum state is not affected by the location of bars. Only the strain of the bar increases as the location becomes outside.

The location can improve the post-yield stiffness without decreasing the ultimate performance. But the location has the limitation, which is the inside of the section to avoid the buckling and the yield of the bar.

4.8.4 Influence of Length of Bars

The length of bars is selected to be the parameter in this study. For the UBRC structure, the bars is installed so as to put the plastic hinge zone of the RC part between the anchors. In this study, we examine three cases of 2D, 3D and 4D (D: length of plastic hinge) (**Figure 4.25**).

From the skeleton curve, the post-yield stiffness increases as the length of bars becomes

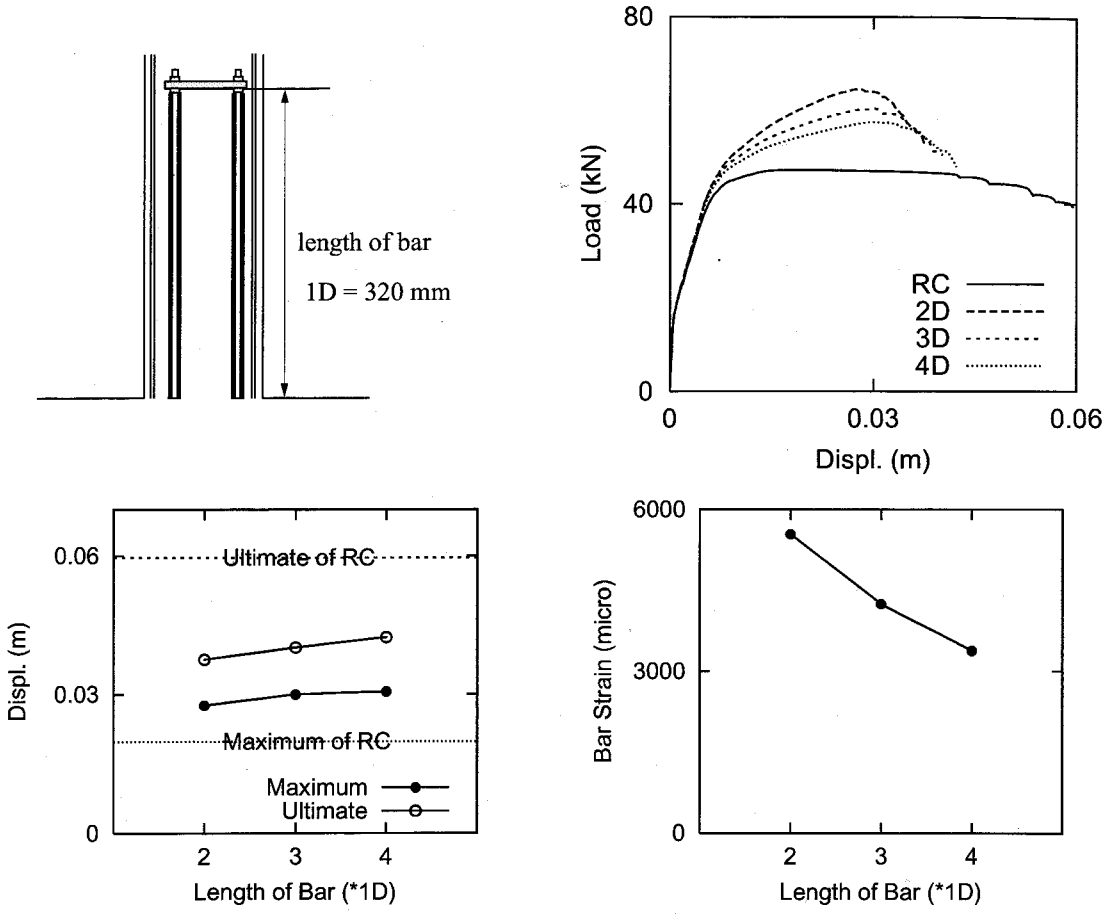

Figure 4.25: Influence of Length of Bars

shorter. And at the same time while the maximum and the ultimate displacement decreases, the strain of the bars increases.

In order to verify the stressing by the bars, the stress distributions of case of 2D and 4D are shown in **Figure 4.26**. At the left of the figures, the bar location is noted. In the case of 4D, the stressing due to the bars' effect can be recognized in the whole length of the pier. On the other hand, in the case of 2D, on Section 6 and 7, the tensile stress remains in the large deformation because these sections are out of the range of the bars. But on Section 5, we can find that the tensile stress is vanishing. The reason for it is the additional moment due to the bars. This results suggest that we should arrange special transverse reinforcements well around the anchor to avoid the failure by the additional moment.

4.8.5 Influence of Gap of Bars at Anchor

In order to verify the effect of the gap at the anchor, we change the length of the gap and analyze the pier. When compressing the bar from the original position, the bar works immediately. But when pulling the bar, it doesn't work until the gap closes. In the analysis,

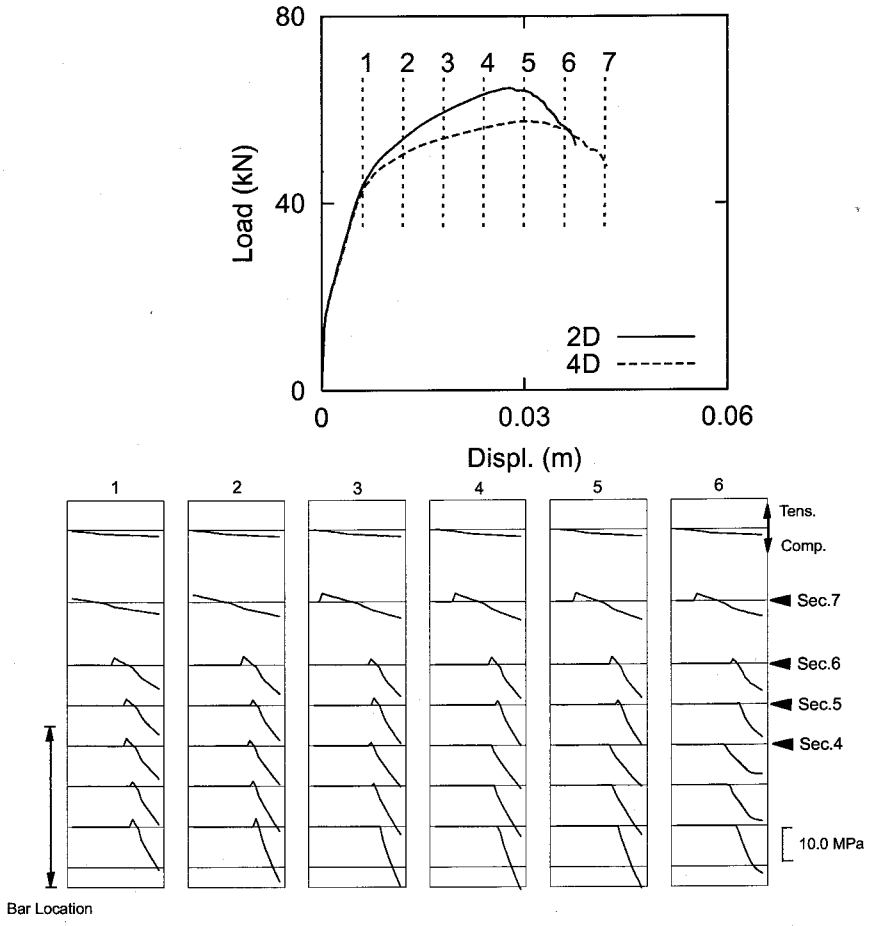

a: Length : 2D

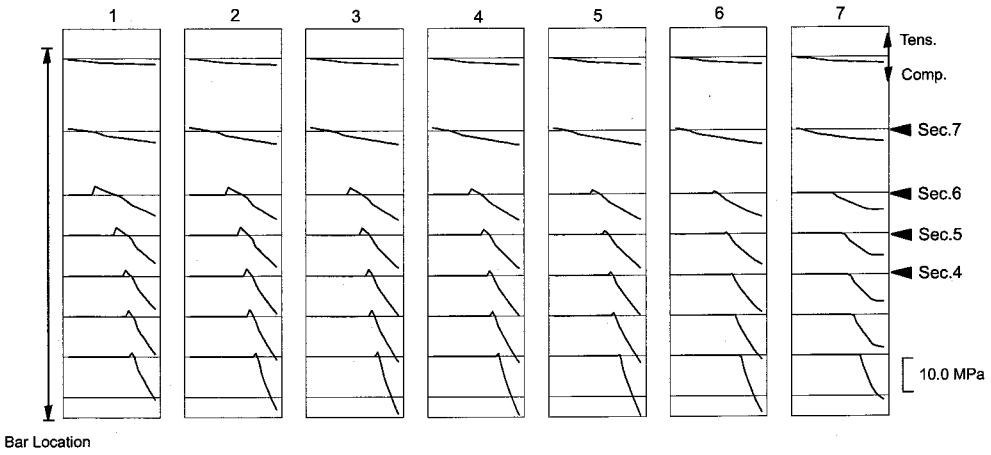

b: Length : 4D

Figure 4.26: Stress Distributions

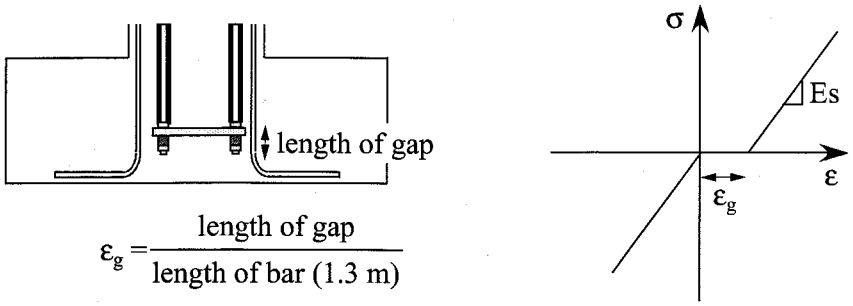

Figure 4.27: Material Property of Bars considering Gap

the gap is taken into account as the nonlinear material property of bars (**Figure 4.27**). The results are shown in **Figure 4.28**.

From the skeleton curve, it is found that the post-yield stiffness is the same regardless of the gap. Only the displacement for the onset of the post-yield stiffness is different. As the result, the maximum and the ultimate displacement increase as the gap increases. Since the ultimate state of the pier is decided by the crushing concrete by the flexural deformation in this study, the maximum restoring force becomes small when the gap is large.

4.8.6 Summary of Parametric Studies

In the previous subsections, we examine the parameters to affect the structural characteristics of UBRC structures. The summary of these studies is shown in **Table 4.3**.

Consider the preliminary designed UBRC structure. If the ultimate strength is lower than the required performance, we may increase the bar ratio. In combination with placing bars outside, with limited decrease of the ultimate deformation, we can increase the strength. If the strength is satisfied with the required performance but the ultimate deformation is lower, we may use the gap and increase the bar ratio a little. Then we keep the strength but increase the deformation. If we need higher post-yield stiffness but the strain of bars exceeds the yield strain, we may increase the bar ratio in place of placing bars outside.

In these parametric studies, the section of the RC part is not selected as a parameter. If we can change the RC section, the various kind of performance can be realized by the UBRC structure.

4.9 Summary

In this study, the UBRC structure was proposed as the high seismic performance structure in the next generation, and the concept and background were described. And, the cyclic loading tests were carried out in order to obtain the fundamental performance. Furthermore the

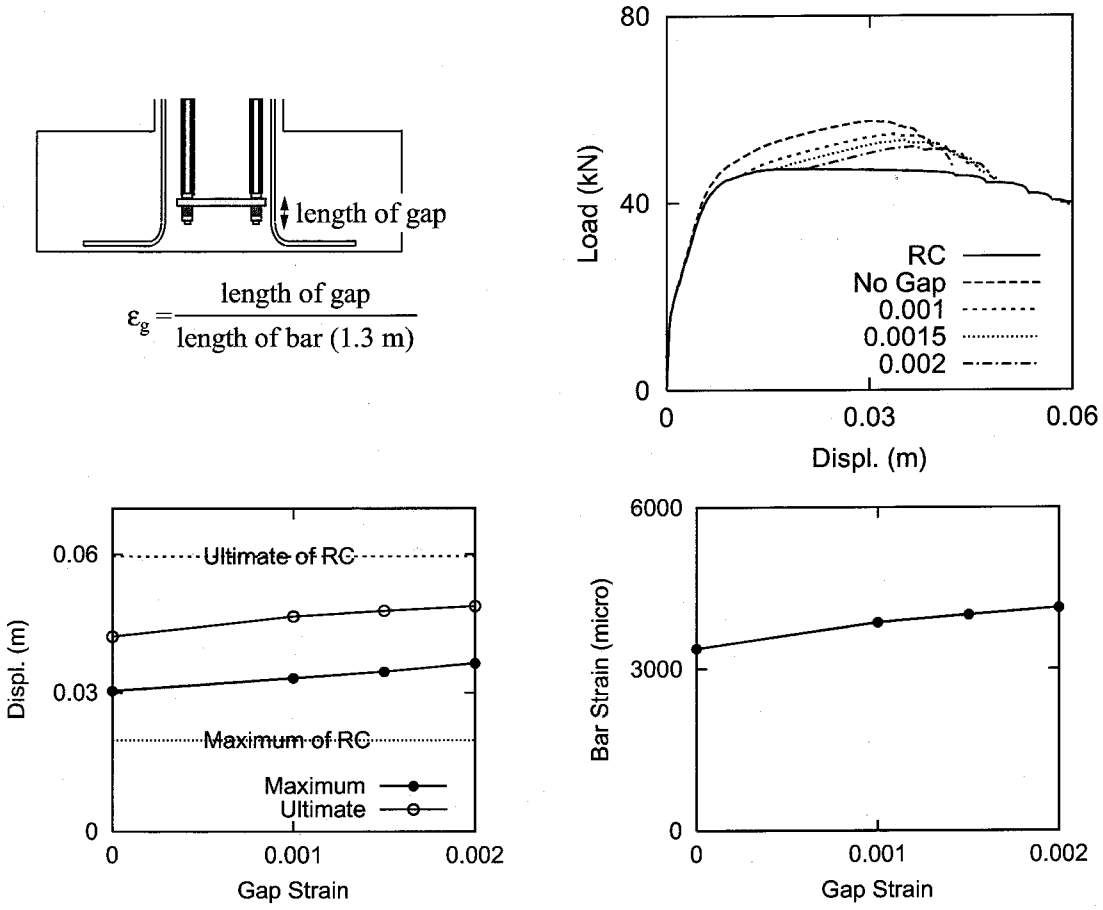

Figure 4.28: Influence of Gap of Bars

Table 4.3: Effect of Parameters

Method	Post-Yield Stiffness	Ultimate (Max.) Displ.	Bar Strain
Increase Bar Ratio	increase	decrease	decrease
Place Outside		constant	increase
Shorten Length		decrease	
Increase Gap	constant	increase	

analytical method for the UBRC structure was developed, and we carried out the parametric studies. From this study, the following results are obtained:

- By installing the unbonded bars, it is possible to easily realize the RC structure with the stable post-yield stiffness.
- The UBRC structure has small residual displacement in comparison with the conventional RC structure by the bar effect.
- The capacity of the energy dissipation is only depend on the amount of longitudinal reinforcement, and never change due to the installation of bars. That is to say, the optimal amount of longitudinal reinforcement for the UBRC structure is the equivalent to that of RC structure in order to expect the energy dissipation.
- From the results of the cyclic loading tests, it can be obtained the equivalent results to the principle got by installing the elastic member into RC structures. This structure can be realized only by installing unbonded bars into RC structure. Therefore this structure can be constructed with simple and easy construction works and low cost.
- The *UnbondBars* object is modeled for the *Method* package of the *Structure* subsystem. In combination with the fiber model object and the unbonded bar object, the behavior of the UBRC structure can be analyzed. Since the method package is different but the the shape object is the same between RC and UBRC structures, the same analytical program for the RC structure can be used for the UBRC structures.
- In order to increase the post-yield stiffness, we have three method; Increase the bar ratio, Place bars outside and Shorten the bar length. By installing the gap at the anchor, the post-yield stiffness doesn't change. Changing these parameters, the various kind of the load – displacement hysteresis can be realized.

References

(1) Editorial Committee for the Report on the Hanshin-Awaji Earthquake Disaster(ed.): *Report on the Hanshin-Awaji Earthquake Disaster, Emergency Repair and Seismic Retrofit (in Japanese)*, Maruzen, 1999.

(2) Iemura, H., Takahashi, Y., Sogabe, N. and Ukai, M.: Developement of High Aseismic Performance RC Piers with Unbonded High Strength Bars (in Japanese), *Proc. of the 1st Symposium on the Enhancement of Earthquake Performance of Infrastructures Based on Investigation into Fracturing Process*, pp. 157–162, 3 2000. Tokyo.

(3) Iemura, H., Takahashi, Y. and Sogabe, N.: Fundamental Study on the RC Piers with Unbonded High Strenght Bars (in Japanese), *Proc. of the 4th Symposium on Ductility Design Method for Bridges*, pp. 433–438, 12 2000. Tokyo.

(4) Iemura, H., Takahashi, Y. and Sogabe, N.: Hybrid Earthquake Loading Test of RC Piers with Unbonded High Strength Bars (in Japanese), *Proc. of the 2nd Symposium on the Enhancement of Earthquake Performance of Infrastructures Based on Investigation into Fracturing Process*, pp. 189–194, 3 2001. Tokyo.

(5) Iemura, H., Takahashi, Y. and Sogabe, N.: Performance Evaluation of UBRC Piers by Hybrid Earthquake Loading Tests (in Japanese), *Proc. of 26th JSCE Earthquake Engineering Symposium*, Vol. 2, pp. 929–932, 8 2001.

(6) Iemura, H., Kato, T., Takahashi, Y. and Maehori, S.: Experimental Study on Seismic Performance of Steel Pipe – Concrete Composite Piers (in Japanese), *Proc. of 10th Japan Earthquake Engineering Symposium*, pp. 2099–2104, 1998.

(7) Kato, T. and Takahashi, Y.: Earthquake Design and Construction of Tall Composite Bridge Piers, *Proc. of 12th World Conference on Earthquake Engineering*, p. No.899, 2000.

(8) Kato, T.: *Research on Inelastic Behavior and Seismic Safety of Steel Pipe – Concnrete Composite Tall Piers (in Japanese)*, PhD Thesis, Kyoto University, 1998.

(9) Iemura, H. and Mikami, T. : Demand Spectra of Yielding Strength and Ductility Factor for Required Seismic Performance Objectives (in Japanese), *Journal of JSCE*, Vol. I-57, No. 689, pp. 333–32, 10 2001.

(10) Japan Road Association: *Seismic Design Specification for Highway Bridges (in Japanese)*, Maruzen Ltd., 1996.

Chapter 5

Application of UBRC Structure

5.1 General Remarks

In the previous chapter, the fundamental characteristics of the UBRC structure are investigated. The results show that the post-yield stiffness can be controlled by the bar parameters. This chapter shows the applications of the UBRC structure. At first, applying to the railway structure, it is shown that the pier can be designed rationally under the two-level seismic design method. This word "rational" means that the applied structure can be satisfied with the required performance with the small amount of reinforcement. Next, applying to the highway bridge structure, the seismic response behavior is investigated by the hybrid earthquake loading tests.

This chapter is described on the basis of the works by Iemura and Takahashi[1,2].

5.2 Application for Railway Structure: Reduce Reinforcement

5.2.1 Two Level Seismic Design Method

After the Hyogo-ken Nanbu Earthquake, the two level seismic design method was proposed as the seismic design of infrastructures[3)4)]. The design method takes two types of design ground motion into account. For a moderate ground motion (called Level I), a bridge should behave in an elastic manner without essential structural damage. For an extreme ground motion (called Level II), a standard bridge should prevent critical failure, while an important bridge should keep the functions with limited damage. Following these proposals, several design specifications were revised[5)6)].

On the other hand, as the design model of a RC structure, the Bridge Design Specifi-

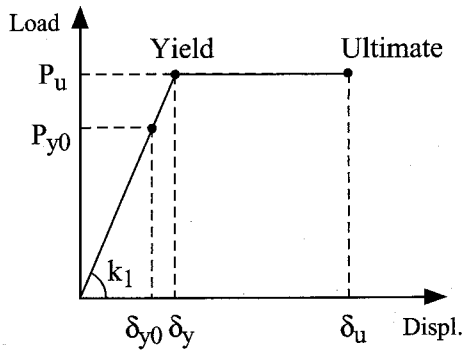

Figure 5.1: Design Load–Displacement Relationship of RC Pier

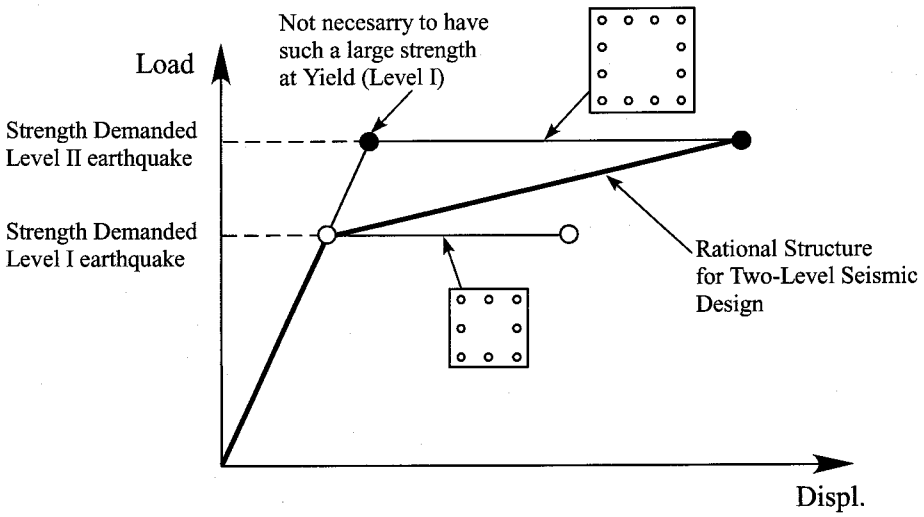

Figure 5.2: Rational Load–Displacement Relationship in Two Level Seismic Design Method

cation uses the perfectly elasto-plastic relationship (**Figure 5.1**)[5]. The Design Standard for Railway Structure uses the tetra-linear model, connecting the crack, yield, maximum and ultimate state[6], but for column type piers, the perfectly elasto-plastic model is recognized to be reasonable from the results of various tests.

When the two level design method is applied for a RC structure, the cross section is usually decided by the Level II design. The required strength by Level II is usually much higher than that by Level I. Since the yield strength and the ultimate state load of the RC structure are almost the same, such a high level of load resistance is required in the yield state although that is essentially required only in the ultimate state. That is to say, the design for Level I is often meaningless. If the post-yield stiffness of the structure can be used effectively, it will be possible that the rational design of a RC structure is carried out by connecting the required performance point of the Level I and Level II (**Figure 5.2**). In this meaning, the UBRC structure with the significant post-yield stiffness can contribute to the rational seismic design.

5.2.2 Railway Rigid Frame Viaduct and Preliminary Design

The objective railway rigid frame viaduct is the railway beam–slab style, and the elevation is shown in **Figure 5.3**. In general, the rigid frame viaduct of the railway structure has large amount of reinforcement. Applying the UBRC structure to the viaduct, the reduction of reinforcement is tried.

In the seismic design of the railway structure, corresponding to the presumed levels of repair and reinforcement of structures that may be required after an intense earthquake, the seismic performance can be categorized into 3 levels as follows[6]:

1. Seismic Performance I: capability of maintaining the original functions without any repair and no excessive displacement occurring during an earthquake.

2. Seismic Performance II: capability of making quick recovery of the original functions with repairs after an earthquake.

3. Seismic Performance III: capability of keeping the overall structure in place without collapse during an earthquake.

For moderate earthquakes (called L1 earthquakes), the structural seismic performance I should be satisfied by all structures. For severe earthquakes (called L2 earthquakes), the seismic performance II should be satisfied by the important structures.

To begin with, the pier as the RC structure for L2 earthquakes is designed, and the designed pier has a 700 mm square cross section and has 24–D32 longitudinal bars. The longitudinal bar ratio is about 3.9 %, which is large amount compared with highway bridge piers (1.0 ~ 1.5 %). On the other hand, the design for L1 earthquakes only requires 16–D32 longitudinal bars in the section (2.6 %). Therefore, for the design concept of the UBRC pier,

1. Only the RC member can be satisfied with Seismic Performance I.

2. The combination of unbonded bars and the RC member can be satisfied with Seismic Performance II.

Under this design philosophy, the cross section is decided as **Figure 5.4**.

It is also possible to reduce the cross section of UBRC member, but in consideration for the workability, in this preliminary design, the cross section is set to be the same as the RC member designed by L1 earthquakes.

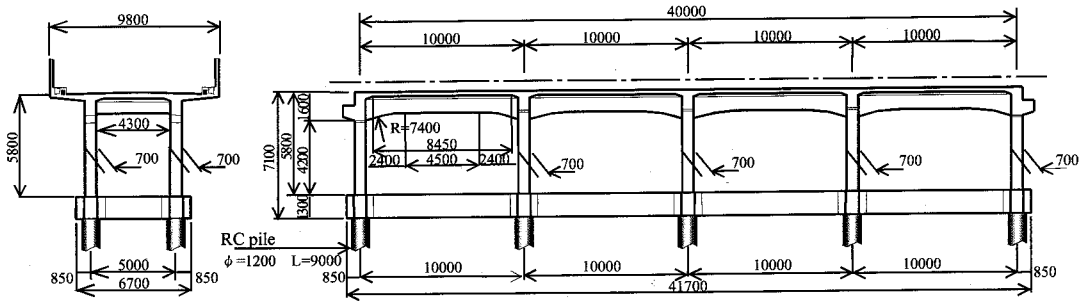

Figure 5.3: Railway Rigid Frame Viaduct Bridge

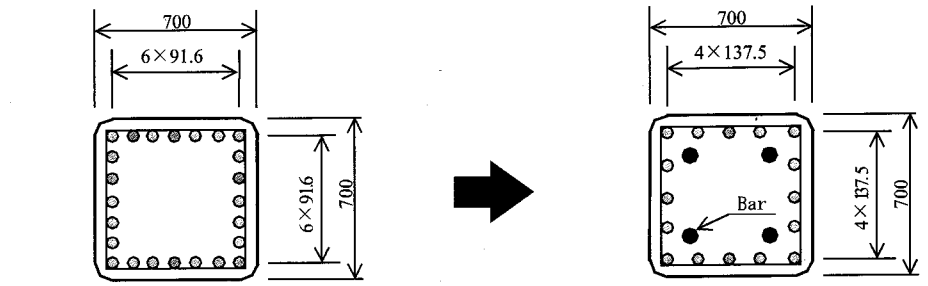

<RC Structure>

- Reinforcement
  - Re-bar SD345 D32 * 24
  - Stirrup SD345 D19 ctc 100
- Concrete 27N/mm²

<UBRC Structure>

- Reinforcement
  - Re-bar SD345 D32 * 16
  - Stirrup SD345 D19 ctc 100
- Concrete 27N/mm²
- Bar (PC rod)
  - φ 32
  - Yield Strength 1185N/mm²
  - Tensile Strength 1331N/mm²

Figure 5.4: Cross Section of RC and UBRC Structure

5.2.3 Description of Test Units and Test Procedure

In order to verify the performance of the UBRC pier by the two level seismic design method, the cyclic loading tests were carried out. In this test we constructed scaled models of the half pier of the rigid frame so as to become the similar moment distribution because the test setup is for single column specimens.

The RC test unit was the 1/2.1875 scale model of the RC pier in the preliminary design for L2 earthquakes (**Figure 5.5**). The number of longitudinal bars and the width between the bars were precisely scaled down.

The UBRC test unit was also the 1/2.1875 scale model of the UBRC pier in the trial design. The arrangement of the longitudinal bars was decided by the section designed by L1 earthquakes, and the configuration of unbonded bars was decided so that the maximum strength was larger than that of RC pier designed by L2 earthquakes. The analytical result is shown in **Figure 5.6**. In the yield state, the restoring force of the UBRC pier is lower than that of the RC pier, but in the large deformation, the UBRC pier becomes stronger than the RC pier. In short, in this structure, the elastic behavior under L1 earthquakes was guaranteed by the RC structure and the required strength of L2 earthquakes was guaranteed by the post-yield stiffness due to the unbonded bars.

The longitudinal bars of the UBRC unit were fewer than the RC unit, and the 4–ϕ17 PC rods were placed in the corner of the cross section. Since the work space became large, the construction work became very easy. For the unbonding treatment, the Hishi Tube by Mitsubishi Plastics, Inc. was used (**Photo 5.1**). This tube is the polyvinylchloride heat shrinkable tube for protecting reinforcement bars from the rust. For the pull-out tests using this tube, the good performance of the unbonding treatment was confirmed.

In the experiments, the horizontal displacement was applied in cycles to displacement ductility factor each of $\mu = \pm 1, \pm 2$, etc. ($\mu = 6$ mm). The axial stress was 1.24 MPa calculated from the superstructure of the assuming pier.

5.2.4 Test Results

Load–Displacement Hysteresis Loops

The hysteresis loops of the RC and UBRC unit are shown in **Figure 5.7**. In case of the RC unit, the restoring force tended to deteriorate gradually after the maximum force (183 kN at the displacement of 0.041 m). On the other hand, the restoring force of the UBRC unit was 171 kN at the displacement of the maximum state of the RC unit, and it increased gradually up to 186 kN at the displacement of 0.077 m along to the stable post-yield stiffness branch. This result was satisfied with the required performance of L2 earthquakes.

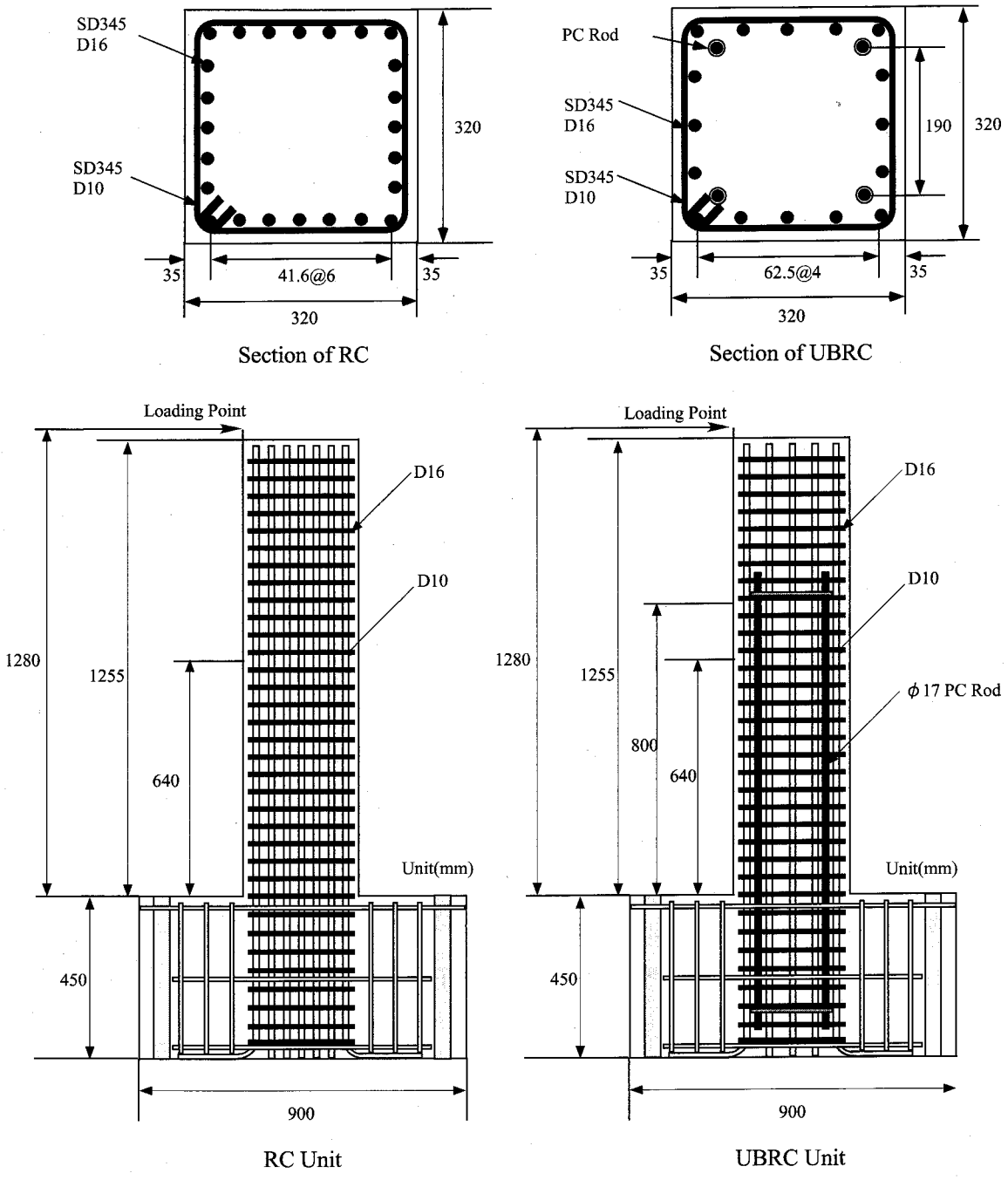

Figure 5.5: Test Units

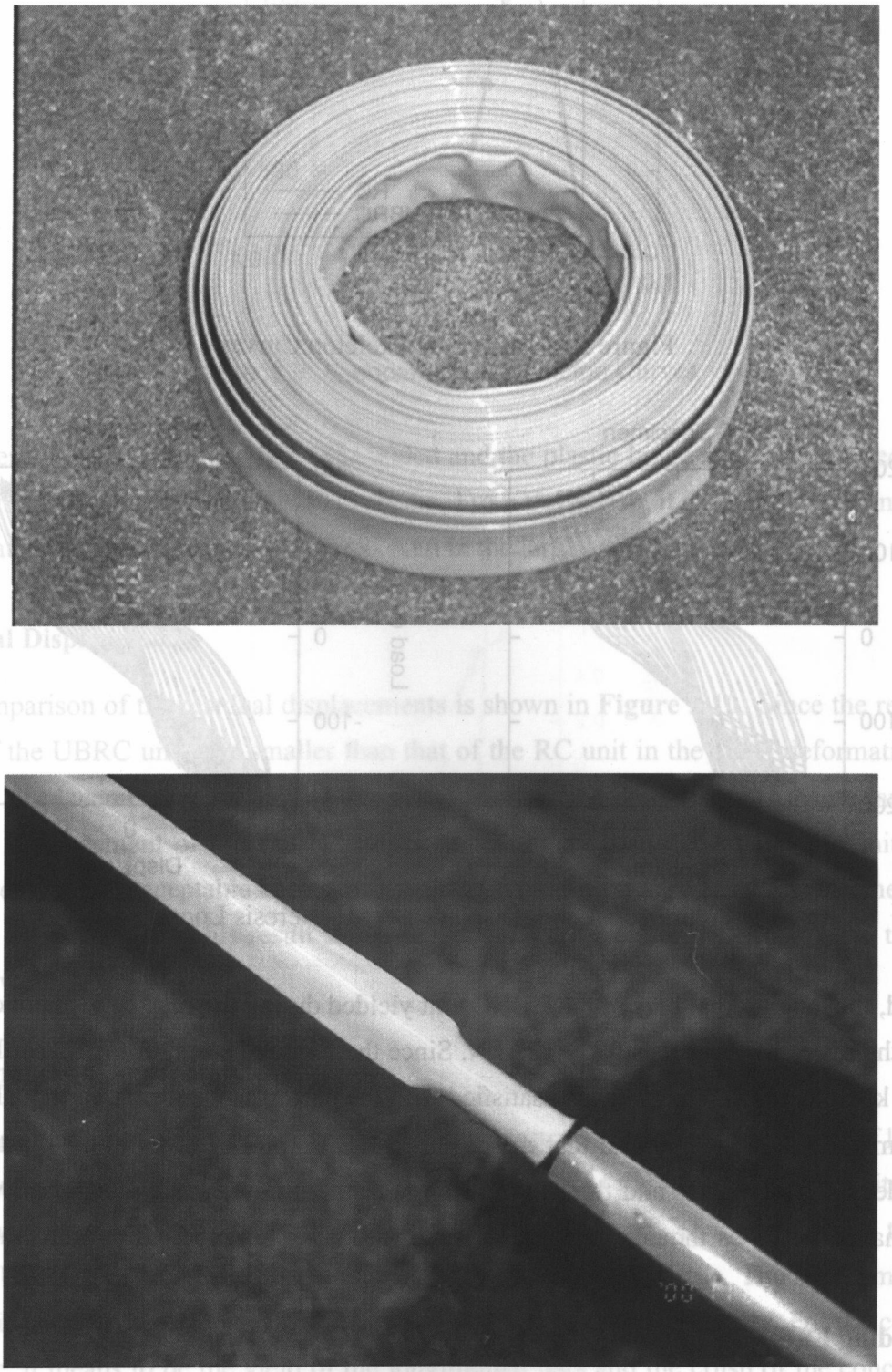

Photo 5.1: Unbond Tube

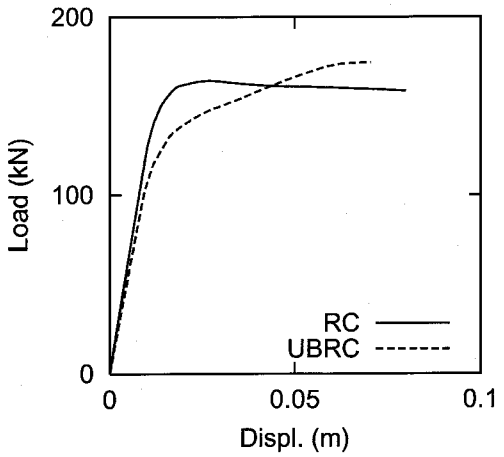

Figure 5.6: Analytical Skeleton Curves

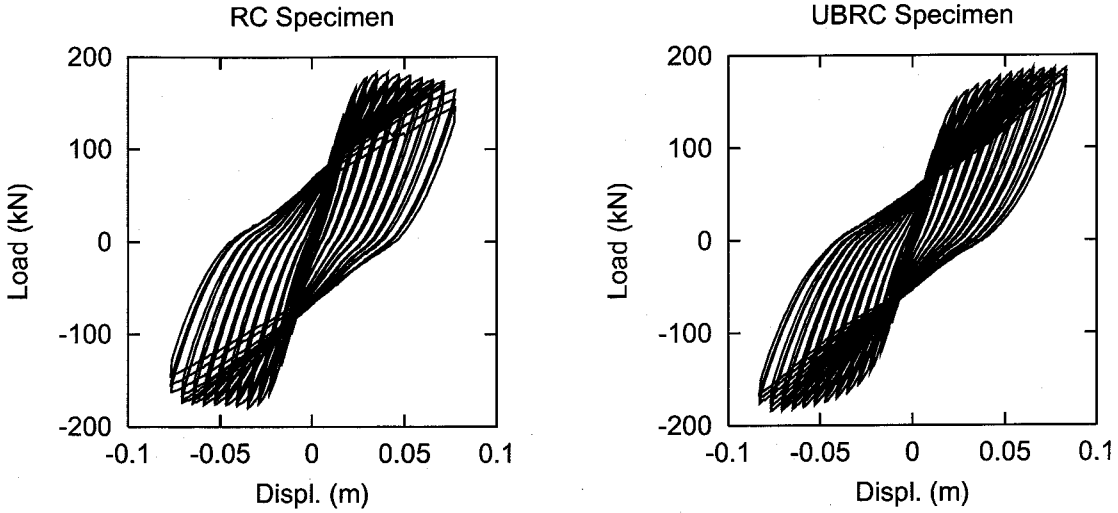

Figure 5.7: Load–Displacement Hysteresis Loops

And, the longitudinal bars of the UBRC unit yielded during the first 2 ~ 3 input cycle, at which the restoring force was 97 ~ 128 kN. Since the required strength for L1 earthquakes was 92 kN, this UBRC unit was also satisfied with the performance for L1 earthquakes.

From the results, it is found that the designed UBRC pier behaves in the elastic manner under L1 earthquakes and the restoring force at the ultimate state is satisfied with the performance for L2 earthquakes in spite of small amount of longitudinal reinforcement.

Unbonding Effect

Figure 5.9 shows the snapshots of the strain distribution of the unbonded bar and the longitudinal bar of the UBRC unit during the loadings (at 1st, 3rd, 5th cycle). If the bars bond to the concrete perfectly, the strain distribution becomes triangle (see the results of longitudinal bars). But the strain distribution of the unbonded bars became constant even in the deforma-

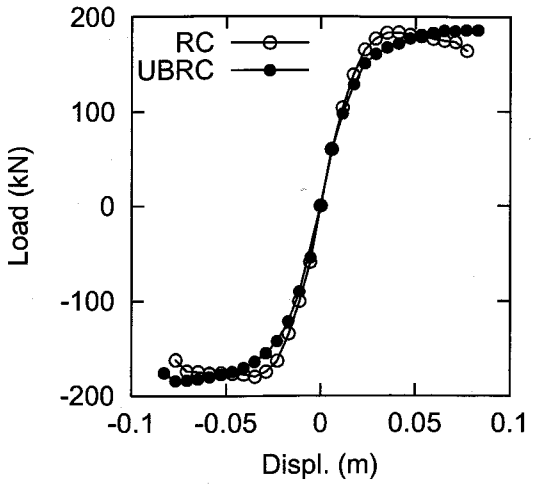

Figure 5.8: Comparison of Skeleton Curves

tion whereas the longitudinal bar had yielded and the plastic hinge zone was formed. And, finally in this test, the bars remained in elastic. From the results, it is clear that the unbonded bars treated by the tube can worked well even in the large deformation.

Residual Displacement

The comparison of the residual displacements is shown in **Figure 5.10**. Since the restoring force of the UBRC unit was smaller than that of the RC unit in the small deformation, the residual displacements were almost the same. And as the deformation became large, the residual displacement of the UBRC unit became smaller than that of the RC unit. This phenomena can be acceptable because we want to avoid the large residual displacement over the 1 % of the height. This result suggests that the elastic restoring force due to the bars worked well.

Performance of Absorbing Energy

The accumulation of absorbed energy is shown in **Figure 5.11**. Since the amount of longitudinal reinforcement of the UBRC unit was lower than that of the RC unit, the capacity of the energy absorption of the UBRC unit was inferior to the RC unit. This result seems to show that the UBRC pier has the low seismic performance, but it is not true. The large amount of hysteretic absorbed energy means the large plastic deformation of the pier. For the concrete structure, it means to be the yield of the longitudinal bars and the crush of the concrete. If the structure with small failure has the equivalent seismic performance of the RC structure, the structure has advantage for the usability and the repairability after earthquakes. Since the UBRC structure can be satisfied with the required performance in the load–displacement relationship, the UBRC structure has the high seismic performance.

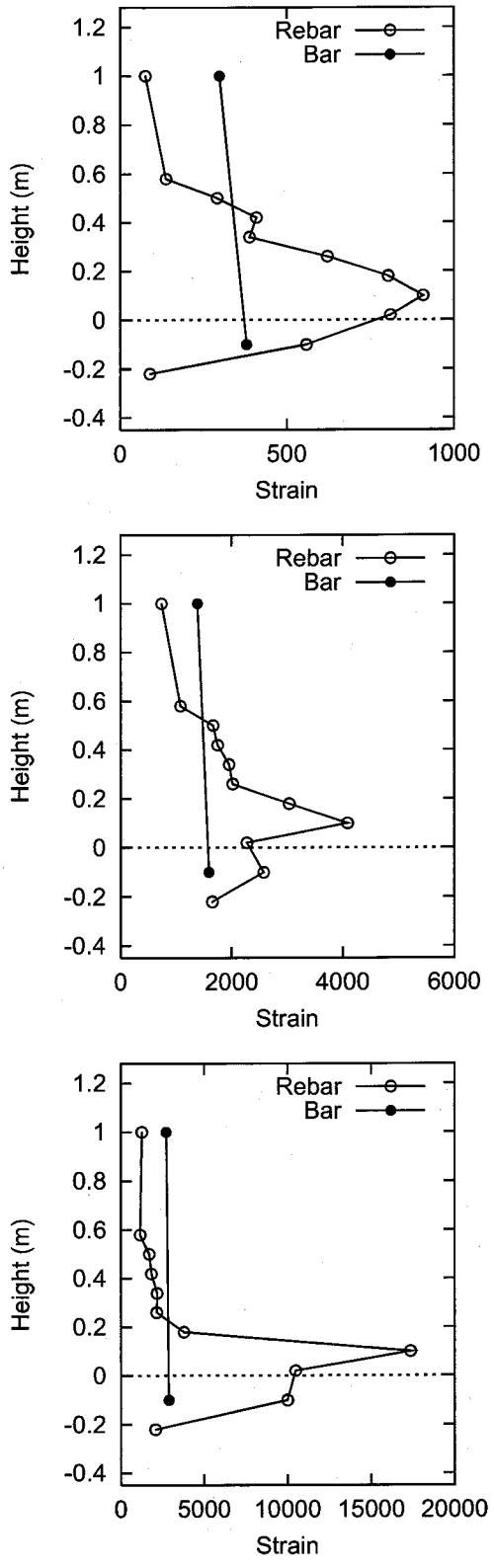

Figure 5.9: Strain Distribution of Bars and Re-bars

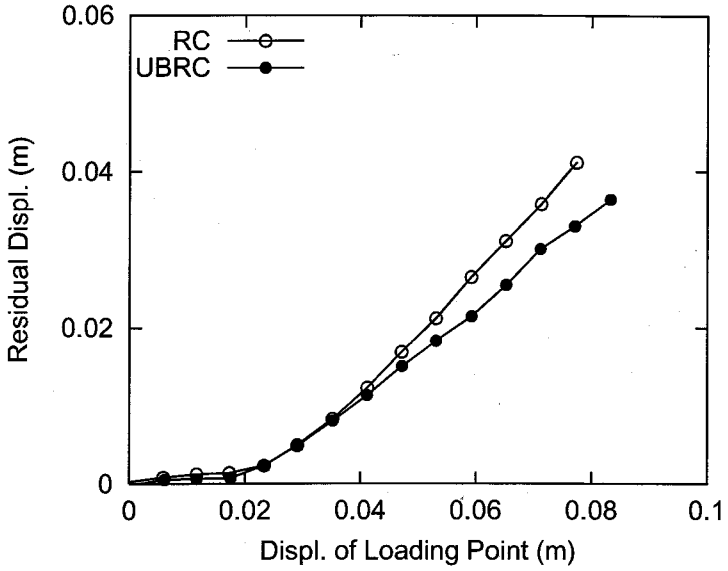

Figure 5.10: Residual Displacement

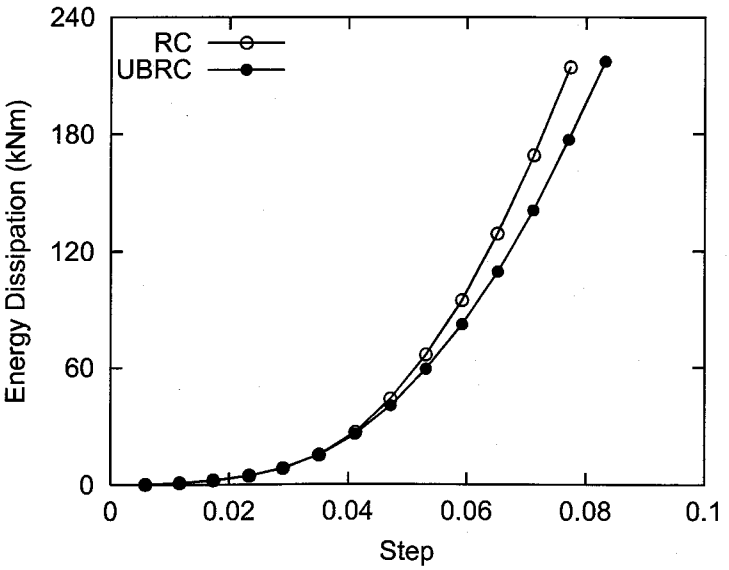

Figure 5.11: Accumulation of Absorbed Energy

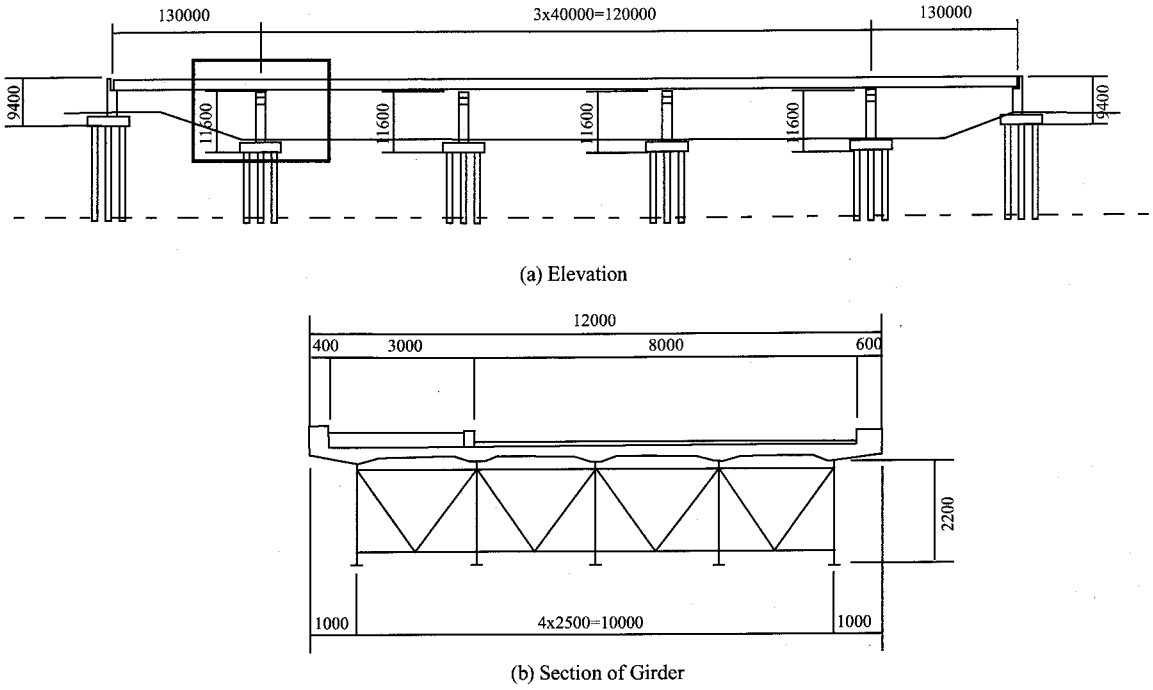

Figure 5.12: Continuous Girder Bridge

5.3 Application for Highway Bridge Structure: Seismic Response

5.3.1 Highway Bridge

The highway bridge used in this study is shown in **Figure 5.12**. The superstructure was the 5 span continuous steel I-girder, and the length of the span was 13 m, 40 m × 3 and 13 m. The pier surrounded by the solid line in **Figure 5.12** was selected as the target pier, and the behavior in the transverse direction was considered in this study. The pier has a 2.4 m square cross section and a height of 9.6 m[7]. 72-D34 were used as the longitudinal reinforcement and D19 transverse hoops were placed in the pitch of 300 mm (**Figure 5.13**).

5.3.2 Description of Test Units and Test Procedure

In order to verify the seismic performance of the UBRC pier, the pseudo dynamics tests were carried out. In this test we constructed three 1/7.5 scale models.

The specimens had a 320 mm square cross section and the loading span of 1.28 m. The reinforcement was 16-D10 as longitudinal bars, D4 stirrups in 40 mm interval and intermediate hoops to adjust the stirrup ratio to that of the assuming pier (**Figure 5.14**). In case of the UBRC pier, PC rods (C-type, ϕ9.2) with the unbonding treatment were installed at 110 mm from the center of the cross section. The both ends of the bars were anchored in

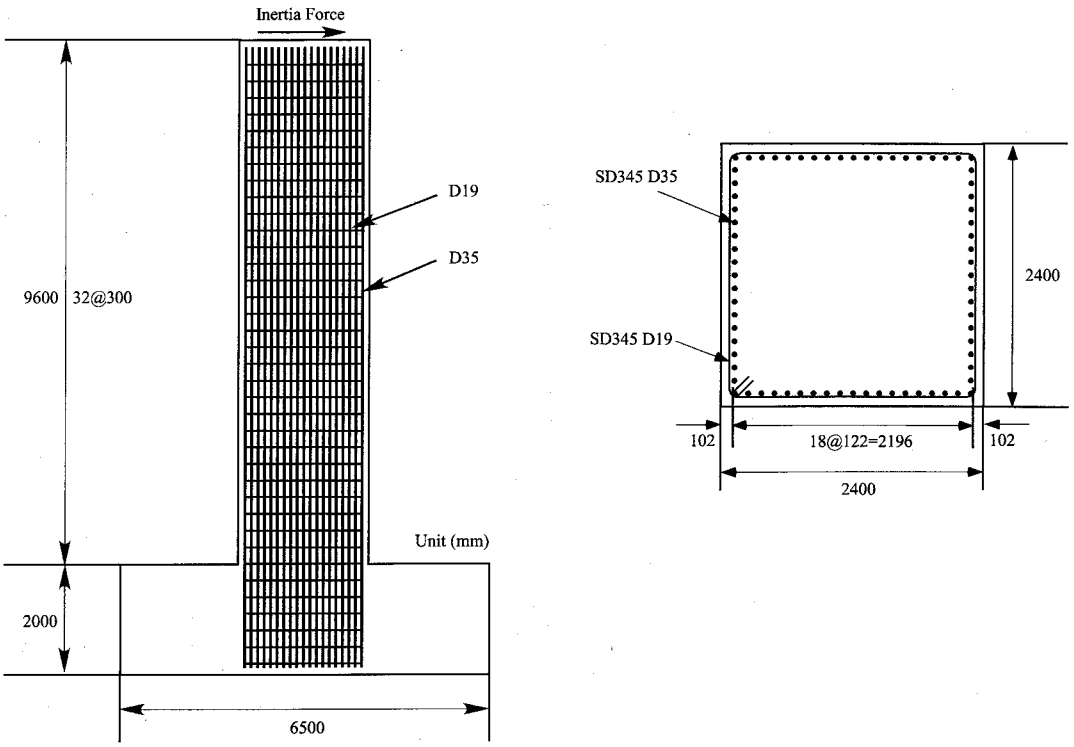

Figure 5.13: Arrangement of Pier

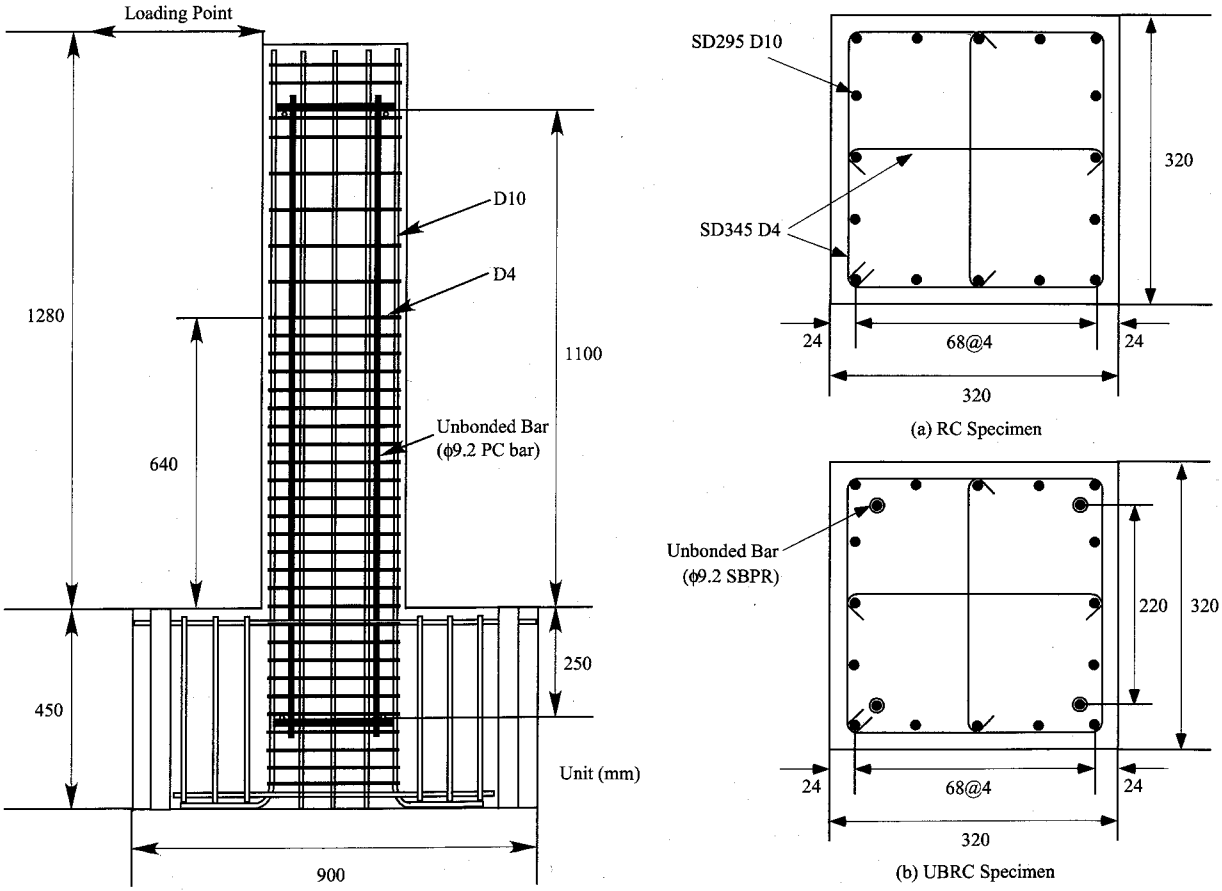

Figure 5.14: Test Units

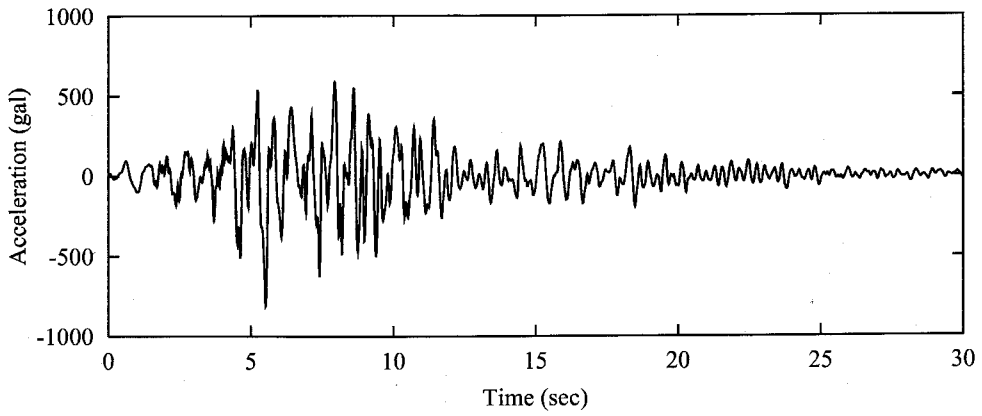

Figure 5.15: Kobe JMA Record (NS Component)

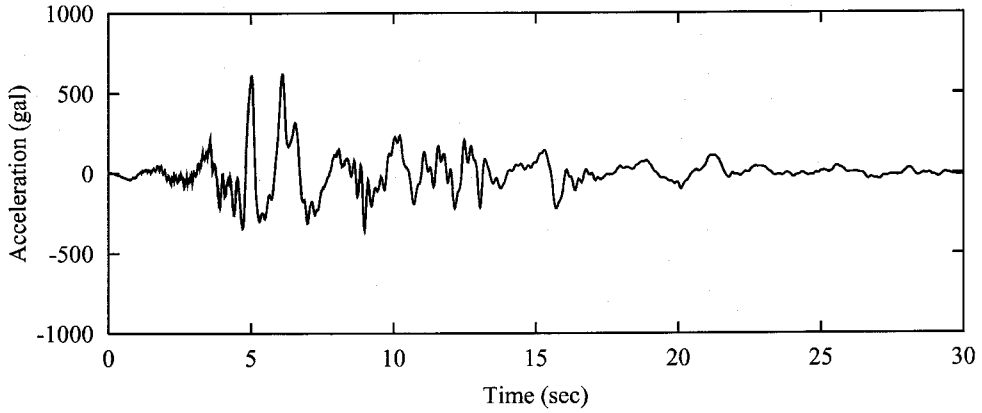

Figure 5.16: Port Island Record (EW Component)

the concrete mechanically.

In the pseudo dynamic test, Kobe JMA record NS component (**Figure 5.15**) and Kobe Port Island record EW component (**Figure 5.16**) were used to examine seismic response characteristics. By considering the similarity law, using the scale model, the tests carried out seismic response calculation for the actual-size structure in the computer[8]. The assuming superstructure weight (Steel I-shape girder) was set to about 5000 kN. In the tests, the axial stress was set to 0.88 MPa.

Parameters of test units and test cases are shown in **Table 5.1**.

Table 5.1: Parameters of Test Units and Test Cases

Test Unit	Input Motion	Stirrup	Bar	Longitudinal Bar
RC-2	Kobe JMA Record NS	D4@40 mm	–	16 – D10
UBRC-3			4×SBPR ϕ9.2 (110 mm)	
UBRC-4	Kobe Pord Island EW			

5.3.3 Results of Pseudo Dynamic Tests

In Case of the Kobe JMA record NS component

The results of RC-2 and UBRC-4 are shown in **Figure 5.17** and **Figure 5.18** respectively. These results were plotted in scale of the real structure.

From the load–displacement hysteresis loop of UBRC-4, the positive post-yield stiffness can be observed. And, the shape of hysteresis loop had the linearity compared with that of RC-2. It is found that the effect of the unbonded bars can be recognized as same as the cyclic loading tests.

From the displacement time histories, the maximum responses in both cases of RC-2 and UBRC-4 were about 30 cm, so no significant difference due to the installation of bars was obtained in this case. One of the reasons for the small difference of the maximum response is that the input motion was insensitive to the variation of post-yield stiffness of the structure. But during 6, 7 seconds, UBRC-4 returned to the original position, but RC-2 returned only to about 0.12 m. As the result, the residual displacement after the earthquake of UBRC-4 was only 1.5 cm, whereas that of the RC-2 was 5 cm. This result shows that by installing unbonded bars, the residual displacement after earthquake can be reduced and the hysteretic behavior can be stabilized.

In Case of the Kobe Port Island Record EW Component

In order to verify the influence of ground motions on the response of structures with post-yield stiffness, the Kobe Port Island record (EW component) (for soft soil) was inputted. Since the test for the RC pier couldn't be carried out using the same input motion, the test results is substituted by the seismic response analysis using the structural properties from RC-2 test unit. As the preliminary examination, it has been confirmed to agree the analytical results with experimental result for RC-2. The analytical results of the RC pier and the experimental result of UBRC-5 are shown in **Figure 5.19** and **Figure 5.20** respectively.

In this case, the maximum displacement response of UBRC-5 was smaller than that of the RC pier. As the result, the residual displacement after earthquake of UBRC-5 was almost zero. Although we have to take care of the characteristics of the input motion, it is found that the residual displacement after earthquakes of the UBRC structure can be reduced by the combination of the small displacement response and the elastic restoring force of the bars.

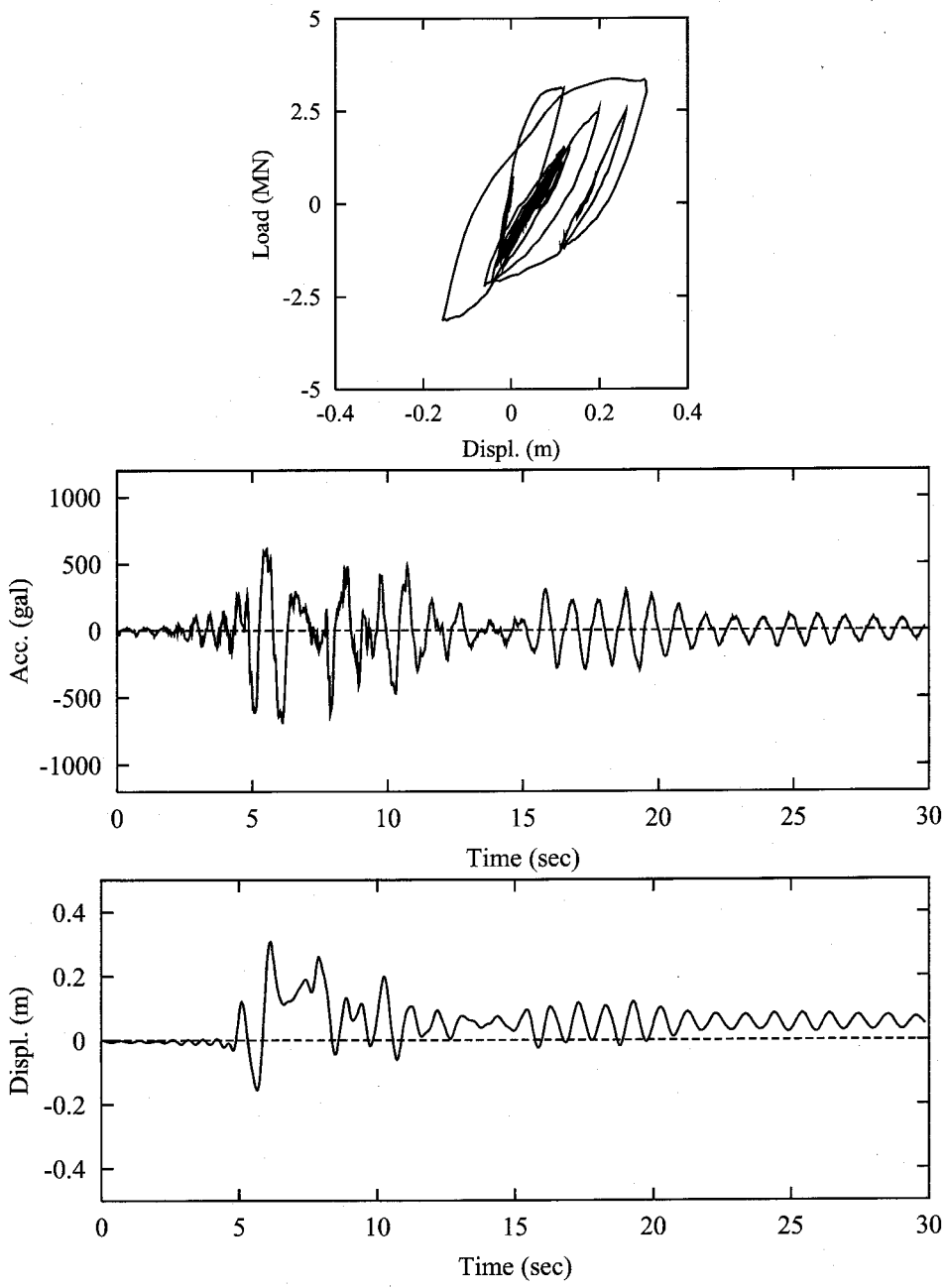

Figure 5.17: Results of Pseudo Dyanamic Test(RC-2)

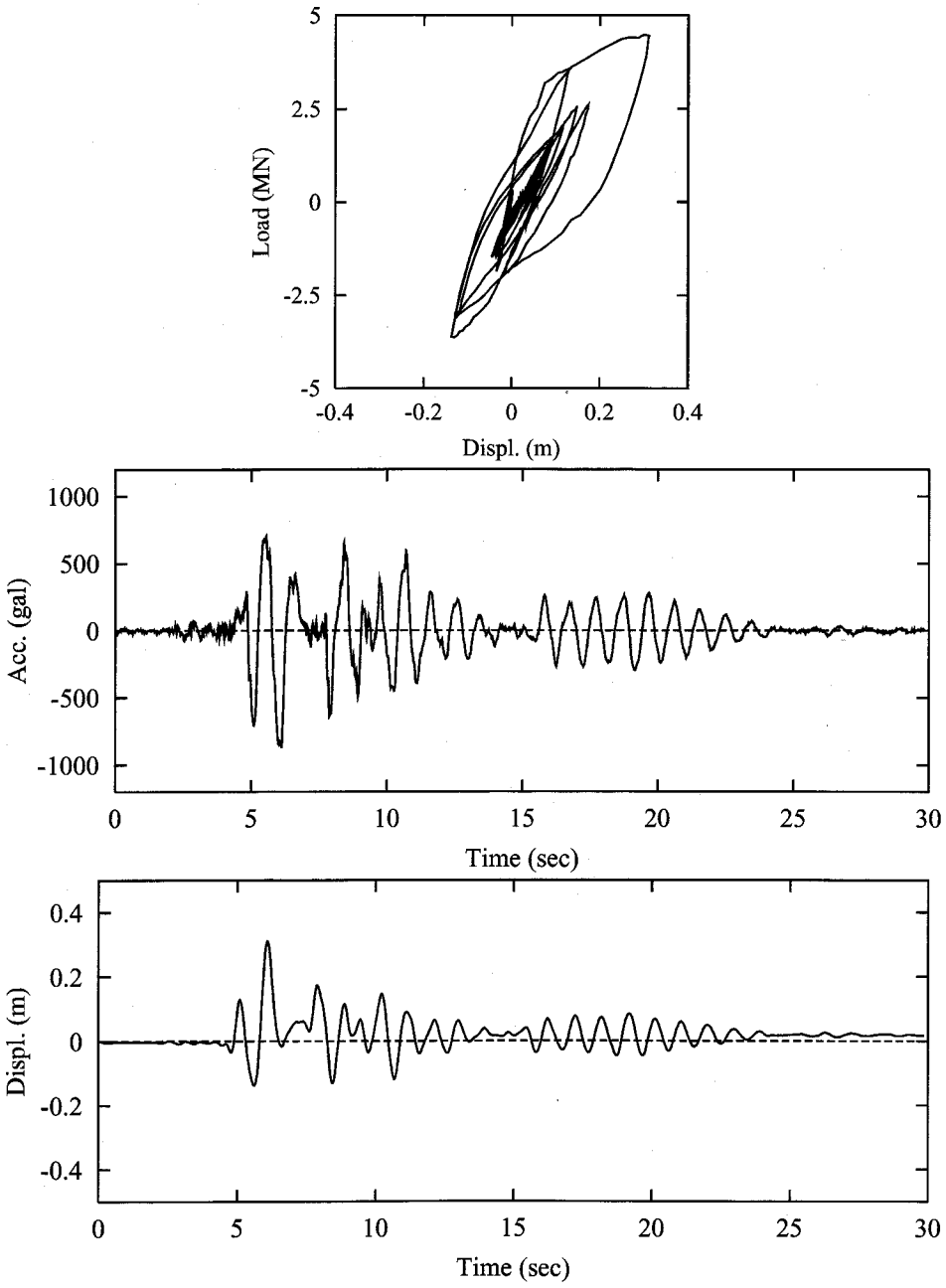

Figure 5.18: Results of Pseudo Dynamic Test(UBRC-4)

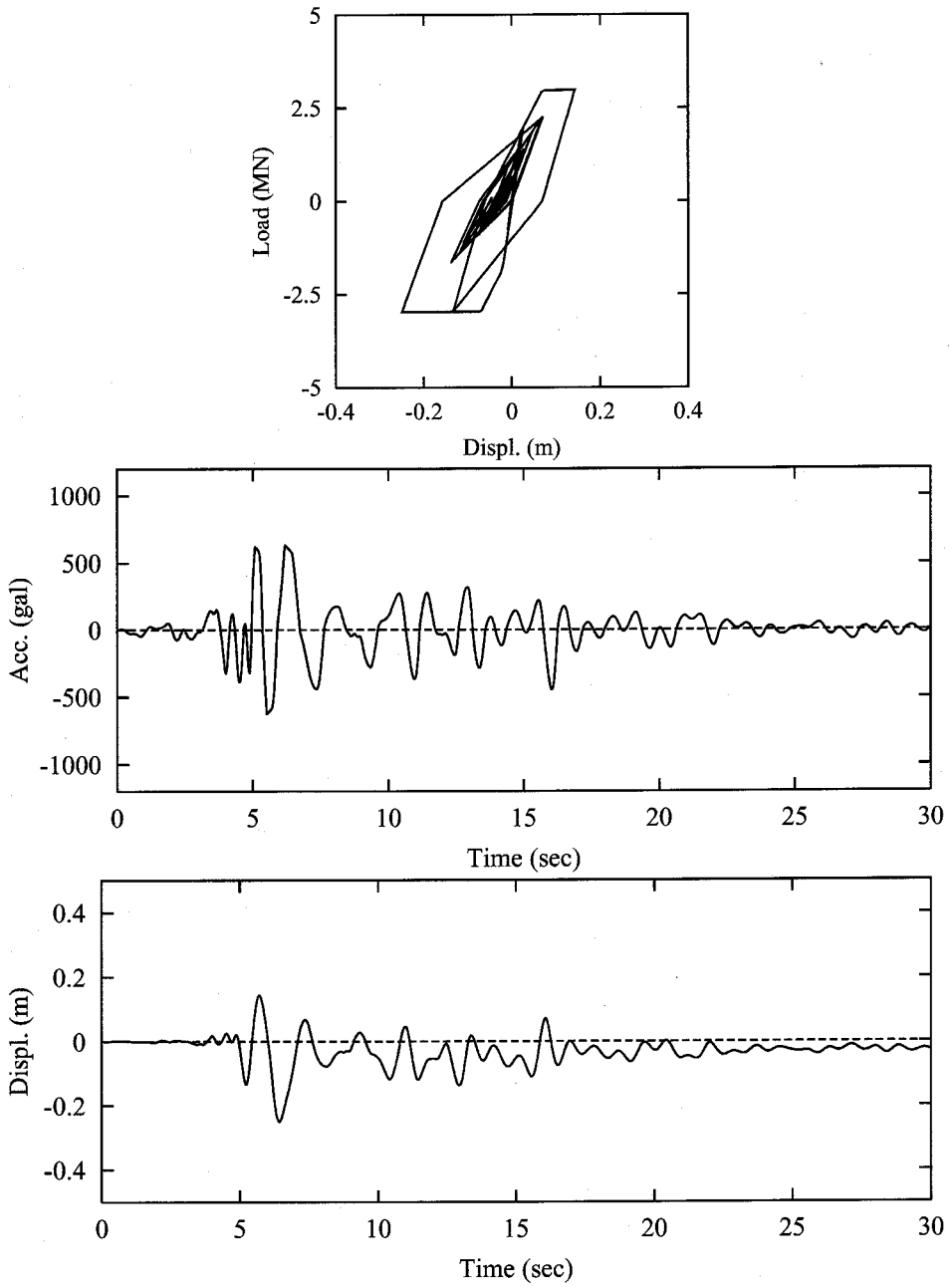

Figure 5.19: Results of Seismic Response Analysis(RC)

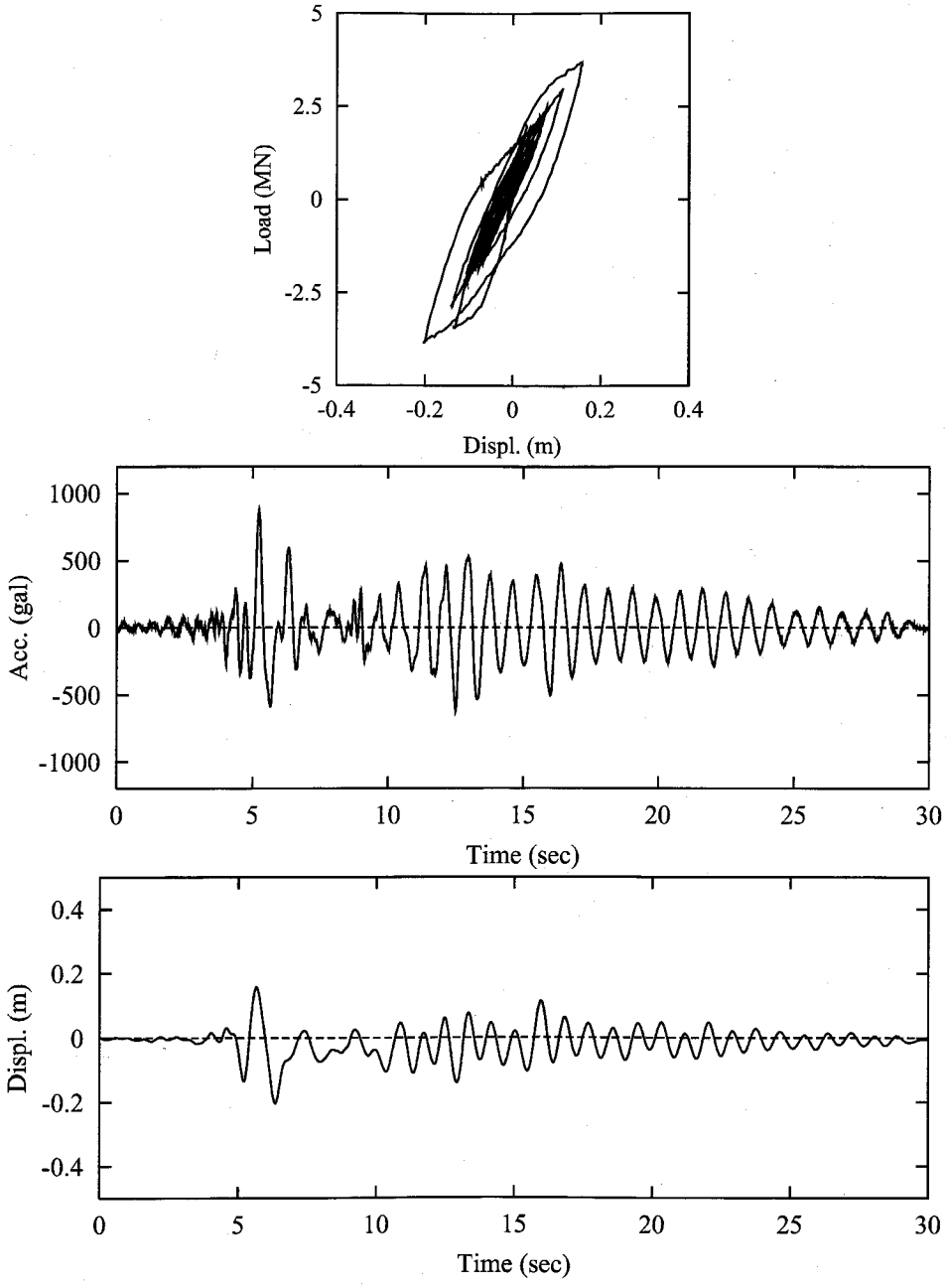

Figure 5.20: Results of Pseudo Dynamic Test(UBRC-5)

5.4 Summary

In this study, the applications of the UBRC structure to the railway and the highway bridge pier are presented. From this study, the following results are obtained:

- The philosophy of the two level seismic design method can be realized easily and rationally by applying UBRC structures with the stable post-yield stiffness.
- The railway RC structures have large amount of longitudinal reinforcement, but applying UBRC structures, the amount of reinforcement can be reduced. Since the RC part of the UBRC structure is decided by L1 earthquakes, it has the economical section. And cooperating with the unbonded bars, it can resist L2 earthquakes. The reduction of reinforcement also make the construction work easy.
- From the results of the pseudo dynamic tests, it is found that the seismic response of the UBRC structures is stable. Especially the residual deformation after earthquakes is certainly small by the combination of the small maximum deformation and the effect of elastic members.
- In the pseudo dynamic tests it is also recognized the bars' effect (stable post-yield stiffness and the small residual deformation). Considering with the easy construction and the low construction cost, the UBRC structure has the high seismic performance.

References

(1) Iemura, H., Takahashi, Y., Iwata, S. and Sogabe, N.: Rational Seismic Design for Railway Elevated Bridges using UBRC Members (in Japanese), *Proc. of 26th JSCE Earthquake Engineering Symposium*, Vol. 2, pp. 921–924, 8 2001.

(2) Iemura, H., Takahashi, Y. and Sogabe, N.: Performance Evaluation of UBRC Piers by Hybrid Earthquake Loading Tests (in Japanese), *Proc. of 26th JSCE Earthquake Engineering Symposium*, Vol. 2, pp. 929–932, 8 2001.

(3) Japan Society of Civil Engineers : Proposal on Earthquake Resistance for Civil Engineering Structures (in Japanese), *Magazine of JSCE*, Vol. 80, No. 7, 1995.

(4) Japan Society of Civil Engineers : Second Proposal on Earthquake Resistance for Civil Engineering Structures (in Japanese), *Magazine of JSCE*, Vol. 81, No. 2, 1996.

(5) Japan Road Association: *Seismic Design Specification for Highway Bridges (in Japanese)*, Maruzen Ltd., 1996.

(6) Railway Technical Research Institute(ed.): *Seismic Design Code for Railway Structures (in Japanese)*, Maruzen, 1999.

(7) Hoshikuma, J., Unjo, S. and Nagaya, K.: Cyclic Loading Tests of Real-Size RC Piers (in Japanese), *Proc. of of the 4th Symposium on Ductility Design Method for Bridges*, pp. 189–194, 1999.

(8) Saizuka, K., Itho, Y., Kiso, E. and Usami, T. : A Consideration on Procedures of Hybrid Earthquake Response Test Taking Account of the Scale Factor (in Japanese), *Journal of JSCE*, Vol. I-30, No. 507, pp. 179–190, 1995.

Chapter 6

Conclusions

An object-oriented structural analysis system has been developed, and the seismic behavior of RC structures have been investigated with the system and the high seismic performance structures are proposed.

The purpose of this research and general remarks on the ground for the development of the new structure were given in Chapter 1. And a review of past studies on the object-oriented approach, the hollow RC tall piers and the high performance concrete structures were also presented there.

In Chapter 2, the structural analysis system is analyzed and designed by the object-oriented procedure. The system is divided into three subsystems : *Structure*, *Load* and *ResponseAnalysis* subsystems, and the analysis is driven by message passing among the subsystems. The analysis system itself is a program code and allows the explicit representation of structures, loads, equations and so on. Each subsystem includes "packages". The *Equation* package is used as the kernel of the *ResponseAnalysis* subsystem. In the *Equation* package, since the algorithms are separated from the equation object, this package becomes robust against adding new algorithms. The *Shape* and the *Method* packages are used in the *Structure* subsystem. The *Shape* package represents the geometry of the structure, and the *Method* package represents how to construct the structural matrices for the analysis. The *Earthquake* package is used in the *Load* subsystems. These packages can improve the modularity of the system and make the system flexible. The object-oriented structural analysis system has the advantage in the research field but also the educational field, by allowing the users to easily understand the inside and to easily extend the function.

In Chapter 3, the seismic response characteristics of RC tall piers with hollow section are investigated by the cyclic loading tests and hybrid earthquake loading tests. From the cyclic loading tests, even in case of the flexural failure, the flexural cracks in the flange part changed into the diagonal cracks in the web part when they progressed into the web part.

Under the cyclic loading, the shear cracks crossed each other in the thin web. The shear deformation increased even by the cyclic loading with constant amplitudes. These results show that importance of the check for the shear resistance of the hollow RC piers. However if the pier has the appropriate amount of the transverse reinforcement and/or the filled section at the bottom, the pier shows a stable seismic response even under a severe earthquake. And as the application of the object-oriented analysis system, the program for the cyclic loading analysis is developed. The analysis system is developed using the *Structure* subsystem, and can simulate the experiment precisely. The reuse of the developed objects for the structural analysis allows an easy development of the analytical system, which is very simple in spite of the nonlinear problem.

In Chapter 4, the Unbonded Bar Reinforced Concrete (UBRC) structure is developed and proposed as the high seismic performance structure. Firstly, the fundamental characteristics are examined through the cyclic loading tests. The structure with the post-yield stiffness shows a stable seismic response. Only by installing the unbonded bars, it is possible to realize the RC structure with the stable post-yield stiffness. The stiffness can be controlled by the selection of the bar parameters, and the capacity of the energy dissipation is controlled by the amount of longitudinal reinforcement. The residual deformation can be reduced by the addition of the elastic restoring force of the bars. According to the parametric studies, there are four methods to change the characteristics of UBRC structures. By the combination of these methods, many kinds of skeleton curves can be obtained. Since this structure can be realized only by installing unbonded bars, it can be constructed with simple and easy construction works. It means that the fairly economical construction is possible. There results suggest that the UBRC structure is a promising approach for the high performance structures in the next generation.

In Chapter 5, the UBRC structure is applied to railway and highway structures. In the application to the railway structure, it is shown that the UBRC structure is suitable for the rational two-level seismic design method. In the two-level seismic design method, the cross section of a RC structure is usually determined by the Level II design, because the required strength by Level II is much higher than that by Level I. Since the load–displacement relationship of a RC pier is of the elasto-plastic type, such a high strength is needed even in the Level I. With the application of the UBRC structure, the rational structure can be constructed without requiring high yield strength. The effect of the rational design can contribute the reduction of the longitudinal reinforcement of the railway structures. And the seismic response of the UBRC structure is investigated for the highway bridge. By installing the unbonded bars, the seismic response becomes stable. Since the structures with the post-yield stiffness sometimes show the small deformation compared with the conventional RC structures, the

residual deformation after earthquakes becomes small by the combination of the small deformation and the effect of elastic members. In terms of the seismic response and the rational design, it is found that the UBRC structure is a high seismic performance structure.

For future studies, the object-oriented analysis system might be extended to the distributed computing. It has been popular to use multi-processor computers and cluster systems of multiple computers, and these philosophy of the cooperation of the multiple computers has the affinity for the message passing between objects. And also the impact on the educational field should be evaluated because the high modularity of the object-oriented system can support the step-by-step development. And for the UBRC structure, it is of great interest to investigate the behavior of the structure with the bond slip between the bars and the concrete. As long as the unbonding behavior is controlled and guaranteed in the large deformation range, the UBRC structure will improve the construction works and the performance for the Level I earthquakes.

Appendix A

Notations of UML

This appendix is described notations of UML used in this dissertation.

class A description of a set of objects that share the same attributes, operations, relationships, and semantics.

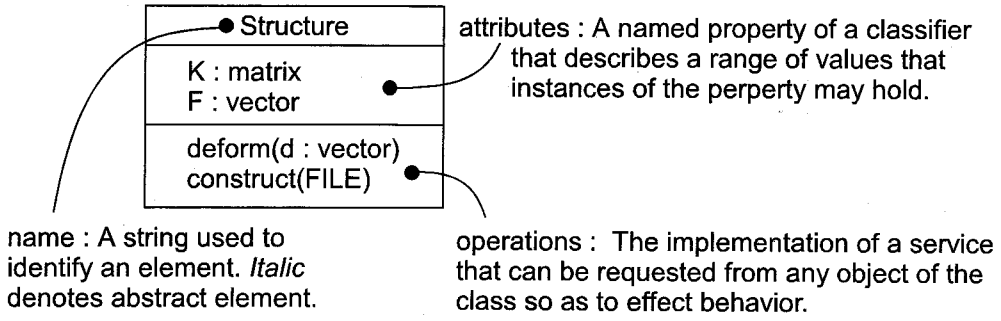

object A concrete manifestation of an abstraction; an entity to which a set of operations can be applied and which has a state that stores the effects of the operations; a synonym for object.

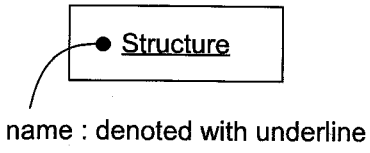

use case A description of a set of sequences of actions, including variants, that a system performs that yields an observable result of value to an actor.

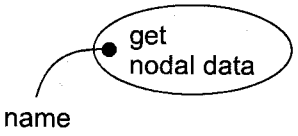

actor A coherent set of roles that users of use cases play when interacting with the use cases.

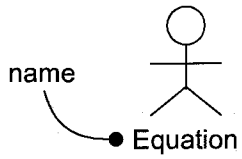

package A general-purpose mechanism for organizing elements into groups.

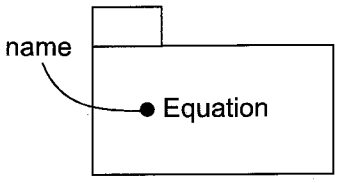

note A graphical symbol for rendering constraints or comments attached to an element or a collection of elements.

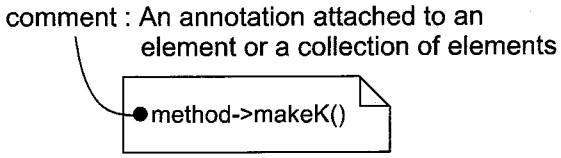

relationship A semantic connection among elements

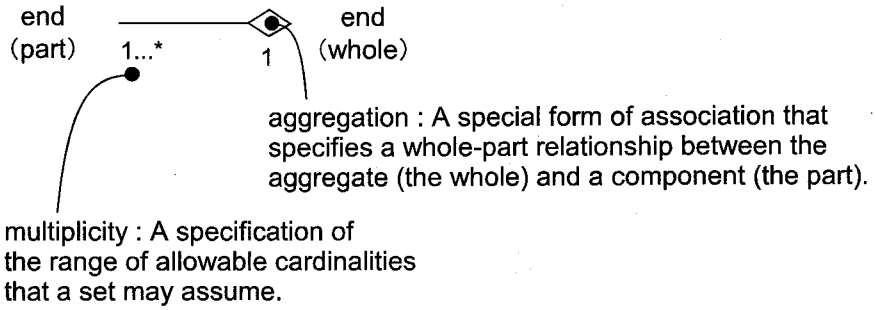

dependency A semantic relationship between two things in which a change to one thing (the independent thing) may affect the semantics of the other thing (the dependent thing).

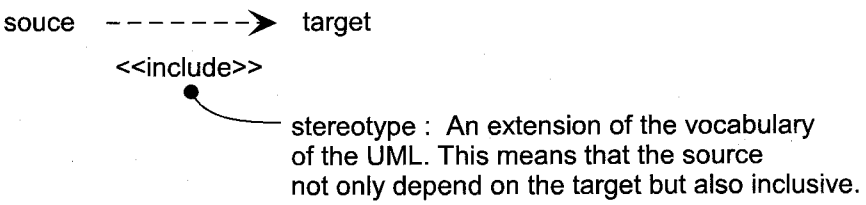

interaction A behavior that comprises a set of messages that are exchanged among a set of objects within a particular context to accomplish a purpose.

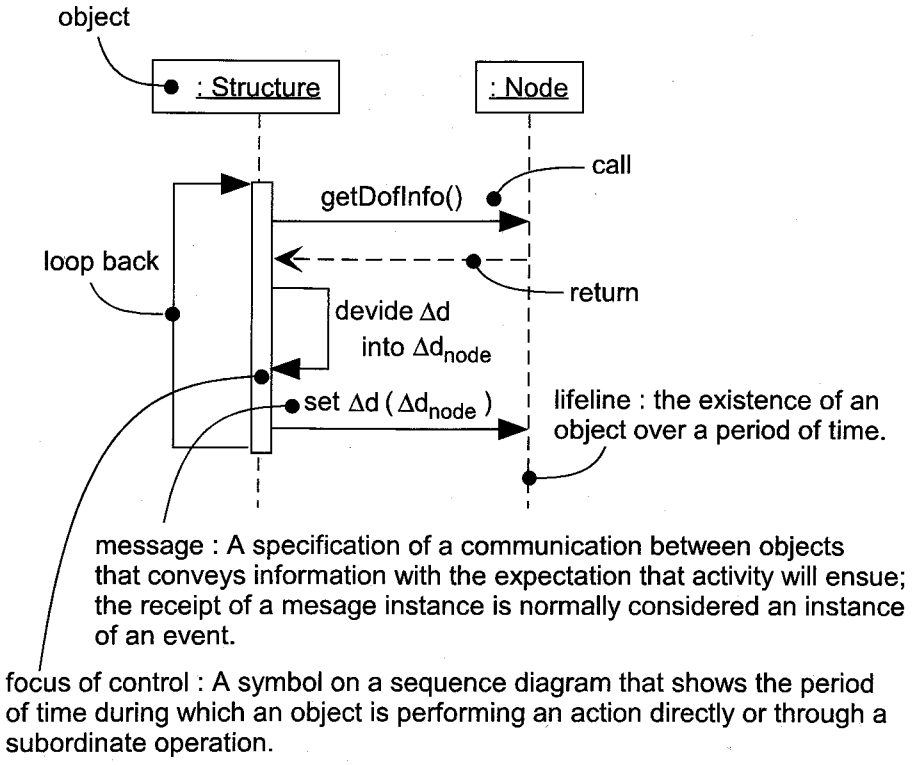

state machine A behavior that specifies the sequences of states an object goes through during its lifetime in response to events, together with its responses to those events.

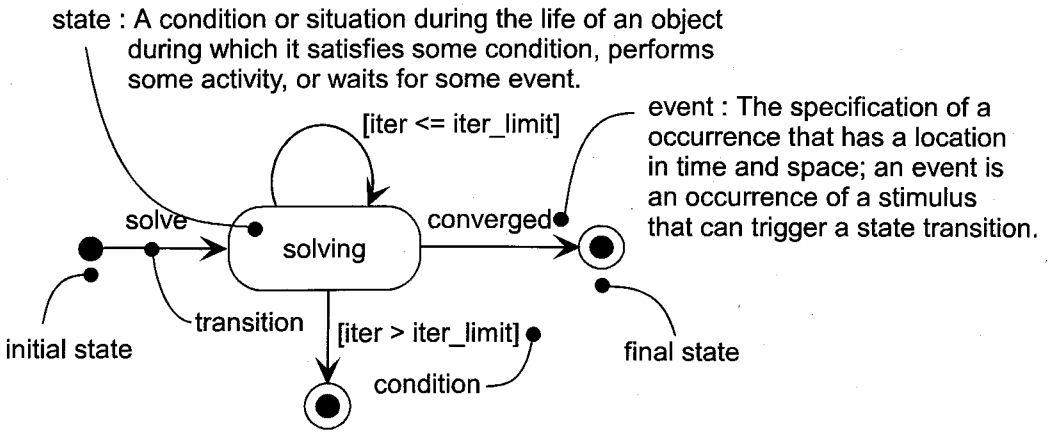

Appendix B

Uniform Expression of Equation

B.1 Uniformed Equations

In order to model the *Equation* package in the *ResponseAnalysis* subsystem, a static/dynamic and linear/nonlinear equation is expressed uniformly as much as possible.

Consider the uniformed equations at time t_{n+1}, iteration $(k-1)$,

$$\hat{\mathbf{K}}_{n+1}^{(k-1)}\Delta\mathbf{d}^{(k)} = \hat{\mathbf{R}}_{n+1}^{(k-1)} \tag{B.1}$$

where $\Delta\mathbf{d}^{(k)}$ is the displacement increment, $\hat{\mathbf{K}}_{n+1}^{(k-1)}$ is the effective stiffness matrix and $\hat{\mathbf{R}}_{n+1}^{(k-1)}$ is the effective load vector. These effective matrices are considered:

$$\hat{\mathbf{K}}_{n+1}^{(k-1)} = \hat{\mathbf{K}}_{dyn} + \mathbf{K}_{n+1}^{(k-1)} \tag{B.2}$$

$$\hat{\mathbf{R}}_{n+1}^{(k-1)} = \hat{\mathbf{R}}_{dyn} - \mathbf{F}_{n+1}^{(k-1)} \tag{B.3}$$

where $\mathbf{K}_{n+1}^{(k-1)}$ is the current tangent stiffness matrix, $\mathbf{F}_{n+1}^{(k-1)}$ is the vector of nodal point forces and $\hat{\mathbf{K}}_{dyn}$ and $\hat{\mathbf{R}}_{dyn}$ are calculated based on the problem type. Therefore the purpose of this appendix is to define them in each problem.

Since an incremental analysis is performed with time step of Δt, the initial conditions in this iteration are $\mathbf{K}_{n+1}^{(0)} = \mathbf{K}_n, \mathbf{F}_{n+1}^{(0)} = \mathbf{F}_n$. For the displacement increment, it is assumed that

$$\Delta\mathbf{d}^{(k)} = \mathbf{d}_{n+1}^{(k)} - \mathbf{d}_{n+1}^{(k-1)} \tag{B.4}$$

Using (B.4), the displacement solution of (B.1) is

$$\mathbf{d}_{n+1}^{(k)} = \mathbf{d}_n + \sum_{i=1}^{k} \Delta\mathbf{d}^{(i)} \tag{B.5}$$

The iteration is continued until appropriate convergence criteria are satisfied.

B.2 Equilibrium Equation

B.2.1 Linear Problem

The linear equilibrium equation is

$$\mathbf{K}\mathbf{d}_{n+1} = \mathbf{R}_{n+1} \tag{B.6}$$

where $\mathbf{K}$ is the stiffness matrix and $\mathbf{d}_{n+1}$ is the displacement solution. In the expression of the incremental manner, the displacement increment is

$$\Delta\mathbf{d}^{(1)} = \mathbf{d}_{n+1} - \mathbf{d}_n = \mathbf{d}_{n+1}^{(1)} - \mathbf{d}_n \tag{B.7}$$

and substituting into (B.6), we have

$$\hat{\mathbf{K}}_{n+1}^{(0)}\Delta\mathbf{d}^{(1)} = \hat{\mathbf{R}}_{n+1}^{(0)} \tag{B.8}$$

where

$$\hat{\mathbf{K}}_{n+1}^{(0)} = \mathbf{K} = \mathbf{K}_n = \mathbf{K}_{n+1}^{(0)} \tag{B.9}$$

$$\hat{\mathbf{R}}_{n+1}^{(0)} = \mathbf{R}_{n+1} - \mathbf{K}\mathbf{d}_n = \mathbf{R}_{n+1} - \mathbf{F}_n = \mathbf{R}_{n+1} - \mathbf{F}_{n+1}^{(0)} \tag{B.10}$$

Comparing (B.9), (B.10) with (B.2), (B.3), we obtain

$$\hat{\mathbf{K}}_{dyn} = \mathbf{0} \tag{B.11}$$

$$\hat{\mathbf{R}}_{dyn} = \mathbf{R}_{n+1} \tag{B.12}$$

B.2.2 Nonlinear Problem

The nonlinear equilibrium equation is

$$\mathbf{K}_{n+1}^{(k-1)}\Delta\mathbf{d}^{(k)} = \mathbf{R}_{n+1} - \mathbf{F}_{n+1}^{(k-1)} \tag{B.13}$$

Comparing (B.13) with (B.2), (B.3), we obtain

$$\hat{\mathbf{K}}_{dyn} = \mathbf{0} \tag{B.14}$$

$$\hat{\mathbf{R}}_{dyn} = \mathbf{R}_{n+1} \tag{B.15}$$

That is, $\hat{\mathbf{K}}_{dyn}$ and $\hat{\mathbf{R}}_{dyn}$ of the nonlinear problem is the same as that of the linear problem.

B.3 Equation of Motion

As shown in B.2, it is enough to obtain $\hat{\mathbf{K}}_{dyn}$ and $\hat{\mathbf{R}}_{dyn}$ in the nonlinear problem.

The nonlinear equation of motion are

$$\mathbf{M}\,\mathbf{a}_{n+1}^{(k)} + \mathbf{C}\,\mathbf{v}_{n+1}^{(k)} + \mathbf{F}_{n+1}^{(k)} = \mathbf{R}_{n+1} \tag{B.16}$$

where $\mathbf{M}$ is the mass matrix, $\mathbf{C}$ is the damping matrix, $\mathbf{a}_{n+1}^{(k)}$ is the acceleration vector and $\mathbf{v}_{n+1}^{(k)}$ is the velocity vector.

To solve this equation, there are many integral methods.

B.3.1 Newmark β Method

Newmark β method is a generalized acceleration method. The following expansions are employed for the velocity and displacement at time t_{n+1}:

$$\mathbf{v}_{n+1}^{(k)} = \mathbf{v}_n + \Delta t\left\{(1-\gamma)\,\mathbf{a}_n + \gamma\,\mathbf{a}_{n+1}^{(k)}\right\} \tag{B.17}$$

$$\mathbf{d}_{n+1}^{(k)} = \mathbf{d}_n + \Delta t\,\mathbf{v}_n + \Delta t^2\left\{\left(\frac{1}{2}-\beta\right)\mathbf{a}_n + \beta\,\mathbf{a}_{n+1}^{(k)}\right\} \tag{B.18}$$

where β, γ are parameters to be chosen to obtain optimum stability and accuracy and Δt is the time interval. Using the relations in (B.4),(B.17) and (B.18), we thus obtain

$$\mathbf{a}_{n+1}^{(k)} = -\left(\frac{1}{2\beta}-1\right)\mathbf{a}_n - \frac{1}{\beta\Delta t}\mathbf{v}_n + \frac{1}{\beta\Delta t^2}\left(\mathbf{d}_{n+1}^{(k-1)} - \mathbf{d}_n + \Delta\mathbf{d}^{(k)}\right) \tag{B.19}$$

$$\mathbf{v}_{n+1}^{(k)} = -\left(\frac{\gamma}{\beta}-2\right)\frac{\Delta t}{2}\mathbf{a}_n - \left(\frac{\gamma}{\beta}-1\right)\mathbf{v}_n + \frac{\gamma}{\beta\Delta t}\left(\mathbf{d}_{n+1}^{(k-1)} - \mathbf{d}_n + \Delta\mathbf{d}^{(k)}\right) \tag{B.20}$$

and substituting into (B.16), we have

$$\left(\hat{\mathbf{K}}_{dyn} + \mathbf{K}_{n+1}^{(k-1)}\right)\Delta\mathbf{d}^{(k)} = \hat{\mathbf{R}}_{dyn} - \mathbf{F}_{n+1}^{(k-1)} \tag{B.21}$$

where

$$\hat{\mathbf{K}}_{dyn} = \frac{\gamma}{\beta\Delta t}\mathbf{C} + \frac{1}{\beta\Delta t^2}\mathbf{M} \tag{B.22}$$

$$\begin{aligned}\hat{\mathbf{R}}_{dyn} = \mathbf{R}_{n+1} &+ \mathbf{M}\left\{\frac{1}{\beta\Delta t^2}\left(\mathbf{d}_n - \mathbf{d}_{n+1}^{(k-1)}\right) + \frac{1}{\beta\Delta t}\mathbf{v}_n + \left(\frac{1}{2\beta}-1\right)\mathbf{a}_n\right\} \\ &+ \mathbf{C}\left\{\frac{\gamma}{\beta\Delta t}\left(\mathbf{d}_n - \mathbf{d}_{n+1}^{(k-1)}\right) + \left(\frac{\gamma}{\beta}-1\right)\mathbf{v}_n + \left(\frac{\gamma}{\beta}-2\right)\frac{\Delta t}{2}\mathbf{a}_n\right\}\end{aligned} \tag{B.23}$$

B.3.2 Wilson θ Method

The basic assumption in the Wilson θ method is that the acceleration varies linearly over the time interval from t_n to $\bar{t}_{n+1} = t_n + \theta\Delta t$, where $\theta \geq 1$ and is determined to obtain optimum stability and accuracy characteristics.

Let τ denote the increase in time, where $0 \leq \tau \leq \theta\Delta t$; then for the time interval t_n to $\bar{t}_{n+1}$, it is assumed that

$$\mathbf{a}(t+\tau)^{(k)} = \mathbf{a}_n + \frac{\tau}{\theta\Delta t}\left(\bar{\mathbf{a}}_{n+1}^{(k)} - \mathbf{a}_n\right) \tag{B.24}$$

where $\bar{\mathbf{a}}_{n+1}^{(k)}$ is the acceleration vector at time $\bar{t}_{n+1}$. Integrating (B.24), we obtain the velocity and the displacement at time $\bar{t}_{n+1}$.

Using the above equations, we have at time $\bar{t}_{n+1}$

$$\bar{\mathbf{v}}_{n+1}^{(k)} = \frac{3}{\theta\Delta t}\left(\bar{\mathbf{d}}_{n+1}^{(k)} - \mathbf{d}_n\right) - 2\,\mathbf{v}_n - \frac{\theta\Delta t}{2}\mathbf{a}_n \tag{B.25}$$

$$\bar{\mathbf{d}}_{n+1}^{(k)} = \mathbf{d}_n + \theta\Delta t\mathbf{v}_n + \frac{\theta^2\Delta t^2}{6}\left(\bar{\mathbf{a}}_{n+1}^{(k)} + 2\,\mathbf{a}_n\right) \tag{B.26}$$

where $\bar{\mathbf{v}}_{n+1}^{(k)}, \bar{\mathbf{d}}_{n+1}^{(k)}$ are the velocity and displacement vector at time $\bar{t}_{n+1}$, iteration (k).

The displacement increment is considered:

$$\Delta\mathbf{d}^{(k)} = \bar{\mathbf{d}}_{n+1}^{(k)} - \bar{\mathbf{d}}_{n+1}^{(k-1)} \tag{B.27}$$

Using the relations in (B.25) to (B.27), we thus obtain

$$\bar{\mathbf{a}}_{n+1}^{(k)} = \frac{6}{\tau^2}\left(\bar{\mathbf{d}}_{n+1}^{(k-1)} - \mathbf{d}_n + \Delta\mathbf{d}^{(k)}\right) - \frac{6}{\tau}\mathbf{v}_n - 2\,\mathbf{a}_n \tag{B.28}$$

$$\bar{\mathbf{v}}_{n+1}^{(k)} = \frac{3}{\tau}\left(\bar{\mathbf{d}}_{n+1}^{(k-1)} - \mathbf{d}_n + \Delta\mathbf{d}^{(k)}\right) - 2\,\mathbf{v}_n - \frac{\tau}{2}\mathbf{a}_n \tag{B.29}$$

Consider the equation of motion (B.16) at time $\bar{t}_{n+1}$. Because the acceleration are assumed to vary linearly, a linearly extrapolated load vector is used; i.e., the equation employed is

$$\mathbf{M}\,\bar{\mathbf{a}}_{n+1}^{(k)} + \mathbf{C}\,\bar{\mathbf{v}}_{n+1}^{(k)} + \bar{\mathbf{F}}_{n+1}^{(k)} = \bar{\mathbf{R}}_{n+1} \tag{B.30}$$

where $\bar{\mathbf{F}}_{n+1}^{(k)}$ is the vector of nodal point forces at $\bar{\mathbf{d}}_{n+1}^{(k)}$ and $\bar{\mathbf{R}}_{n+1} = \mathbf{R}_n + \theta\,(\mathbf{R}_{n+1} - \mathbf{R}_n)$. Substituting (B.28) and (B.29) into (B.30), the equation at time $\bar{t}_{n+1}$ is obtained:

$$\left(\bar{\hat{\mathbf{K}}}_{dyn} + \bar{\mathbf{K}}_{n+1}^{(k-1)}\right)\Delta\mathbf{d}^{(k)} = \bar{\hat{\mathbf{R}}}_{dyn} - \bar{\mathbf{F}}_{n+1}^{(k-1)} \tag{B.31}$$

where

$$\bar{\bar{\mathbf{K}}}_{dyn} = \frac{6}{\tau^2}\mathbf{M} + \frac{3}{\tau}\mathbf{C} \tag{B.32}$$

$$\begin{aligned}\bar{\bar{\mathbf{R}}}_{dyn} = \mathbf{R}_n &+ \theta(\mathbf{R}_{n+1} - \mathbf{R}_n) \\ &+ \mathbf{M}\left\{\frac{6}{\tau^2}\left(\mathbf{d}_n - \bar{\mathbf{d}}_{n+1}^{(k-1)}\right) + \frac{6}{\tau}\mathbf{v}_n + 2\,\mathbf{a}_n\right\} \\ &+ \mathbf{C}\left\{\frac{3}{\tau}\left(\mathbf{d}_n - \bar{\mathbf{d}}_{n+1}^{(k-1)}\right) + 2\,\mathbf{v}_n + \frac{\tau}{2}\mathbf{a}_n\right\}\end{aligned} \tag{B.33}$$

To obtain the solution at time t_{n+1}, at first, the displacement $\bar{\mathbf{d}}_{n+1}$ from (B.30) is obtained. And substituting into (B.24) evaluated at $\tau = \Delta t$, we obtain the solutions.

B.3.3 Operator Splitting Method

This method relies on a predictor–corrector approach and doesn't require any numerical iteration. The corrector displacement is obtained by the Newmark β method. With this method, it is assumed that

$$\mathbf{K}\mathbf{d}_{n+1} - \mathbf{F}_{n+1} \approx \mathbf{K}\tilde{\mathbf{d}}_{n+1} - \tilde{\mathbf{F}}_{n+1} \tag{B.34}$$

$$\tilde{\mathbf{d}}_{n+1} = \mathbf{d}_n + \Delta t\,\mathbf{v}_n + \frac{\Delta t^2}{4}\mathbf{a}_n \tag{B.35}$$

where $\mathbf{K}$ is the linear stiffness, $\tilde{\mathbf{d}}_{n+1}$ is the predictor displacement vector and $\tilde{\mathbf{F}}_{n+1}$ is the vector of nodal point forces when the $\tilde{\mathbf{d}}_{n+1}$ have been imposed.

Substituting (B.34) into (B.16), the equation of motion in the Operator–Splitting method is obtained:

$$\mathbf{M}\,\mathbf{a}_{n+1} + \mathbf{C}\,\mathbf{v}_{n+1} + \left(\mathbf{K}\mathbf{d}_{n+1} + \tilde{\mathbf{F}}_{n+1} - \mathbf{K}\tilde{\mathbf{d}}_{n+1}\right) = \mathbf{R}_{n+1} \tag{B.36}$$

Predictor phase:

Evaluate a predictor displacement vector with (B.35).

Corrector phase:

Based on the Newmark β method, the equations for the displacement and velocity at time t_{n+1} are

$$\mathbf{d}_{n+1}^{(k)} = \tilde{\mathbf{d}}_{n+1} + \Delta t^2\beta\,\mathbf{a}_{n+1} \tag{B.37}$$

$$\mathbf{v}_{n+1}^{(k)} = \mathbf{v}_n + \Delta t\left\{(1-\gamma)\,\mathbf{a}_n + \gamma\,\mathbf{a}_{n+1}^{(k)}\right\} \tag{B.38}$$

Transforming (B.37), we have

$$\mathbf{a}_{n+1} = \frac{1}{\Delta t^2 \beta}\left(\mathbf{d}_{n+1} - \tilde{\mathbf{d}}_{n+1}\right) \tag{B.39}$$

and substituting (B.38) and (B.39) into (B.36), we have

$$\left(\hat{\mathbf{K}}_{dyn} + \mathbf{K}\right)\Delta\tilde{\mathbf{d}} = \hat{\mathbf{R}}_{dyn} - \tilde{\mathbf{F}}_{n+1} \tag{B.40}$$

where

$$\hat{\mathbf{K}}_{dyn} = \frac{\gamma}{\beta\Delta t}\mathbf{C} + \frac{1}{\beta\Delta t^2}\mathbf{M} \tag{B.41}$$

$$\hat{\mathbf{R}}_{dyn} = \mathbf{R}_{n+1} - \mathbf{C}\{\mathbf{v}_n + \Delta t(1-\gamma)\mathbf{a}_n\} \tag{B.42}$$

$$\Delta\tilde{\mathbf{d}} = \mathbf{d}_{n+1} - \tilde{\mathbf{d}}_{n+1} \tag{B.43}$$

Solve (B.40) for $\mathbf{d}_{n+1}$.

Updating phase:

Using (B.39) and (B.38), we obtain the acceleration and the velocity vector at time t_{n+1}.

Appendix C

Fiber Model Formulation of Timoshenko Beam

C.1 Basic Assumptions in Timoschenko Beam

C.1.1 Displacement Field

Considering beam bending analysis with the effect of shear deformations, we retain the assumption that a plane section originally normal to the neutral axis remains plane, but because of shear deformations this section does not remain normal to the neutral axis. The longitudinal displacement at (x,y) is

$$u(x,y) = u_0(x) - y\theta(x) \tag{C.1}$$

where $u_0(x)$ is a longitudinal displacement at the neutral axis of the section and $\theta(x)$ is a total rotation of the section originally normal to the neutral axis of the beam. The transverse displacement at (x,y) is

$$v(x,y) = v_0(x) \tag{C.2}$$

where $v_0(x)$ is a transverse displacement at the neutral axial of the section. The total rotation is given by the rotation of the tangent to the neutral axis and the shear deformation,

$$\theta(x) = \frac{dv}{dx} - \beta \tag{C.3}$$

where β is the rotation angle due to the shearing deformation.

C.1.2 Relationship between Strain and Displacement

In the theory of small deformation, the longitudinal strain is

$$\epsilon_x = \frac{\partial u}{\partial x} \tag{C.4}$$

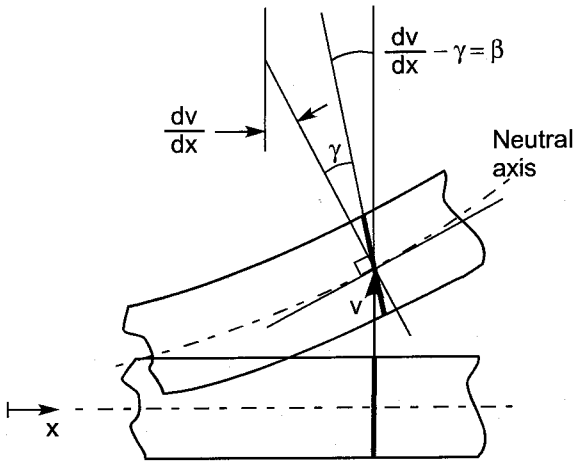

Figure C.1: Deformation of Cross Section

The shearing strain is

$$\gamma_{xy} = \frac{\partial u}{\partial y} + \frac{\partial v}{\partial x} \tag{C.5}$$

Using (C.3), we have

$$\epsilon_x = \frac{du_0}{dx} - y\frac{d\theta}{dx} = \epsilon_0 - y\phi \tag{C.6}$$

$$\gamma_{xy} = -\theta + \frac{dv}{dx} = \beta \tag{C.7}$$

C.1.3 Principle of Virtual Work

Using the general expression of the principle of virtual work, we have

$$\int_V \left(\overline{\epsilon_x}\sigma_x + \overline{\gamma_{xy}}\tau_{xy}\right) dV = \int_L p\delta v dx \tag{C.8}$$

where $\overline{\epsilon_x}$ is the virtual longitudinal strain, $\overline{\gamma_{xy}}$ is the virtual shearing strain and q is the distributed transverse load along the beam.

or

$$I_1 + I_2 = I_3 \tag{C.9}$$

where

$$I_1 = \int_V \overline{\epsilon_x}\sigma_x dV \tag{C.10}$$

$$I_2 = \int_V \overline{\gamma_{xy}}\tau_{xy} dV \tag{C.11}$$

$$I_3 = \int_L p\delta v dx \tag{C.12}$$

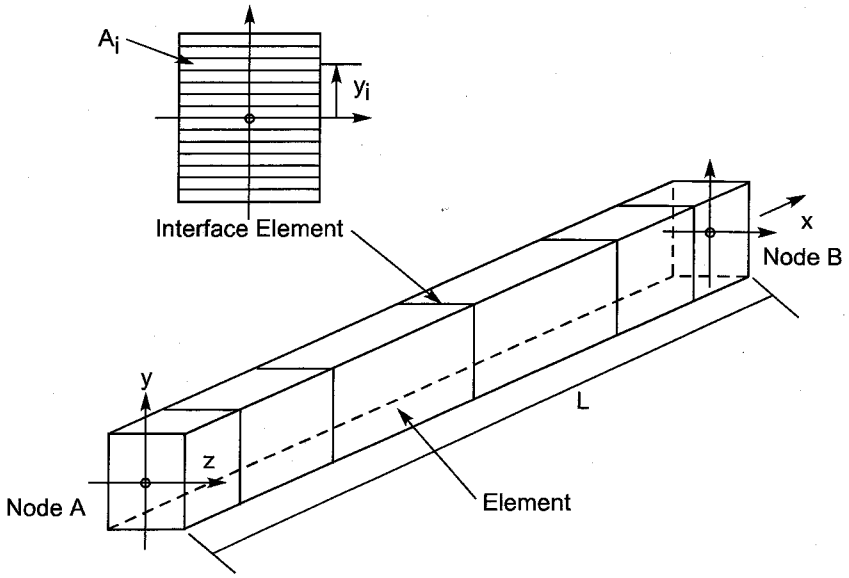

Figure C.2: Formulation of Fiber Model

C.2 Fiber Model Formulation

C.2.1 Constitutive Relationship

Assuming that the deformation state for the interface element at time t is defined by ${}^t\epsilon_0$, ${}^t\gamma_{xy}$ and ${}^t\phi$, deformations for the time $t + \Delta t$ are:

$$ {}^{t+\Delta t}\epsilon_0 = {}^t\epsilon_0 + \Delta\epsilon_0 \tag{C.13} $$

$$ {}^{t+\Delta t}\gamma_{xy} = {}^t\gamma_{xy} + \Delta\gamma_{xy} \tag{C.14} $$

$$ {}^{t+\Delta t}\phi_0 = {}^t\phi_0 + \Delta\phi_0 \tag{C.15} $$

Substituting (C.13) and (C.15) into (C.6), we have

$$ \Delta\epsilon_i = \Delta\epsilon_0 - y_i\Delta\phi \tag{C.16} $$

where y_i is a distance from the neutral axis to the centroid of i-th fiber. And

$$ \Delta\gamma_i = \Delta\gamma_{xy} \tag{C.17} $$

Based on the strain state in all fiber point, corresponding tangent and shear modulus and stress levels, ${}^tE_i$, ${}^tG_i$, ${}^t\sigma_i$ and ${}^t\tau_i$, can be obtained directly from the adopted stress–strain relations. The interface element incremental forces can be obtained using the following three equations:

$$ \Delta N = \sum_{i=1}^{n} A_i\Delta\sigma_i = \sum_{i=1}^{n} E_iA_i\Delta\epsilon_i \tag{C.18} $$

$$\Delta Q = \sum_{i=1}^{n} A_i \Delta\tau_i = \sum_{i=1}^{n} G_i A_i k \Delta\gamma_i \tag{C.19}$$

$$-\Delta M = \sum_{i=1}^{n} A_i \Delta\sigma_i y_i = \sum_{i=1}^{n} E_i A_i y_i \Delta\epsilon_i \tag{C.20}$$

where A_i is a discrete area associated to each fiber and k is the shear correction factor. If in (C.18) and (C.20), incremental strains are expressed in terms of incremental interface element deformations, (C.16), the following equations are obtained:

$$\Delta N = \left(\sum_{i=1}^{n} E_i A_i\right)\Delta\epsilon_0 + \left(\sum_{i=1}^{n} E_i A_i y_i\right)\Delta\phi \tag{C.21}$$

$$-\Delta M = \left(\sum_{i=1}^{n} E_i A_i y_i\right)\Delta\epsilon_0 + \left(\sum_{i=1}^{n} E_i A_i y_i^2\right)\Delta\phi \tag{C.22}$$

which can be expressed in matrix form,

$$\begin{Bmatrix} \Delta N \\ -\Delta M \end{Bmatrix} = \begin{bmatrix} \sum E_i A_i & \sum E_i A_i y_i \\ \sum E_i A_i y_i & \sum E_i A_i y_i^2 \end{bmatrix} \begin{Bmatrix} \Delta\epsilon_0 \\ \Delta\phi \end{Bmatrix} \tag{C.23}$$

or

$$\sigma_x = \mathbf{D}_f \boldsymbol{\epsilon}_x \tag{C.24}$$

And in terms of the shear stress, we have

$$\Delta Q = \sum G_i A_i k \, \Delta\gamma_{xy} = D_s \, \Delta\gamma_{xy} \tag{C.25}$$

C.2.2 Shape Function

the displacement increment vector of the interface element is

$$\mathbf{U} = \{u, v, \theta\}^T = \mathbf{N}\mathbf{d} \tag{C.26}$$

where $\mathbf{N}$ is the interpolation function and the $\delta\mathbf{d}$ is the nodal displacement increment.

$$\mathbf{d} = \left\{\Delta u^A, \Delta v^A, \Delta\theta^A, \Delta u^B, \Delta v^B, \Delta\theta^B\right\}^T \tag{C.27}$$

Using the interpolations

$$\mathbf{N} = \begin{bmatrix} N_1 & 0 & 0 & N_2 & 0 & 0 \\ 0 & N_1 & 0 & 0 & N_2 & 0 \\ 0 & 0 & N_1 & 0 & 0 & N_2 \end{bmatrix} \tag{C.28}$$

where

$$\xi = x/L$$
$$N_1 = 1 - \xi \quad N_2 = \xi$$

and L is the length of the beam.

C.2.3 Strain – Nodal Displacement Increment Transformation Matrix

In the fiber model, it is necessary to consider the longitudinal strain and the curvature at the interface element. The strain increment vector of the interface element is

$$\epsilon_x = \{\Delta\epsilon_0, \Delta\phi\}^T = \mathbf{B}_f\mathbf{d} \tag{C.29}$$

$$\Delta\gamma_{xy} = \mathbf{B}_s\mathbf{d} \tag{C.30}$$

where $\mathbf{B}_f$ and $\mathbf{B}_s$ are the strain–nodal displacement increment transformation matrices.

Using (C.28), $\mathbf{B}_f$ is obtained:

$$\begin{aligned}\mathbf{B}_f &= \begin{bmatrix} \frac{dN_1}{dx} & 0 & 0 & \frac{dN_1}{dx} & 0 & 0 \\ 0 & 0 & \frac{dN_2}{dx} & 0 & 0 & \frac{dN_2}{dx} \end{bmatrix} \\ &= \begin{bmatrix} -\frac{1}{L} & 0 & 0 & -\frac{1}{L} & 0 & 0 \\ 0 & 0 & \frac{1}{L} & 0 & 0 & \frac{1}{L} \end{bmatrix}\end{aligned} \tag{C.31}$$

And using (C.3) and (C.5), $\mathbf{B}_s$ is obtained:

$$\begin{aligned}\mathbf{B}_s &= \begin{bmatrix} 0 & \frac{dN_1}{dx} & -N_1 & 0 & \frac{dN_2}{dx} & -N_2 \end{bmatrix} \\ &= \begin{bmatrix} 0 & -\frac{1}{L} & \frac{x}{L} - 1 & 0 & \frac{1}{L} & -\frac{x}{L} \end{bmatrix}\end{aligned} \tag{C.32}$$

C.2.4 Bending Stiffness Matrix

Substituting (C.6) into (C.10), the following equation is obtained:

$$\begin{aligned} I_1 &= \int_V \overline{\epsilon_x}\sigma_x dV = \int_V \left(\overline{\epsilon_0} - y\overline{\phi}\right)\sigma_x dV \\ &= \int_L\int_A \overline{\epsilon_0}\sigma_x dA dx + \int_L\int_A -y\overline{\phi}\sigma_x dA dx && \text{(C.33)} \\ &= \int_L \overline{\epsilon_0}\int_A \sigma_x dA dx + \int_L \overline{\phi}\int_A -y\sigma_x dA dx && \text{(C.34)} \\ &= \int_L \overline{\epsilon_0}N(x)dx + \int_L -\overline{\phi}M(x)dx && \text{(C.35)} \\ &= \int_L \begin{Bmatrix} \overline{\epsilon_0} \\ \overline{\phi} \end{Bmatrix}^T \begin{Bmatrix} N \\ -M \end{Bmatrix}_x dx && \text{(C.36)} \end{aligned}$$

where$\{\}_x$ denotes the value of the section at x.

Substituting (C.24) and (C.29) into (C.36), we have

$$I_1 = \int_L \overline{\mathbf{d}}^T\, \mathbf{B}_f^T\, \mathbf{D}_f\, \mathbf{B}_f\, \mathbf{d}\, dx \tag{C.37}$$

Based on the principle of virtual work, the bending stiffness matrix is obtained:

$$\mathbf{K}_f = \int_L \mathbf{B}_f^T\, \mathbf{D}_f\, \mathbf{B}_f\, dx \tag{C.38}$$

C.2.5 Shearing Stiffness Matrix

From (C.11), the following equation is obtained:

$$\begin{aligned} I_2 &= \int_V \overline{\gamma_{xy}} \tau_{xy} dV \\ &= \int_L \overline{\gamma_{xy}} \int_A \tau_{xy} dA dx \\ &= \int_L \overline{\gamma_{xy}} Q dx \end{aligned} \tag{C.39}$$

Substituting (C.24) and (C.30) into (C.39), we have

$$I_2 = \int_L \overline{\mathbf{d}}^T \mathbf{B}_s^T D_s \mathbf{B}_s \mathbf{d} \, dx \tag{C.40}$$

Based on the principle of virtual work, the bending stiffness matrix is obtained:

$$\mathbf{K}_s = D_s \int_L \mathbf{B}_s^T \mathbf{B}_s \, dx \tag{C.41}$$

Usually in order to calculate (C.41), the two point Gauss–Legendre integration is used. But the resultant exhibits the very stiff behavior (shear locking). To avoid the locking, the one point Gauss–Legendre integration is used.

C.2.6 Tangent Stiffness Matrix

As the result, the tangent stiffness matrix of the Timoschenko beam is obtained:

$$\mathbf{K} = \mathbf{K}_f + \mathbf{K}_s \tag{C.42}$$

Appendix D

Modeling Methods of Finite Element of Structure

The objective analytical methods for elements in this study are the finite element method, the fiber model analysis, the moment–curvature model and the spring model(load–displacement model). In this appendix, these analytical methods are reviewed in order to handle them as uniformly as possible.

D.1 Finite Element Method

In the finite element method, the characteristic matrices is made by the volume integral based on the stress–strain relationship.

Each characteristic matrix expresses as follows:

- Strain Increment Vector **E**

$$\delta\mathbf{E} = \{\delta\varepsilon\} \tag{D.1}$$

- Displacement Increment Vector (in Element Coordinate System) $\delta\mathbf{u}$

$$\delta\mathbf{u} = \left\{ \delta u_r^A \quad \delta u_s^A \quad \delta u_t^A \quad \delta u_r^B \quad \delta u_s^B \quad \delta u_t^B \right\}^T \tag{D.2}$$

- Displacement Increment Vector (in Global Coordinate System) $\delta\mathbf{U}$

$$\delta\mathbf{U} = \left\{ \delta U_r^A \quad \delta U_s^A \quad \delta U_t^A \quad \delta U_r^B \quad \delta U_s^B \quad \delta U_t^B \right\}^T \tag{D.3}$$

- Linear Strain–Nodal Displacement Increment transformation matrix **B**

$$\mathbf{B} = \left[-\frac{1}{L} \quad y\left(\frac{6}{L^2} - \frac{12x}{L^3}\right) \quad y\left(\frac{4}{L} - \frac{6x}{L^2}\right) \quad \frac{1}{L} \quad y\left(-\frac{6}{L^2} + \frac{12x}{L^3}\right) \quad y\left(\frac{2}{L} - \frac{6x}{L^2}\right) \right] \tag{D.4}$$

- Stress–Strain Material Property Matrix **D**

$$\mathbf{D} = [E_t] \tag{D.5}$$

- Linear Strain Incremental Stiffness Matrix **K**

$$\mathbf{K} = \int_V \mathbf{B}^T \cdot \mathbf{D} \cdot \mathbf{B}\, dV \tag{D.6}$$

- Vector of Nodal Point Forces Equivalent to the Element Stress **F**

$$\mathbf{F} = \int_V \mathbf{B}^T \cdot \{\sigma\}\, dV \tag{D.7}$$

D.2 Fiber Model Analysis

In the fiber model analysis, the characteristic matrices is made by the line integral of the sectional characteristic matrices based on the area and the stress–strain relationship of each fiber.

Each characteristic matrix expresses as follows: Here, the strain increment vector **E**, the displacement increment vector $\delta\mathbf{u}, \delta\mathbf{U}$ are the same of the finite element method.

- Linear Strain–Nodal Displacement Increment transformation matrix **B**

$$\mathbf{B} = \begin{bmatrix} -\frac{1}{L} & 0 & 0 & \frac{1}{L} & 0 & 0 \\ 0 & -\frac{6}{L^2} + \frac{12x}{L^3} & -\frac{4}{L} + \frac{6x}{L^2} & 0 & \frac{6}{L^2} - \frac{12x}{L^3} & -\frac{2}{L} + \frac{6x}{L^2} \end{bmatrix} \tag{D.8}$$

- Force–Strain Material Property Matrix **D**

$$\mathbf{D} = \begin{bmatrix} \sum A_i E_i & \sum A_i E_i y_i \\ sym. & \sum A_i E_i y_i^2 \end{bmatrix} \tag{D.9}$$

- Linear Strain Incremental Stiffness Matrix **K**

$$\mathbf{K} = \int_L \mathbf{B}^T \cdot \mathbf{D} \cdot \mathbf{B}\, dL \tag{D.10}$$

- Vector of Nodal Point Forces Equivalent to the Element Stress **F**

$$\mathbf{F} = \int_L \mathbf{B}^T \cdot \begin{Bmatrix} \sum A_i \sigma_i \\ \sum A_i \sigma_i y_i \end{Bmatrix} dL \tag{D.11}$$

Here, L : length of element, $E_i, A_i, y_i, sigma_i$: tangent stiffness, area, arc length from the center, stress of fiber i, respectively.

D.3 Moment–Curvature Model

In the moment–curvature model, the characteristic matrices is made by the line integral of the sectional characteristic matrices based on the moment–curvature relationship of each section.

Each characteristic matrix expresses as follows: Here, the strain increment vector **E**, the displacement increment vector $\delta\mathbf{u}, \delta\mathbf{U}$, Linear Strain–Nodal Displacement Increment transformation matrix **B** and Linear Strain Incremental Stiffness Matrix **K** are the same of the fiber model analysis.

- Force–Strain Material Property Matrix **D**

$$\mathbf{D} = \begin{bmatrix} EA & 0 \\ sym. & k \end{bmatrix} \tag{D.12}$$

- Vector of Nodal Point Forces Equivalent to the Element Stress **F**

$$\mathbf{F} = \int_L \mathbf{B}^T \cdot \begin{Bmatrix} EA\varepsilon \\ M \end{Bmatrix} dL \tag{D.13}$$

Here, E : Young's modulus of material, A : sectional area, k : tangent stiffness of moment–curvature relationship, ε : axial strain and M : moment.

D.4 Spring Model

In axial and lateral direction, the load–displacement relationship is used, and in rotational direction, the moment–rotational angle relationship is used.

- Linear Displacement Incremental Stiffness Matrix **K**

$$\mathbf{K} = \begin{bmatrix} k_A & 0 & 0 & -k_A & 0 & 0 \\ & k_H & 0 & 0 & -k_H & 0 \\ & & k_R & 0 & 0 & -k_R \\ & & & k_A & 0 & 0 \\ & sym. & & & k_H & 0 \\ & & & & & k_R \end{bmatrix} \tag{D.14}$$

- Vector of Nodal Point Forces Equivalent to the Element Stress **F**

$$\mathbf{F} = \begin{Bmatrix} P_A & P_H & M_R & -P_A & -P_H & -M_R \end{Bmatrix}^T \tag{D.15}$$

Here, k_A, k_H, k_R : sprint stiffness of axial, lateral and rotational direction, respectively, P_A, P_H, M_R : spring force of axial, lateral and rotational direction, respectively.